Universidad
Autónoma de Madrid

Facultad de Ciencias
Departamento de Física Teórica

Consejo Superior
de Investigaciones Científicas

Instituto de Física Teórica
IFT–UAM/CSIC

Dynamics of D-branes on local Calabi-Yau geometries

Memoria de Tesis Doctoral presentada ante la Facultad de Ciencias,
Sección de Ciencias Físicas, de la Universidad Autónoma de Madrid,
por **Iñaki García-Etxebarria,**

Trabajo dirigido por el Doctor **D. Ángel M. Uranga,**
Investigador Científico del Instituto de Física Teórica IFT
y
Consejo Superior de Investigaciones Científicas.

Madrid, 4 de febrero de 2008.

Acknowledgements

On the professional level I owe a lot to my advisor Angel Uranga. He was the one who patiently guided my first steps in string theory, always having time for explaining whatever basic concept had me confused at the time. When I started becoming more independent, he always supported and encouraged me to explore my own ideas. Working with someone with such a sharp mind and clear vision of so many aspects of string theory was always enormously pleasurable and didactic, and thanks to Angel's extremely nice personality, it was also a lot of fun.

I also want to thank Fouad Saad, with whom I have spent so many hours working. Collaborating with him was always a very enriching experience, and I learnt a lot from our long discussions about any aspect of string theory that came in our way. On a more personal level, I also learnt very much from him as a person, and always enjoyed immensely interacting with him.

Thanks go also to the institutions that kindly hosted me during my different stays abroad: the theory division of L'École Polytechnique, the theory department of Princeton University, and the CERN theory division. I keep excellent memories of all these places.

I also want to thank Sebastian Franco for a nice collaboration, and most importantly for generously devoting some of his time to being a nice host for my stay in Princeton in such a crucial moment of his life. I sincerely appreciate it.

Special thanks go to the secretaries of the UAM, IFT and CERN theory departments: Juan Carlos, Isabel, Diana de Toth, and Nanie Perrin, who thanks to their competence (and what in my mind can only be ascribed to big amounts of white magic) many times made dealing with the administration something bearable, instead of the usual dadaist nightmare.

I must also thank the Basque Government for funding my Ph.D. studies through a BFI Fellowship, and the European Union for support for part of my stay in CERN in the form of a Marie Curie grant.

On a more personal level, I want to thank my parents, brother and grandmother for support during the thesis, and always being ready to lend a hand whenever I needed some help with something. Also thanks for supporting my decisions, weird as they might have seen sometimes.

During these last three years I have met a lot of other people that deserve a lot of thanks for helping make me a better person. The list is long, but some of the names that come to mind most easily are Afri, Alfonso, Antón, Daniel, Davide, Elodie, Felipe, Jose Oñorbe, Leila, Marc, Sergio Montañez and Tomás. I am surely omitting quite a few people, so sorry if you are not on the list, and feel free to jump in.

Finally, my most heartfelt thanks go to Nao, who with her kindness and intelligence made my days full of light and joy.

Contents

Chapter 1

Introduction

All experiments so far in particle physics support one theoretical model: the standard model of particle physics [1, 2, 3], extended with masses for the neutrinos to account for oscillations. Its predictions match experiment quite beautifully. Until evidence against it is presented, perhaps coming from the LHC, there is no need to modify it. Still, there are reasons for not feeling completely satisfied by it. Let us describe a few:

- The modern accepted theory of gravity, general relativity, does not fit well within the theoretical framework of quantum field theory. Namely it is non-renormalizable. This means that the behavior at short scales is not well defined: the theory as formulated requires specifying an infinite number of unknown constants (the coefficients of the irrelevant operators) if it is going to describe arbitrarily large energies, so it loses predictivity in this regime. Building a theory that reproduces gravity at long scales and is still well defined at arbitrarily short scales proves to be very hard, with very few candidates to date.

- For some time the renormalizability of the standard model was interpreted as a necessary consistency requirement for the theory. Nowadays the viewpoint has changed, and the renormalizability is understood as coming from the fact that the standard model is the low energy effective theory valid only below some energy threshold. Near that threshold we should start seeing deviations that can be accounted for by including non-renormalizable terms suppressed by the new physics scale. A usual suspect for this scale is something like 1 TeV, the new physics being given by the Minimal Supersymmetric Standard Model (MSSM). Even if this is not the case, at the Planck scale quantum gravity effects are expected to become an essential part of the description, so the standard model should break down there.

- There are a few (around 30) free numerical parameters in the standard model once one fixes the gauge group and the representations. While

this might not seem much taking into account the amount of results it accurately predicts, it would be nice to have a better understanding of the nature of these numbers: whether there are hidden relations between them due to some more fundamental theory or they are just environmental properties of the vacuum we happen to live in. Lacking an experimentally verified more fundamental theory, not much else can be said about what is fundamental and what environmental.

- In the same way that the constants above can be varied in some range without spoiling the consistency of the theory, it is relatively easy to come up with different matter contents or gauge groups. The representation where the (fermionic) matter in the standard model lives does look definitively mysterious:

$$(3,2)_{1/6} + (\bar{3},1)_{-2/3} + (\bar{3},1)_{1/3} + (1,2)_{-1/2} + (1,1)_1 + (1,1)_0 \quad (1.1)$$

  replicated three times. The first number describes the $SU(3)$ representation, the second the $SU(2)$ representation and subindex the hypercharge. All the fermions are taken to have left chirality, hence the bars. I have included a singlet corresponding to the right handed neutrinos present in the see-saw mechanism. This complicated structure demands explanation. One reasonable possibility when taking MSSM coupling constant unification into account is that the standard model is the low energy effective theory for a theory with a unified gauge group that gets broken at some high scale.

- The color interactions are CP-invariant in the standard model except for the θ angle, which in principle can take any value between 0 and 2π. To date no CP-violations have been measured in the strong interaction sector, implying strong upper bounds on θ (it must be smaller than 10^{-9}). Its smallness requires a rather delicate cancellation between two conceptually different entities, namely the phase of the determinant of the quark mass matrix and the coefficient for the topological term in the QCD Lagrangian (it is quantum chiral anomalies that link these two things). This is called in the literature the Strong CP problem [4].

- As briefly mentioned above neutrino oscillation experiments have shown quite convincingly that neutrinos have mass, although the exact details are still unclear and require further measurements. One popular mechanism for achieving natural neutrino masses is the see-saw mechanism, which introduces both Majorana and Dirac mass terms for the neutrinos. In order to do this one needs to extend the spectrum of the standard model by right handed neutrinos ν_R as done above. If we allow for lepton number violation, then neutrinos can have both a Dirac mass term

$$m_D \overline{\nu_L} \nu_R, \quad (1.2)$$

and a Majorana mass term

$$m_M \overline{\nu_R^C} \nu_R. \tag{1.3}$$

The mass scale m_D is usually assumed to be of the order of the electroweak breaking scale, while the Majorana mass is taken to be close to the GUT scale since it is not protected by any chirality arguments. Diagonalizing the mass matrix with these values for m_D and m_M results in neutrino masses consistent with observation. If this is the proper mechanism, by naturalness arguments it hints strongly to new physics at the scale m_M.

- A final very important point where the standard model needs to be extended concerns the explanation of the cosmological data concerning the energy content of the observed universe. Matter described by the standard model accounts only for something like 5% of the observed energy, while dark matter accounts for 25%. Various mechanisms have been postulated to explain the nature of dark matter, extending the standard model in different directions. For example, many supersymmetric models automatically include some interesting candidates for dark matter such as the neutralino and the gravitino. The remaining 70% of the energy content of the universe is called dark energy, and it can be described by introducing a cosmological constant term in Einstein's equations. The microscopic origin of this parameter is unknown at present, without even a good candidate for explaining its observed small but nonzero value.

I think that this is enough motivation for exploring alternatives that extend the standard model in different ways.

One mainstream way of thinking of physics beyond the standard model is in terms of string theory. I will not attempt to review it here since there is by now a plethora of good textbooks available at different levels of sophistication. A short selection of accessible introductory texts is [5, 6, 7, 8, 9, 10, 11, 12, 13, 14, 15].

String theory provides a framework where the question of unification of gravity and relativistic field theory receives a satisfactory answer, in fact providing a consistent description of physics for all energy scales. A fundamental virtue of string theory is that it is relatively easy to find solutions of it which reduce at low energies to conventional general relativity and field theory. It can in this way be thought of as a ultraviolet consistent theory capable of encompassing all known interactions.

Nevertheless, just invoking string theory does not solve the issues just discussed. We will adopt the bottom-up perspective here, and try to build string theory models that resemble the experimental observations. These models automatically include gravity in a consistent way, but most of the

questions posed above might remain unanswered in this approach[1]. In any case, we believe it is a step in the right direction. It should also be interesting to see how does a successful string theory embedding of the standard model plus the standard cosmological model look like. It could be that the exact string theory background for the observed universe gives us hints about some yet undiscovered physical principle organizing the observed interactions.

Another approach one could take for discussing phenomenology in the context of string theory is the top-bottom approach, where one tries to solve string theory and see how does the solution look for a particular observer. This has at least two important disadvantages with respect to the bottom-up approach. First, solving string theory seems to be a Herculean task. Not even the nonperturbative off-shell description of the theory is known in the general case. The second problem is that even if one restricts oneself to the better understood corners of the theory (the low-energy sector of compactifications with fluxes, to put one example of a relatively well understood limit of the theory) one still obtains a multitude of consistent solutions. When trying to predict observable signatures out of the huge number of solutions the theory seems to admit, a number of important conceptual problems arise. The study of how to overcome these problems and predict observable consequences for our universe from first principles is referred to as the study of the landscape[2]. It remains an active, although very controversial, area of research. One recent review for the adventurous explorer is [16].

Let us come back to our favored bottom-up approach. Here we are on firmer ground, but the road is still very bumpy. It is worth stressing that to this day there is no complete embedding of the standard model in string theory, and neither of the available cosmological data. Nevertheless lots of progress has been made, and it is fair to say that there exist mechanisms for embedding most popular model building scenarios in string theory, even if many details still have to be worked out and no precision matching has yet been achieved. In this work we continue along this direction: we provide tools by which different model building scenarios may be studied in string theory, but we will not try to do any precision matching between our toy models and the real world. We will be much more explicit below about which scenarios we embed, and with which limitations.

The theoretical appeal of string theory goes much further than its model building possibilities. In recent times it has been found that many deep physical questions find nice concrete formulations in string theory, and in this way lots of insight has been gained lately about some puzzles of modern physics. Particularly seminal was the microscopic understanding of D-branes

[1] Most string model building targets the MSSM, where some of the problems discussed above are alleviated.

[2] Although in practise one often is satisfied with counting the number of vacua with a desired property inside the set of all possible vacua. In this way the muddy but essential problem of defining a probability wave function over the set of vacua is avoided.

in string theory by Polchinski [17]. This provided an extremely important tool to explore the nonperturbative properties of string theory. Shortly following Polchinki's discovery a number of important advances where done, and much light was shed on some fascinating questions. Let me devote a few lines to shortly describing some of these questions.

Chronologically the first discovery was the partial understanding of the web of dualities that restores unity in string theory. It fact, the proposal for the existence of M-theory [18, 19] happened prior to the discovery of D-branes, although D-branes are essential for completing the web of dualities. Understanding the precise way in which the different string theories are connected by dualities allowed to translate problems which were hard in one description into problems which were easy in a different picture. More generally, it provided a multitude of examples in which the degrees of freedom of a string theory admit an equivalent description in terms of a seemingly different theory.

In the same line of dual descriptions, but even more striking, came the AdS/CFT conjecture [20, 21, 22]. It illustrates in a particular class of instances the holographic principle for theories of quantum gravity [23]. In its simplest form, the AdS/CFT correspondence asserts the equality of type IIB string theory formulated in the $AdS_5 \times S^5$ background and $\mathcal{N} = 4$ SYM theory in four dimensions.

Another important development is the description of the microstates of some classes of black holes in terms of D-branes, starting with [24] (see [25] for a recent review). This showed explicitly how the thermodynamics encoded in the Bekenstein-Hawking entropy formula is reproduced in string theory from the statistical mechanics of bound states of D-branes with the appropriate macroscopic charges.

As the last important series of physical developments we will be mentioning here we have the multitude of advances in the understanding of four dimensional supersymmetric gauge theories, specially of their strong coupling dynamics. In many cases, even if the results themselves can be expressed and motivated in pure gauge theory language, the string theory embedding of the results clarifies the picture immensely. Let us mention just a couple of beautiful branches of this subject. First we have Seiberg duality, [26] provides a nice review. See also [27] for a review of how to embed this in string theory in terms of webs of branes, along the lines of the discussion in the next chapters. Another nice development is the solution of $\mathcal{N} = 2$ SYM by Seiberg and Witten [28]. Here one finds that the Seiberg-Witten curve encoding the properties of the solution admits a beautiful geometrical realization when the $\mathcal{N} = 2$ system is lifted to string theory [29, 30].

Although further from the central topics of this thesis, string theory has also been a fertile ground for mathematics. Particularly fruitful has been topological string theory, a simplified version of string theory (see [31, 32] for pedagogical introductions to the subject). It is simple enough to

be solvable in some instances[3], but it is nevertheless nontrivial enough to reproduce interesting aspects of the string physics described in the previous paragraphs. In particular it contains essential information about the BPS sector of string theory. We will be implicitly using results originally derived in the topological string theory context in the main text. We will not go into the beautiful formal aspects of the mathematics of string theory here, but let us highlight the concept of mirror symmetry, since it will prove to be essential for some of the developments of later chapters. The physical statement of mirror symmetry (somewhat simplified, but enough for our purposes) is that there exist pairs of "mirror" Calabi-Yau spaces $(\mathcal{M}, \mathcal{W})$ such that type IIA string compactified in one member of the pair is equivalent to type IIB compactified in the other. A nice review of mirror symmetry is [35].

Key to the work described in this thesis was another advance that also became possible thanks to the introduction of D-branes in string theory. It was soon realized that the world volume theory of D-branes located at singular points in the geometry could have a very involved field content, typically with gauge groups with many factors and a number of chiral fields in bifundamentals of the factors. Furthermore, involved superpotentials would appear. The first and simplest example to be analyzed was the case of the abelian orbifold singularities [36]. This was soon generalized, and it was found that branes at toric singularities provided a tractable environment where very interesting quiver gauge theories could be constructed. We give a short review of this area in Appendix C.

Such local scenarios have a number of advantages in string model building. The main one is probably that they are largely insensitive to the way in which the singularity is embedded in the complete Calabi-Yau (which eventually we must do in order to incorporate gravity), and how we choose to stabilize closed string moduli. This will give us some freedom when we decide to embed the configuration in a compact Calabi-Yau in order to obtain a more realistic model. Another virtue of branes at local singularities is that they fit quite well into the warped throat scenario (see [37] for the general philosophy). A more technical reason is that local geometries are in many cases easier to work with. Specially in the case of toric geometry, all the information about the geometry we will need in order to build the holomorphic sector of our models can be encoded in a simple way in terms of purely algebraic data. In some cases such as the $L^{a,b,c}$ family one can even write down the explicit Ricci-flat metric for the local Calabi-Yau singularity [38, 39].

In this thesis we will be describing some interesting dynamics of branes at local Calabi-Yau geometries that prove to be useful for model building

[3]Many interesting problems in topological string theory can be reformulated in terms of gauged zero dimensional quantum theories, called matrix models. These can be solved exactly in many cases [33]. See [34] for an excellent review of these topics.

purposes.

In more detail, we will focus on configurations of branes in type II string theory. The main picture will be the one where our system is described by fractional D3 branes at toric singularities, but occasionally we will consider instead formulations related by duality where crucial aspects of the constructions are more evident, and in fact usually manifested geometrically. For example, in Chapter 3 we will work mainly with webs of D and NS branes in type IIA. These so-called Hanany-Witten configurations [40] can be T-dualized to branes at $L^{a,b,a}$ singularities in type IIB. Similarly, the Ooguri-Vafa geometries of Chapter 6 can be mapped, via two T-dualities, to Hanany-Witten configurations, and from there to branes at singularities in type IIB.

As an illustration of the usage of the tools we will develop, we will show in detail how to build some toy models of gauge mediated supersymmetry breaking in Chapter 7. In any case, regardless of the final fate of models of gauge mediated supersymmetry breaking when confronted with experimental data, many of the ideas we present here are of interest by themselves, and shed some light on interesting aspects of the theory.

In particular, the attempts to embed the metastable vacua of ISS in string theory discussed in Chapters 3 and 4 are interesting in their own right. They provide relatively controlled settings where supersymmetry is spontaneously broken in string theory.

In the same way, the results in Chapter 5 are of interest for getting a better understanding of the physics of branes at singularities. They provide a nice link between the smoothing of the singular geometry and the deformations of the gauge theory using some beautiful ideas of mirror symmetry.

The analysis of the continuity of the nonperturbative potential in Chapter 6 also applies to a multitude of scenarios, and not just the one presented here. The study of multi D-instanton effects we start in Chapter 6 is expected to be important for any phenomenon where both D-instantons and motion in closed string moduli space are involved.

Organization

Let us present here an overview of how this work is organized.

We start in Chapter 3 by describing a string theory lift of the metastable solution found by Intriligator, Seiberg and Shih [41]. The lift is in terms of webs of branes in type IIA string theory. We also describe a M-theory lift of the metastable configuration, and a number of possible generalizations of the construction to other gauge theories. This chapter follows [42].

Chapter 4 is devoted to another realization of the ISS vacua in string theory, this time described in terms of branes at toric singularities in type

IIB. This realization is more demanding technically, but will prove to be more useful for our model building purposes. This chapter follows [43].

In Chapter 5 we will study how the resolutions and deformations of the singularity are represented in terms of the gauge theory living in the world volume of the D-brane located at the singularity. This chapters follows [44].

Chapter 6 discusses some more formal aspects of the continuity of the nonperturbative superpotential generated by D-instantons. This kind of superpotential could be used to give naturally small values to some unnaturally small parameters entering the construction of the previous chapters. This chapter follows [45].

Finally Chapter 7 puts the pieces together, and shows how to construct models of gauge mediated supersymmetry breaking in string theory in a simple way just by putting branes in appropriately smoothed singularities. We illustrate the construction via some simple toy models. This chapter follows [46].

The appendices contain short reviews of some background material relevant for the discussion in the main text, and most importantly a list of further references.

Capítulo 2

Introducción

(Spanish translation of Chapter 1)

Hasta el día de hoy todos los experimentos en física de partículas están de acuerdo con un modelo teórico: el modelo estándar de física de partículas [1, 2, 3], extendido con masas para los neutrinos para explicar sus oscilaciones. Sus predicciones concuerdan con los experimentos perfectamente. Hasta que se presente evidencia en contra de este modelo, quizá a partir de los datos obtenidos en el LHC, no hay necesidad de modificarlo. Aún así hay razones para no sentirse completamente satisfecho. Algunas de estas razones son:

- La teoría moderna de la gravedad, la relatividad general, no casa muy bien en el formalismo de la teoría cuántica de campos. En particular, es no renormalizable. Esto significa que su comportamiento a escalas pequeñas no está bien definido: la teoría tal y como está formulada requiere especificar un número infinito de constantes desconocidas (los coeficientes de los operadores irrelevantes) si le pedimos que describa energías arbitrariamente grandes, de modo que pierde predictividad en este régimen. Resulta que construir una teoría que sea compatible con la relatividad general a bajas energías pero que esté bien definida a cualquier escala es muy difícil, con muy pocos candidatos hasta la fecha.

- Durante algún tiempo la renormalizabilidad del modelo estándar se interpretó como algo requerido para que la teoría fuese consistente. Hoy en día el punto de vista ha cambiado, y el hecho de que la teoría sea renormalizable se interpreta como que el modelo estándar es a una teoría efectiva a largas distancias, válida por encima de un umbral de escalas determinado. Cerca de ese umbral deberíamos empezar a ver diferencias, que podemos tener en cuenta introduciendo términos no renormalizables suprimidos por la escala de nueva física. Un sospechoso habitual para esta escala es 1 TeV, y la nueva física estaría descrita por el MSSM (*Minimal Supersymmetric Standard Model*). Incluso aunque no sea éste el caso, a la escala de Planck los efectos de gravedad

cuántica se vuelven una parte esencial de cualquier descripción del sistema, lo que implica que a esas energías el modelo estándar debería dejar de ser válido.

- Hay unos cuantos (30 más o menos) parámetros numéricos indeterminados en el modelo estándar una vez fijado el grupo gauge y las representaciones. Aunque esto no parezca mucho comparado con la cantidad de resultados que predice con precisión, sería bueno tener una mejor comprensión del origen de estos números: entender si hay relaciones ocultas entre ellos debidas a teorías más fundamentales o son simplemente propiedades ambientales del vacío en el que nos encontramos. Dado que no tenemos una teoría fundamental verificada experimentalmente, no se puede decir mucho más sobre esta cuestión.

- Del mismo modo que las constantes del modelo estándar pueden ser alteradas en cierto intervalo sin afectar a la consistencia de la teoría, es relativamente sencillo obtener diferentes contenidos de materia o interacciones. La representación en la que se encuentra la materia fermiónica del modelo estándar es ciertamente misteriosa:

$$(3,2)_{1/6} + (\bar{3},1)_{-2/3} + (\bar{3},1)_{1/3} + (1,2)_{-1/2} + (1,1)_1 + (1,1)_0 \quad (2.1)$$

  repetida tres veces. El primer número describe la representación de $SU(3)$, el segundo la representación de $SU(2)$ y el subíndice la hypercarga. Todos los fermiones tienen quiralidad *left*, es ésta la razón de las representaciones conjugadas. He incluido un singlete correspondiente a los neutrinos *right* presentes en el mecanismo de *see-saw*. Esta estructura requiere una explicación. Una posibilidad razonable cuando uno toma en cuenta la unificación de los acoplos en el MSSM es que el modelo estándar es una teoría efectiva a bajas energías para una teoría con un grupo gauge unificado que se rompe al del modelo estándar a una escala alta.

- También tenemos el ángulo θ de QCD, que viola CP. La interacciones fuertes son invariantes CP en el modelo estándar con la excepción de este ángulo, que en principio puede tomar cualquier valor entre 0 y 2π. No se ha observado ninguna violación de CP en el sector de interacciones fuertes, lo que implica cotas superiores bastantes importantes para θ (debe ser menor que 10^{-9}). El que sea tan pequeño requiere una cancelación bastante sutil entre dos entidades conceptualmente bastante distintas: la fase del determinante de la matriz de masas de los quarks y el coeficiente para el término topológico en el Lagrangiano de QCD (son las anomalías quirales las que relacionan estos dos términos). Esto se conoce en la literatura como el problema CP fuerte [4].

- Como hemos mencionado brevemente un poco más arriba los experimentos de oscilación de neutrinos han mostrado de manera bastante

convincente que éstos tienen masa, aunque los detalles exactos aún no están completamente claros y requieren más medidas. Un mecanismo popular para conseguir masas de neutrinos naturales es el mecanismo del *see-saw*, que introduce términos de masa tanto Majorana como Dirac para los neutrinos. Para que esto sea posible uno debe extender el espectro del modelo estándar con neutrinos *right* ν_R como hemos hecho arriba. Si permitimos violaciones del número leptónico, entonces los neutrinos pueden tener un término de masa tanto de Dirac

$$m_D \overline{\nu_L} \nu_R, \tag{2.2}$$

como de Majorana

$$m_M \overline{\nu_R^C} \nu_R. \tag{2.3}$$

La escala de masa m_D se toma normalmente alrededor de la escala electrodébil, mientras que la masa de Majorana se toma cerca de la escala de unificación, dado que no está protegida por ningún argumento de quiralidad. Si uno diagonaliza la matriz de masas con estos valores para m_D y m_M uno obtiene valores compatibles con lo observado. Si éste es el mecanismo correcto detrás de las oscilaciones de neutrinos, apunta a nueva física a la escala m_M.

- Finalmente, un aspecto en el que el modelo estándar debe ser extendido es en el tratamiento de los datos cosmológicos sobre el contenido de energía del universo. La materia descrita por el modelo estándar es alrededor del 5 % de la energía observada, mientras que la materia oscura compone alrededor del 25 %. Se han propuesto varios mecanismos para explicar la materia oscura, extendiendo el modelo estándar en diferentes direcciones. Por ejemplo, muchos modelos supersimétricos automáticamente incluyen algunos candidatos interesantes para ser materia oscura, tales como el neutralino y el gravitino. El 70 % restante de la energía del universo se denomina energía oscura, y puede ser descrita introduciendo un término de constante cosmológica en las ecuaciones de Einstein. El origen microscópico de este parámetro no se conoce de momento, y no hay ni siquiera buenos candidatos para explicar su valor pequeño pero distinto de cero.

Creo que esto es motivación suficiente para explorar alternativas que extienden el modelo estándar en diferentes sentidos.

Una manera común de pensar en física más allá del modelo estándar es la teoría de cuerdas. No intentaré dar aquí una descripción de ésta dado que ya hay una multitud de libros de texto de calidad. Una pequeña selección de introducciones a la materia accesibles es [5, 6, 7, 8, 9, 10, 11, 12, 13, 14, 15].

La teoría de cuerdas provee un formalismo en el que la gravedad y la teoría cuántica de campos se unifican. De hecho da una descripción consistente de todas las escalas de energía. Una virtud fundamental de la teoría

de cuerdas es que es relativamente sencillo encontrar soluciones de ésta que reproducen a bajas energías la teoría cuántica de campos y la relatividad general. De esta manera, puede ser considerada como una teoría consistente en el ultravioleta capaz de reproducir todas las interacciones conocidas.

De todos modos, no resolvemos los problemas descritos más arriba simplemente invocando el formalismo de teoría de cuerdas. Adoptaremos aquí el enfoque *bottom-up*, en el que uno trata de construir modelos de teorías de cuerdas con fenomenología similar a la observada. Estos modelos automáticamente incluyen gravedad de manera consistente, pero la mayoría de las cuestiones descritas mas arriba se quedan sin solución[1]. Aun así, creemos que es un paso en la dirección correcta. También debería ser interesante ver cómo es un modelo de cuerdas que reproduzca de manera correcta la física observada. Podría ser que el vacío de teoría de cuerdas para el universo observado nos dé pistas importantes sobre nuevos principios físicos que pongan algo de orden en las interacciones conocidas.

Otro enfoque que se podría adoptar es el enfoque *top-bottom*, en el que se intentan resolver las ecuaciones de teoría de cuerdas y ver qué fenomenología tiene la solución. Este enfoque tiene al menos dos defectos importantes comparado con el *bottom-up*. El primero es que resolver teoría de cuerdas es un trabajo hercúleo. Ni siquiera se conoce la formulación completa de la teoría en el caso general. El segundo problema es que incluso si uno se restringe al sector mejor comprendido de la teoría (la teoría a bajas energías de una compactificación con flujos, por poner un ejemplo de un límite de la teoría que se entiendo relativamente bien) aún se obtienen una multitud de soluciones consistentes. Si se intentan obtener consecuencias observables a partir de la gran cantidad de soluciones que la teoría parece admitir, uno debe afrontar problemas conceptuales bastante importantes. El estudio de cómo resolver estos problemas y predecir consecuencias observables para nuestro universo a partir de primeros principios se denomina habitualmente el estudio del *landscape*[2]. Esta línea de investigación sigue siendo muy activa, aunque también muy controvertida. Un resumen reciente para el explorador osado es [16].

Volvamos a nuestro enfoque *bottom-up*. Aquí estamos en tierra más firme, aunque todavía hay muchos obstáculos. Es importante mencionar que al día de hoy no hay una descripción completa del modelo estándar en el marco de la teoría de cuerdas, y tampoco de los datos cosmológicos. No obstante se ha progresado mucho, y se puede decir que hay mecanismos para reproducir los modelos de fenomenología más populares en teoría de cuerdas, aunque

[1] La mayor parte de la fenomenología de cuerdas trata de construir el MSSM, en el que los problemas descritos más arriba encuentran soluciones parciales.

[2] Aunque en la práctica a menudo uno se conforma con contar el número de vacíos con una propiedad determinada dentro del conjunto total de vacíos. De este modo se evita el peliagudo pero esencial problema de definir una función de onda de probabilidad sobre el conjunto de vacíos.

aún hay muchos detalles por fijar y de momento no se ha obtenido una concordancia precisa. En este trabajo seguimos en esta línea: construimos herramientas para reproducir diferentes modelos de fenomenología en teoría de cuerdas, pero no intentamos hacer ninguna comparación precisa entre nuestros modelos ilustrativos y el mundo real. Más abajo seremos mucho más explícitos sobre qué tipo de modelos obtenemos, y con qué limitaciones.

El atractivo teórico de la teoría de cuerdas va más allá de sus posibilidades fenomenológicas. En los últimos tiempos se ha encontrado que muchas preguntas físicas profundas tienen formulaciones concretas y hermosas en teoría de cuerdas, y de este modo se ha aprendido mucho recientemente sobre algunos enigmas de la física teórica moderna. Particularmente importante fue el descubrimiento por Polchinski de la descripción microscópica de las D-branas en teoría de cuerdas [17]. Esto nos dio una herramienta muy potente para explorar las propiedades no perturbativas de la teoría de cuerdas. Gracias al avance de Polchinski pronto se obtuvieron resultados muy importantes, y algunas preguntas fascinantes obtuvieron respuestas. En los siguientes párrafos haré un pequeño resumen de algunos de estos avances.

Cronológicamente el primer descubrimiento fue la comprensión parcial de la red de dualidades que unifican la teoría de cuerdas. De hecho, la propuesta de la existencia de la teoría M [18, 19] antecede al descubrimiento de las D-branas, aunque las D-branas son esenciales para completar la red de dualidades. El descubrimiento de cómo formulas unas teorías de cuerdas en forma de otras permite traducir problemas complicados en una descripción a problemas sencillo en otra. De manera más general, los argumentos de dualidad nos dan ejemplos en los que los grados de libertad de una teoría de cuerdas admiten una descripción equivalente en términos de otra teoría de cuerdas en apariencia bien distinta.

En la misma línea de descripciones duales, pero aún más sorprendente, vino la conjetura AdS/CFT [20]. Esta conjetura ilustra es un ejemplo del principio holográfico para las teorías de gravedad cuántica [23]. En su forma más sencilla, la correspondencia AdS/CFT afirma que la teoría de cuerdas tipo IIB formulada en $AdS_5 \times S^5$ es equivalente a la teoría SYM $\mathcal{N} = 4$ en cuatro dimensiones.

Otro avance impactante es la descripción de los micro-estados de cierta clase de agujeros negros en términos de D-branas, empezando por [24] (véase [25] para un resumen reciente). Esto mostró explícitamente cómo la termodinámica descrita por la fórmula de Bekenstein-Hawking para la entropía aparece en teoría de cuerdas como la mecánica estadística de los estados ligados de D-branas con las cargas macroscópicas pertinentes.

El último de la serie de avances importantes que mencionaremos aquí concierne a los importantes descubrimientos en teoría de campos supersimétrica en cuatro dimensiones, especialmente la compresión de su sector fuertemente acoplado. Aunque en muchos casos los resultados pueden ser moti-

vados y obtenidos puramente en teoría de campos, su formulación en teoría de cuerdas suele clarificar el resultado enormemente. Un par de avances que queremos destacar aquí son los siguientes. Primero tenemos la dualidad de Seiberg, [26] es un buen resumen. Véase también [27] para una explicación detallada de cómo formular estos resultados en términos de teoría de cuerdas, de manera similar a la discusión que haremos en capítulos posteriores. Otro desarrollo interesante es la solución de SYM $\mathcal{N} = 2$ por Seiberg y Witten [28]. Aquí nos encontramos con que la curva de Seiberg-Witten que codifica las propiedades de la solución aparece de forma puramente geométrica cuando el sistema se formula en teoría de cuerdas [29, 30].

Aunque esto se aleja más del núcleo central de esta tesis, la teoría de cuerdas también ha sido muy fructífera para las matemáticas. Particularmente rica ha sido la teoría de cuerdas topológicas, una versión simplificada de la teoría de cuerdas (véanse [31, 32] para introducciones pedagógicas a la materia). Es suficientemente simple como para ser completamente resoluble en algunos casos[3], pero suficientemente rica como para reproducir algunos aspectos interesantes de la física de cuerdas descrita más arriba. En particular, contiene información esencial sobre el sector BPS de teoría de cuerdas. En este trabajo utilizaremos implícitamente muchos resultados derivados en el contexto de cuerdas topológicas. No hablaremos mucho en esta tesis de los hermosos aspectos matemáticos de la teoría de cuerdas, pero el concepto de *mirror symmetry* merece mención especial dado que haremos abundante uso de él en capítulos posteriores. Este principio afirma (simplificaré un poco lo que afirma mirror symmetry, pero es suficientemente preciso para nuestros propósitos) que existen pares de espacios Calabi-Yau $(\mathcal{M}, \mathcal{W})$ tales que la teoría de cuerdas IIA compactificada en un miembro del par es equivalente a la IIB en el otro miembro del par. Una buena introducción a mirror symmetry se puede encontrar en [35].

Esencial para el trabajo descrito en esta tesis es otro avance que también devino posible gracias a la introducción de las D-branas en teoría de cuerdas. Resulta ser que la teoría que aparece en el volumen de la D-brana cuando ésta está en un punto singular puede llegar a tener un contenido de materia y una dinámica gauge muy ricas, con superpotenciales complicados. El primer ejemplo en ser estudiado, que es también uno de los más sencillos, fue el caso de D-branas en orbifolds abelianos [36]. Esto fue prontamente generalizado, y se encontró que las branas en singularidades tóricas son un sistema particularmente tratable donde teorías gauge complejas e interesantes podían ser construidas con facilidad. El Apéndice C contiene una pequeña introducción a la materia.

[3] Muchos problemas interesantes en teoría de cuerdas topológicas pueden ser reformulados en términos de teorías gauge de cero dimensionales, denominadas modelos de matrices. Estos pueden ser resueltos de manera exacta en muchos casos [33]. Véase [34] para una introducción excelente a estos temas.

Estos escenarios locales tienen bastantes ventajas a la hora de construir modelos de cuerdas. Probablemente su principal virtud es que en gran medida no dependen de cómo completemos la singularidad local a un Calabi-Yau (algo que deberemos hacer si queremos incluir la gravedad en nuestros modelos), y cómo decidamos estabilizar los moduli de cuerda cerrada. Esto nos da bastante libertad para construir modelos realistas. Otra virtud de las construcciones de branas en singularidades es que encajan bien en la imagen de gargantas warpeadas (véase [37] para un resumen de la filosofía de este enfoque). Una razón más técnica es que las geometrías locales son en muchos casos más fáciles de manejar. En particular en el caso de geometría tórica, toda la información que necesitamos para construir el sector holomorfo de nuestros modelos se puede codificar de manera sencilla en términos puramente algebraicos. En algunos casos, tales como la familia $L^{a,b,c}$, uno puede incluso escribir explícitamente la métrica Ricci-plana para la singularidad Calabi-Yau [38, 39].

En esta tesis describiremos algunas propiedades dinámicas de D-branas en geometrías Calabi-Yau locales que resultan ser interesantes para los propósitos de fenomenología.

Más en detalle, nos centraremos en configuraciones de branas en teoría de cuerdas tipo II. La imagen en la que nos centraremos será la de D3 branas fraccionarias en singularidades tóricas pero a veces estudiaremos imágenes relacionadas a través de dualidades, en las cuales ciertos aspectos de nuestras construcciones serán más sencillos de ver, a menudo de forma puramente geométrica. Por ejemplo, en el Capítulo 3 trabajaremos principalmente con configuraciones de D y NS branas en tipo IIA. Éstas configuraciones, conocidas como Hanany-Witten [40], pueden ser dualizadas a branas en singularidades $L^{a,b,a}$ en tipo IIB. Del mismo modo, las geometrías de Ooguri-Vafa en el Capítulo 6 pueden ser mapeadas, a través de dos T dualidades, a configuraciones de Hanany-Witten, y de ahí a branas en singularidades en teoría de cuerdas tipo IIB.

Como muestra de las técnicas que desarrollamos, en el Capítulo 7 mostraremos cómo construir algunos modelos de juguete de GMSB[4]. En cualquier caso, e independientemente del destino final de los modelos de GMSB al enfrentarse a los datos experimentales, muchas de las ideas que presentamos aquí son interesantes por sí mismas, e iluminan aspectos interesantes de la teoría.

En particular, los intentos de modelizar los vacíos meta-estables de ISS en teoría de cuerdas que discutimos en los Capítulos 3 y 4 son interesantes por sí solos. Son ejemplos de situaciones relativamente controladas en las que la supersimetría está espontáneamente rota en teoría de cuerdas.

Del mismo modo, los resultados del Capítulo 5 son interesantes para conseguir una mejor comprensión de las branas en singularidades. Nos dan

[4] *Gauge Mediated Supersymmetry Breaking.*

un vínculo entre los suavizados de la geometría y las deformaciones de la teoría gauge utilizando algunas potentes ideas de mirror symmetry.

El análisis de la continuidad del superpotencial no perturbativo en el Capítulo 6 también tiene relevancia en muchos otros contextos, y no sólo en el presentado aquí. El estudio de los efectos multi-instantónicos que iniciamos en el Capítulo 6 promete ser importante para cualquier fenómeno en el que tanto D-instantones como translaciones en el espacio de moduli de cuerda cerrada estén involucrados.

Organización

A continuación presentaremos cómo está organizado este trabajo.

Comenzamos en el Capítulo 3 describiendo una configuración de cuerdas que reproduce la solución meta-estable de Intriligator, Seiberg y Shih [41]. Esta configuración es en términos de redes de branas en teoría de cuerdas tipo IIA. También describimos el *lift* a teoría M de la configuración meta-estable, y unas cuantas posibles generalizaciones de la construcción a otras teorías gauge. Este capítulo está basado en [42].

El Capítulo 4 trata de otra posible configuración de cuerdas análoga a los vacíos ISS. En este caso la configuración es en términos de branas en singularidades tóricas en teoría de cuerdas tipo IIB. Esta configuración es técnicamente más complicada, pero nos resultará más conveniente a la hora de construir nuestros modelos. Este capítulo está basado en [43].

En el Capítulo 5 discutiremos cómo las posibles resoluciones y deformaciones de la singularidad tórica afectan a la teoría de la D-brana localizada en la singularidad. Este capítulo está basado en [44].

El Capítulo 6 discute algunos aspectos formales de la continuidad del superpotencial no perturbativo generado por D-instantones. Este tipo de superpotenciales podría ser utilizado para dar valores naturalmente pequeños a algunos parámetros artificialmente pequeños en los capítulos anteriores. Este capítulo está basado en [45].

Finalmente el Capítulo 7 junta las piezas, y muestra cómo construir modelos de GMSB en teoría de cuerdas de manera sencilla, simplemente poniendo branas en singularidades adecuadamente suavizadas. Este capítulo está basado en [46].

Los apéndices contienen breves resúmenes de material necesario para una mejor comprensión del texto.

Chapter 3

Metastable vacua in string theory

It is always interesting to understand quantum field theories in terms of string theory, as this sometimes clarifies aspects that are obscure in the gauge theory description. Good examples of this phenomenon are [29, 47, 48] where one finds that some essential properties (such as the Seiberg-Witten curve [28, 49]) of a certain class of $\mathcal{N} = 2$ and $\mathcal{N} = 1$ gauge theories can be read quite easily from the M-theory lift of brane configurations describing at low energies the gauge theory we are interested in, or the description of Seiberg duality in terms of webs of branes, as reviewed in [50].

In this spirit, we will proceed in this chapter to describe the IIA and M-theory lift of the metastable vacua Intriligator, Seiberg and Shih (henceforth referred to as ISS) found in massive SQCD [41]. We shortly review some important points of their discussion in Appendix A.

Finding this lift will allow us to easily find some other families of gauge theories that are expected to exhibit metastable nonsupersymmetric vacua. We describe these generalizations in Section 3.3.

It is possible to link the configurations described in this chapter to configurations of branes at singularities similar to those studied in the next chapters by compactifying one dimension and applying T-duality, one example of the kind of manipulations one should do is [51]. A closer link between ISS vacua and branes at singularities will be described in Chapter 4, where we will directly realize susy breaking metastable vacua in a particular class of branes at toric singularities.

The construction described in this chapter was first discussed in [42], see also [52] and [53]. We will not discuss here many other aspects and realizations of metastable vacua in string theory that have been studied recently in the literature, a non exhaustive sample of some interesting approaches is [54, 55, 56, 57, 58, 59, 60, 61, 62, 63].

This chapter is organized as follows. In Section 3.1 we describe the brane

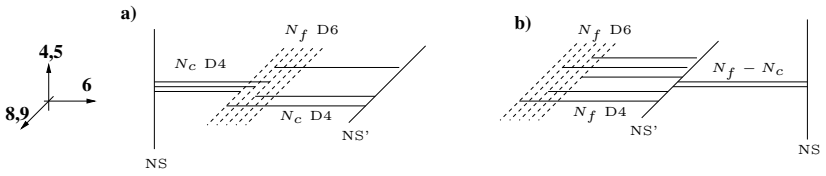

Figure 3.1: The type IIA brane configurations for $SU(N_c)$ SYM with N_f (massless) flavors (a) and its Seiberg dual theory (b).

configuration in type IIA describing the metastable vacuum. In Section 3.2 we show a M-theory lift of this type IIA configuration. Finally in Section 3.3 we use the brane picture to argue for the existence of metastable vacua in a number of nontrivial gauge theories.

3.1 Type IIA configuration

An efficient way to realize supersymmetric gauge field theories in string theory is to embed them as the effective gauge theory on the world-volume of configurations of D- and NS-branes. These Hanany-Witten setups [40] have been successfully employed in the study of four-dimensional gauge theories with $\mathcal{N} = 2$ and $\mathcal{N} = 1$ supersymmetry (see e.g. [64, 29, 48, 47, 65] and [27] for a review with more complete references). In this section we describe the type IIA brane configuration that corresponds to the ISS non-supersymmetric local minimum, and understand some of its classical properties.

A convenient starting point is the type IIA brane configuration of $\mathcal{N} = 1$ $SU(N_c)$ SYM with N_f flavors[1]. We consider one NS-brane stretching along the coordinates 012345, one NS-brane (denoted NS'-brane) stretching along 012389, N_c color D4-branes stretching along 0123 and suspended in x^6 between the NS- and NS'-branes, and N_f flavor D6-branes stretching along 0123789. See [64, 27] for more details. We consider the configuration for zero flavor masses (namely, the D6's have all the same position as the NS' in 45). The configuration is shown in Figure 3.1a.

Notice that the D4-branes can in general split in pieces as they are able to end on the D6-branes. Notice also the familiar s-rule [40] which imposes that there is at most one D4-brane piece connecting the NS-brane with a

[1]This configuration can be obtained from the one describing $\mathcal{N} = 2$ SQCD with $SU(N_c)$ gauge group by rotating the NS' (originally parallel to the NS) [66]. The relative angle θ between the NS and NS' branes dictates the mass of the adjoint chiral superfield $|\mu(\theta)| = \tan\theta$. In the limit in which the NS and NS' become orthogonal $\mu \to \infty$. Integrating out the adjoint chiral superfield we are left with $\mathcal{N} = 1$ $SU(N_c)$ SQCD with vanishing superpotential. Although this viewpoint is useful in the derivation of the M-theory lift of the type IIA configuration, in this section we directly discuss the final rotated configuration.

given D6-brane. The number of D4-brane pieces connecting the NS'-brane with a given D6-brane is on the other hand arbitrary.

Following the operations in [64, 27], it is straightforward to obtain the brane configuration describing the Seiberg dual theory. Sketchily, one considers moving the NS across the D6-branes (process in which the N_c finite D4-brane pieces joining them disappear, and $N_f - N_c$ new finite D4-brane pieces appear), and then across the NS'. The final configuration is shown in Figure 3.1b. Notice the familiar realization of the meson vevs as the position in $8, 9$ of the N_f D4-branes pieces suspended between the D6-branes and the NS'-brane.

3.1.1 The susy breaking vacuum

Let us now consider the type IIA configurations and the above processes in the presence of non-zero flavor massless, by moving off the D6-branes in the directions 45. Consider for simplicity the case where all flavor masses are equal.

The introduction of flavor masses corresponds in the magnetic field theory to the introduction of the linear term in the mesons that triggers supersymmetry breaking. Recall that there is a non-supersymmetric set of vacua, where the dual quarks have non-trivial vevs (fixed by the flavor masses), and which is parametrized by pseudo-moduli encoded in an $N_c \times N_c$ block of the mesonic matrix.

These features are nicely reproduced by the type IIA configuration. When the D6-branes are moved off in 45, the $N_f - N_c$ D4-branes joining them to the NS-brane move along 45 and maintain the same supersymmetry. However, the N_f D4-brane pieces joining them to the NS'-brane misalign with respect to them, leading to a non-trivial F-term. The F-term can be partially canceled by recombining $N_f - N_c$ of such D4-branes with the D4-branes joining the D6- and the NS-branes. This recombination corresponds to the fact that $N = N_f - N_c$ entries in the dual quarks acquire non-zero vevs to minimize the F-term. Notice that the appropriate breaking of the global symmetry is nicely reproduced. For shortness, we sometimes denote D4'-branes the D4-branes suspended between the D6- and the NS'-brane.

The configuration for the supersymmetry-breaking configuration is shown in Figure 3.2. This configuration is the starting point of our studies[2]. Notice that the $N_f - N_c$ D4'-branes joining the D6-branes to the NS'-brane are free to move in the directions $8, 9$, hence reproducing (most of) the classical

[2]This brane setup has been well investigated in the past in order to study the deformation corresponding to adding terms linear in the mesons to the magnetic superpotential (see for example [27]. The only new ingredient is to allow the rank of the quark mass matrix of the electric theory (linear couplings in the magnetic dual) to be larger than N_c. This brane setup was discussed by various attendants to a group meeting at the Institute for Advanced Study.

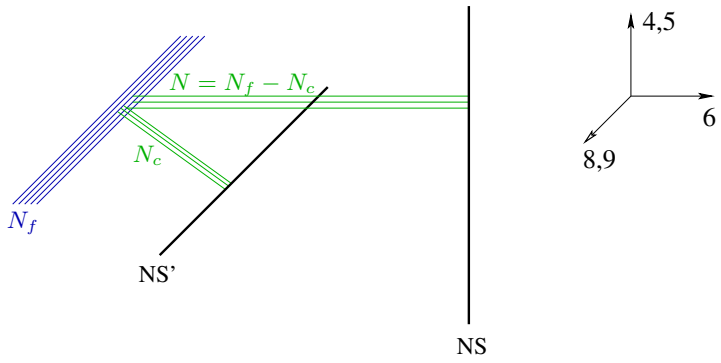

Figure 3.2: Type IIA brane configuration corresponding to the SUSY breaking minimum.

moduli space of non-supersymmetric vacua of the field theory (notice that the pseudo-modulus θ is not manifest in the geometry[3]).

It is very interesting to consider more general situations, with arbitrary non-zero masses. Recall that in the field theory analysis in [41], the non-supersymmetric vacua are obtained when the vevs for the dual quarks φ_0, $\tilde{\varphi}_0$ are given by the N largest masses (out of the N_f mass parameters). In configurations where some vev is given by one of the N_c smallest masses, a classically unstable mode appears.

This behavior is easily reproduced by the type IIA configuration. The different flavor masses correspond to different $4, 5$ positions for the different D6-branes. The brane setup corresponding to the classical non-supersymmetric configuration suggested in ISS is shown in Figure 3.3. In this configuration, the N_c D4-branes connected to the NS'-brane end on the N_c D6-branes which are closest (i.e. those associated with the N_c smallest mass parameters). This is in order to minimize the energy of the configuration. In addition, the remaining N D4-branes connected to the NS-brane, end on the farthest N D6-branes (i.e. those associated with the N largest mass parameters). The reason for this is clarified in the next paragraph. Recall that the position in $4, 5$ of these D4-branes is related to the dual quark vevs, so we have indeed found the configuration realizing the ISS vacuum for different masses.

It is now easy to realize what goes wrong if one considers the configuration where a dual quark vev is given by one of the N_c smallest masses. Clearly, there is one D6-brane on which two D4-brane pieces (one connecting to the NS-brane and other to the NS'-brane) coincide. Since these D4-branes are non-supersymmetric with respect to each other, an open string tachyon

[3]The pseudo-modulus θ is defined such that $\langle\varphi_0\rangle = \mu e^{\theta}\mathbb{I}_N$ and $\langle\tilde{\varphi}_0\rangle = \mu e^{-\theta}\mathbb{I}_N$, see [41] and Section 4.1.

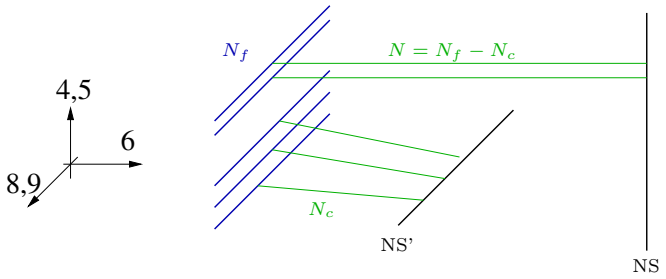

Figure 3.3: The non-supersymmetric type IIA configuration reproducing the non-supersymmetric ISS field theory minimum for arbitrary flavor masses.

develops at their intersection. This is precisely the unstable mode which appears in the field theory analysis. Notice that the stretched open string leading to the tachyon is a component of the meson field Φ, in agreement with this interpretation[4]. Notice also that this tachyon only appears at the origin in the mesonic (pseudo)moduli space, in agreement with the field theory analysis. However one cannot try to avoid this classical instability by moving off in the (pseudo)moduli space, since quantum corrections (see later) lift it dynamically pushing the configuration towards the origin.

The above brane configuration can also be used to study the situation of SQCD with $N_{f,0}$ massless and $N_{f,1}$ massive flavors. These models have been discussed in [68] from the field theory viewpoint. In particular, it was shown that the magnetic dual exhibits supersymmetry breaking by the rank condition for $N_{f,0} < N_c$, and that in this case one does not have a meta-stable minimum, but rather a saddle point with a runaway direction parametrized by the mesons formed by the massless quarks (and which becomes the runaway triggered by the Affleck-Dine-Seiberg superpotential in the large field region).

The above brane configuration provides a simple explanation of these facts. We consider the type IIA brane configuration in which $N_{f,0}$ D6-branes sit at the origin in the directions $4, 5$. If $N_{f,0} < N_c$, then $N = N_f - N_c < N_{f,1}$ and there are some of the $N_{f,1}$ D6-branes associated with non-zero masses which are not endpoints of the N D4-branes in the D4/NS5 system. These D6-branes can be used as endpoints of the D4-branes in the D4/NS' system and lead to non-supersymmetric configurations. If on the other hand $N_{f,0} > N_c$, then $N > N_{f,1}$ and the N D4-branes in the D4/NS system occupy all the $N_{f,1}$ massive flavor D6-branes (and some more). Hence the D4-branes in the D4/NS' system are forced to end on the massless flavor D6-branes, leading to a final supersymmetric configuration. Thus one reproduces the

[4]One may be surprised by the fact that an open string tachyon is captures by a field theory analysis. In fact, similar phenomena occur in other non-supersymmetric tachyonic D-brane configurations, in the regime of small supersymmetry breaking, see e.g. [67].

above mentioned condition to have rank supersymmetry breaking.

The above discussion leads to an important observation. There is a dynamical 's-rule' in the non-supersymmetric configurations of our interest, which prevents a D4-brane and a D4'-brane to end on the same D6-brane. Although more manifest in the case of different masses, this conclusion is general and valid in the case of equal masses. This has an important implication on the structure of the M5-brane describing the M-theory lift of our type IIA configurations.

3.1.2 The metastable vacuum in the electric theory

Once we have identified the structure of the supersymmetry breaking metastable minimum in the brane configuration realizing the magnetic theory, it is possible to obtain it in the brane realization of the electric theory. This is simply obtained by undoing the Seiberg duality, namely by crossing back the NS'- and NS-branes. The resulting configuration is shown in Figure 3.4b. The supersymmetric configuration corresponding to the supersymmetric minima of the theory is shown in Figure 3.4a.

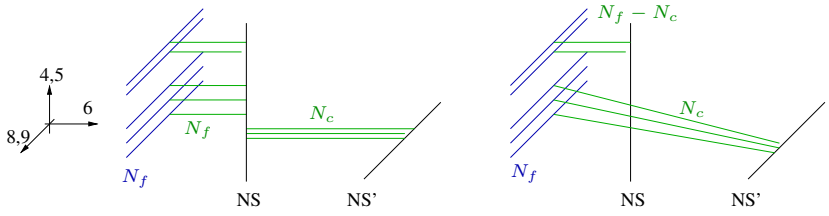

Figure 3.4: Figure (a) shows the brane configuration describing the supersymmetric minimum of the electric theory. Figure (b) shows the supersymmetry breaking meta-stable vacua in the brane configuration realizing the electric theory.

3.1.3 Longevity of the metastable vacuum

As discussed in [41], the longevity of the meta-stable SUSY breaking vacuum depends on its distance to the SUSY vacua in field space and the height of the potential barrier separating them. Both of them can be estimated by considering a simple trajectory connecting the minima.

The separation between vacua is determined by the expectation value of Φ at the supersymmetric minimum, the type IIA brane setup provides a simple visualization of the barrier height. The $\varphi_0 = \tilde{\varphi}_0 = 0$ point corresponds to no recombination of the D4-branes. The increase in length of the branes accounts for the additional potential energy.

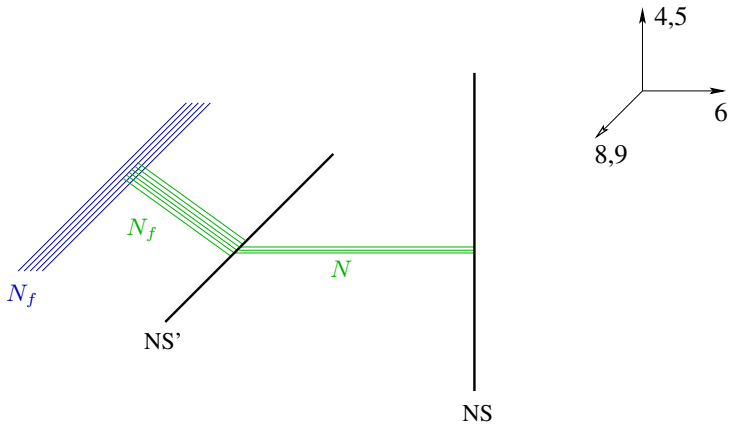

Figure 3.5: Brane configuration describing the $\varphi_0 = \tilde{\varphi}_0 = 0$ point used to estimate the height of the potential barrier.

3.2 M-theory curve

Let us now lift the previous brane configuration to M-theory. Both the D4 branes and the NS5 branes lift to M5 branes in M-theory, and whether it is a D4 or a NS5 depends on whether it wraps the M-theory circle or not. The D6 has quite a different lift, as it lifts to a Taub-NUT space (one way for thinking about this object is by analogy with the magnetic monopole, where the role of the $U(1)$ electromagnetism gauge fiber is played here by the M-theory circle). So our objective consists, ignoring spacetime as usual, of describing the two (real) dimensional surface described by the M5 brane in the 456789(10) directions. There is no interesting structure in the 7 direction, as the D6 brane is extended there and the original D4-NS system does not extend in that direction, so it is a fair assumption to think that the M-theory lift of the NS-D4 system will not wrap that direction. We will ignore it in the following. That leaves us with 45689(10), a 6 dimensional space, where the (10) direction is a circle fibered non trivially over 459, with the winding number at infinity giving the D6 brane charge.

An important remark is in order at this point. Properly speaking, the brane configurations in M-theory we will find describe theories in the same universality class of the original theory, see for example the discussion in section 5 of [47]. In particular, holomorphic quantities of the field theory are expected to be computable in the M-theory lift.

In our setup we will be interested in a non-supersymmetric vacuum of the supersymmetric theory, which *a priori* needs not survive the M-theory lift (and indeed it does not, see [53]). The M-theory state we build reduces at vanishing string coupling to the metastable type IIA configuration, and it captures various features of the IIA configuration such as its pseudo-moduli.

Nevertheless, it is important to notice that this M-theory lift possesses non-holomorphic boundary conditions, and thus the asymptotic behavior of our M-theory curve differs from the one of the M-theory lift of the supersymmetric configuration. As a result, it cannot be interpreted as a state with spontaneously broken supersymmetry in M-theory. Instead, it corresponds to a state in a theory with a Lagrangian that breaks supersymmetry explicitly. This issue was emphasized and investigated in detail in [53].

This being said, let us construct the lift to M-theory of the metastable type IIA configuration. In order to properly understand the resulting geometry it is convenient to discuss first some technical points about the complex structure of Taub-NUT spaces. Let us devote the Section 3.2.1 to do so. With this knowledge we will come back to the construction of our non-supersymmetric M-theory vacua in Section 3.2.2.

3.2.1 An aside on hyper-Kähler geometry

The description of the M-theory geometry together with its complex structure is most natural from the quaternionic geometry point of view, but perhaps this is a bit unfamiliar, so let us give here a short discussion of the matters involved.

Hyper-Kähler construction of the multicenter Taub-NUT spaces

Let us describe the (multicenter) Taub-NUT space as a hyper-Kähler quotient, following the reasoning in [69]. In order to build the Taub-NUT in this way, we start from the manifold $\mathcal{M}$ given by $d+1$ copies of $\mathbb{H}$, where d is the number of centers in our space and $\mathbb{H}$ is a copy of $\mathbb{R}^4$ with flat hyper-Kähler metric. Let us take as coordinates in $\mathcal{M}$ the quaternions w and q_a, where a goes from 1 to d.

Now consider the abelian group G of rank d acting on the manifold, this group is isomorphic to $\mathbb{R}^d$ locally. The moment map for this group acting on $\mathcal{M}$ is given by

$$\mu_a = \frac{1}{2}\mathbf{r}_a + \mathbf{y}, \tag{3.1}$$

where $\mathbf{r}_a = q_a i \bar{q}_a$ (no sum in a, and boldface denotes three dimensional vectors) and $\mathbf{y} = (w - \bar{w})/2$. Under the a-th factor of G, q_a transforms with a $+1$ $U(1)$ charge, w gets translated and the rest of the coordinates remain invariant. Let us consider the set of vectors $\mathbf{e}_a$. Then we define our Taub-NUT space as:

$$X = \mu^{-1}(\mathbf{e})/G, \tag{3.2}$$

where the a index is implicit. Namely, we consider all points in $\mathcal{M}$ such that their moment maps μ_a give $\mathbf{e}_a$, and then quotient the resulting space by the action of G. With the metric inherited from the flat $\mathcal{M}$ one gets the

multicenter Taub-NUT space with the standard metric:

$$ds^2 = \frac{1}{4}V d\mathbf{r}^2 + \frac{1}{4}V^{-1}(d\tau + \vec{\omega}\cdot d\mathbf{r})^2, \tag{3.3}$$

with $\nabla \times \vec{\omega} = \vec{\nabla}V$ and

$$V = 1 + \sum_{a=1}^{d} \frac{1}{|\mathbf{r} - \mathbf{e}_a|}, \tag{3.4}$$

so we can identify the values of the moment maps with the positions of the centers of the Taub-NUTs.

Complex structure for these spaces

In this section we will try to understand better the structure as a complex manifold of the space we just built following [29]. Recall that a quaternion can be written as $q = a + ib + jc + kd$, where i, j and k satisfy the $SU(2)$ Lie group algebra, so we can think of them as the Pauli matrices, and a, b, c and d are real numbers. This structure reflects the hyper-Kähler nature of the manifold, we can associate choosing a complex structure (in the S^2 of possible complex structures) with privileging i, say, and then decomposing the quaternion q into two complex numbers w_1 and w_2 given by:

$$w_1 = a + ib \tag{3.5}$$
$$w_2 = c + id, \tag{3.6}$$

the decomposition being motivated by $q = a + ib + j(c + id)$. We have the freedom of choosing any combination of i, j and k as determining a complex structure, so we have essentially the freedom of choosing a direction in $\mathbb{R}^3$. Note also that the 3-vector structure of the moment maps also comes from ijk, so rotating the directions of the base space for the Taub-NUT (i.e., ordinary rotations in the type IIA picture) roughly corresponds to choosing different complex structures. This will be the basic idea in what follows.

Let us privilege a complex structure and then separate q_a into the complex variables y_a and z_a, and w into v and v', such that the action of G in these complex variables is given by:

$$y_a \to e^{i\theta_a} y_a \tag{3.7}$$
$$z_a \to e^{-i\theta_a} z_a \tag{3.8}$$
$$v \to v \tag{3.9}$$
$$v' \to v' - \sum_{a=1}^{d} \theta_a. \tag{3.10}$$

Also, when we pick a complex structure, namely a direction in 3 space, the moment map can be divided into the longitudinal part (a real part $\mu_{\mathbb{R}}$)

and a complex (transverse) part $\mu_{\mathbb{C}}$. In the type IIA picture the latter corresponds to the projection of the D6 brane position into the 45 plane in which the NS brane is sitting, and the former to the x^6 position of the brane, which as we will see below does not appear in the defining equations for the NS factor of the M theory curve in the complex structure in which it is holomorphic.

The components of $\mu_{\mathbb{C}}, a$ give the equations:

$$y_a z_a = v - e_a, \tag{3.11}$$

where e_a is the projection of $\mathbf{e}_a$ in the 45 plane. We can define then the manifold X in terms of the G invariants and any constraints between them. In terms of the invariants $y = e^{iv'} \prod_{a=1}^{d} y_a$, $z = e^{-iv'} \prod_{a=1}^{d} z_a$ and v, the defining equation for the resulting space is given by:

$$yz = \prod_{a=1}^{d} (v - e_a), \tag{3.12}$$

which is the equation we have been using in the main text for the Taub-NUT.

Rotating the complex structure

We have described how to obtain the equations for the Taub-NUT in a given complex structure, but in our system there are two different relevant complex structures with no holomorphic relation between them, and we expect that the y, z and v parameters describing the Taub-NUT in the complex structure in which the NS factor of the M theory curve is holomorphic have a complicated non-holomorphic relation with the parameters y', z' and v' describing the curve in the complex structure where the NS' factor is holomorphic. In this section we describe how to obtain explicit relations between both sets of coordinates.

The basic idea has already been described. What we notice is that rotations of the moment maps have two interpretations, one as rotations in the space of complex structures of the hyper-Kähler manifold and the other as rotations in the Type IIA theory. Since in the type IIA theory the rotation necessary for going from the direction associated with the NS factor being holomorphic (i.e., x^6) to the direction in which the NS' factor is holomorphic ($x^6 \cos\theta + x^4 \sin\theta$, where θ is the rotation angle, given by the masses and the position in x^6 of the D6 branes) is easy to determine with simple trigonometry, the appropriate change in complex structure is simple to determine too. For example, let us identify the ijk directions in quaternion space with the 645 directions in the type IIA picture. With this convention, the complex structure making the NS factor holomorphic is given by privileging i, and splitting the quaternionic coordinates as $q_a =$

$(a+ib)+j(c+id) = (y_a, z_a)$. Now we rotate in order to obtain the expressions in the coordinates where NS' is holomorphic. The effect in ijk is given by:

$$\begin{pmatrix} i \\ j \\ k \end{pmatrix} \to \begin{pmatrix} \cos\theta & -\sin\theta & 0 \\ \sin\theta & \cos\theta & 0 \\ 0 & 0 & 1 \end{pmatrix} \begin{pmatrix} i \\ j \\ k \end{pmatrix} \equiv \begin{pmatrix} I \\ J \\ K \end{pmatrix}. \tag{3.13}$$

We now want to split the moment maps into complex coordinates where I is now the privileged complex structure. We just substitute and read components, let us do it for some generic q:

$$\begin{aligned} q &= a + bi + cj + dk = a + b(I\cos\theta + J\sin\theta) + c(J\cos\theta - I\sin\theta) + dk \\ &= a + I(b\cos\theta - c\sin\theta) + J(b\sin\theta + c\cos\theta + Id). \end{aligned} \tag{3.14}$$

From here we read what the new y and z are, and since we have the expressions of $abcd$ in terms of the original y and z (for example, $b = -i/2(y - \bar{y})$), this completely determines the new variables as a non-holomorphic function of the old ones and the θ angle.

3.2.2 Back to M-theory

Now that we understand better the structure as a complex manifold of the multicenter Taub-NUT space let us apply this knowledge in order to lift the metastable IIA brane configuration to M-theory.

In particular, it is simple to realize that the configuration, at least for the massless case, factorizes into two curves which are holomorphic in different complex structures. The hyper-Kähler structure then strongly suggests that the rotation in complex structure space can be mapped to the rotation in type IIA that we need in order to go from one factor of the curve to the other. Let us assume this and describe each factor in its natural complex structure, with the understanding that one system of holomorphic coordinates can be expressed in terms of the other as described in the previous section.

The curves

Let us start by describing the lift of the D4/NS system, which is locally $\mathcal{N} = 2$ supersymmetric. It is conventional to introduce in this kind of setups complex coordinates given by $v = x_4 + ix_5$ and $w = x_8 + ix_9$. The ambient Taub-NUT can then be described by the equation:

$$yz = \left[\prod_{i=N_c+1}^{N} (v - \mu_i)\right] (v - \mu)^{N_c}, \tag{3.15}$$

where μ is associated with the masses of the corresponding flavor, given by their positions in the 45 directions. Note that we have set the masses of the

N_c lightest flavors equal, this is required in order to have a supersymmetric D4/NS' system[5].

Once we have described the ambient space we want to find the holomorphic curve described by the D4/NS system. Here we can use standard arguments describing this factor in $\mathcal{N} = 2$ theories, see for example [48]. What we do in the end consists of taking the usual $\mathcal{N} = 1$ lift described in the literature and rotating one of the factors as suggested by the hyper-Kähler structure. The equation we write for the D4/NS is then the one we find in the literature:

$$z - \prod_{i=N_c+1}^{N} (v - \mu_i) = 0 \tag{3.16}$$

$$w = 0. \tag{3.17}$$

We see that when $v = \mu_i$ the curve goes to $z = 0$. This describes the curve going to the location of the corresponding center of the Taub-NUT geometry, which is at $yz = 0$. This factorizes, the curve wraps the $z = 0$, y arbitrary component (the one to the right, in our language).

We can also describe the NS'/D4 system reusing known results from the literature. For this factor we have to introduce adapted complex coordinates, in which the curve is holomorphic. The Taub-NUT will still be of the same form:

$$y'z' = \left[\prod_{i=N_c+1}^{N} (v' - \mu'_i)\right] (v' - \mu')^{N_c}, \tag{3.18}$$

where the primes describe the adapted coordinates. The holomorphic curve is also easily described:

$$z' - \prod_{i=N_c+1}^{N} (w - w_i) = 0 \tag{3.19}$$

$$v' = 0, \tag{3.20}$$

where the difference with the previous case arises mainly from the fact that the NS' is rotated with respect to the NS. We have not rotated the w coordinate as only a rotation in 456 space is needed to go from one system to the other, so we expect w to be still a good holomorphic coordinate. The w_i describe mesonic (pseudo)moduli, they have an interpretation similar to that in the IIA configuration as pieces of the curve sliding along the 89 directions.

Each factor is holomorphic in some complex structure, and thus area minimizing by itself. The resulting curve is thus non-holomorphic but (locally in curve space) area minimizing. This statement encodes the fact that we have a non supersymmetric metastable minimum of M-theory.

[5]We are assuming here equal x^6 positions for the D6 branes, otherwise we could have different masses here.

3.2.3 Pseudomoduli stabilization

An important point for the comparison with field theory is the fate of the pseudomoduli. We know that in field theory they get a mass at one loop, so we should see a similar effect in the M-theory configuration. Although we have not studied this in detail, the configuration seems able to reproduce this lifting at first order.

Namely, as we have seen, pseudomoduli of the gauge theory get mapped to the positions in 89 of the branes in the NS'/D4 system. These are holomorphic parameters, so we do not expect them to get corrections from self-interactions in the NS'/D4 system (similarly to the Coleman-Weinberg formula for pseudomoduli stabilization, where only the supersymmetry breaking spectrum contributes). The corrections should then come from the interactions with the other (relatively non holomorphic) NS/D4 system. In the supergravity approximation this effect comes mainly from annulus exchange between both factors. It is easiest to estimate it in the IIA picture (very similar arguments can be put forward in the M theory picture). Namely, we start with the observation that relatively supersymmetric D4 branes exert no force on each other because of the cancellation between gravity (attractive) and RR-form (repulsive) forces. When we misalign them the RR-form force gets less repulsive, and a net attraction arises (which in the short distance regime is represented by the tachyon that triggers recombination). So in the IIA setup we expect the net effect to be an attraction between the D4/NS and D4/NS' branes. This should stabilize the mesonic moduli at the origin of moduli space, which is what we find in the gauge theory analysis.

From the point of view of a proper M-theory analysis one should solve for the appropriate back-reacted background, something along this lines has been done in [70] in a holomorphic context.

3.3 Generalizations

Once we understand the IIA lift of the configuration we can generalize to more complicated cases with relative ease. Let us discuss some interesting cases. Most of them have already been described in the literature in the electric phase.

3.3.1 Symplectic and orthogonal gauge groups

It is straightforward to carry out a similar discussion for the metastable minima in the $SO(N_c)$ and $USp(N_c)$ theories with N_f massive flavors. In fact, the type IIA configurations realizing these gauge theories, and their Seiberg duality properties, have been studied in [71]. We sketch the new features of this construction, referring the reader to this reference (see also [27] for a review) for details.

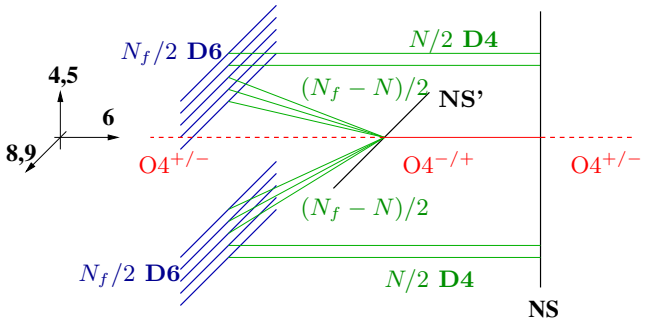

Figure 3.6: The type IIA brane configuration for the non-supersymmetric minimum of the $SO(N_c)$ and $USp(N_c)$ gauge theories with N_f massive flavors. For clarity we have shown the situation for different flavor masses. The horizontal solid/dashed line corresponds to the O4-plane, and its change of charge as it crosses the NS- and NS'-branes is shown as a change between dashed and solid. For the $SO(N_c)$ theory we have $N = N_f - N_c + 4$, and it corresponds to choosing the O4-plane to have negative charge in the middle interval, and positive on the semi-infinite pieces. For the $USp(N_c)$ theory we have $N = N_f - N_c - 4$ and the O4-plane charge is positive in the middle interval.

These gauge groups are described in string theory by the introduction of orientifold planes. The required configurations have been described in [71, 27]. In particular we will describe $SO(N_c)$ and $USp(N_c)$ theories with N_f massive flavors in the fundamental.

The only additional ingredient is the introduction of an O4 plane stretching in the 01236 directions (i.e., parallel to the D4 branes going from the D6 branes to the NS branes). When the O4 plane crosses the NS or NS' branes it flips its charge.

The introduction of the orientifold plane forces us to include the images (in the covering space) of the D4 branes under the orientifold symmetry. The gauge theory living in the D4 branes world volume has a reduced gauge symmetry, due to the projection, from $SU(N_c)$ to $USp(N_c)$ or $SO(N_c)$ depending on the charge we choose for the orientifold plane (positive or negative).

One last subtlety concerns the Hanany-Witten effect in the presence of O4-planes. The O4 plane has ± 4 units of D4 brane charge, which contribute to the calculation of the magnetic gauge group rank. The result is $N = N_f - N_c \pm 4$, with plus sign for SO groups and minus sign for USp group.

The final magnetic theory configuration is given in Figure 3.6.

One thing we observe is that there appears to be an instability where the NS' meets the orientifold plane, as two mutually non supersymmetric stacks of D4 branes meet there and this usually induces a tachyon. In terms of the gauge theory analysis there appears to be no tachyon, so we just take the classical stability of the configuration as given. Further analysis needs to be done in order to guarantee that the open string tachyon is completely

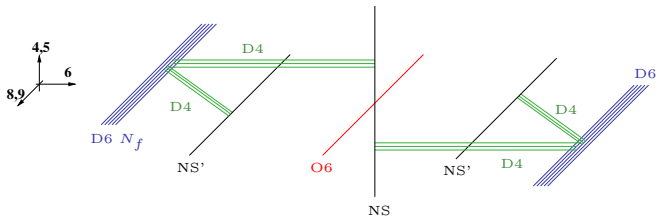

Figure 3.7: The type IIA brane configuration describing the non-supersymmetric meta-stable minimum in the $SU(N_c)$ theory with non-chiral matter in the symmetric or antisymmetric representations (corresponding to the choice of positive or negative O6-plane charge), plus massive flavors.

removed by the action of the orientifold and the NS'. A similar analysis was done in [72], the analysis for our configuration should follow the same lines.

Another important difference with the $SU(N_c)$ case is that the D4-NS' factor is non holomorphic by itself even in the case with equal flavor masses. This will probably make the M-theory lift more difficult, as we cannot write the configuration as two factors each holomorphic in a different complex structure.

3.3.2 $SU(N_c)$ with non-chiral matter in $\square\square$ or $\begin{smallmatrix}\square\\\square\end{smallmatrix}$

It is possible to obtain theories with non-chiral matter in the symmetric or antisymmetric representations of $SU(N_c)$ by the introduction of O6 planes along 0123789, this has been done in [73]. Dualizing the electric theory and obtaining the metastable vacuum proceeds then as usual, the result is shown in Figure 3.7.

3.3.3 $SU(N_c)$ with chiral matter in the $\begin{smallmatrix}\square\\\square\end{smallmatrix} + \overline{\square\square} + 8\square$

Building four dimensional chiral theories from IIA brane configurations is more involved than in the IIB case. A simple reason is that the branes in IIA have an odd number of world volume dimensions (for example 5 for D4 branes), and there is no chirality in odd dimensions. It is still possible to build chiral configurations, though, via more involved setups. We present here one such example, taken from [74, 75, 76]. The main new ingredient in this setup is an O6 plane passing through the NS', which gives one multiplet in the symmetric, another in the conjugate symmetric, and 8 multiplets in the fundamental of $SU(N_c)$. The resulting configuration is shown in Figure 3.8. Chirality comes as follows: the NS' acts as a domain wall in the O6 world volume (in the 7 direction in particular) such that the O6 charge is different in both sides. This introduces a tadpole in the NS' world volume theory unless one cancels it with 8 semi infinite in the 7 direction (half) D6-branes ending on it, which give the required chiral flavors. Related topics are discussed in [77, 78].

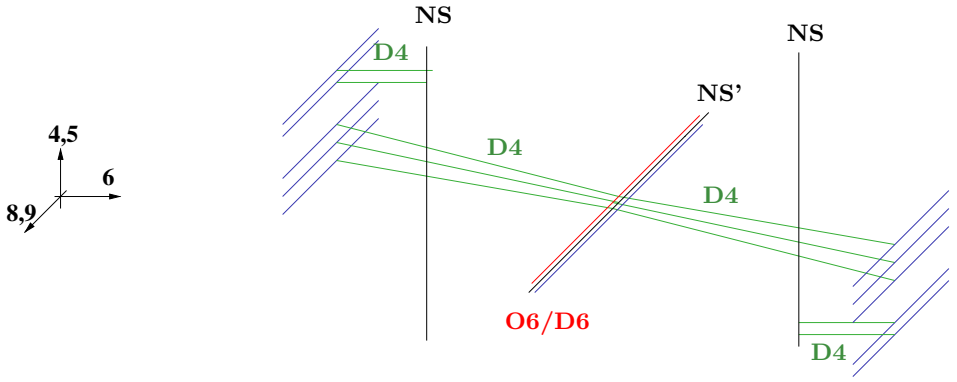

Figure 3.8: The type IIA brane configuration describing the non-supersymmetric meta-stable minimum in the chiral $SU(N_c)$ theory with matter in antisymmetric, conjugate symmetric and fundamental representations. Here O6/D6 stands for the system of the split O6-plane and the 8 half D6-branes.

Chapter 4

Susy breaking in runaway quiver theories

In Chapter 3 we have discussed a possible embedding of the ISS metastable vacuum in string theory. In this chapter we will go one step forward and describe a construction that, while more technically demanding, will allow for some interesting model building possibilities, which we discuss in Chapter 7. In particular we will focus our attention on D-branes located at toric singularities, and we will use the language of dimer models to encode the relevant properties of the resulting theory in the world volume of the brane.

This chapter uses heavily dimer model ideas, the reader unfamiliar with them is advised to read Appendix C for a short introduction to the relevant background material, and a list of references. Appendix B might also be interesting for some background in toric geometry, although we will not use toric geometry explicitly in this chapter.

We will consider the class of fractional branes called *DSB* in the classification of [79], namely brane configurations that develop a non-perturbative Affleck-Dine-Seiberg type superpotential in the infrared, removing the classical supersymmetric vacua and giving rise to runaway dibaryonic directions. We will see how, upon the addition of an appropriate number of light enough massive flavours, these kinds of theories generically develop ISS-like metastable vacua.

We will not prove this result in full generality for this class of branes, but we will do so for some interesting infinite families of geometries, suggesting that the result is fully general. We will also develop general tools that simplify the analysis enormously, rendering the check for existence or nonexistence of metastable vacua in any particular example a simple task.

The connection between metastable vacua and DSB branes was originally hinted at in [68], where the dP_1 case was studied. The generalization to the much wider class of DSB branes described in this chapter was done in [43], which we will follow here.

An important caveat of the construction described here is that often there are fields in the world volume of the brane with are decoupled at tree level from the rest (for instance Z_{12} in the dP_1 case discussed in Section 4.2). This means in particular that they are pseudomoduli, and cannot be lifted at one-loop since they lack tree level couplings to the sector breaking susy. They will certainly couple at higher orders, but going to higher than one-loop in our construction becomes much more demanding technically, mainly due to the fact that gauge dynamics in the magnetic dual start playing an important role. The fate of these (pseudo-)flat directions at higher loop orders remains unknown as of this writing.

The plan for this chapter is as follows. We will start in Section 4.1 by revisiting the stabilization of the pseudomoduli in the ISS case in the Feynman diagram language, introducing the technical tools we will need along the way. In order to get a taste for the complications one faces in general, in Section 4.2 we will apply these tools to one of the simplest geometries of interest, the complex cone over dP_1. We will use the lessons learned in the dP_1 case in Section 4.3, where we will describe how the analysis goes for any arbitrary toric singularity. We illustrate these considerations in a number of interesting classes of singularities in Section 4.4.

4.1 The ISS model revisited

Let us revisit the ISS model described in Appendix A in a language slightly different from the usual one. We will be particularly interested in the one-loop masses of the classically massless fields, the so-called pseudo-Goldstones. These one-loop corrections are traditionally computed using the Coleman-Weinberg potential, as described in Section A.2. The Coleman-Weinberg formula gives the complete one-loop scalar potential for the theory for any arbitrary vev (so we can obtain the mass for any field by taking the second derivative with respect to that field). This technique, although elegant and powerful, is rather complicated for the rather involved quiver theories we are interested in. In general it requires the diagonalization of an arbitrary $N \times N$ mass matrix, something which cannot be done analytically.

We are just interested in the one-loop correction to the pseudomoduli masses around a particular ansatz for our fields, so we do not need the full power of the Coleman-Weinberg formula. We will find that a more straightforward approach based on the computation of Feynman diagrams does the job nicely, and allows us to obtain simple analytic expressions for the pseudomoduli masses. If these masses are positive, this will imply that the vacuum ansatz we have chosen is correct.

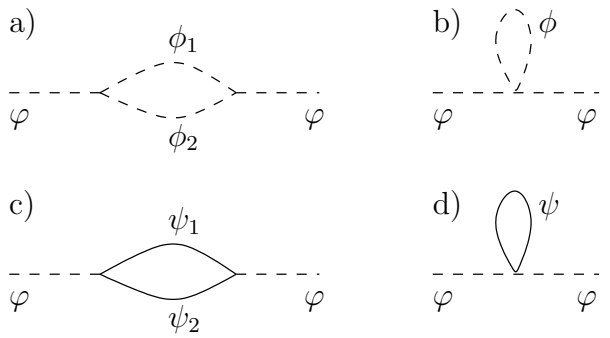

Figure 4.1: Feynman diagrams contributing to the one-loop two point function. The dashed line denotes bosons and the solid one fermions.

4.1.1 Basic amplitudes

Let us start with a quick discussion of the basic building blocks for all amplitudes we will calculate in the rest of this chapter. Here we will be just listing for future reference the results of some easy one-loop Feynman diagram computations, so the reader uninterested in the detailed form of the expressions is advised to jump to Section 4.1.3, where we illustrate the use of these results, coming back as desired to this section for the origin of the formulas quoted there.

We are interested in computing two point functions for the pseudomoduli at one loop, and in Section 4.1.4 also tadpole diagrams. There are just a few kinds of diagrams entering in the calculation, which we will present now for the two-point function, see Figure 4.1. The (real) bosonic fields are denoted by ϕ_i and the (Weyl) fermions by ψ_i. The pseudomodulus we are interested in is denoted by φ.

Bosonic contributions

These come from two terms in the Lagrangian. First there is a diagram coming from terms of the form (Figure 4.1b):

$$\mathcal{L} = \ldots + \lambda\varphi^2\phi^2 - \frac{1}{2}m^2\phi^2, \tag{4.1}$$

giving an amplitude (we will be using dimensional regularization)

$$i\mathcal{M} = \frac{-2i\lambda}{(4\pi)^2}m^2\left(\frac{1}{\epsilon} - \gamma + 1 + \log 4\pi - \log m^2\right). \tag{4.2}$$

The other contribution comes from the diagram in Figure 4.1a:

$$\mathcal{L} = \ldots + \lambda\varphi\phi_1\phi_2 - \frac{1}{2}m_1^2\phi_1^2 - \frac{1}{2}m_2^2\phi_2^2, \tag{4.3}$$

which contributes to the two point function with an amplitude:

$$i\mathcal{M} = \frac{i\lambda^2}{(4\pi)^2}\left(\frac{1}{\epsilon} - \gamma + \log 4\pi - \int_0^1 dx \log \Delta\right), \tag{4.4}$$

where here and in the following we denote $\Delta \equiv x m_1^2 + (1-x)m_2^2$.

Fermionic contributions

The relevant vertices here are again of two possible kinds, one of which is nonrenormalizable. The cubic interaction comes from terms in the Lagrangian given by the diagram in Figure 4.1c:

$$\mathcal{L} = \ldots + \varphi(a\psi_1\psi_2 + a^*\bar{\psi}_1\bar{\psi}_2) + \frac{1}{2}m_1(\psi_1^2 + \bar{\psi}_1^2) + \frac{1}{2}m_2(\psi_2^2 + \bar{\psi}_2^2). \tag{4.5}$$

We are assuming real masses for the fermions here, in the configurations we study this can always be achieved by an appropriate field redefinition. The contribution from such vertices is given by:

$$\begin{aligned} i\mathcal{M} \;=\; & \int_0^1 dx \left\{ \frac{-2im_1m_2}{(4\pi)^2}(a^2 + (a^2)^*)\left(\frac{1}{\epsilon} - \gamma + \log 4\pi - \log\Delta\right)\right. \\ & \left. - \frac{8i|a|^2}{(4\pi)^2}\Delta\left(\frac{1}{\epsilon} - \gamma + \log 4\pi + \frac{1}{2} - \log\Delta\right)\right\}. \end{aligned} \tag{4.6}$$

The other fermionic contribution, which one does not need as long as one is dealing with renormalizable interactions only (but which we will need soon when analyzing the pseudomodulus θ), is given by terms in the Lagrangian of the form (Figure 4.1d):

$$\mathcal{L} = \ldots + \lambda\varphi^2(\psi^2 + \bar{\psi}^2) + \frac{1}{2}m(\psi^2 + \bar{\psi}^2), \tag{4.7}$$

which contributes to the total amplitude with:

$$i\mathcal{M} = \frac{8\lambda m i}{(4\pi)^2}m^2\left(\frac{1}{\epsilon} - \gamma + 1 + \log 4\pi - \log m^2\right). \tag{4.8}$$

4.1.2 The basic superpotentials

The amplitudes in the previous section are the basic ingredients entering the computation, but in general the number of diagrams contributing to the two point amplitudes is quite big, so calculating all the contributions by hand can get quite involved in particular examples[1]. Happily, one finds that complicated models (such as dP_1 or dP_2, studied later on in this chapter) reduce to performing the analysis for only two different superpotentials, which we analyze in this section.

[1]The authors wrote the computer program in `http://cern.ch/inaki/pm.tar.gz` which helped greatly in the process of computing the given amplitudes for the relevant models.

The symmetric case

We want to study in this section a superpotential of the form:

$$W = h(X\phi_1\phi_2 + \mu\phi_1\phi_3 + \mu\phi_2\phi_4 - \mu^2 X). \tag{4.9}$$

This model is a close cousin of the basic O'Raifeartaigh model. We are interested in the one loop contribution to the two point function of X, which is massless at tree level.

From the (F-term) bosonic potential one obtains the following terms entering the one loop computation:

$$\begin{aligned} V &= \left[|hX\phi_2|^2 + |h|^2\mu(X\phi_2\phi_3^* + X^*\phi_2^*\phi_3) + |h|^2\mu(X\phi_1\phi_4^* + X^*\phi_1^*\phi_4)\right] \\ &+ |h|^2\mu^2(\phi_1\phi_2 + \phi_1^*\phi_2^*) + \sum_{i=1}^{4}|h|^2\mu^2|\phi_i|^2 \end{aligned} \tag{4.10}$$

In order to do the computation it is useful to diagonalize the mass matrix by introducing ϕ_+ and ϕ_- such that:

$$\phi_1 = \frac{1}{\sqrt{2}}(\phi_+ + i\phi_-) \qquad \phi_2 = \frac{1}{\sqrt{2}}(\phi_+ - i\phi_-) \tag{4.11}$$

and ϕ_a, ϕ_b such that:

$$\phi_3^* = \frac{1}{\sqrt{2}}(\phi_a + i\phi_b) \qquad \phi_4^* = \frac{1}{\sqrt{2}}(\phi_a - i\phi_b). \tag{4.12}$$

With these redefinitions the bosonic scalar potential decouples into identical ϕ_+ and ϕ_- sectors, giving two decoupled copies of:

$$\begin{aligned} V &= |h|^2|X|^2|\phi_+|^2 + |h|^2\mu^2(|\phi_+|^2 + |\phi_a|^2) \\ &\quad + |h|^2\mu(X\phi_+\phi_a + X^*\phi_+^*\phi_a^*) - \frac{|h|^2\mu^2}{2}\left(\phi_+^2 + (\phi_+^2)^*\right). \end{aligned} \tag{4.13}$$

Calculating the amplitude consists simply of constructing the (very few) two point diagrams from the potential above and plugging the formulas above for each diagram (the fermionic part is even simpler in this case). The final answer is that in this model the one loop correction to the mass squared of X is given by:

$$\delta m_X^2 = \frac{|h^4|\mu^2}{8\pi^2}(\log 4 - 1). \tag{4.14}$$

The generalized asymmetric case

The next case is slightly more complicated, but will suffice to analyze completely all the models we encounter. We will be interested in the one loop

contribution to the mass of the pseudomoduli Y in a theory with superpotential:

$$W = h(X\phi_1\phi_2 + \mu\phi_1\phi_3 + \mu\phi_2\phi_4 - \mu^2 X) + k(rY\phi_1\phi_5 + \mu\phi_5\phi_7), \quad (4.15)$$

with k and r arbitrary complex numbers. The procedure is straightforward as above, so we will just quote the result. We obtain an amplitude given by:

$$i\mathcal{M} = \frac{-i}{(4\pi)^2}|h^2 r\mu|^2 \mathcal{C}\left(\frac{|k|^2}{|h|^2}\right), \quad (4.16)$$

where we have defined $\mathcal{C}(t)$ as:

$$\mathcal{C}(t) = \frac{t}{2-t}\left(\log 4 - \frac{t}{t-1}\log t\right). \quad (4.17)$$

Note that this is a positive definite function, meaning that the one loop correction to the mass is always positive, and the pseudomoduli get stabilized for any (nonzero) value of the parameters. Also note that the limit of vanishing t with $|r|^2 t$ fixed (i.e., vanishing masses for ϕ_5 and ϕ_7, but nonvanishing coupling of Y to the supersymmetry breaking sector) gives a nonvanishing contribution to the mass of Y.

4.1.3 The ISS metastable minimum

Armed with the results found in the previous section, let us come back to the ISS case, and try to compute the masses of the pseudomoduli using Feynman diagram techniques. The strategy to apply is the same in this example as in the general case, and consists of the following:

- First we choose an ansatz for the classical minimum to become the one-loop vacuum. It is natural to propose a point of maximal enhanced symmetry. In particular, close to the origin in the space of vevs for M there exist an R-symmetry, whose breaking by gauge interactions (via anomalies) is negligible in that region. The connection between unbroken R-symmetry and susy breaking is well known [80]. Hence the natural candidate for the one-loop minimum is

$$q = \tilde{q}^{\mathrm{T}} = \begin{pmatrix} \mu \\ 0 \end{pmatrix}, \quad (4.18)$$

  with the rest of the fields set to 0. This initial ansatz for the one-loop minimum is eventually confirmed by the positive square masses at one-loop found in the computations described below. In our more general discussion of meta-stable minima in runaway quiver gauge theories, our ansatz for the one-loop minimum is a direct generalization of the above (and is similarly eventually confirmed by the one-loop mass computation).

- Then we expand the field linearly around this vacuum, and identify the set of classically massless fields. We refer to these as pseudomoduli (with some abuse of language, since there could be massless fields which are not classically flat directions due to higher potential terms)
- As a final step we compute one-loop masses for these pseudomoduli by evaluating their two-point functions via conventional Feynman diagrams, as explained in detail in Section 4.1.1

In the particular case of the ISS model, we expand around the ansatz 4.18 in the following way:

$$q = \begin{pmatrix} \mu + \frac{1}{\sqrt{2}}(\xi_+ + \xi_-) \\ \frac{1}{\sqrt{2}}(\rho_+ + \rho_-) \end{pmatrix}, \quad \tilde{q}^{\mathrm{T}} = \begin{pmatrix} \mu + \frac{1}{\sqrt{2}}(\xi_+ - \xi_-) \\ \frac{1}{\sqrt{2}}(\rho_+ - \rho_-) \end{pmatrix}, \quad M = \begin{pmatrix} Y & Z \\ \tilde{Z}^{\mathrm{T}} & \Phi \end{pmatrix}, \tag{4.19}$$

where we have taken linear combinations of the fields in such a way that the bosonic mass matrix is diagonal. This will also be convenient in Section 4.1.4, where we discuss the Goldstone bosons in greater detail.

We now expand the ISS magnetic superpotential

$$W_{\text{magnetic}} = h\,(\mathrm{Tr}\,\tilde{q}Mq - \mu^2 \mathrm{Tr}\,M) \tag{4.20}$$

in terms of these fluctuations in order to obtain

$$\begin{aligned} W &= \sqrt{2}\mu\xi_+ Y + \frac{1}{\sqrt{2}}\mu Z\rho_+ + \frac{1}{\sqrt{2}}\mu Z\rho_- + \frac{1}{\sqrt{2}}\mu\rho_+\tilde{Z} - \frac{1}{\sqrt{2}}\mu\rho_-\tilde{Z} \\ &\quad + \frac{1}{2}\rho_+^2\Phi - \frac{1}{2}\rho_-^2\Phi - \mu^2\Phi + \dots, \end{aligned} \tag{4.21}$$

where we have not displayed terms of order three or higher in the fluctuations, unless they contain Φ, since they do not enter the one loop computation we will perform. Note also that we have set $h = 1$ and we have removed the trace (the matricial structure is easy to restore later on, here we restrict to the simplest case). The massless bosonic fluctuations are given by $\mathrm{Re}\,\rho_+$, $\mathrm{Im}\,\rho_-$, Φ and ξ_-. The first two together with $\mathrm{Im}\,\xi_-$ are Goldstone bosons, as explained in Section 4.1.4. Thus the pseudomoduli we are interested in are given by Φ and $\mathrm{Re}\,\xi_-$. Let us focus on Φ (the case of $\mathrm{Re}\,\xi_-$ admits a similar discussion). In this case the relevant terms in the superpotential simplify further, and just the following superpotential contributes:

$$W = \mu Z\frac{1}{\sqrt{2}}(\rho_+ + \rho_-) + \mu\tilde{Z}\frac{1}{\sqrt{2}}(\rho_+ - \rho_-) + \frac{1}{2}\rho_+^2\Phi - \frac{1}{2}\rho_-^2\Phi - \mu^2\Phi$$

which we recognize, up to a field redefinition, as the symmetric model of Section 4.1.2. We can thus directly read the result

$$\delta m_\Phi^2 = \frac{|h|^4\mu^2}{8\pi^2}(\log 4 - 1). \tag{4.22}$$

This matches the value given in [41], which was found using the Coleman-Weinberg potential.

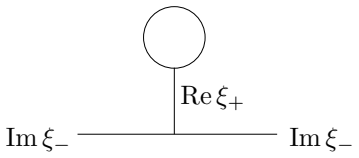

Figure 4.2: Schematic tadpole contribution to the $\mathrm{Im}\,\xi_-$ two point function. Both bosons and fermions run in the loop.

4.1.4 Goldstone bosons

One aspect of our technique that merits some additional explanation concerns the Goldstone bosons. The one-loop computation of the masses for the fluctuations associated to the symmetries broken by the vacuum, using just the interactions described in Section 4.1.1, leads to a non-vanishing result. This puzzle is however easily solved by realizing that certain (classically massive) fields have a one-loop tadpole. This leads to a new contribution to the one-loop Goldstone two-point amplitude, given by the diagram in Figure 4.2. Adding this contribution the total one-loop mass for the Goldstone bosons is indeed vanishing, as expected. This tadpole does not affect the computation of the one-loop pseudomoduli masses (except for $\mathrm{Re}\,\xi_+$, but its mass remains positive) as it is straightforward to check.

The structure of this cancellation can be understood by recalling the derivation of the Goldstone theorem for the 1PI effective potential, as we now discuss. The proof can be found in slightly more detail, together with other proofs, in [2]. Let us denote by V the 1PI effective potential. Invariance of the action under a given symmetry implies that

$$\frac{\delta V}{\delta \phi_i}\Delta\phi_i = 0, \tag{4.23}$$

where we denote by $\Delta\phi_i$ the variation of the field ϕ_i under the symmetry, which will in general be a function of all the fields in the theory. Taking the derivative of this equation with respect to some other field ϕ_k

$$\frac{\delta^2 V}{\delta\phi_i\delta\phi_k}\Delta\phi_i + \frac{\delta V}{\delta\phi_i}\cdot\frac{\delta\Delta\phi_i}{\delta\phi_k} = 0. \tag{4.24}$$

Let us consider how this applies to our case. At tree level, there is no tadpole and the above equation (truncated at tree level) states that for each symmetry generator broken by the vacuum, the value of $\Delta\phi_i$ gives a nonvanishing eigenvector of the mass matrix with zero eigenvalue. This is the classical version of the Goldstone theorem, which allows the identification of the Goldstone bosons of the theory.

For instance, in the ISS model in the previous section (for $N_f = 2$), there are three global symmetry generators broken at the minimum described

around (4.18). The $SU(2) \times U(1)$ symmetry of the potential gets broken down to a $U(1)'$, which can be understood as a combination of the original $U(1)$ and the t_z generator of $SU(2)$. The Goldstone bosons can be taken to be the ones associated to the three generators of $SU(2)$, and correspond (for μ real) to $\mathrm{Im}\,\xi_-$, $\mathrm{Im}\,\rho_-$ and $\mathrm{Re}\,\rho_+$, in the parametrization of the fields given by equation (4.19).

Even in the absence of tree-level tadpoles, there could still be a one-loop tadpole. When this happens, there should also be a non-trivial contribution to the mass term for the Goldstone bosons in the one-loop 1PI potential, related to the tadpole by the one-loop version of (4.24). This relation guarantees that the mass term in the physical (i.e. Wilsonian) effective potential, which includes the 1PI contribution, plus those of the diagram in Figure 4.2, vanishes, as we described above.

In fact, in the ISS example, there is a non-vanishing one-loop tadpole for the real part of ξ_+ (and no tadpole for other fields). The calculation of the tadpole at one loop is straightforward, and we will only present here the result

$$i\mathcal{M} = \frac{-i|h|^4\mu^3}{(4\pi)^2}(2\log 2). \tag{4.25}$$

The 1PI one-loop contribution to the Goldstone boson mass is also simple to calculate, giving the result

$$i\mathcal{M} = \frac{-i|h|^4\mu^2}{(4\pi)^2}(\log 2). \tag{4.26}$$

Using the variations of the relevant fields under the symmetry generator, e.g. for t_z,

$$\Delta\mathrm{Re}\,\xi_+ = -\mathrm{Im}\,\xi_- \tag{4.27}$$

$$\Delta\mathrm{Im}\,\xi_- = \mathrm{Re}\,\xi_+ + 2\mu. \tag{4.28}$$

we find that the (4.24) is satisfied at one-loop.

$$\left\langle \frac{\delta^2 V}{\delta\phi_i\delta\phi_k}\Delta\phi_i + \frac{\delta V}{\delta\phi_i}\cdot\frac{\delta\Delta\phi_i}{\delta\phi_k} \right\rangle = m^2_{\mathrm{Im}\,\xi_-}\cdot 2\mu + (\mathrm{Re}\,\xi_+\text{tadpole})\cdot(-1) = 0. \tag{4.29}$$

A very similar discussion applies to t_x and t_y.

The above discussion of Goldstone bosons can be similarly carried out in all examples we discuss. Hence, it will be enough to carry out the computation of the 1PI diagrams discussed in Section 4.1.1, and verify that they lead to positive squared masses for all classically massless fields (with Goldstone bosons rendered massless by the additional diagrams involving the tadpole).

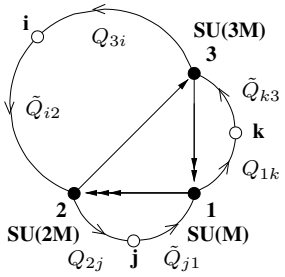

Figure 4.3: Extended quiver diagram for a dP_1 theory with flavors, from [68].

The general lesson

We can extract a general lesson from the analysis of the ISS case we just did. We have already described it, but let us emphasize them here once more in a condensed version since it constitutes the backbone of the more complicated analysis we will attempt in the following sections.

It is the following: Computing the one-loop correction to the pseudomoduli masses around some ansatz for the real quantum vacuum in pseudomoduli space (which we choose in analogy to the ISS case, and needs to be justified by getting positive masses for the pseudomoduli) reduces to some very simple Feynman diagram gymnastics, which can furthermore be quite systematized. In the end, one can construct the two-point function (the mass term) from the elementary building blocks in Section 4.1.2.

In the rest of this chapter we will see how this idea works in a wide variety of configurations of DSB branes in toric singularities.

4.2 A case study: dP_1

One of the simplest geometries with fractional branes of the DSB kind is the complex cone of dP_1, which we study in this section. This case was already studied in detail in [68]. We will redo the analysis in that paper with our new tools, and reproduce their results. In fact, we will be able to do better and provide nice analytic expressions for the masses as functions of the parameters in the gauge theory Lagrangian. This analysis was done numerically in some directions in parameter space in [68], our analytic results match the numeric results in that paper.

The quiver for the theory we wish to study is shown in Figure 4.3. It is given by the usual dP_1 quiver with ranks $(0, M, 2M, 3M)$ for the nodes (the rank assignment is for M fractional branes), and the addition of $N_{f,1}$ flavor nodes coming from noncompact D7 branes coming near the singularity, as described in Appendix C.4.

The superpotential for this theory is the one for dP_1 plus some cubic

couplings to the flavors, in detail:

$$\begin{aligned} W &= \lambda(X_{23}X_{31}Y_{12} - X_{23}Y_{31}X_{12}) \\ &+ \lambda'(Q_{3i}\tilde{Q}_{i2}X_{23} + Q_{2j}\tilde{Q}_{j1}X_{12} + Q_{1k}\tilde{Q}_{k3}X_{31}) \\ &+ m_3 Q_{3i}\tilde{Q}_{k3}\delta_{ik} + m_2 Q_{2j}\tilde{Q}_{i2}\delta_{ji} + m_1 Q_{1k}\tilde{Q}_{j1}\delta_{kj}, \end{aligned} \tag{4.30}$$

where the subindices denote the groups under which the field is charged. The first line is the superpotential of the theory of fractional brane, the second line describes 77-73-37 couplings between the flavor branes and the fractional brane, and the last line gives the flavor masses. Note that there is a massless field, denoted Z_{12} in [68], that does not appear in the superpotential. This is one of the decoupled fields mentioned in the introduction to this chapter.

We are interested in gauge factors in the free magnetic phase. This is the case for the $SU(3M)$ gauge factor in the regime

$$M + 1 \leq N_{f,1} < \frac{5}{2}M. \tag{4.31}$$

To apply Seiberg duality on node 3, we introduce the dual mesons:

$$\begin{array}{rclcrcl} M_{21} &=& \frac{1}{\Lambda}X_{23}X_{31} & ; & N_{k1} &=& \frac{1}{\Lambda}\tilde{Q}_{k3}X_{31} \\ M'_{21} &=& \frac{1}{\Lambda}X_{23}Y_{31} & ; & N'_{k1} &=& \frac{1}{\Lambda}\tilde{Q}_{k3}Y_{31} \\ N_{2i} &=& \frac{1}{\Lambda}X_{23}Q_{3i} & ; & \Phi_{ki} &=& \frac{1}{\Lambda}\tilde{Q}_{k3}Q_{3i} \end{array} \tag{4.32}$$

and we also replace the electric quarks Q_{3i}, $\tilde{Q}_{k3}$, X_{23}, X_{31}, Y_{31} by their magnetic duals $\tilde{Q}_{i3}$, Q_{3k}, X_{32}, X_{13}, Y_{13}. The magnetic superpotential is given by rewriting the confined fields in terms of the mesons and adding the coupling between the mesons and the dual quarks,

$$\begin{aligned} W &= h\,(\,M_{21}X_{13}X_{32} + M'_{21}Y_{13}X_{32} + N_{2i}\tilde{Q}_{i3}X_{32} \\ &+ N_{k1}X_{13}Q_{3k} + N'_{k1}Y_{13}Q_{3k} + \Phi_{ki}\tilde{Q}_{i3}Q_{3k}\,) \\ &+ h\mu_0\,(\,M_{21}Y_{12} - M'_{21}X_{12}\,) + \mu'\,Q_{1k}N_{k1} + \mu'\,N_{2i}\tilde{Q}_{i2} \\ &- h\mu^2 \mathrm{Tr}\,\Phi + \lambda'\,Q_{2j}\tilde{Q}_{j1}X_{12} + m_2 Q_{2i}\tilde{Q}_{i2} + m_1 Q_{1i}\tilde{Q}_{i1}. \end{aligned} \tag{4.33}$$

This is the theory we want to study. In order to simplify the treatment of this example we will disregard any subleading terms in m_i/μ', and effectively integrate out N_{k1} and N_{2i} by substituting them by 0. This is not necessary, and indeed the computations in the next sections for more complicated theories will be exact. We do it here in order to compare results with [68].

As in the ISS model, this theory breaks supersymmetry via the rank condition. The fields $\tilde{Q}_{i3}$, Q_{3k} and Φ_{ki} are the analogs of q, $\tilde{q}$ and M in the ISS case discussed above. This motivates a vacuum ansatz analogous to the

one in equation (4.18), giving rise to the following linear expansion:

$$\begin{array}{ccccc}
\Phi = \begin{pmatrix} \phi_{00} & \phi_{01} \\ \phi_{10} & \phi_{11} \end{pmatrix} & ; & \tilde{Q}_{i3} = \begin{pmatrix} \mu e^{\theta} + Q_{3,1} \\ \tilde{Q}_{3,2} \end{pmatrix} & ; & Q_{3i}^{\mathrm{T}} = \begin{pmatrix} \mu e^{-\theta} + Q_{3,1} \\ Q_{3,2} \end{pmatrix} \\
\tilde{Q}_{k1} = \begin{pmatrix} \tilde{Q}_{1,1} \\ y \end{pmatrix} & ; & Q_{2j} = \begin{pmatrix} Q_{2,11} & x \\ Q_{2,21} & x' \end{pmatrix} & ; & M_{21} = \begin{pmatrix} M_{21,1} \\ M_{21,2} \end{pmatrix} \\
Y_{13} = (Y_{13}) & ; & X_{12}^{\mathrm{T}} = \begin{pmatrix} X_{12,1} \\ X_{12,2} \end{pmatrix} & ; & X_{32}^{\mathrm{T}} = \begin{pmatrix} X_{32,1} \\ X_{32,2} \end{pmatrix} \\
Y_{12}^{\mathrm{T}} = \begin{pmatrix} Y_{12,1} \\ Y_{12,2} \end{pmatrix} & ; & N'_{k1} = \begin{pmatrix} N'_{k1,1} \\ z \end{pmatrix} & ; & M'_{21} = \frac{\lambda'}{h\mu_0} \begin{pmatrix} M'_{21,1} \\ M'_{21,2} \end{pmatrix} \\
 & & X_{13} = (X_{13})\,. & &
\end{array} \tag{4.34}$$

Note that we have chosen to introduce the nonlinear expansion in θ in order to reproduce the results found in the literature in their exact form[2]. Note also that for the sake of clarity we have not been explicit about the ranks of the different matrices. They can be easily worked out (or for this case, looked up in [68]), and we will restrict ourselves to the 2 flavor case where the matrix structure is trivial. As a last remark, we are not being explicit either about the definitions of the different couplings in terms of the electric theory. This can be done easily (and as in the ISS case they involve an unknown coefficient in the Kähler potential), but in any event, the existence of the meta-stable vacua can be established for general values of the coefficients in the superpotential. Hence we skip this more detailed but not very relevant discussion.

The next step consists in expanding the superpotential and identifying the massless fields. We get the following quadratic contributions to the superpotential:

$$\begin{aligned}
W_{\mathrm{mass}} &= 2h\mu\phi_{00}\tilde{Q}_{3,1} + h\mu\phi_{01}\tilde{Q}_{3,2} + h\mu\phi_{10}Q_{3,2} \\
&+ h\mu_0 M_{21,1}Y_{12,1} + h\mu_0 M_{21,2}Y_{12,2} - \lambda' M'_{21,1}X_{12,1} - \lambda' M'_{21,2}X_{12,2} \\
&+ h\mu N'_{k1,1}Y_{13} - h_1\mu\tilde{Q}_{1,1}X_{13} - h_2\mu Q_{2,11}X_{32,1} - h_2\mu Q_{2,21}X_{32,2}.
\end{aligned}$$

The fields massless at tree level are x, x', y, z, ϕ_{11}, θ, $Q_{3,2}$ and $\tilde{Q}_{3,2}$. Three of these are Goldstone bosons as described in the previous section. For real μ they are $\mathrm{Im}\,\theta$, $\mathrm{Re}\,(\tilde{Q}_{3,2}+Q_{3,2})$ and $\mathrm{Im}\,(\tilde{Q}_{3,2}-Q_{3,2})$. We now show that all other classically massless fields get masses at one loop (with positive squared masses).

As a first step towards finding the one-loop correction, notice that the supersymmetry breaking mechanism is extremely similar to the one in the ISS model before, in particular it comes only from the following couplings in the superpotential:

$$W_{\mathrm{rank}} = hQ_{3,2}\tilde{Q}_{3,2}\phi_{11} - h\mu^2\phi_{11} + \ldots \tag{4.35}$$

[2]A linear expansion would lead to identical conclusions concerning the existence of the meta-stable vacua, but to one-loop masses not directly amenable to comparison with results in the literature.

This breaks the spectrum degeneracy in the multiplets $Q_{3,2}$ and $\tilde{Q}_{3,2}$ at tree level, so we refer to them as the fields with broken supersymmetry.

Let us compute now the correction for the mass of x, for example. For the one-loop computation we just need the cubic terms involving one pseudomodulus and at least one of the broken supersymmetry fields, and any quadratic term involving fields present in the previous set of couplings. From the complete expansion one finds the following supersymmetry breaking sector:

$$W_{\text{symm.}} = h\phi_{11}Q_{3,2}\tilde{Q}_{3,2} + h\mu\phi_{01}\tilde{Q}_{3,2} + h\mu\phi_{10}Q_{3,2} - h\mu^2\phi_{11}. \tag{4.36}$$

The only cubic term involving the pseudomodulus x and the broken supersymmetry fields is

$$W_{\text{cubic}} = -h_2\, x\, \tilde{Q}_{3,2}X_{32,1}, \tag{4.37}$$

and there is a quadratic term involving the field $X_{32,1}$

$$W_{\text{mass coupling}} = -h_2\mu Q_{2,11}X_{32,1}. \tag{4.38}$$

Assembling the three previous equations, the resulting superpotential corresponds to the *asymmetric* model in Section 4.1.2, so we can directly obtain the one-loop mass for x:

$$\delta m_x^2 = \frac{1}{16\pi^2}|h|^4\mu^2\mathcal{C}\left(\frac{|h_2|^2}{|h|^2}\right). \tag{4.39}$$

Proceeding in a similar way, the one-loop masses for ϕ_{11}, x', y and z are:

$$\begin{aligned}
\delta m_{\phi_{11}}^2 &= \frac{1}{8\pi^2}|h|^4\mu^2(\log 4 - 1) \\
\delta m_{x'}^2 &= \frac{1}{16\pi^2}|h|^4\mu^2\mathcal{C}\left(\frac{|h_2|^2}{|h|^2}\right), \\
\delta m_y^2 &= \frac{1}{16\pi^2}|h|^4\mu^2\mathcal{C}\left(\frac{|h_1|^2}{|h|^2}\right) \\
\delta m_z^2 &= \frac{1}{16\pi^2}|h|^4\mu^2(\log 4 - 1).
\end{aligned} \tag{4.40}$$

There is just one pseudomodulus left, $\operatorname{Re}\theta$, which is qualitatively different to the others. With similar reasoning, one concludes that it is necessary to study a superpotential of the form

$$W = h(X\phi_1\phi_2 + \mu e^{\theta}\phi_1\phi_3 + \mu e^{-\theta}\phi_2\phi_4 - \mu^2 X). \tag{4.41}$$

Due to the non-linear parametrization, the expansion in θ shows that there is a term quadratic in θ which contributes to the one-loop mass via a vertex with two bosons and two fermions, the relevant diagram is shown in Figure 4.1d. The result is a vanishing mass for $\operatorname{Im}\theta$, as expected for a Goldstone

boson (the one-loop tadpole vanishes in this case), and a non-vanishing mass for $\mathrm{Re}\,\theta$

$$\delta m^2_{\mathrm{Re}\,\theta} = \frac{1}{4\pi^2}|h|^4\mu^4(\log 4 - 1). \tag{4.42}$$

We conclude by mentioning that all squared masses are positive, thus confirming that the proposed point in field space is the one-loop minimum. As shown in [68], this minimum is parametrically long-lived against tunneling to the runaway regime.

Summary

Let us restate the main points of what we have just found, since the main features of the dP_1 case will be shared by all cases we will discuss below. When one takes the theory of (fractional DSB) D3 branes located at a dP_1 singularity, and adds massive flavors with specific couplings, one finds that the theory has a non supersymmetric metastable minimum, with the caveat that there is a pseudomoduli Z_{12} whose fate is unknown. Since apparently nothing protects its mass when supersymmetry is broken, one expects it to develop a nonzero value when higher order corrections are taken into account, but there is always the possibility of getting a tachyonic mass, which would mean that the vacuum is unstable against decay into some other vacuum (perhaps at infinity). Assuming that the correction is positive and nonzero, then this theory provides us with a simple way to build interesting vacua for gauge mediated supersymmetry breaking in terms of string theory. We will apply these ideas in a particular example in Chapter 7.

A couple of important points were not discussed above, but they are worth mentioning. First, it is possible to estimate the decay probability for the metastable configuration using semi classical methods, one gets that it is possible to have the metastable vacuum arbitrary stable by tuning the parameters of the original superpotential.

The second point concerns the large field behavior of the dP_1 theory. One can analyze it in the same way as we did it for ISS, and one finds that there is a runaway towards infinity in field space.

Detailed discussion of both points can be found in the original literature [41, 68].

4.3 The general case

In the previous section we showed how to argue for the existence of metastable vacua on configurations of DSB fractional branes in the particular case of the complex cone over dP_1, once light massive flavors are included. In this section we generalize the arguments for general DSB branes. We will show how to add D7–branes in a specific manner so as to generate the appropriate

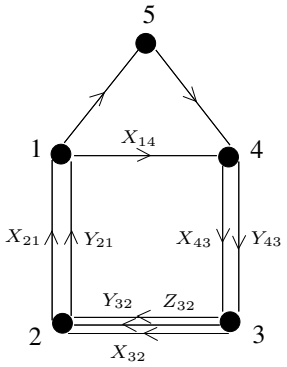

Figure 4.4: Quiver diagram used to illustrate general results. It does not correspond to any geometry in particular.

cubic flavor couplings and mass terms. Once this is achieved, we describe the structure of the Seiberg dual theory.

The results of our analysis show that, with the specified configuration of D7–branes, the determination of metastability is greatly simplified and only involves looking at the original superpotential. Thus, although we do not prove that DSB branes on arbitrary singularities generate metastable vacua, we show how one can determine the existence of metastability in a very simple and systematic manner.

The discussion in this section is perhaps a bit too technical, so in order to make it slightly more palatable have chosen to sketch the main point first in Section 4.3.1, leaving the details for Section 4.3.2. Examples of how can apply these ideas to specific examples can be found in Section 4.4.

4.3.1 A general argument

Construction of the flavored theories

Consider a general quiver gauge theory arising from branes at singularities. As we have argued previously, we focus on DSB branes, so that there is a gauge factor satisfying $N_{f,0} < N_c$, which can lead to supersymmetry breaking by the rank condition in its Seiberg dual, as argued in [68]. To make the general analysis more concrete, let us consider a quiver like that in Figure 4.4. We will also assume that the gauge factor to be dualized corresponds to node 2. This system does not correspond to any particular geometry, we choose to study it just because it illustrates the general structure nicely. In what follows we analyze the structure of the fields and couplings in the Seiberg dual, and reduce the problem of studying the metastability of the theory with flavors to analyzing the structure of the theory in the absence of flavors.

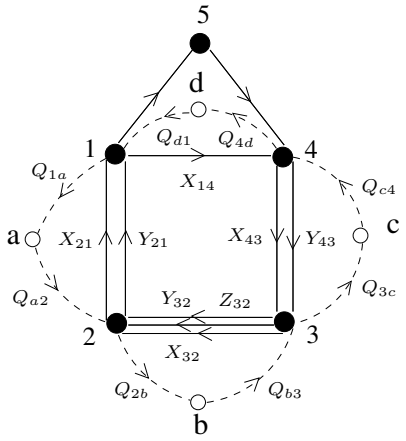

Figure 4.5: Quiver diagram with flavors. White nodes denote flavor groups.

Let us introduce flavors in this picture. As discussed originally in [68] and reviewed in Appendix C.4, we can introduce a supersymmetric D7-brane for each bifundamental X_{ab} in the quiver theory. This D7 acts as a flavor group, and the massless strings from the D7 to the D3 are the flavored quarks Q_{bi}, $\tilde{Q}_{ia}$, where the subindices denote under which groups the quarks transform. For example, Q_{bi} transforms in the fundamental of the gauge factor b and the antifundamental of the flavor group i living in the D7. We also have to include a cubic coupling $X_{ab}Q_{bi}\tilde{Q}_{ia}$ in the superpotential, coming from worldsheet instantons in the mirror type IIA picture, for example.

Let us choose to introduce the following specific set of D7 branes. Take a superpotential coupling of the D3-brane quiver gauge theory, involving fields charged under the node to be dualized (the node 2 in our example). This corresponds to a loop in the quiver. Let us choose, for instance, $X_{32}X_{21}X_{14}Y_{43}$ in Figure 4.4. For any bi-fundamental chiral multiplet in this coupling, we introduce a set of $N_{f,1}$ of the corresponding D7-brane. This leads to a set of flavors for the different gauge factors, in a way consistent with anomaly cancellation.

We show the resulting flavored quiver in Figure 4.5. We also have to include the cubic 73-33-37 couplings in the superpotential[3]

$$W_{flavor} = \lambda' \left(X_{32}Q_{2b}Q_{b3} + X_{21}Q_{1a}Q_{a2} + X_{14}Q_{4d}Q_{d1} + Y_{43}Q_{3c}Q_{c4} \right) \quad (4.43)$$

Finally, we introduce mass terms for all flavors of all involved gauge factors:

$$W_{mass} = m_2 Q_{a2}Q_{2b} + m_3 Q_{b3}Q_{3c} + m_4 Q_{c4}Q_{4d} + m_1 Q_{d1}Q_{1a} \quad (4.44)$$

[3]Here we assume the same prefactor for each coupling for simplicity, but the conclusions hold for arbitrary non-zero couplings.

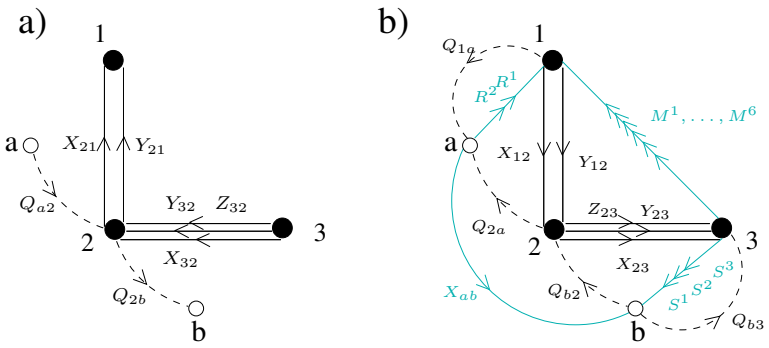

Figure 4.6: a) Relevant subquiver for Seiberg dualizing node 2. b) The Seiberg dual subquiver.

These mass terms break the flavor group into a diagonal subgroup. In the brane picture we have that the various D7 branes recombine into a single brane, which we pull away slightly from the singularity.

Seiberg duality and one-loop masses

Let us choose the number of D7 branes in such a way that node 2 is in the free magnetic phase. This allows us to study the infrared behaviour of the theory in a very simple way by going to the Seiberg dual theory, where gauge dynamics become unimportant in a first approximation (since the dual is infrared-free).

The relevant subquiver for the purposes of doing Seiberg duality is shown in Figure 4.6a, and its Seiberg dual in Figure 4.6b. The M's are mesons with indices in the gauge groups, R's and S's are mesons with only one index in the flavor group, and X_{ab} is a meson with both indices in the flavor groups. The original cubic superpotential and flavor mass superpotentials become

$$\begin{aligned} W_{flavor\,dual} &= \lambda' \left(S^1_{3b} Q_{b3} + R^1_{a1} Q_{1a} + X_{14} Q_{4d} Q_{d1} + Y_{43} Q_{3c} Q_{c4} \right) \\ W_{mass\,dual} &= m_2 \underline{X_{ab}} + m_3 Q_{b3} Q_{3c} + m_4 Q_{c4} Q_{4d} + m_1 Q_{d1} Q_{1a} \end{aligned}$$

In addition we have the extra meson superpotential

$$\begin{aligned} W_{mesons} &= h(\underline{X_{ab} \tilde{Q}_{b2} \tilde{Q}_{2a}} + R^1_{a1} \tilde{X}_{12} \tilde{Q}_{2a} + R^2_{a1} \tilde{Y}_{12} \tilde{Q}_{2a} + S^1_{3b} \tilde{Q}_{b2} \tilde{X}_{23} \\ &+ S^3_{3b} \tilde{Q}_{b2} \tilde{Z}_{23} + M^1_{31} \tilde{X}_{12} \tilde{X}_{23} + M^2_{31} \tilde{X}_{12} \tilde{Y}_{23} + M^3_{31} \tilde{X}_{12} \tilde{Z}_{23} \\ &+ S^2_{3b} \tilde{Q}_{b2} \tilde{Y}_{23} + M^4_{31} \tilde{Y}_{12} \tilde{X}_{23} + M^5_{31} \tilde{Y}_{12} \tilde{Y}_{23} + M^6_{31} \tilde{Y}_{12} \tilde{Z}_{23}). \end{aligned}$$

The crucial point is that we always obtain terms of the kind underlined above, namely a piece of the superpotential reading $m_2 X_{ab} + h X_{ab} \tilde{Q}_{b2} \tilde{Q}_{2a}$. This leads to tree level supersymmetry breaking by the rank condition, as

announced. Moreover the superpotential fits in the structure of the generalized asymmetric O'Raifeartaigh model studied in Section 4.1.2, with X_{ab}, $\tilde{Q}_{b2}$, $\tilde{Q}_{2a}$ corresponding to X, ϕ_1, ϕ_2 respectively. The multiplets $\tilde{Q}_{b2}$ and $\tilde{Q}_{2a}$ are split at tree level, and X_{ab} is massive at 1-loop. From our study of the generalized asymmetric case, any field which has a cubic coupling to the supersymmetry breaking fields $\tilde{Q}_{b2}$ or $\tilde{Q}_{2a}$ is one-loop massive as well. Using the general structure of W_{mesons}, a little thought shows that all dual quarks with no flavor index (e.g. $\tilde{X}$, $\tilde{Y}$) and all mesons with one flavor index (e.g. R or S) couple to the supersymmetry breaking fields.

Thus they all get one-loop masses (with positive squared mass). Finally, the flavors of other gauge factors (e.g. Q_{b3}) are massive at tree level from W_{mass}.

The bottom line is that the only fields which do not get mass from these interactions are the mesons with no flavor index, and the bi-fundamentals which do not get dualized (uncharged under node 2). All these fields are related to the theory in the absence of extra flavors, so they can be already stabilized at tree-level from the original superpotential. So, the criteria for a metastable vacua is that the original theory, *in the absence of flavors* leads, after dualization of the node with $N_f < N_c$, to masses for all these fields (or more mildly that they correspond to directions stabilized by mass terms, or perhaps higher order superpotential terms).

The argument is completely general, and leads to an enormous simplification in the study of the theories. In Section 4.4 we describe several examples.

4.3.2 The detailed proof

In the previous section we omitted some important but not specially enlightening technical details for the sake of clarity. We provide these technical details in this section. The reader uninterested in how the argument above is made waterproof can skip this section, and jump instead to Section 4.4, where we illustrate the discussion above in a variety of examples.

We will describe here how to take into account the matricial structure, and show that all fields, except for Goldstone bosons, get positive squared masses at tree-level or at one-loop.

For the choice of D7 branes shown in Figure 4.5 we get the following superpotential terms (we are omitting the part of the superpotential not involving the flavors):

$$\begin{aligned} W_{flavor} &= \lambda' \left(X_{32} Q_{2b} Q_{b3} + X_{21} Q_{1a} Q_{a2} + X_{14} Q_{4d} Q_{d1} + Y_{43} Q_{3c} Q_{c4} \right) \\ W_{mass} &= m_2 Q_{a2} Q_{2b} + m_3 Q_{b3} Q_{3c} + m_4 Q_{c4} Q_{4d} + m_1 Q_{d1} Q_{1a} \end{aligned} \quad (4.45)$$

which becomes after dualizing node 2:

$$\begin{aligned} W_{flavor\,dual} &= \lambda' \left(S^1_{3b} Q_{b3} + R^1_{a1} Q_{1a} + X_{14} Q_{4d} Q_{d1} + Y_{43} Q_{3c} Q_{c4} \right) \\ W_{mass\,dual} &= m_2 \underline{X_{ab}} + m_3 Q_{b3} Q_{3c} + m_4 Q_{c4} Q_{4d} + m_1 Q_{d1} Q_{1a} \\ W_{mesons} &= h \left(\underline{X_{ab} \tilde{Q}_{b2} \tilde{Q}_{2a}} \right. \\ &+ R^1_{a1} \tilde{X}_{12} \tilde{Q}_{2a} + R^2_{a1} \tilde{Y}_{12} \tilde{Q}_{2a} \\ &+ S^1_{3b} \tilde{Q}_{b2} \tilde{X}_{23} + S^2_{3b} \tilde{Q}_{b2} \tilde{Y}_{23} + S^3_{3b} \tilde{Q}_{b2} \tilde{Z}_{23} \\ &+ M^1_{31} \tilde{X}_{12} \tilde{X}_{23} + M^2_{31} \tilde{X}_{12} \tilde{Y}_{23} + M^3_{31} \tilde{X}_{12} \tilde{Z}_{23} \\ &+ \left. M^4_{31} \tilde{Y}_{12} \tilde{X}_{23} + M^5_{31} \tilde{Y}_{12} \tilde{Y}_{23} + M^6_{31} \tilde{Y}_{12} \tilde{Z}_{23} \right) \end{aligned} \tag{4.46}$$

The crucial point is that the underlined terms appear for any quiver gauge theory with flavors introduced in the way we have described. As explained in the previous section, supersymmetry is broken by the rank condition due to the F-term of the dual meson associated to the massive flavors. Our vacuum ansatz is (we take $N_f = 2$ and $N_c = 1$ for simplicity; this does not affect our conclusions)

$$\tilde{Q}_{b2} = \begin{pmatrix} \mu \mathbf{1}_{N_c} \\ 0 \end{pmatrix} \quad ; \; q\tilde{Q}_{2a} = (\mu \mathbf{1}_{N_c} \,;\, 0) \tag{4.47}$$

with all other vevs set to zero. We parametrize the perturbations around this minimum as

$$\tilde{Q}_{b2} = \begin{pmatrix} \mu + \phi_1 \\ \phi_2 \end{pmatrix} \quad ; \; \tilde{Q}_{2a} = (\mu + \phi_3 \,;\, \phi_4) \quad ; \; X_{ab} = \begin{pmatrix} X_{00} & X_{01} \\ X_{10} & X_{11} \end{pmatrix} \tag{4.48}$$

so the underlined terms give when expanded:

$$\begin{aligned} h X_{ab} \tilde{Q}_{b2} \tilde{Q}_{2a} - h\mu^2 X_{ab} &= h X_{11}\, \phi_2\, \phi_4 - h\mu^2 X_{11} + h\mu\, \phi_2\, X_{01} + h\mu\, \phi_4\, X_{10} \\ &+ h\mu\, \phi_1\, X_{00} + h\mu\, \phi_3\, X_{00} + h\, \phi_1\, \phi_3 X_{00} \\ &+ h\, \phi_2\, \phi_3 X_{01} + h\, \phi_1\, \phi_4 X_{10} \end{aligned} \tag{4.49}$$

It is important to note that all the fields in (4.48) will have quadratic couplings only in the underlined term (4.49). Thus, one can safely study these terms only. The conclusions will be independent of the other terms in the superpotential. Diagonalizing (4.49) gives

$$\begin{aligned} h X_{ab} \tilde{Q}_{b2} \tilde{Q}_{2a} - h\mu^2 X_{ab} &= h X_{11} \phi_2 \phi_4 - h\mu^2 X_{11} + h\mu \phi_2 X_{01} + h\mu \phi_4 X_{10} \\ &+ \sqrt{2} h\mu \phi_+ X_{00} + \frac{h}{2} \phi_+^2 X_{00} - \frac{h}{2} \phi_-^2 X_{00} \\ &+ \frac{h}{\sqrt{2}} (\xi_+ - \xi_-) \phi_2 X_{01} + \frac{h}{\sqrt{2}} (\xi_+ + \xi_-) \phi_4 X_{10} \end{aligned} \tag{4.50}$$

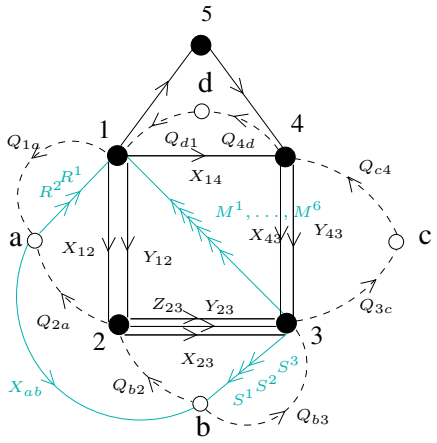

Figure 4.7: Quiver after Seiberg duality on node 2.

where

$$\xi_+ = \frac{1}{\sqrt{2}}(\phi_1 + \phi_3) \quad ; \quad \xi_- = \frac{1}{\sqrt{2}}(\phi_1 - \phi_3) \tag{4.51}$$

This term is the generalized asymmetric case studied in Section 4.1.2 with

$$X_{11} \to X \,;\, \phi_4 \to \phi_1 \,;\, \phi_2 \to \phi_2 \,;\, X_{10} \to \phi_3 \,;\, X_{01} \to \phi_4 \tag{4.52}$$

So here X_{11} is the linear term that breaks supersymmetry, and ϕ_2, ϕ_4 are the broken supersymmetry fields. In (4.50), the only massless fields at tree-level are X_{11} and ξ_-. Comparing to the ISS case in Section 4.1 shows that $\mathrm{Im}\,\xi_-$ is a Goldstone boson and X_{11}, $\mathrm{Re}\,\xi_-$ get mass at tree-level. As for ϕ_2 and ϕ_4, setting $\rho_+ = \frac{1}{\sqrt{2}}(\phi_2 + \phi_4)$ and $\rho_- = \frac{1}{\sqrt{2}}(\phi_2 - \phi_4)$ gives us $\mathrm{Re}\,(\rho_+)$ and $\mathrm{Im}\,(\rho_-)$ massless and the rest massive. Following the discussion in Section 4.1, $\mathrm{Re}\,(\rho_+)$ and $\mathrm{Im}\,(\rho_-)$ are just the Goldstone bosons of the broken $SU(N_f)$ symmetry[4].

We have shown so far that the dualized flavors (e.g. $\tilde{Q}_{b2}$, $\tilde{Q}_{2a}$) and the mesons with two flavor indices (e.g. X_{ab}) get mass at tree-level or at 1-loop unless they are Goldstone bosons. Now, we need to verify that this is the case for the remaining fields.

The complete Seiberg dual of the original quiver diagram is shown in Figure 4.7. The dualized bi-fundamentals come in two classes. The first are the ones that initially (before dualizing) had cubic flavor couplings, there will always be only two of those (e.g. $\tilde{X}_{12}$, $\tilde{X}_{23}$). The second are those that did not have initially cubic couplings to flavors, there is an arbitrary number of those (e.g. $\tilde{Y}_{12}$, $\tilde{Y}_{23}$, $\tilde{Z}_{23}$).

[4]In the case where the flavor group is $SU(2)$, these Goldstone bosons are associated to the generators t_x and t_y.

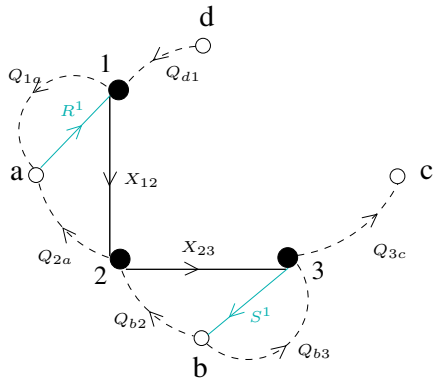

Figure 4.8: Relevant part of the dual quiver for the first class of bifundamentals.

We will start by analyzing the fields in the first class. Figure 4.8 shows the relevant part of the quiver for these fields. Recalling the superpotential terms (4.46), we see that there are several possible sources of tree-level masses. For instance, these can arise in $W_{flavor\,dual}$ and $W_{mass\,dual}$. Also, remembering our assignation of vevs in (4.47), tree-level masses can also arise in W_{mesons} from cubic couplings involving the broken supersymmetry fields (e.g. $\tilde{Q}_{b2}$, $\tilde{Q}_{2a}$).

The first class of bi-fundamentals (e.g. $\tilde{X}_{12}$, $\tilde{X}_{23}$) only appear in W_{mesons} coupled to their respective mesons (e.g. R^1, S^1). In turn these mesons will appear in quadratic terms in $W_{flavor\,dual}$ coupled to flavors (e.g. $S^1_{3b}Q_{b3}$ and $R^1_{a1}Q_{1a}$), and these flavors each appear in one term in W_{mass}. Thus there are two sets of three terms which are coupled at tree-level and which always couple in the same way. Consider for instance the term

$$\begin{aligned}
\lambda'\, S^1_{3b}Q_{b3} \,+\, m_3 Q_{b3}Q_{3c} \,+\, h\, S^1_{3b}\tilde{Q}_{b2}\tilde{X}_{23} \;&=\; \lambda'\,(S_1\ S_2)\begin{pmatrix}B_1\\B_2\end{pmatrix} + m_1(C_1\ C_2)\begin{pmatrix}B_1\\B_2\end{pmatrix} \\
&+\; h\,(S_1\ S_2)\begin{pmatrix}\mu+\phi_1\\ \phi_2\end{pmatrix}\tilde{X}_{23} \\
&=\; \lambda'(S_1B_1+S_2B_2) + m_1(B_1C_1+B_2C_2) \\
&+\; h\mu\, S_1\,\tilde{X}_{23} \,+\, h\, S_1\,\phi_1\,\tilde{X}_{23} \,+\, h\, S_2\,\phi_2\,\tilde{X}_{23}
\end{aligned} \tag{4.53}$$

where S_i, B_i, C_i and $\tilde{X}_{23}$ are the perturbations around the minimum. Diagonalizing (which can be done analytically for any values of the couplings), we get that all terms except one get tree-level masses, the massless field being:

$$Y = m_1 S_2 - \lambda' C_2 \tag{4.54}$$

This massless field has a cubic coupling to $\phi_2\,\tilde{X}_{23}$ and gets mass at 1-loop

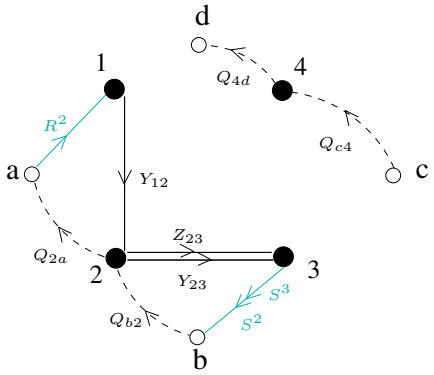

Figure 4.9: Relevant part of the dual quiver for the second class of bifundamentals.

since ϕ_2 is a broken supersymmetry field, as described in Section 4.1.2.

Figure 4.9 shows the relevant part of the quiver for the second class of bi-fundamentals (i.e. those that are dualized but do not have cubic flavor couplings).

These fields and their mesons only appear in one term, so will always couple in the same way. Taking as an example

$$\begin{aligned} h\, R_{a1}^2 \tilde{Y}_{12} \tilde{Q}_{2a} &= \begin{pmatrix} R_1 \\ R_2 \end{pmatrix} \tilde{Y}_{12}\, (\mu + \phi_3\,;\, \phi_4) \\ &= \mu R_1\, \tilde{Y}_{12} \,+\, R_1\, \phi_3\, \tilde{Y}_{12} + R_2\, \phi_4\, \tilde{Y}_{12} \end{aligned} \tag{4.55}$$

This shows that R_1 and $\tilde{Y}_{12}$ get tree-level masses and R_2 gets a mass at 1-loop since it couples to the broken supersymmetry field ϕ_4. The only remaining fields are flavors like Q_{c4}, Q_{4d}, which do not transform in a gauge group adjacent to the dualized node (i.e. not adjacent in the quiver loop corresponding to the superpotential term used to introduce flavors). These are directly massive from the tree-level W_{mass} term.

So, as stated, all fields except those that appear in the original superpotential (i.e. mesons with gauge indices and bi-fundamentals which are not dualized) get masses either at tree-level or at one-loop. So we only need to check the dualized original superpotential to see if we have a metastable vacua.

4.4 Some additional examples

The considerations in the previous section might seem a bit formal. In this section we will show how they apply to numerous examples, and allow us to check for the existence of ISS-like metastable vacua in a variety of interesting setups of DSB branes at toric singularities, which flavor D7 branes appropriate added.

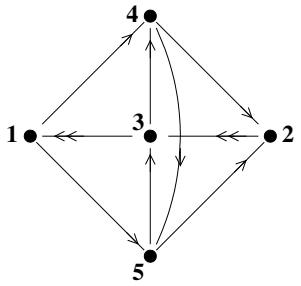

Figure 4.10: Quiver diagram for the dP_2 theory.

4.4.1 The complex cone over dP_2

Let us start by a DSB brane in the complex cone over dP_2. This theory provides another quiver theory with runaway behavior [79]. The quiver diagram for dP_2 is given in Figure 4.10, and the superpotential is given by:

$$\begin{aligned} W &= X_{34}X_{45}X_{53} - X_{53}Y_{31}X_{15} - X_{34}X_{42}Y_{23} + Y_{23}X_{31}X_{15}X_{52} \\ &+ X_{42}X_{23}Y_{31}X_{14} - X_{23}X_{31}X_{14}X_{45}X_{52} \end{aligned} \tag{4.56}$$

We consider a set of M DSB fractional branes, corresponding to choosing ranks $(M, 0, M, 0, 2M)$ for the corresponding gauge factors. The superpotential in this case reduces to:

$$W = -\lambda X_{53}Y_{31}X_{15} \tag{4.57}$$

We also introduce flavors as described in Appendix C.4. The resulting quiver is depicted in Figure 4.11. As described in the general analysis, we have to add the cubic 33-37-73 coupling to the superpotential. We also choose to separate the D7 branes slightly from the singularity, giving mass terms to the flavors. The resulting superpotential we want to analyze is thus given by:

$$\begin{aligned} W_{total} &= -\lambda X_{53}Y_{31}X_{15} - \lambda'(Q_{1i}\tilde{Q}_{i3}Y_{31} + Q_{3j}\tilde{Q}_{j5}X_{53} + Q_{5k}\tilde{Q}_{k1}X_{15}) \\ &+ m_1 Q_{1i}\tilde{Q}_{k1} + m_2 Q_{3j}\tilde{Q}_{i3} + m_5 Q_{5k}\tilde{Q}_{j5} \end{aligned} \tag{4.58}$$

where $1, 2, 3$ are the gauge group indices and i, j, k are the flavor indices.

We will choose ranks such that the $U(2M)$ node is in the free magnetic phase, namely:

$$M + 1 \;\leq\; N_{f,1} \;<\; 2M \tag{4.59}$$

After Seiberg duality the dual gauge factor is $SU(N)$ with rank $N = N_{f,1} - M$ and dynamical scale Λ. To get the matter content in the dual, we replace the microscopic flavors Q_{5k}, $\tilde{Q}_{j5}$, X_{53}, X_{15} by the dual flavors $\tilde{Q}_{k5}$, Q_{5j},

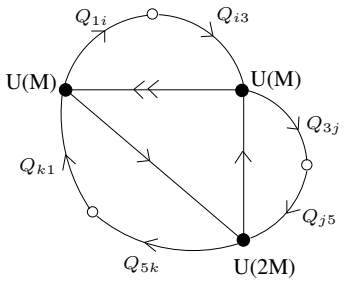

Figure 4.11: Quiver diagram for the dP_2 theory with M DSB fractional branes and flavors appropriately introduced.

X_{35}, X_{51}. We will be working in the magnetic description only in the rest of this section, so hopefully the similarity between the notation for the electric and magnetic theories is not confusing. We also have the mesons related to the fields in the electric theory by

$$\begin{array}{lllllll} M_{1k} & = & \frac{1}{\Lambda} X_{15} Q_{5K} & ; & \tilde{N}_{j3} & = & \frac{1}{\Lambda} \tilde{Q}_{j5} X_{53} \\ M_{13} & = & \frac{1}{\Lambda} X_{15} X_{53} & ; & \tilde{\Phi}_{jk} & = & \frac{1}{\Lambda} \tilde{Q}_{j5} Q_{5k} \end{array} \tag{4.60}$$

There is a cubic superpotential coupling the mesons and the dual flavors

$$W_{mes.} = h(M_{1k}\tilde{Q}_{k5}X_{51} + M_{13}X_{35}X_{51} + \tilde{N}_{j3}X_{35}Q_{5j} + \tilde{\Phi}_{jk}\tilde{Q}_{k5}Q_{5j}) \tag{4.61}$$

where $h = \Lambda/\hat{\Lambda}$ with $\hat{\Lambda}$ given by $\Lambda_{elect}^{3N_c-N_f}\,\Lambda^{3(N_f-N_c)-N_f} = \hat{\Lambda}^{N_f}$, and Λ_{elect} the dynamical scale of the electric theory. Writing the classical superpotential in terms of the new fields gives

$$\begin{array}{rcl} W_{clas.} & = & -\,h\,\mu_0\,M_{13}Y_{31} \,+\, \lambda'\,Q_{1i}\tilde{Q}_{i3}Y_{31} \,+\, \mu'\,\tilde{N}_{j3}Q_{3j} \,+\, \mu'\,M_{1k}\tilde{Q}_{k1} \\ & + & m_1 Q_{1i}\tilde{Q}_{k1} \,+\, m_3 Q_{3j}\tilde{Q}_{i3} \,-\, h\mu^{\,2}\mathrm{Tr}\,\Phi \end{array} \tag{4.62}$$

where $\mu_0 = \lambda\Lambda$, $\mu' = \lambda'\Lambda$, and $\mu^{\,2} = -m_5\hat{\Lambda}$. So the complete superpotential for the Seiberg dual theory is

$$\begin{array}{rcl} W_{dual} & = & -\,h\,\mu_0\,M_{13}Y_{31} \,+\, \lambda'\,Q_{1i}\tilde{Q}_{i3}Y_{31} \,+\, \mu'\,\tilde{N}_{j3}Q_{3j} \,+\, \mu'\,M_{1k}\tilde{Q}_{k1} \\ & + & m_1 Q_{1i}\tilde{Q}_{k1} \,+\, m_3 Q_{3j}\tilde{Q}_{i3} \,-\, h\mu^{\,2}\mathrm{Tr}\,\Phi \\ & + & h\,(\,M_{1k}\tilde{Q}_{k5}X_{51} \,+\, M_{13}X_{35}X_{51} \,+\, \tilde{N}_{j3}X_{35}Q_{5j} \,+\, \tilde{\Phi}_{jk}\tilde{Q}_{k5}Q_{5j}\,) \end{array} \tag{4.63}$$

This superpotential has a sector completely analogous to the ISS model, triggering supersymmetry breaking by the rank condition. This suggests the following ansatz for the one-loop vacuum

$$Q_{5k} = \tilde{Q}_{5k}^{\mathrm{T}} = \begin{pmatrix} \mu \\ 0 \end{pmatrix}, \tag{4.64}$$

with all other vevs set to zero. Following our technique as explained above, we expand fields at linear order around this point. Focusing on $N_{f,1} = 2$ and $N_c = 1$ for simplicity (the general case can be easily recovered), we have

$$\tilde{Q}_{k5} = \begin{pmatrix} \mu + \delta\tilde{Q}_{5,1} \\ \delta\tilde{Q}_{5,2} \end{pmatrix} \quad ; \quad Q_{5k} = (\mu + \delta Q_{5,1}\,;\, \delta Q_{5,2}) \quad ; \quad \Phi = \begin{pmatrix} \delta\Phi_{0,0} & \delta\Phi_{0,1} \\ \delta\Phi_{1,0} & \delta\Phi_{1,1} \end{pmatrix}$$

$$\tilde{Q}_{k1} = \begin{pmatrix} \delta\tilde{Q}_{1,1} \\ \delta\tilde{Q}_{1,2} \end{pmatrix} \; ; \; Q_{1i} = (\delta Q_{1,1}\,;\, \delta Q_{1,2}) \; ; \; \tilde{Q}_{i3} = \begin{pmatrix} \delta\tilde{Q}_{3,1} \\ \delta\tilde{Q}_{3,2} \end{pmatrix} \; ; \; Q_{3j} = (\delta Q_{3,1}\,;\, \delta Q_{3,2})$$

$$\tilde{N}_{j3} = \begin{pmatrix} \delta\tilde{N}_{3,1} \\ \delta\tilde{N}_{3,2} \end{pmatrix} \; ; \; M_{1k} = (\delta M_{1,1}\,;\, \delta M_{1,2}) \; ; \; M_{13} = \delta M_{13} \; ; \; Y_{31} = \delta Y_{31} \; ; \; X_{51} = \delta X_{51}$$

$$X_{35} = \delta X_{35} \tag{4.65}$$

Inserting this into equation (4.63) gives

$$\begin{aligned} W_{dual} &= -h\,\mu_0\,\delta M_{13}\delta Y_{31} + \lambda'\,\delta Q_{1,1}\delta\tilde{Q}_{3,1}\delta Y_{31} + \lambda'\,\delta Q_{1,2}\delta\tilde{Q}_{3,2}\delta Y_{31} \\ &+ \mu'\,\delta\tilde{N}_{3,1}\delta Q_{3,1} + \mu'\,\delta\tilde{N}_{3,2}\delta Q_{3,2} + \mu'\,\delta M_{1,1}\delta\tilde{Q}_{1,1} + \mu'\,\delta M_{1,2}\delta\tilde{Q}_{1,2} \\ &+ m_1\delta Q_{1,1}\delta\tilde{Q}_{1,1} + m_1\delta Q_{1,2}\delta\tilde{Q}_{1,2} + m_3\delta Q_{3,1}\delta\tilde{Q}_{3,1} + m_3\delta Q_{3,2}\delta\tilde{Q}_{3,2} \\ &- h\mu^2\delta\Phi_{11} + h\,(\,\mu\delta M_{1,1}\delta X_{51} + \delta M_{1,1}\delta\tilde{Q}_{5,1}\delta X_{51} + \delta M_{1,2}\delta\tilde{Q}_{5,2}\delta X_{51} \\ &+ \delta M_{13}\delta X_{35}\delta X_{51} + \mu\delta X_{35}\delta\tilde{N}_{3,1} + \delta X_{35}\delta\tilde{N}_{3,1}\delta Q_{5,1} + \delta X_{35}\delta\tilde{N}_{3,2}\delta Q_{5,2} \\ &+ \mu\delta\tilde{Q}_{5,1}\delta\Phi_{00} + \mu\delta Q_{5,1}\delta\Phi_{00} + \delta Q_{5,1}\delta\tilde{Q}_{5,1}\delta\Phi_{00} + \mu\delta\Phi_{01}\delta\tilde{Q}_{5,2} \\ &+ \delta Q_{5,1}\delta\Phi_{01}\delta\tilde{Q}_{5,2} + \mu\delta\Phi_{10}\delta Q_{5,2} + \delta\tilde{Q}_{5,1}\delta\Phi_{10}\delta Q_{5,2} + \delta\tilde{Q}_{5,2}\delta\Phi_{11}\delta Q_{5,2}). \end{aligned}$$

We now need to identify the pseudomoduli, in other words the massless fluctuations at tree level. We focus then just on the quadratic terms in the superpotential

$$\begin{aligned} W_{mass} &= -h\,\mu_0\,\delta M_{13}\delta Y_{31} \\ &+ \mu'\,\delta\tilde{N}_{3,1}\delta Q_{3,1} + m_3\delta Q_{3,1}\delta\tilde{Q}_{3,1} + h\mu\delta X_{35}\delta\tilde{N}_{3,1} \\ &+ \mu'\,\delta\tilde{N}_{3,2}\delta Q_{3,2} + m_3\delta Q_{3,2}\delta\tilde{Q}_{3,2} \\ &+ \mu'\,\delta M_{1,1}\delta\tilde{Q}_{1,1} + m_1\delta Q_{1,1}\delta\tilde{Q}_{1,1} + h\mu\delta M_{1,1}\delta X_{51} \\ &+ \mu'\,\delta M_{1,2}\delta\tilde{Q}_{1,2} + m_1\delta Q_{1,2}\delta\tilde{Q}_{1,2} \\ &+ h\mu\delta\tilde{Q}_{5,1}\delta\Phi_{00} + h\mu\delta Q_{5,1}\delta\Phi_{00} \\ &+ h\mu\delta\Phi_{01}\delta\tilde{Q}_{5,2} + \mu\delta\Phi_{10}\delta Q_{5,2}. \end{aligned} \tag{4.66}$$

We have displayed the superpotential so that fields mixing at the quadratic level appear in the same line. In order to identify the pseudomoduli we have to diagonalize[5] these fields.

[5] As a technical remark, let us note that it is possible to set all the mass terms to be real by an appropriate redefinition of the fields, so we are diagonalizing a real symmetric matrix.

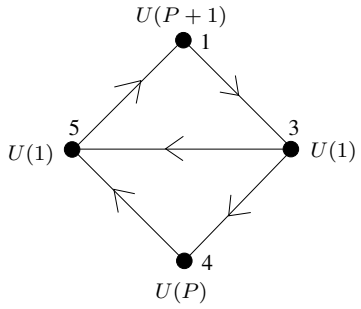

Figure 4.12: Quiver diagram for the dP_3 theory with a DSB brane.

Note that the structure of the mass terms corresponds to the one described in the general analysis done in Section 4.3, in particular around equation (4.53). From the analysis performed there we know that upon diagonalization, fields mixing in groups of four (i.e., three mixing terms in the superpotential, for example the $\delta M_{1,1}$, $\delta\tilde{Q}_{1,1}$, $\delta Q_{1,1}$, δX_{51} mixing) get nonzero masses, while fields mixing in groups of three (two mixing terms in the superpotential, for example $\delta M_{1,2}$, $\delta\tilde{Q}_{1,2}$ and $\delta Q_{1,2}$) give rise to two massive perturbations and a massless one, a pseudomodulus.

We then just need to study the fate of the pseudomoduli. From the general analysis, the pseudomoduli coming from the mixing terms are

$$\begin{aligned} Y_1 &= m_3\delta\tilde{N}_{3,2} - \mu'\delta\tilde{Q}_{3,2}\,, \\ Y_2 &= m_1\delta M_{1,2} - \mu'\delta Q_{1,2}\,, \\ Y_3 &= h\mu(\delta Q_{5,1} - \delta\tilde{Q}_{5,1})\,. \end{aligned} \tag{4.67}$$

In order to continue the analysis, one just needs to change basis to the diagonal fields and notice that the one loop contributions to the pseudomoduli are described again by the asymmetric model of Section 4.1.2, so they receive positive definite contributions. The exact analytic expressions can be easily found with the help of some computer algebra program, but we omit them here since they are quite unwieldy.

4.4.2 The complex cone over dP_3

Let us go on to a more complicated example, the complex cone over dP_3. The details are very similar to the cases we have studied above, so we will be sketchier and just show the main features of the analysis. DSB branes for this system have already been considered in [79].

The quiver is shown in Figure 4.12 and the superpotential is

$$W = X_{13}X_{35}X_{51} \tag{4.68}$$

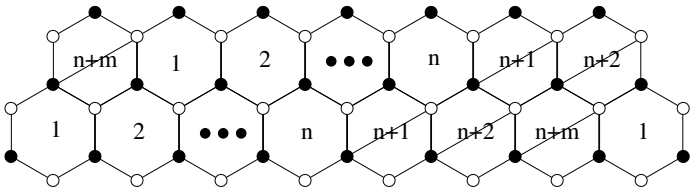

Figure 4.13: Dimer for $Y^{(p,q)}$. The dots indicate $n-3$ hexagons we have not drawn.

Node 1 has $N_f < N_c$ so upon addition of massive flavors and dualization will lead to supersymmetry breaking by the rank condition. Following the procedure of the previous section, we add $N_{f,1}$ flavors coupling to the bifundamentals X_{13}, X_{35} and X_{51}. Node 1 is in the free magnetic phase for $P+1 \leq N_{f,1} < \frac{3}{2}P+\frac{1}{2}$. Dualizing node 1, the above superpotential becomes

$$W = X_{35}M_{53} \tag{4.69}$$

where M_{53} is the meson $X_{51}X_{13}$. So, following the results of the previous section, we can conclude that this DSB fractional brane generates a metastable vacua with all pseudomoduli lifted.

4.4.3 The $Y^{p,q}$ family

Consider D3-branes at the real cones over the $Y^{p,q}$ Sasaki-Einstein manifolds [81, 82, 83, 84], whose field theory were determined in [85]. The theory admits a fractional brane [86] of DSB kind, which namely breaks supersymmetry and lead to runaway behavior [79, 87]. The analysis of metastability upon addition of massive flavors for arbitrary $Y^{p,q}$'s is much more involved than previous examples. Already the description of the field theory on the fractional brane is complicated. Even for the simpler cases of $Y^{p,1}$ and $Y^{p,p-1}$ we study in this section the superpotential contains many terms. In this section we do not provide a general proof of metastability, but rather consider the more modest aim of showing that all directions related to the runaway behavior in the absence of flavors are stabilized by the addition of flavors. We expect that this will guarantee full metastability, since the fields not involved in our analysis parametrize directions orthogonal to the runaway at infinity.

The dimer for $Y^{p,q}$ is shown in Figure 4.13 and consists of a row of n hexagons and $2m$ quadrilaterals which are just halved hexagons [87]. The labels (n,m) are related to (p,q) by

$$n = 2q \quad ; \quad m = p - q \tag{4.70}$$

We will show that we can obtain metastable vacua for fractional branes at cones over the $Y^{p,1}$ and $Y^{p,p-1}$ geometries. Although there is no obvi-

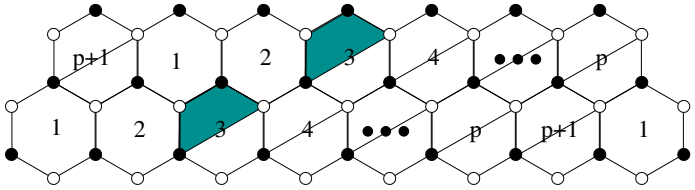

Figure 4.14: Dimer for $Y^{(p,1)}$. We have drawn in color the empty node for the DSB brane. In Figure 4.15 we reproduce the ranks for the nodes involved in the metastability analysis.

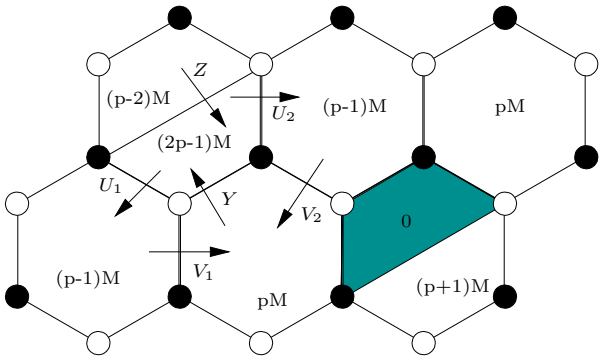

Figure 4.15: Part of the $Y^{(p,1)}$ dimer relevant for the metastability analysis. We indicate the ranks and the fields involved in the analysis.

ous generalization for arbitrary $Y^{p,q}$'s, our results strongly suggest that the existence of metastable vacua extends to the complete family.

The $Y^{p,1}$ case

The dimer for the theory on the DSB fractional brane in the $Y^{p,1}$ case is shown in Figure 4.14. It is a periodic array made from a row of two full hexagons, followed by $p-1$ cut hexagons (the shaded quadrilateral has $N_c = 0$). The quadrilateral with rank $(2p-1)M$ has $N_f < N_c$, and as shown in [87] induces the ADS superpotential triggering the runaway. The relevant part of the dimer is shown in Figure 4.15, where V_1 and V_2 are the fields that run to infinity [87]. This node will lead to supersymmetry breaking by the rank condition in the dual. It is in the free magnetic phase for $M+1 \leq N_{f,1} < pM + \frac{M}{2}$. The piece of the superpotential involving the V_1 and V_2 terms is

$$W = YU_2V_2 - YU_1V_1. \tag{4.71}$$

In the dual theory, the dual superpotential makes the fields massive. Hence, the theory has a metastable vacua where the runaway fields are stabilized.

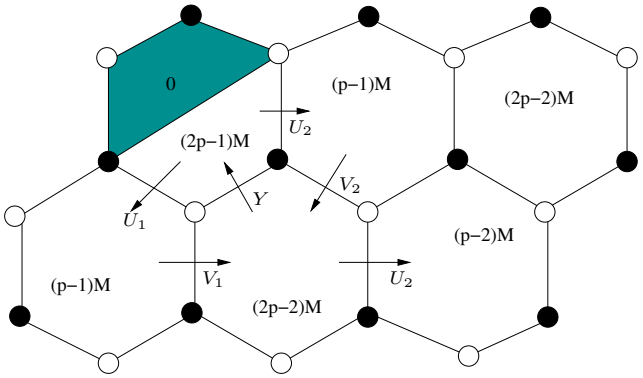

Figure 4.16: Part of the $Y^{(p,p-1)}$ dimer relevant for the metastability analysis. We indicate the ranks and the fields involved in the analysis.

The $Y^{p,p-1}$ case

The analysis for $Y^{p,p-1}$ is similar. The node with the highest rank is again the $(2p-1)M$ one, and it also gives an ADS superpotential [87]. The relevant part of the dimer is shown in Figure 4.16. We see that the runaway direction is described by the fields V_1 and V_2. Upon addition of $N_{f,1}$ flavors, the relevant node is in the free magnetic phase for $M+1 \leq N_{f,1} < pM + \frac{M}{2}$. Considering the superpotential, it is straightforward to show that the runaway fields become massive. Complementing this with our analysis in previous sections, we conclude that the theory has a metastable vacua where the runaway fields are stabilized.

Chapter 5

Resolved and deformed dimer models

In this chapter we leave the study of the realization of metastable vacua in local geometries, and focus instead on some interesting aspects of the physics of branes at toric singularities.

We will discuss how geometric operations in the local toric geometry such as resolutions and deformations are realized in the gauge theory of branes located on it. Readers unfamiliar with toric geometry or dimer models are advised to read Appendices B and C at this point for a short introduction to the main ideas we will be using here, and a list of references to the relevant literature.

One possible application of the considerations in this chapter is to the construction of models of gauge mediated supersymmetry breaking, as we show in Chapter 7. The results discussed here are also useful for quickly finding the gauge theory describing branes at arbitrary toric singularities. This can easily be done by embedding into a big orbifold and partially resolving.

The contents of this chapter were first discussed in [44] and [46].

5.1 Resolving the singularity

In terms of the web diagrams, resolving the singularity corresponds to giving a finite length to one of the interior segments, representing a blowup of a $\mathbb{P}^1$ in the toric geometry. The close relation between the Riemann surface Σ and the toric diagram suggests a way of reading the effect in the dimer, and hence in the gauge theory, of the blowup. The rest of this section will be devoted to making this heuristic connection concrete, both in general and in particular examples.

The basic idea is that one should identify which external legs of the web diagram go to which side. In the dimer this divides the zig-zag paths into

two sets, since as we describe in Appendix C we have a one to one mapping between zig-zag paths and external legs. Let us call the zig-zag paths in the first set paths of type 1 and those in the second set paths of type 2. In turn, since each edge is crossed by exactly two zig-zag paths, this divides the set of edges into three, namely those where two zig-zags of type 1 meet, those were two of type 2 meet, and those where zig-zag paths of mixed type meet. Let us denote this as edges of type 1, 2 and 3 respectively.

In terms of the mirror surface, a resolution consists of sending a given set of external legs to infinity (actually finite distance, but we will be ignoring the corresponding massive mediators for now). Then the theory divides into two sectors, one corresponding to each side. In terms of dimer diagrams, what we have is that the original dimer diagram decomposes into two subdimers[1], that we can call 1 and 2. The subdimer 1 is obtained from the original dimer diagram by removing all edges of type 2, and similarly for the subdimers of type 2. Edges of type 3 remain in both diagrams. This can be seen quite intuitively from the mirror, since edges of type 1 and 2 are localized in one side of the resolution, while edges of type 3 can communicate with both sectors.

In terms of the gauge theory, what we have done is a Higgsing of the original theory, where we assign the following vacuum expectation values to bifundamentals:

$$\Phi_1 = \begin{pmatrix} 0 & 0 \\ 0 & v \end{pmatrix}, \qquad \Phi_2 = \begin{pmatrix} v & 0 \\ 0 & 0 \end{pmatrix}, \qquad \Phi_3 = \begin{pmatrix} 0 & 0 \\ 0 & 0 \end{pmatrix}, \tag{5.1}$$

where Φ_i denotes the vev for the fields of type i. We see that these vevs force us to introduce Fayet-Iliopoulos terms in order to cancel the D-terms and remain in a supersymmetric vacuum. Also, they trigger the recombination of some gauge factors into their diagonal combinations, which in terms of the dimer is represented as the recombination of the two faces adjacent to the edge that gets a vev.

One thing that we should prove is that this assignation of vevs is indeed a flat direction, so we can resolve the singularity while remaining in a supersymmetric minimum, this is done in Section 5.1.2.

Let us discuss all this is greater detail by means of a simple example, the double conifold. We want to study what happens in the gauge theory of D3 branes located at this singularity when one switches on Fayet-Iliopoulos terms[2] in such a way that the singularity gets to resolved to two conifold

[1] As in the rest of this work, we will often call *subdimer* a dimer diagram that results from removing some edges from some dimer graph. The terminology is not entirely correct, as a dimer is conventionally what we call an edge.

[2] This point is subtle, since generically the $U(1)$ factors are massive due to the Green-Schwartz mechanism, and hence disappear from the low energy effective theory. It is possible nevertheless to work with them and include their massive couplings at a later stage, see [88]. Otherwise the deformations we are considering are described by vevs of some suitable baryonic operators.

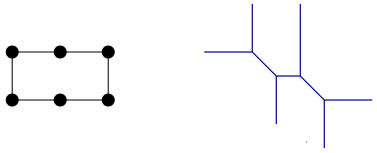

Figure 5.1: The toric diagram and web diagram of the double conifold singularity $xy = s^2w^2$. For clarity, we show the web diagram for a slightly resolved geometry.

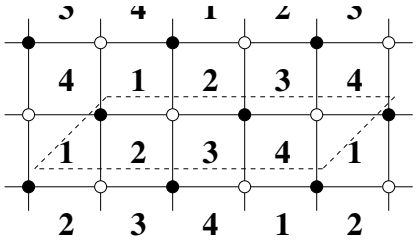

Figure 5.2: Dimer diagram corresponding to the double conifold singularity in Figure 5.1. The dashed line corresponds to the unit cell of the periodic tiling.

singularities. The geometry admits a different non minimal resolution, going into two $\mathbb{C}^2/\mathbb{Z}_2 \times \mathbb{C}$ singularities. We show the toric and web diagram representation of such a resolution in Figure 5.3. The original geometry for the double conifold is presented in Figure 5.1, and the corresponding dimer diagram in Figure 5.2.

With the techniques described above finding out the effect in the gauge theory of such a resolution will be simple. First we have to draw the zig-zag paths in the dimer, we show them in Figure 5.4. Next we find the homotopy charges of these zig-zag paths in order to associate them with external legs of the web diagram. In Figure 5.5a we describe the tiling of the mirror Riemann surface Σ (which is a punctured sphere, since the toric diagram for the double conifold has no interior points), while in Figure 5.5b we have drawn the associated web diagram.

Next we perform the resolution in the mirror geometry. We have to select which external legs in the web diagram go to which side of the resolution. Since we want to resolve into two conifolds, the choice is simple, a schematic representation of one such choice is represented in Figure 5.6. Note that when separating the Riemann surface into two pieces new punctures appear (G in Figure 5.6) in the two factors. In the subdimers these are represented as new zig-zags paths that we have to draw so each edge is crossed exactly by two zig-zag paths. What this condition means is that the resulting Riemann surfaces are completely tiled by local patches. In Figure 5.6b the new path G allows us to completely cover the resulting spheres.

Once we have such a splitting of zig-zag paths it is easy to construct the resulting gauge theories at the two remaining singularities, it is done as

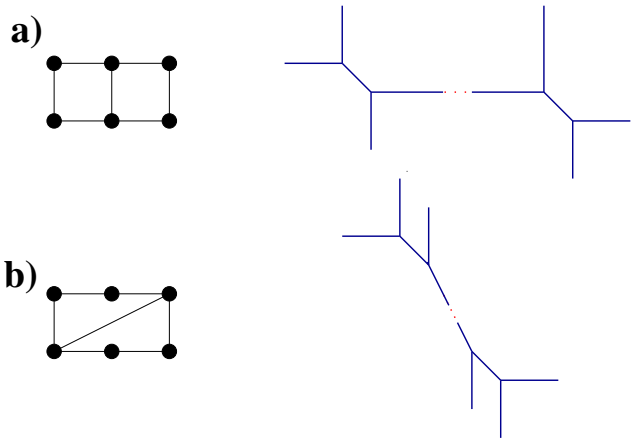

Figure 5.3: Partial resolution of the double conifold singularity of Figure 5.1, splitting the initial singularity into (a) two isolated conifold singularities; (b) two $\mathbb{C}^2/\mathbb{Z}_2$ (times $\mathbb{C}$) singularities. The distance between the daughter singularities is controlled by the size of the $\mathbf{S}^2$ corresponding to the dotted segment in the associated web diagram. For clarity the web diagrams of the left-over singularities are shown for slightly resolved geometries.

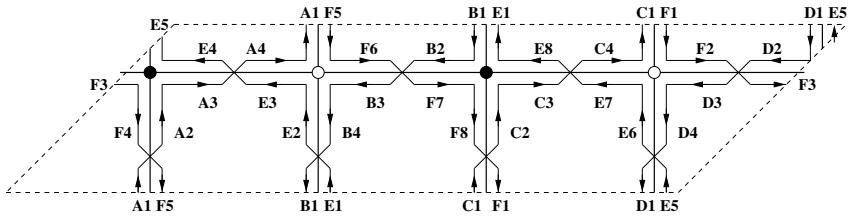

Figure 5.4: Zig-zag paths for the dimer diagram of the double conifold.

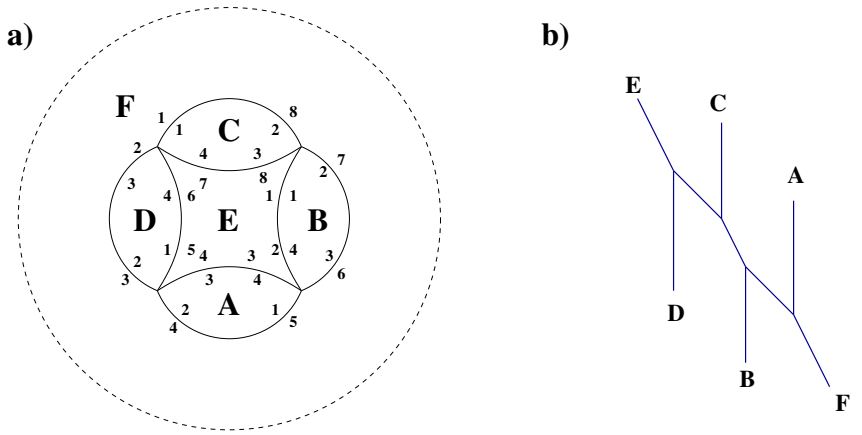

Figure 5.5: a) Tiling of the Riemann surface for the double conifold. We have indicated the adjacency relations we read from the dimer. The $\mathbb{P}^1$ is represented as the compactified complex plane (the dashed line represents infinity). b) The web diagram where we have associated external legs with zig-zag paths according to their (p, q) charge.

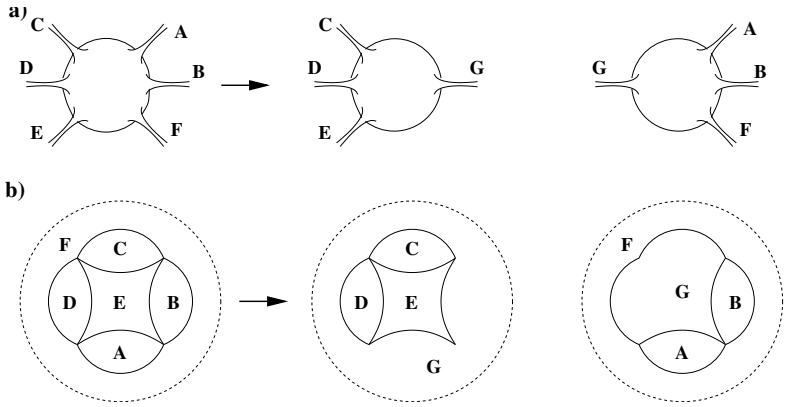

Figure 5.6: Schematic representation of the factorization of Σ. The new puncture G is shown. a) represents the factorization in terms of the Riemann surface emphasizing the similarity with the web diagram description while b) emphasizes the effect on the tiling.

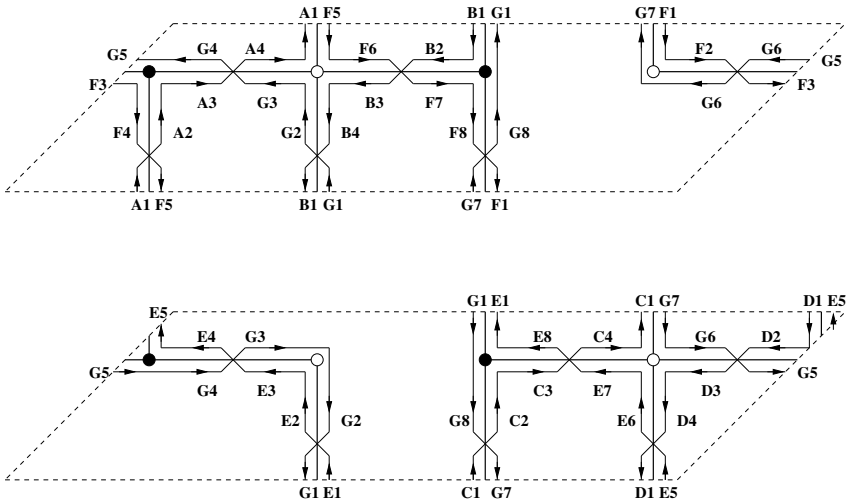

Figure 5.7: Zig-zag paths corresponding to the two daughter theories in the splitting of the double conifold singularity into two conifold singularities, with the corresponding dimers shown as thick lines.

follows. Let us center in the conifold singularity associated to the zig-zag paths A, B, F and G, the other one is similar. We draw in the original dimer A, B and F and "close" the drawing by drawing G. This last zig-zag path should only complete the edges where one zig-zag path is already present, but it should not follow edges where there is no zig-zag path. Another, simpler, way of saying this is that in order to get the gauge theory at the first singularity we remove all edges where none of A, B and F appear, and then draw the zig-zags of the resulting dimer, which are A, B, F and G. The net result is drawn in Figure 5.7.

We see that in Figure 5.7 there are massive nodes, that is quadratic superpotential terms, that we need to integrate out in order to obtain the final infrared theory. We have done this in Figure 5.8, once one integrates out the massive nodes the dimer model for the conifold is immediately recognizable.

Another example: dP_3 going to two SPPs

Let us present an slightly more involved example, where the factorization lowers the genus of Σ. The principles are the same, but a few new interesting features arise in this case. We will consider the splitting of the complex cone over dP_3 into two suspended pinch point (SPP) singularities. The toric diagram for the resolution is shown in Figure 5.9, the dimer diagram (for the most symmetric phase) of the gauge theory is shown in Figure 5.10 and the unit cell of the dimer diagram with the zig-zag paths is in Figure 5.11.

We will not describe the process in detail, but from Figure 5.9 one can easily see that the resolution will involve two auxiliary paths instead of just

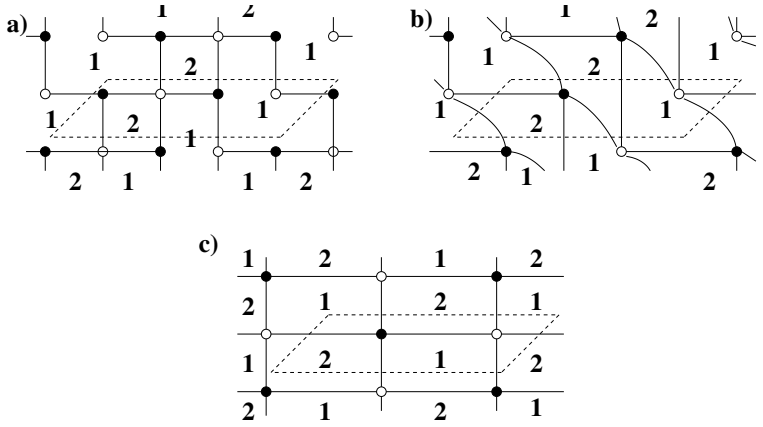

Figure 5.8: (a) Dimer diagram corresponding to the first picture in Figure 5.7. Figure (b) shows the dimer of the theory after integrating out massive modes. An equivalent diagram is shown in Figure (c), where one recognizes the dimer diagram of the conifold theory.

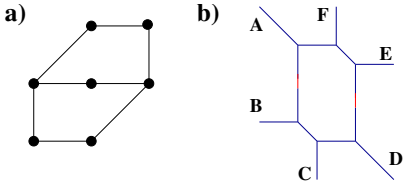

Figure 5.9: The toric diagram and web diagram of the complex cone over dP_3, in a splitting to two SPP singularities. For clarity, the web diagrams of the left-over SPP singularities are shown for slightly resolved geometries. External legs are denoted as the corresponding zig-zag path in Figure 5.11.

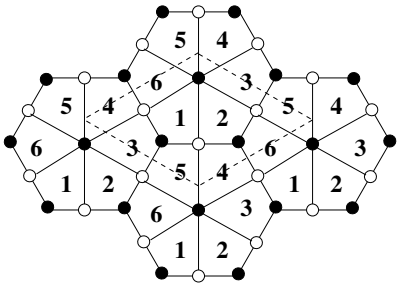

Figure 5.10: The dimer diagram for the gauge theory of D3-branes on the complex plane over dP_3.

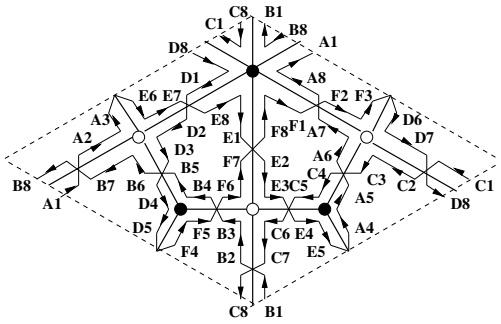

Figure 5.11: The set of zig-zag paths for the dimer of Figure 5.10.

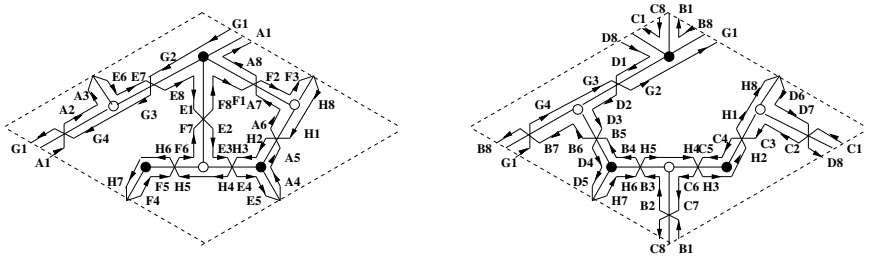

Figure 5.12: The two dimers obtained upon the splitting by small resolution shown in Figure 5.9. They can be shown to be equivalent to two copies of the SPP dimer diagram.

one as in the previous example. The rest of the procedure is essentially the same, and when one removes edges of the appropriate type, one ends up with a gauge theory with a moduli space that classically corresponds to the SPP singularity, as it is easy to check with standard methods (in fact one advantage of the current method is that no checking is necessary, as we know the resulting geometry by construction). The final dimers describing the SPP geometry are shown in Figure 5.12.

5.1.1 Perfect matchings

It is also interesting to study the effect of the partial resolution in terms of perfect matchings. We will center as usual in the case of the double conifold, other cases as similar. The perfect matchings for the double conifold dimer are shown in Figure 5.13, and their positions in the toric diagram are shown in Figure 5.14a.

Figure 5.14b was found just by examining which perfect matchings remain in which dimer after the resolution. It is in fact possible to give a nice explanation in terms of the Riemann surface Σ. Namely, the difference between perfect matchings p_1 and p_2 (for example) is a cycle in the Riemann surface that after resolution remains completely in one of the sides, so the

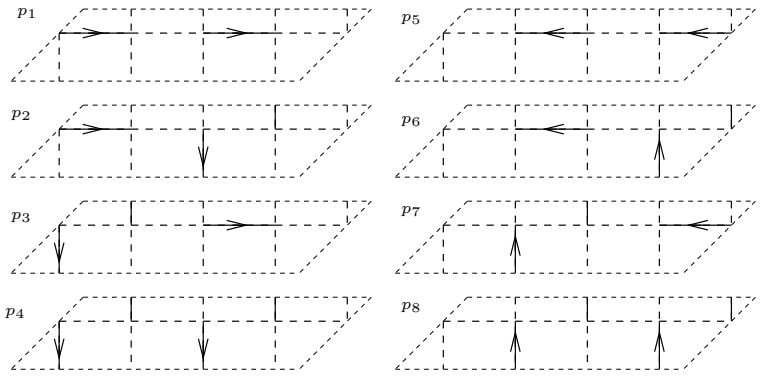

Figure 5.13: The eight perfect matchings for the dimer diagram of the double conifold.

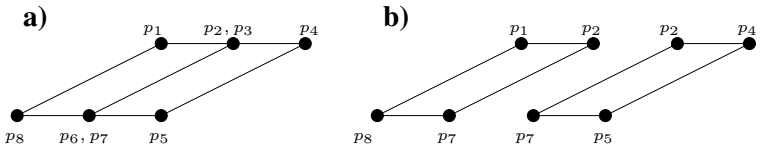

Figure 5.14: In a partial resolution, the original perfect matchings descending to perfect matchings of one or the other subdimer end up located at one or the other toric sub-diagram, as shown here for the resolution of the double conifold to two conifolds.

corresponding perfect matchings appear in the toric diagram of the remaining singularity. A different class of cycles is provided by p_1 and p_4, which give rise to one cycles that stretch from one conifold to the other, and are thus not present at the massless level. The interpretation of this in terms of the toric diagrams is that p_1 and p_4 end up in different sides. The last case is that of p_3 (and p_6). When combined with any of the other perfect matchings they give rise to one cycles that go from one singularity to the other, and thus are removed from the final configuration.

5.1.2 Gauge theory interpretation

Most of the concepts above can be given a meaning in the pure gauge analysis, showing that the dimer encodes a lot of nontrivial gauge theory information in a very simple way.

One thing that we have not checked until now because we lacked technology was that of the flatness of the resolutions we are considering. Namely, we have to make sure that switching on Fayet-Iliopoulos terms does not break the non abelian D-terms and the F-terms.

The easiest to discuss are the F-terms. According to the discussion in Appendix 5.1.1 in any resolution some of the original perfect matchings stay at one side of the toric diagram (meaning that all the corresponding edges

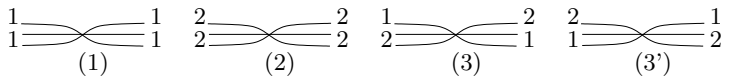

Figure 5.15: The four possible types of edges, classified according to the zig-zag paths meeting at the edge.

are either of type 3 or of type 1) and some others stay in the other side (so all the corresponding edges are of type 3 or 2). Now a basic fact that is easy to check using consistency of the zig-zag paths construction is that the existence of an edge of type 3 touching a node guarantees the existence of another edge of type 3 touching the node, so there are always at least two edges of type 3 if there is any. Also, if an edge if touched by edges of type 1 and 2, consistency of the resolution in terms of zig-zag paths again tells us that there are at least 2 edges of type 3 through any edge[3]. Remember that we were assigning the following set of vevs to the bifundamentals:

$$\Phi_1 = \begin{pmatrix} 0 & 0 \\ 0 & v \end{pmatrix}, \qquad \Phi_2 = \begin{pmatrix} v & 0 \\ 0 & 0 \end{pmatrix}, \qquad \Phi_3 = \begin{pmatrix} 0 & 0 \\ 0 & 0 \end{pmatrix}. \tag{5.2}$$

Then the existence of two edges of type 3 per node assures us that the F-terms conditions are satisfied, as they will always read $0 = 0$.

Nonabelian D-terms are more technical, but it can still be shown that they remain flat under the previous assignation of vevs.

As described previously, we divide the set of zig-zag paths into two disjoint sets, where each set admits a dual interpretation as the set of external legs in the web diagram that we take to infinity. Let us denote collectively the elements belonging to the first set as 1 and those belonging to the other set as 2.

Consider a given face in the dimer diagram, and orient its edges by running through them counterclockwise (this is just a convention). Each edge can then be classified into 4 types depending on which kind of zig-zag paths intersect over it. We will denote the four kinds as type 1, 2, 3 and $3'$, see Figure 5.15, where edges of type 3 and $3'$ are distinguished by the orientation[4].

In this fashion, we assign to each face a (periodic) string of symbols given by the kind of edges we encounter when traversing the face counterclockwise. A typical string will then look like:

$$\ldots 3'1323'3 \ldots$$

[3]In fact there are exactly two in any consistent resolution, as we will prove in Section 5.1.3. We will only need here that there are at least two.

[4]The similar notation for edges and zig-zag paths is introduced in order to (hopefully) improve the readability. In the rest of this section we mostly deal with edges, so this should not cause too much confusion.

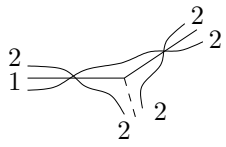

Figure 5.16: Inconsistent pasting of edges ($3'2$). Note that the only constraints come from the joining of the interior zig-zag paths. The exterior ones can be arbitrary as they do not need to be joined (in the absence of bi-valent nodes) since they "run off" along some extra edge, denoted by the dashed line in the drawing.

where we have written just the period. It is easy to realize that any valid string should satisfy a few rules which we can read from the dimer diagram. Namely there are some sequences of symbols that are not allowed, for example $3'2$. To see this, focus on the zig-zag paths "interior" to the edge. The given sequence would tell us that a type 1 zig-zag path exits the $3'$ vertex from the right, and then joins a type 2 zig-zag path in the next edge, see Figure 5.16. This is obviously not allowed. The other disallowed sequences are $13'$, 23, 31, 33, $3'3'$, 12 and 21.

We can then associate to the most general face in a dimer a sequence of symbols not containing these forbidden words. It is easy to convince oneself that in any such string, at least one of the following substitutions applies and gives rise to another consistent sequence with two symbols removed in the period ("$\cdot$" denotes the empty word):

$$\begin{array}{llllllll} 11 & \longrightarrow \cdot & ; & 22 \longrightarrow \cdot & ; & 33' \longrightarrow \cdot & ; & 3'3 \longrightarrow \cdot \\ 132 & \longrightarrow 3 & ; & 23'1 \longrightarrow 3' & & & & \end{array}$$

As an example, applying the rules one would get the following sequence of strings:

$$3'133'1132 \longrightarrow 3'11132 \longrightarrow 3'132 \longrightarrow 3'3 \longrightarrow \cdot$$

Since we can always apply one of these rules, and all of them reduce the length of the string by two, we have found that it is always possible to reduce an arbitrary string to nothing. The interesting fact about these operations is that on the field theory side they do not change the value of the D-term. Essentially, the first four rules preserve the D-term value because the disappeared edges correspond to a fundamental and an antifundamental with the same vev, hence with canceling contributions to the D-term. For the last two rules, the disappeared edges have vevs whose contributions add up to the trace of an $SU(N)$ generator, which is zero. What this means is that the value of the D-term for all possible faces in a dimer is given by the D-term of the empty sequence, which is equal to zero.

As an example, let us study the configuration depicted in Figure 5.17. The periodic string we associate with the face is given by $\ldots 223'132 \ldots$.

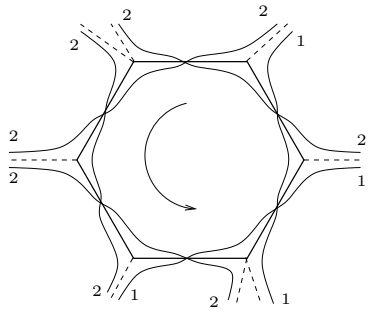

Figure 5.17: A possible face in a dimer, where we have indicated the relevant classification for the zig-zag paths. External edges are denoted by the dashed lines, and the arrow indicates the traversal direction used in the text when enumerating the edges.

Applying the rules we have described a possible reduction to nothing would be:

$$223'132 \longrightarrow 23'32 \longrightarrow 22 \longrightarrow \cdot$$

This proves that the D-term for the relevant gauge group vanishes.

5.1.3 Details of the massive sector

Here we will provide the detailed description in the gauge theory description of the set of states becoming massive in the partial resolution of the singularity. The discussion in this section follows mainly Appendix A in [46].

The following discussion will be slightly technical, so for clarity let us summarize here the main results we will obtain:

1. For each edge which disappears in the i^{th} daughter dimer diagram, there is a massive vector multiplet in the adjoint of the $U(N_i)$ gauge factor corresponding to that location (i.e. that arising from the diagonal of the gauge factors of the two faces the edge used to separate in the initial theory).

2. For each face in the original dimer diagram, we obtain two massive vector multiplets in the bi-fundamental $(N_1, \overline{N_2})$ and its conjugate, of the gauge factors at the corresponding location.

3. For each edge present in both daughter dimer diagrams, there is one $(N_1, \overline{N_2})$ chiral multiplet in the corresponding bi-fundamental representation (i.e. charged under faces separated by the edge) becoming massive. The dimer diagram ensures that globally, these types chiral multiplets pair up consistently to form massive scalar multiplets.

4. If the daughter dimer diagrams contain bi-valent nodes (nodes with two edges) the corresponding edges each describe a massive scalar multiplet in the bi-fundamental of the two faces they separate.

5. For each D7-brane passing through an edge of type 1 there is a massive scalar multiplet in the fundamental representation of the $U(N_2)$ gauge factor corresponding to the resulting recombined face. Similarly for edges of type 2. When there are N_7 D7 branes across such an edge the massive multiplet transforms as $(N_{D3}, \overline{N_7})$.

The detailed justification of these rules will be the subject of the rest of this section.

In a partial resolution, the dimer diagram leads to two daughter dimer diagrams. Denote F, E, V and F_i, E_i, V_i, $i = 1, 2$ the number of faces, edges and vertices in the initial and daughter diagrams. Recall they satisfy the Euler formulas $F - E + V = 0$, $F_i - E_i + V_i = 0$. Also, each daughter dimer diagram has the same vertices as the initial one, hence $V_i = V$. Finally, we denote N_i the number of D3-branes at the i^{th} daughter singularity, and $N = N_1 + N_2$ the initial number.

The number of gauge bosons becoming massive in the Higgs mechanism associated to the partial resolution (namely $U(N)^F \to U(N_1)^{F_1} \times U(N_2)^{F_2}$) is

$$\begin{aligned} n_V &= F(N_1 + N_2)^2 - F_1(N_1)^2 - F_2(N_2)^2 \\ &= (F - F_1)N_1^2 + (F - F_2)N_2^2 + 2FN_1N_2 \end{aligned} \tag{5.3}$$

The number of chiral multiplets which become massive is

$$\begin{aligned} n_{ch} &= E(N_1 + N_2)^2 - E_1(N_1)^2 - E_2(N_2)^2 \\ &= (E - E_1)N_1^2 + (E - E_2)N_2^2 + 2EN_1N_2 \end{aligned} \tag{5.4}$$

Of these latter, n_V of them are eaten by the massless vector multiplets to lead to massive vector multiplets. Using the Euler formulas and $V_i = V$ we have

$$(F - F_i) - (E - E_i) = F - E - (F_1 - E_1) = 0 \tag{5.5}$$

implying

$$F - F_i = E - E_i. \tag{5.6}$$

Hence $(E - E_i)N_i^2$ chiral multiplets are eaten by the $(F - F_i)N_i^2$ vector multiplets, and similarly $2FN_1N_2$ chiral multiplets out of the $2FN_1N_2$ are eaten by the corresponding vector multiplets. The remaining chiral multiplets, which are $2(E - F)N_1N_2 = 2VN_1N_2$ in number, pair up into massive scalar multiplets via superpotential terms as we show below.

Now, let us try to describe in detail how all the multiplets become massive. Consider first the $(F - F_1)N_1^2$ disappeared vector multiplets. The

disappearance is due to the fact that some faces in the initial diagram recombine in the first daughter diagram. They do so because there are $(E-E_1)$ edges which have disappeared, due to the vev of the $N_1 \times N_1$ block in the corresponding bi-fundamental. This shows that the $(F-F_1)N_1^2$ vector multiplets eat up the $(E-E_1)N_1^2$ chiral multiplets, leading to $F-F_1 = E-E_1$ massive vector multiplets in the adjoint of the $U(N_1)$ gauge symmetry of the corresponding recombined face. Similarly for the $(F-F_2)N_2^2$ vector and chiral multiplets. This is rule number **1** above.

In order to understand the additional $2FN_1N_2$ disappeared vector multiplets, it is useful to have a more precise picture of how the edges of a face in the initial diagram can behave. Notice that for a given face in the original dimer diagram, it is impossible that all edges are of type 3 (present in both sub-dimers). If all edges in a face would be of type 3, and given the fact that at each node there can only be two edges of type 3 (this will be proven below), then that face would correspond to a cycle on the Riemann surface wrapping the new puncture G coming from the resolution. However, since this cycle corresponds to a face in the dimer, its (p,q) charge would be zero, which is impossible. Thus every face has to have at least two edges which are not of type 3, so either two edges of the face are of type 1, i.e. disappear from sub-dimer 2, (or two are of type 2) or one edge is of type 1 and another of type 2 (see Figure 5.18). We denote these two cases (a) and (b).

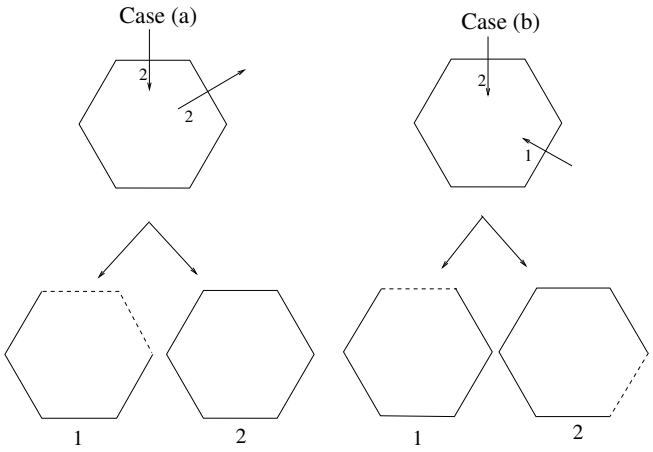

Figure 5.18: Two possible configuration of edges for a face.

The $2FN_1N_2$ disappeared vector multiplets arise from open strings stretching between subdimers 1 and 2, at the same face location in both. They become massive by eating up chiral multiplets associated to open strings stretching between both sub-dimers, across disappeared edges. In case (a), the coupling occurs as shown in Figure 5.19.

The vector multiplets (shown as wavy arrows) A_{12} and B_{21} couple to the

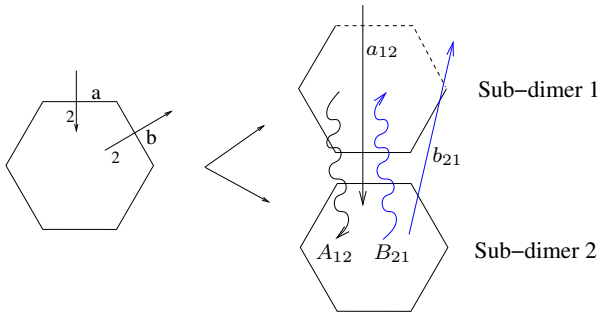

Figure 5.19: Coupling between chiral and vector multiplets for the case when a face has two edges of the same type.

chiral multiplets a_{12} and b_{21} respectively (which stretch across edges a and b respectively). In case (b), the coupling occurs as shown in Figure 5.20.

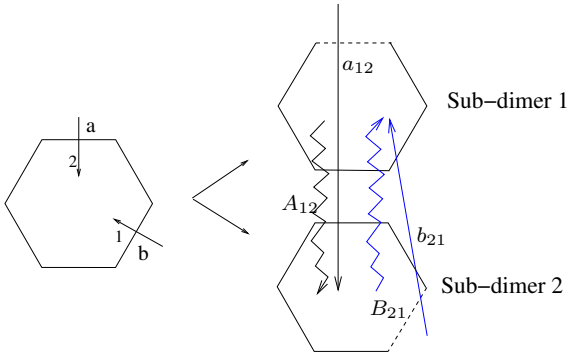

Figure 5.20: Coupling between chiral and vector multiplets for the case when a face has one edge of each type.

The vector multiplets A_{12} and B_{21} couple to a_{12} and b_{21} respectively. a_{12} and b_{21} stretch across edges a and b respectively. This can be easily generalised to a face with an arbitrary assignation of edges. The above discussion shows that for each face in the original dimer diagram, we obtain two massive vector multiplets in the bi-fundamental $(N_1, \overline{N_2})$ and its conjugate, of the gauge factors at the corresponding location. This is rule number **2** above.

Let us now consider the remaining $2(E - F)N_1N_2 = 2VN_1N_2$ chiral multiplets. As we show, they become massive due to the V superpotential terms. These chiral multiplets arise from open strings stretching between the two dimer diagrams (with both orientations), across edges of type 3. The fact that each superpotential term leads to a mass for a chiral multiplet in the $(N_1, \overline{N_2})$ and $(\overline{N_1}, N_2)$ (of the faces separated by the corresponding

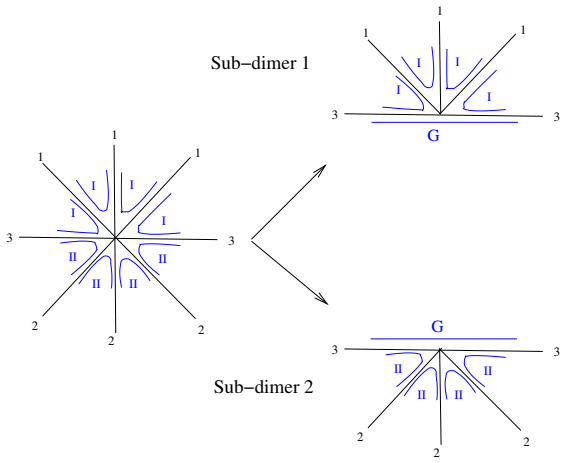

Figure 5.21: Resolution for the case when only two edges at a given node are of type 3. G represents the new puncture which arises in the resolution

edge) follows from the fact that each node has necessarily two edges of type 3, as we show below. In other words, all fields in the superpotential term, except the two chiral multiplets, acquire vevs, leading to a mass term for the latter. Hence one recovers rule number **3** above.

The property that each node necessarily has two edges of type 3 can be shown as follows. In a partial resolution, the zig-zag paths of the original dimer diagram are split in two sets I and II. That is, the daughter dimer diagram 1 is obtained by removing the zig-zag paths II and adding the zig-zag path G which correspond to the new puncture. Similarly for dimer diagram 2, with the zigzag G being the same but with opposite orientation. Now, at each node, two edges of type 1 and 2 have to be separated by at least one edge of type 3. A little thought shows that if there are more than two edges of type 3 at any given node, the zig-zags G in both subdimers cannot be the same. This is illustrated in Figures 5.21 and 5.22. In the first figure one sees that when only two edges of type 3 are present at a given node, then they separate the graph into two regions of type 1 and 2 respectively. Now, in the daughter dimer diagram 1 (resp. 2) all edges of type 2 (resp. 1) are absent. Hence the zigzag G of the new puncture passes through the boundary of region 1 (resp. 2), consistently leading to the same G with opposite orientation in the two diagrams. The situation for a node with more than two edges of type 3 is shown in Figure 5.22. Since it clearly leads to paths G which are not the same in the two dimer diagrams, we conclude that such node structure is not possible.

One small subtlety is that for a given edge of type 3, there are actually two chiral multiplets becoming massive. These correspond to open strings stretching across this edge and going from the first daughter dimer diagram

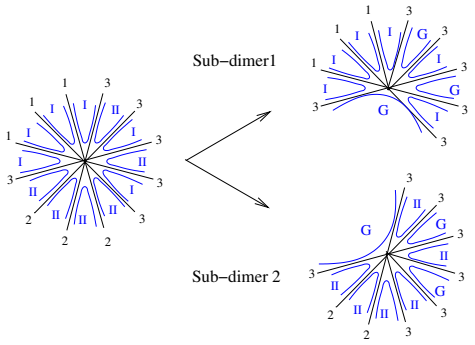

Figure 5.22: Resolution for the case when more than two edges at a given node are of type 3. G represents the new puncture which arises in the resolution.

to the second and vice-versa. Each superpotential term pairs only one of these chiral multiplets (coupling it to only one of the chiral multiplets in the other adjacent type 3 node). And for a given edge of type 3, both modes acquire mass thanks to the two superpotential terms at the nodes of the edge.

Rule number **4** just encodes the trivial fact that a quadratic term in the superpotential (i.e. a bivalent node in dimer language) is a mass term for the involved fields.

Including D7-branes

So far we have described all rules except for the last one, rule number **5**. In order to obtain this last rule we should recall the description of the D7 flavor branes in terms of the dimer construction, which we review in Appendix C.4. D7 branes are represented as segments across an edge in the dimer diagram (leading to 37, 73 states coupling to the corresponding 33 bi-fundamental in the D3-brane gauge theory).

The rules for the massive spectrum can be easily read from the Riemann surface description. Namely, we resolve by separating the Riemann surface into two parts determined by the punctures contained in them. When a D7 stretches between two punctures located in different factors of the resulting resolved geometry it survives in both subdimers. This can be intuitively understood since the D7 smoothly deforms into (from the point of view of one of the factors in the resolution) a D7 that goes from one of the original punctures into infinity along the new puncture that arises when resolving. This configuration is as supersymmetric as the original configuration, so it remains in the final dimer configuration. The gauge theory picture supports this intuitive derivation, see below.

If the D7 stretches along punctures that go to the same factor of the resolution then it disappears from the theory describing the gauge theory

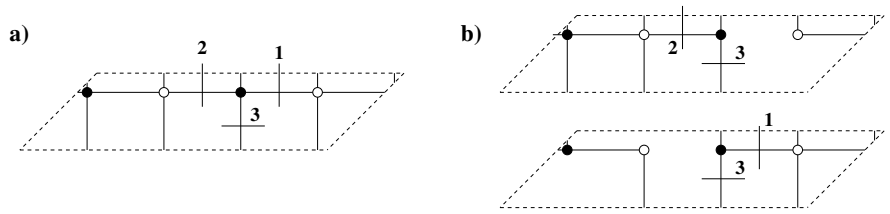

Figure 5.23: The fate of different D7-branes in a partial resolution. D7-branes associated to edges of type 1 resp. 2 become D7-branes absent in the first resp. second dimer diagram, hence passing through the second resp. first daughter singularity. For type 3 edges, the D7-branes remains in both daughter dimer diagrams, hence passes through both daughter singularities.

on the D3s located at the other remaining singularity.

These rules can be described in an equivalent way by focusing just in the dimer diagram and talking in terms of edges. The rules are then:

- When the D7 intersects an edge of type 3 it survives in both subdimers.
- When the D7 intersects an edge of type 1 or 2 it only survives in the corresponding subdimer.

So we have that the D7 survives when the associated edge in the dimer diagram survives. This can also be seen from the gauge theory, where a 33 vev turns the cubic coupling 73-33-37 into mass terms for the 37 open strings. Rule number **5** is a simple restatement of these facts. In Figure 5.23 we illustrate these matters in the case of the double conifold resolution.

5.2 Deforming the singularity

In some cases there is another way to smooth a toric singularity. The case of the conifold is illustrative again. As reviewed in Appendix B the conifold is topologically a real cone over $\mathbf{S}^3 \times \mathbf{S}^2$, and the singularity corresponds to the case where both spheres collapse to zero size at the origin of the cone. Resolving the singularity corresponds to making the $\mathbf{S}^2$ finite in size, but it is also possible to make the 3-sphere finite in size in the base, and this also smooths out the singularity. This is called a complex deformation, and it is described in more detail in Appendix B.3.2. In terms of the description of the conifold as a subvariety of $\mathbb{C}^4$, resolution corresponds to adding a Fayet-Iliopoulos term:

$$|z_1|^2 + |z_2|^2 - |z_3|^2 - |z_4|^2 = \xi, \tag{5.7}$$

while the complex deformation corresponds to:

$$z_1^2 + z_2^2 + z_3^2 + z_4^2 = \epsilon, \tag{5.8}$$

where ϵ is some complex number we can choose to be real positive by redefining the coordinates.

Physically, deformation is triggered by adding fractional branes to the system. Fractional D3 branes can be understood as D5 branes in collapsed 2-cycles (such as the one in the base of the conifold). In some cases these branes trigger a geometrical transition such that the 2-cycle the fractional brane was wrapping disappears, a finite size 3-cycle appears instead and the brane is converted to 3-form flux in the cycle. The case of the conifold has been studied in [89], and generalized to arbitrary toric singularities in [90], see also [79].

This process can also be nicely described in terms of the gauge theory living in the world volume of the D3 branes. Putting fractional branes corresponds to changing the ranks of the gauge factors in an anomaly free way such that the beta functions no longer vanish. In the case of "deformation branes" (in the sense of [79], the fractional brane of the conifold is one example) the resulting dynamics of the gauge theory triggers a quantum deformation of the moduli space in the infrared[5], such that the moduli space is described again by equation 5.8.

As the last and simplest description of the complex deformation we have the description in terms of web diagrams. It corresponds to separating the original web diagram into two subwebs in equilibrium. In the dual description as a toric diagram, it corresponds to decomposing the original toric diagram into a Minkowski sum [91].

For clarity we will discuss the case of the complex deformation of the double conifold into a conifold. The derivation of the result is clearest from the point of view of the Riemann surface. There the deformation brane wraps a one cycle in such a way that Σ is divided into two regions and the complex deformation is represented by contracting this one cycle into a point in such a way that we separate the Riemann surface into two pieces, they corresponding to the two remaining singularities after the deformation (in our case one of the "singularities" is just flat space, so the resulting singularity is just given by the conifold). We can read the effect of the deformation in the gauge theory by following which edges and vertices go to which side of the resulting surface. This procedure turns out to reproduce the heuristic method described in [79]. An equivalent way of phrasing the procedure is saying that we cut the Riemann surface and then glue the boundaries. The double conifold example is in Figure 5.24. The web diagram description can be found in Figure 5.25.

The discussion in terms of dimer diagrams follows from the mirror picture in quite a straightforward way. In particular we can easily read the new set of edges, the superpotentials and the faces. An easy way to organize all this information without the complication of visualizing the Riemann surface

[5] I.e., in the infrared we have $N_f = N_c$ in the usual Seiberg classification.

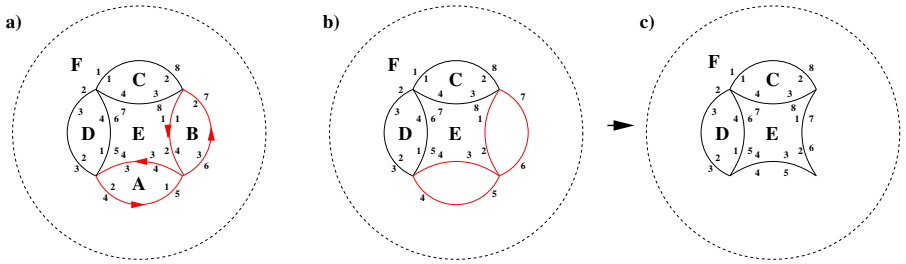

Figure 5.24: The geometric transition in the mirror. (a) The fractional brane defines a one cycle in the Riemann surface. (b) We cut along this one cycle. (c) Gluing the boundaries of the daughter Riemann surface then gives us the resulting conifold geometry after integrating out the massive mode.

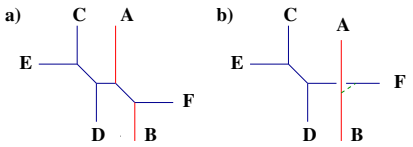

Figure 5.25: Complex deformation of the double conifold into a conifold singularity.

consists of reading the adjacency relations we have to impose in order to do the gluing of the Riemann surface. The result for the double conifold is shown in Figure 5.26, where we also show the zig-zag paths (a proper identification of these greatly facilitates the gluing in practice, although they are not strictly needed according to the procedure we have given).

The case of dP_3

Let us study a slightly more involved geometry we are already somewhat familiar with, namely the complex cone over the third del Pezzo surface, or dP_3 for short. We have shown the dimer diagram for this geometry in Figure 5.10, and the set of zig-zag paths in Figure 5.11. We will introduce a fractional brane that increases the rank of the gauge factors 1, 3 and 5 by the same amount. The gauge theory analysis of [90] tells us that a complex deformation of the moduli space is triggered in this case.

According to the procedure described above, the first thing one should do consists of building the one cycle in the Riemann surface given by the fractional brane. This is done in Figure 5.27. We see that the cycle separates the Riemann surface into two patches with the topology of discs.

Let us focus on the punctures F, D and B. One finds the final Riemann surface by cutting out the FDB triangle and contracting its boundary to a point. We see that we get a two sphere, as expected since the resolution we are considering, looking to the set of zig-zag paths remaining (see Figure 5.28), should give flat space, which has genus 0.

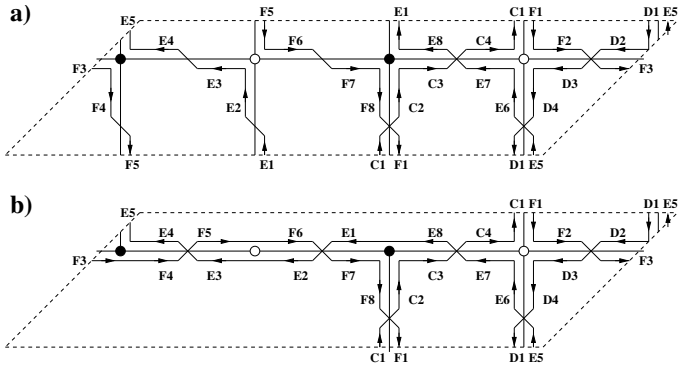

Figure 5.26: a) Zig-zag paths of the original dimer corresponding to the punctures in Σ. b) The closing of the open boundary to get the resulting mirror geometry implies adjacency relations that allow to reconstruct the edges of the dimer diagram associated to the D3-branes in the complex deformed geometry. In this case we recover the dimer diagram of a conifold, as expected from a complex deformation of the double conifold, see Figure 5.25.

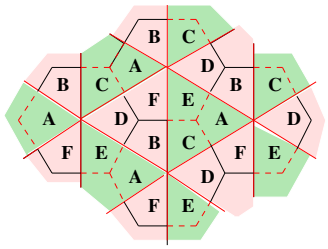

Figure 5.27: The mirror Riemann surface for dP_3 is a torus with six punctures, which is depicted as a periodic array (the fact that it formally looks like the original dimer diagram is accidental, and not true for a general singularity). The total 1-cycle that corresponds to the fractional brane in the discussion corresponds to a triangular path enclosing the punctures A, C, E. It separates the Riemann surface in two pieces, shown in different color, each with the topology of a disk.

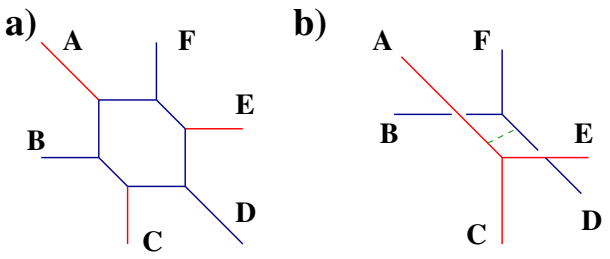

Figure 5.28: Complex deformation of the cone over dP_3 to a smooth space. The sub-webs describing the left over singularities actually describe two copies of (locally) flat space.

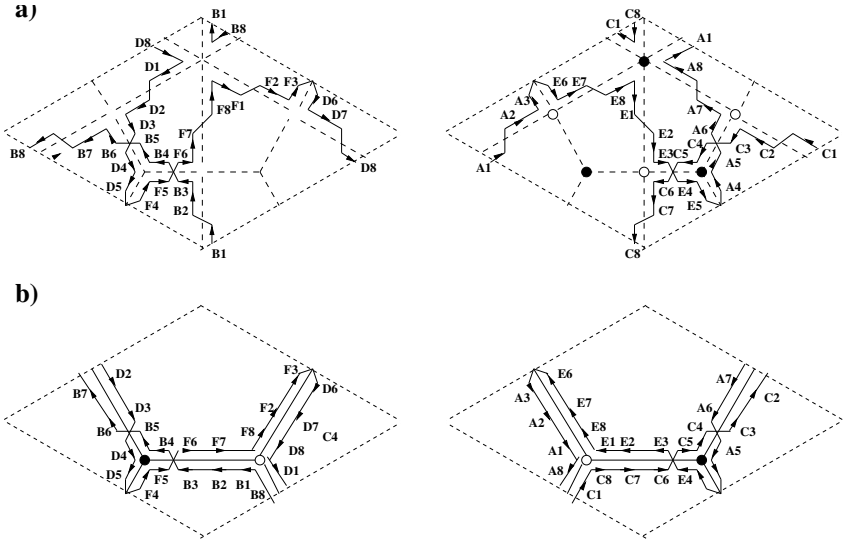

Figure 5.29: The effect of the complex deformation on the dimer diagram of dP_3. Figure a) shows the two sets of zig-zag paths corresponding to the two pieces of Riemann surface obtained after cutting along the 1-cycle defined by the fractional brane discussed in the main text. Figure b) shows the new zig-zag paths obtained upon imposing the adjacency relations implied by the gluing of boundaries of the Riemann surfaces. Notice these adjacency relations are completely natural from the viewpoint of zig-zag paths; they simply amount to pairing unpaired pieces in a consistent way.

The interpretation of this operation in the dimer is not difficult once one has described the action on Σ. We show it in Figure 5.29.

There are a couple of complementary observations we can make from the Riemann surface interpretation. First, according to the analysis in [79], there exist different types of fractional branes according to their infrared behavior. In particular only one kind trigger an infrared deformation of the moduli space. In the Riemann surface picture this is easy to see, deformation branes are those that divide the Riemann surface into two sets such that the sum of the (p, q) charges in each side adds up to 0. The deformation is then represented by cutting along the one cycle, as we have described. The other types of branes do not allow for this.

The second observation relates to the rule that a deformation is described in terms of web diagrams as dividing the web in two subwebs in equilibrium. This can be easily seen in the Riemann surface. The one-cycle along which we cut the Riemann surface divides the set of punctures into two sets. In our construction, punctures have an associated (p, q) charge given by the homotopy charge of the corresponding zig-zag path in the dimer diagram. The other property we need to show equilibrium is that the (p, q) charge of a one-cycle in the Riemann surface is given by the sum of the charges of the

punctures it surrounds. Since the fractional brane one-cycle is contractible by construction in the remaining geometry, this shows that the two sets of legs have (p, q) charge zero.

5.2.1 Perfect matchings

It is possible to study the deformation process in terms of perfect matchings as we did for the resolution. This gives a nice link with the mathematical literature [92, 93], which associates complex deformations of the geometry with decompositions of the toric diagram into Minkowski sum components[6]. We will show it in detail for the case of dP_3, the general case is easy to study.

The basic idea is studying where do differences of perfect matchings, which define one cycles in Σ, go under the complex deformation. In particular, in order to find the relative position of two perfect matchings p_i and p_j in one of the resulting sub-singularities one cuts along the fractional brane and contracts the border to a point. This might have changed the (p, q) charge of the one-cycle defined by the difference of perfect matchings, as some of the punctures it used to surround no longer exist in the daughter geometry. One just draws the resulting cycle in Σ and adds up the (p, q) charges of the punctures it surrounds. This will give the relative position vector (perhaps rotated 90 degrees depending on convention, as explained before) for the two perfect matchings in the toric diagram.

In practice, the above procedure, despite being unambiguous, is hard to visualize sometimes. There is a simplified procedure that also gives correct results, although in some cases it might not be applicable. In the cases we found only the simplest deformations could not be analyzed with this last method, but in these cases tracing the physics in the Riemann surface is simple enough.

The basic idea is the following: one looks in the dimer to the cycle defined in the original geometry and performs the pasting in the dimer as explained above (one particular example is Figure 5.26). When pasting edges one is defining equivalence relations between the edges, which one can then lift to equivalence classes of perfect matchings in the natural way. Once one has the equivalence classes, we just draw the corresponding toric diagram starting from the original one and drawing at the same position equivalent matchings.

Either way one decides to do it, the steps are similar. First one has to identify the perfect matchings. We do it for one phase of dP_3 in Figure 5.30. We also illustrate the location of the perfect matchings in the toric diagram in Figure 5.31. Applying the method of equivalence classes, one then obtains the geometry after the deformation. The result is shown in Figure 5.32, where we see how we recover the web diagram of flat space, meaning that

[6]The Minkowski sum consists essentially in "sliding" one of the terms in the sum along the edges of the others. See the Appendix in [79] for a better explanation with drawings.

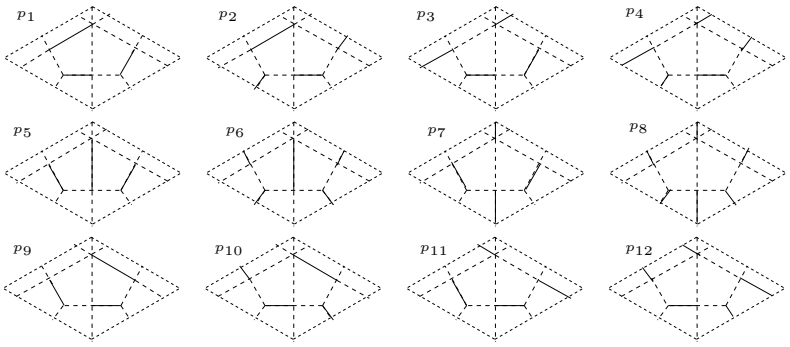

Figure 5.30: Perfect matchings for the dimer of dP_3, shown in 5.10.

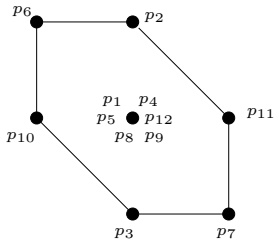

Figure 5.31: Location in the toric diagram of dP_3 of the perfect matchings of Figure 5.30.

the resulting geometry is smooth (since the other part of the Riemann surface is similar).

5.2.2 Gauge theory interpretation

Complex deformations of the geometry are related to the introduction of fractional branes and thus duality cascades, as described in [90]. In the gauge theory description a fractional brane appears an anomaly-free assignation of ranks of the gauge factors such that not all ranks are equal. The fractional brane for the conifold, for example, is given by the gauge group $SU(2M) \times SU(M)$ instead of the usual $SU(M) \times SU(M)$. This is usually denoted simply by giving the rank vector $(2M, M)$. The different ranks make the β function no longer vanishing, and in the infrared a quantum deformation of the moduli space occurs[7].

Let us study in detail the case of the double conifold being deformed to the conifold from the point of view of the gauge theory. We will phrase the

[7] This happens only for some types of fractional branes, called *deformation* branes [79]. The other possible types of fractional branes are *DSB* branes, which lift the vacuum due to an ADS superpotential (they were the focus of Chapter 4), and $\mathcal{N} = 2$ branes, for which supersymmetric directions still remain, corresponding to flat directions in which the fractional brane can move.

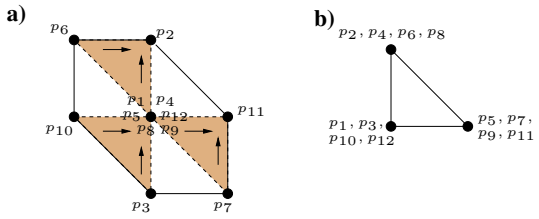

Figure 5.32: a) The location of the equivalence classes of matchings describes the toric diagram of the first daughter geometry. In this case we recover the toric diagram of a smooth space, precisely the dual of the sub-web diagram corresponding to the legs B, D, F in Figure 5.28. Notice that all matchings in each vertex are equivalent (so their real multiplicity in the toric diagram is 1. b) The equivalence relation between perfect matchings can be regarded as the contraction of certain triangles in the toric diagram.

description in terms of dimer diagrams, since many gauge theory phenomena admit a nice pictorial description in this language. The easiest way to see the resulting geometry is studying the gauge theory on the world volume of probe D3 branes, this is what we will be doing in the following.

The fractional brane and D3 probe system we will consider is given by the rank vector $(M, 2M, M, M)$. The corresponding dimer appears in Figure 5.33a. With this assignation of ranks, the second factor runs fastest, and confines first when we run towards the IR (we start from equal couplings). The IR theory can then be described by Seiberg dualizing this second factor. This is shown in Figure 5.33b, where we describe the theory in terms of mesons of the second factor[8]. A quick counting shows that we are in the $N_f = N_c$ case, so the nontrivial geometry of the moduli space is to be found in the mesonic branch. This means that we can ignore the baryons in what follows, just setting them to 0. The standard analysis tells us that the moduli space is deformed quantum mechanically from the classical constraint $\det \mathcal{M} = 0$ into $\det \mathcal{M} = \epsilon$ (typically ϵ is some power of the dynamical scale Λ of the theory.). We recognize the equations for the deformation of the double conifold, where the moduli space is parametrized by the mesonic vevs (which are good variables, according to geometric invariant theory). This is manifest in the $M = 1$ case, where the mesons become complex numbers.

One can in fact follow all the previous discussion in terms of the dimer diagram. Once the confining factor has confined and we can describe the theory in the Seiberg dual phase (Figure 5.33c) the remaining quantum deformed superpotential appears as shown in Figure 5.33d. The resulting tiling is no longer a tiling of the torus, as some edges cross without intersecting. This is a reflection of the fact that a deformed toric geometry is no longer toric. In order to satisfy the quantum constraint we have to give vevs to some mesons, we have done it for the mesons describing the flat space sector

[8]This is similar to the description of Seiberg duality in terms of dimers, see [94].

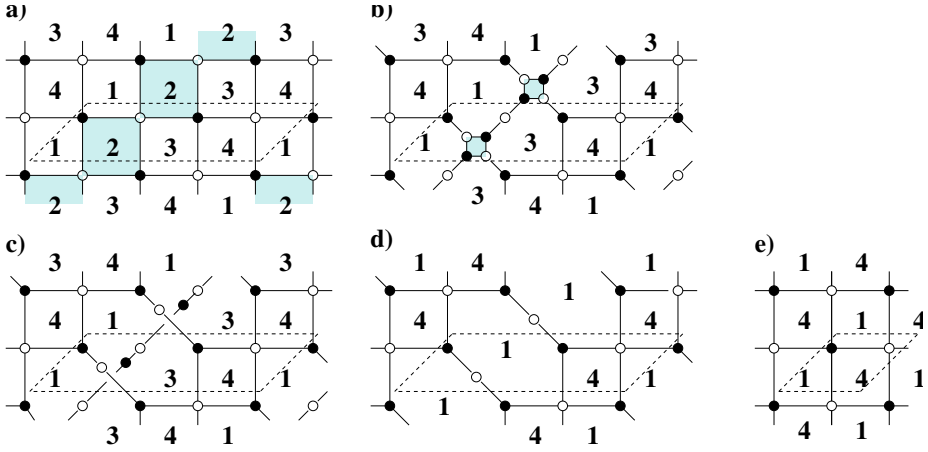

Figure 5.33: Dimer diagram representation of the gauge theory analysis of D3-branes probing the complex deformation of the double conifold to the conifold. (a) shows the fractional branes upon consideration. In (b) we introduce the mesons of the corresponding gauge factor. In (c) the gauge factor of the fractional branes confines and disappears. They leave behind a non-perturbative contribution to the superpotential of the mesons, implementing their quantum deformed constraint. The fact that the deformed space is not a toric variety is reflected by the fact that the dimer diagram is 'non-planar' with edges passing through each other without intersection. In (d) we show the dimer diagram obtained when some mesons acquire a vev to saturate the quantum constraint. The resulting dimer diagram is equivalent to (e), which corresponds to the conifold theory.

of the deformation. This means that we are focusing on the conifold part. As we can see in Figure 5.33d, the resulting dimer does indeed describe the conifold.

We can do the same analysis for the case of dP_3 being deformed into flat space, this is shown in Figure 5.34.

Another thing to note is that all this analysis nicely matches the discussion in terms of zig-zag paths. Namely, the rules for pasting edges are exactly those we use for constructing mesons. Confinement is described by the removal of the zig-zag paths that bound the confining face. This process leaves some edges with only one zig-zag path, which we proceed to paste, as described in the previous sections, in order to obtain a consistent dimer. It is easy to realize, for example by studying any particular example, that the consistent pasting is given by the construction of the appropriate mesons for the confining faces.

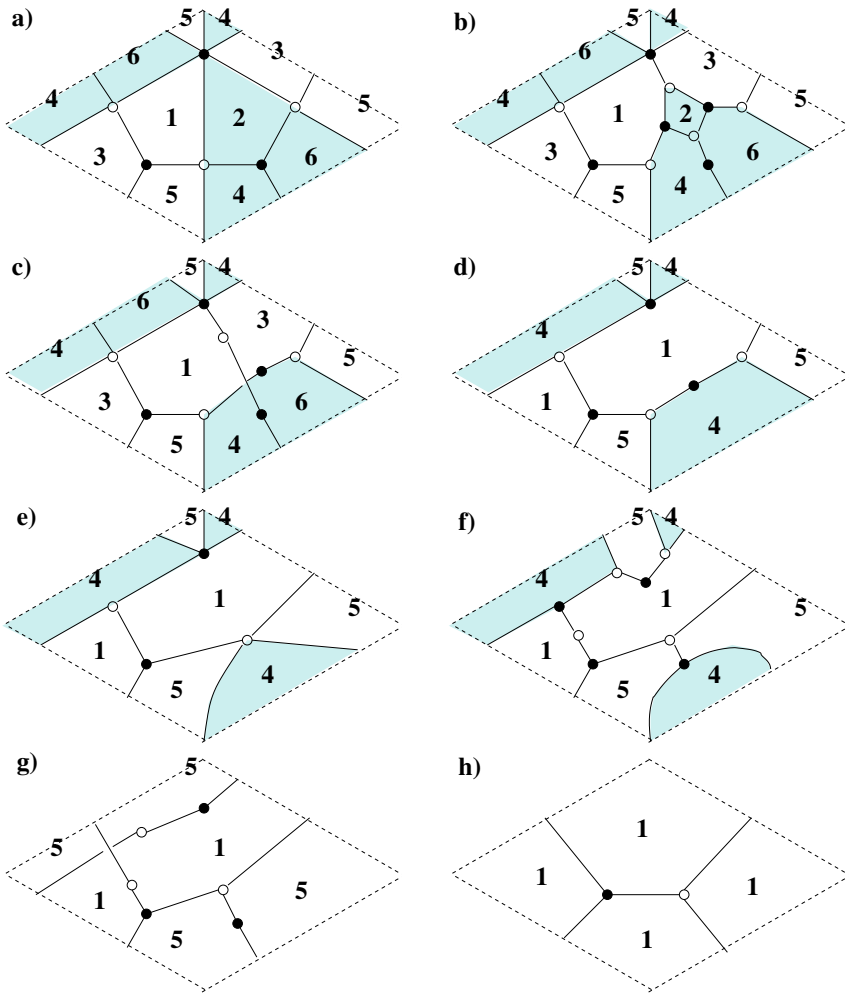

Figure 5.34: Dimer diagram representation of the gauge theory analysis of D3-branes probing the complex deformation of the cone over dP_3 to a smooth geometry. (a) shows the fractional branes upon consideration. In (b) we introduce the mesons of the gauge factor 2. In (c) the gauge factor 2 confines and induces a non-perturbative superpotential (associated to the quantum constraint on the mesons). In (d) the quantum constraint is saturated by giving vevs to certain mesons, which break the gauge factors 1 and 3, and 4 and 6, to their diagonal combinations, respectively denoted 1 and 4 in the following. After integrating out one bi-valent node (e), the gauge factor 4 has $N_f = N_c$, so we introduce its mesons (f). In (g) the gauge factor 4 confines and induces a non-perturbative superpotential. After giving vevs to some mesons, and integrating out bi-valent nodes, we obtain the dimer diagram (g), corresponding to D3-branes in a smooth geometry.

Chapter 6

Continuity of nonperturbative effects

We have shown in Chapter 4 how to engineer metastable vacua by putting branes at toric singularities. D7 branes enter in an essential way by providing the string realization of the light flavors in the ISS construction. In Chapter 7 we will show how to join together local models with such features in order to construct interesting scenarios of gauge mediated supersymmetry breaking.

Nevertheless, this setup has the unpleasant feature of requiring that some parameters entering the construction are unnaturally small in order for our approximations to be justified. The ISS setup requires flavor masses much smaller than the dynamical scale of the theory in order for the approximations to be well controlled, and the metastable vacuum long-lived.

Such unnaturally small parameters in the superpotential can be rendered natural if they appear dynamically, that is: they are absent at tree level (and by supersymmetric non renormalization theorems, absent at all loops) but appear as a consequence of nonperturbative effects. The nonperturbative effects we will be focusing on will be D-instantons. These are D-branes localized in the spacetime directions and extended in the internal space. For completeness we have included a short review of D-instanton physics in Appendix D. The reader unfamiliar with the recent D-instanton literature is advised to read this appendix before entering the following sections. In Appendix D.4 we review a simple example, originally studied in [55], where D-instantons generate mass terms dynamically in a theory describing D-branes in a toric singularity.

The question which we will be answering in this chapter concerns the continuity of the nonperturbative terms generated by the D-instantons when the moduli of the geometrical background are varied. In particular, as one moves in complex structure moduli for a type IIA local Calabi-Yau geometry (such as the ones we will be considering), one finds that D-instantons might decay into two (or more). We will see many explicit examples of this later in

the chapter. The important point here is that, if the complete superpotential is continuous in closed string moduli space as holomorphicity arguments suggest, then the decay products must interact in such a way as to reproduce the effect of the original single instanton. We will find that this is indeed the case in the configurations we study. This phenomenon was well known in the $\mathcal{N} = 4$ and $\mathcal{N} = 2$ literature, but here we will be finding multi instanton processes in the $\mathcal{N} = 1$ context, a region relatively unexplored so far.

Let us note at this point that the usage of *perturbative* and *nonperturbative* in this chapter refers always to the string coupling, matching the usage in field theory. Nonperturbative corrections in α' are also important, and in fact give rise, via disk diagrams with appropriate insertions of boundary changing operators, to some perturbative (in g_s) couplings between the massless open string modes. These couplings will play a key role in our discussion.

This discussion about continuity of the nonperturbative superpotential is somewhat orthogonal to the model building considerations of the rest of this work, and of independent theoretical interest by itself. We have included it here in the belief that it will be of relevance for many detailed model building proposals incorporating D-instanton effects.

Let us make a last remark before entering into details. D-instantons with too many zero modes to contribute to the superpotential typically induce higher F-terms. Whether these are continuous under instanton decay and recombination is also an interesting question which we do not answer here. Nevertheless, we will find that these higher F-terms play an important role in our discussion.

This chapter is organized as follows. We start in Section 6.1 by shortly reviewing the main properties of the local geometries we will be playing with. In Section 6.2 we discuss continuity of non-gauge instanton effects under instanton decay and recombination. In Section 6.3 we turn our attention to the more familiar but technically more challenging gauge instantons. In Section 6.4 we blur a bit the distinction between these two kinds by showing how motions in moduli space can turn continuously non-gauge instanton effects into gauge nonperturbative dynamics, and vice versa. We finish in Section 6.5 by discussing some implications of the discussions in this chapter for F-theory compactifications.

6.1 Ooguri-Vafa geometries

Here we describe a set of geometries which we will use in several of our explicit examples below. They are non-compact geometries, but they suffice to study instanton effects and transitions as long as they involve just the local structure of compact cycles (see footnote 8 for one example where non-compactness is relevant to the discussion).

Let us consider the following class of local Calabi-Yau manifolds, described by:

$$\begin{aligned} xy &= \prod_{k=1}^{P}(z-a_k) \\ x'y' &= \prod_{k'=1}^{P'}(z-b'_k) \end{aligned} \tag{6.1}$$

This kind of geometry is a particular case of those considered in [95]. It describes two $\mathbb{C}^*$ fibrations, parametrized by x, y and x', y', varying over the complex plane z, degenerating at the locations a_i, b_i respectively. In this geometry on can construct Lagrangian 3-cycles by considering segments joining pairs of degeneration points on the base, and fibering the two $\mathbb{S}^1$'s in the two $\mathbb{C}^*$ fibers. Segments joining pairs of a-type degenerations or pairs of b-type degenerations lead to 3-cycles with topology $\mathbb{S}^2 \times \mathbb{S}^1$. Segments joining a- and b-type degenerations lead to 3-cycles with topology $\mathbb{S}^3$. Let us introduce the notation $[p_1, p_2]$ for the 3-cycle associated to the pair of degeneration points p_1, p_2, whatever their type.

Introducing the holomorphic 3-form

$$\Omega \;=\; \frac{dx}{x}\,\frac{dx'}{x'}\,dz \tag{6.2}$$

the 3-cycle $[p_1, p_2]$ is calibrated by the form $e^{i\theta}\Omega$, where θ is the angle of the segment $[p_1, p_2]$ with the real axis in the z-plane. Namely $Im(e^{i\theta}\Omega)|_{[p_1,p_2]} = 0$, where $|_{[p_1,p_2]}$ denotes restriction to the 3-cycle. Hence, segments which are parallel in the z-plane define 3-cycles which preserve a common supersymmetry. We will be interested in configurations where all degenerations are on (or near) the real axis.

We will consider stacks of 4d space filling D6-branes and/or euclidean D2-branes wrapping the different 3-cycles, and describe the nonperturbative superpotentials arising from these configurations. The open string modes and their interactions are easy to determine. For instance, each stack of N D6-branes on a 3-cycle leads to a $U(N)$ gauge group in a vector multiplet of $\mathcal{N} = 1$ supersymmetry for 3-cycles of $\mathbb{S}^3$ topology, and of $\mathcal{N} = 2$ supersymmetry for 3-cycles of $\mathbb{S}^2 \times \mathbb{S}^1$ topology. The angle θ introduced above determines the precise supersymmetry preserved by the corresponding set of branes. Also, two D6-branes wrapping two 3-cycles involving one common degeneration point lead to a vector-like pair of bi-fundamental chiral multiplets, arising from open strings in the intersection of 3-cycles (which is topologically $\mathbb{S}^1$, coming from the $\mathbb{C}^*$ that does not degenerate at the intersection).

As discussed in [95] one can perform T-dualities along the two $\mathbb{S}^1$ directions, and map the configuration to a Hanany-Witten setup of P NS-branes

(along 012345) and P' NS'-branes (along 012389), with D4-branes (along 01236) suspended among them, in a flat space geometry with a noncompact x^6 direction (in contrast to the usual Hanany-Witten configurations describing systems such as the conifold). The gauge theory content described above follows from the standard rules in this setup (see [27]). This picture also facilitates the computation of the superpotential, whose general discussion we skip, but which we present in our concrete example below.

6.2 Non-gauge D-brane instanton effects

In this section we consider "exotic" D-brane instantons (i.e. instantons arising from D-branes wrapping internal cycles different from those wrapped by the spacetime filling branes in the model). For simplicity we restrict ourselves to perturbative type IIA Calabi-Yau compactifications in the absence of fluxes. The aim of this section is to show the continuity of the nonperturbative superpotential across the lines of marginal stability for the instantons. We show that the microscopic mechanism underlying this continuity reveals interesting new properties of D-brane instanton physics, including multi-instanton processes and nonperturbative lifting of fermion zero modes.

As we review in Appendix D, in perturbative type II models (and in the absence of additional ingredients like 3-form fluxes), for instantons to have just the two fermion zero modes required to contribute to the superpotential they should be mapped to themselves under the orientifold action and have an $O(1)$ Chan-Paton symmetry. This constrains the possible splittings of the instanton in walls of marginal stability, for instance an $O(1)$ instanton cannot split into two $O(1)$ instantons, as we show in Section 6.2.3. Still, there is enough freedom to have non-trivial splitting of instantons that contribute to the superpotential, as we now discuss in some simple examples.

6.2.1 $O(1)$ instanton splitting as $O(1) \times U(1)$ instantons

Configuration and marginal stability line

In this section we consider one simple example of an $O(1)$ instanton A, which contributes to the nonperturbative superpotential, and can reach a line of marginal stability on which it splits as an O(1) instanton B and a $U(1)$ instanton (described as a brane C and its image C').

Consider a geometry of the kind introduced in Section 6.1, with two degenerations a_1, b_1 located at $z = \pm t/2$, with $t \in \mathbb{R}$, and two degenerations a_2, b_2 located at $z = \pm s/2 + i\epsilon$, with $s, \epsilon \in \mathbb{R}$, and $s < t$ for concreteness, see Figure 6.1. Namely

$$\begin{aligned} x^2 + y^2 &= (z + t/2)(z - s/2 - i\epsilon) \\ x'^2 + y'^2 &= (z + s/2 - i\epsilon)(z - t/2) \end{aligned} \tag{6.3}$$

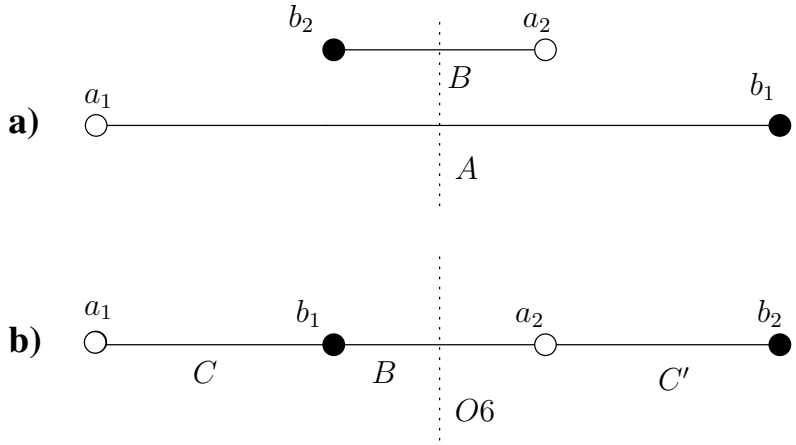

Figure 6.1: Example of an $O(1)$ instanton A (figure a) splitting into an $O(1)$ instanton B and a $U(1)$ instanton C and its image C' (figure b).

Consider modding out the geometry by the orientifold action $\Omega R(-1)^{F_L}$, where R is the antiholomorphic involution

$$z \to -\overline{z} \quad ; \quad (x, y) \leftrightarrow \left(\overline{x}', \overline{y}'\right) \tag{6.4}$$

The set of fixed points defines an O6-plane along the imaginary z axis. This orientifold exchanges degenerations of a and b type. The parameters s, t, ϵ belong to chiral multiplets associated to complex structure moduli invariant under the orientifold action. We choose the O6-plane charge such that it leads to $O(1)$ Chan-Paton symmetry for D2-brane instantons on 3-cycles defined by horizontal segments crossing it.

For generic non-zero ϵ there are two $O(1)$ instantons in this configurations, corresponding to D2-branes on the segments $[a_1, b_1]$ (denoted instanton A) and $[b_2, a_2]$ (denoted instanton B). Each has just two fermion zero modes, and therefore leads to a contribution to the nonperturbative superpotential

$$W \;=\; f_1 e^{-T} \;+\; f_2 e^{-S} \tag{6.5}$$

where T, S are the closed string chiral multiplets whose real parts are given by the moduli t, s controlling the size of the wrapped 3-cycles. Here f_i are prefactors given by one-loop determinants, which depend on the Kahler moduli (but not on the complex structure moduli).

When ϵ is taken to zero, the four degenerations align, and the instanton A reaches a line of marginal stability, and splits into an instanton of type B, and a $U(1)$ instanton corresponding to a D2-brane on $[a_1, b_2]$ and its orientifold image on $[a_2, b_1]$ (denoted C and C' respectively). Since the complete superpotential should behave continuously in this motion in moduli

space, there should be suitable instanton processes reproducing it. There are only two basic instantons, namely the $O(1)$ instanton B on $[b_2, a_2]$, which indeed reproduces the e^{-S} term in (6.5), and the $U(1)$ instanton C (with its image C'), which has four fermion zero modes and does not contribute to the superpotential. Hence, there is no instanton which reproduces the e^{-T} term. The resolution of the puzzle lies in understanding the mutual influence of different instantons, and can be understood in different ways as we now describe.

The 2-instanton process

In order to show that the 2-instanton process contributes to the superpotential, we have to discuss the structure of zero modes in the 2-instanton configuration, and how they are saturated. This will involve the saturation of additional zero modes due to higher order interactions on the instanton world-volume effective action.

Let us briefly describe the structure of zero modes in the different sectors. We refer to the instantons C, B as 1, 2 in this section.

• In the 11 sector (and its $1'1'$ image), the open string sector feels a background with 8 supercharges, half of which are broken by the instanton. We have a $U(1)$ gauge symmetry (although there are no gauge bosons), four bosonic zero modes x_1^μ corresponding to the 4d translational Goldstones, and four fermionic zero modes θ_1^α, $\tilde{\theta}_{1\,\dot{\alpha}}$, corresponding to the Goldstinos. Note that the Lorentz symmetry under which these are chiral spinors is a global symmetry from the instanton volume viewpoint.

• The 22 sector is sensitive to the orientifold action and hence feels a background with 4 supercharges, half of which are broken by the instanton. The orientifold projection truncates part of the spectrum, as compared with the above $U(1)$ instanton case. There is an $O(1) \equiv \mathbb{Z}_2$ gauge symmetry, and four bosonic zero modes x_2^μ.

• Consider now the spectrum from open string stretching at the 12 intersection (and its image 1'2). Locally around it, the background admits 16 supersymmetries, half of which are broken by the D-branes. The massless modes thus form a hypermultiplet under the unbroken 8 supersymmetries. We have two complex bosonic zero modes φ_{12}, φ_{21}, with charges $+1$ and -1 under the $U(1)_1$ gauge symmetry of the instanton 1, and four fermionic zero modes, χ_{12}^α, χ_{21}^α, with charges $+1$ and -1 under $U(1)_1$. Alternatively, these can be conjugated to $\overline{\chi}_{21\,\dot{\alpha}}$, $\overline{\chi}_{12\,\dot{\alpha}}$, with charges -1, $+1$. Let us call the chiral superfields in the hypermultiplet Φ_{12} and Φ_{21}.

Let us now describe the couplings of these modes on the volume of the instanton. They are analogous (upon dimensional reduction) to the couplings that would appear if we would have D6-branes instead of D2-branes. There is a first term which describes the mass terms of the open strings between

the two instantons when they are separated in the 4d direction

$$S_{kinetic} = (x_1^\mu - x_2^\mu)^2 \left(|\varphi_{12}|^2 + |\varphi_{21}|^2\right) + i(x_1^\mu - x_2^\mu) \left\{ \overline{\chi}_{12}\sigma_\mu\chi_{12} - \overline{\chi}_{21}\sigma_\mu\chi_{21} \right\} \tag{6.6}$$

These terms are related to the couplings to gauge bosons in the D6-D6 system. There are also terms involving the neutral fermion zero modes θ, $\tilde{\theta}$ (analogous to the couplings to gauginos in the D6-D6 system), given by[1]:

$$S_\lambda = (\chi_{12}\,(\theta_1 - \theta_2))\varphi_{12}^* - (\chi_{21}\,(\theta_1 - \theta_2))\varphi_{21}^* + (\overline{\chi}_{12}\tilde{\theta})\varphi_{12} - (\overline{\chi}_{21}\tilde{\theta})\varphi_{21} \tag{6.7}$$

Notice that the combination $\theta_1 + \theta_2$ is decoupled, and corresponds to the two Goldstinos of the combined two-instanton system. We also have a D-term potential (the same arising in a D6-D6-brane system):

$$S_D = \left(|\varphi_{12}|^2 - |\varphi_{21}|^2 \right)^2 \tag{6.8}$$

Finally, there are quartic couplings involving the fields in the 12 sector. The local intersection preserves 8 supercharges, but the interaction is induced by effects that preserve only 4 supercharges (due to the different nature of degenerations at the intersection and adjacent to it). The interaction can be obtained from a superpotential of the form

$$W \simeq \left(\Phi_{12}\Phi_{21} \right)^2 \tag{6.9}$$

This in fact identical to the superpotential that would be obtained for D6-branes. The underlying reason is that both D2- and D6-branes have identical boundary states of the internal CFT (and a flip of DD to NN boundary conditions in the 4d part), thereby leading to essentially the same correlation functions.

Thus we obtain fermion-scalar interactions of the form

$$S_{\chi^2\varphi^2} = \chi_{12}\varphi_{21}\chi_{12}\varphi_{21} + 2\chi_{12}\chi_{21}\varphi_{12}\varphi_{21} + \varphi_{12}\chi_{21}\varphi_{12}\chi_{21} + \text{h.c.} \tag{6.10}$$

and the F-term scalar potential

$$S_F = |\varphi_{21}\varphi_{12}\varphi_{21}|^2 + |\varphi_{12}\varphi_{21}\varphi_{21}|^2 \tag{6.11}$$

Let us now consider the role of this complete instanton effective action in the generation of a nonperturbative superpotential. Notice that the contribution to the superpotential is dominated by configurations of overlapping instantons, namely when $x_1 - x_2 = 0$, as follows. A large non-zero separation gives large masses to the open strings between the instantons (consistent with the equation (6.6)), so we can integrate out these fields and set their vevs to zero, making the couplings in (6.7) vanish. Then we cannot saturate

[1] Similar couplings in the context of a D2-instanton intersecting its orientifold image have been described in [96].

the $\theta_1 - \theta_2$ zero modes, and the integral vanishes. So let us focus for simplicity[2] in the case $x_1 - x_2 = 0$. In this case we have an instanton action given by $S_{2\text{inst}} = S_\lambda + S_D + S_{\chi^2\varphi^2} + S_F$. The pieces relevant for the saturation of zero modes will be S_λ and $S_{\chi^2\varphi^2}$. We can soak up $(\theta_1 - \theta_2)$ by bringing down two insertions of $(\chi_{12}\,(\theta_1 - \theta_2))\varphi^*_{12}$ from S_λ. Similarly we can soak up $\tilde{\theta}$ by bringing down two insertions of $(\overline{\chi}_{12}\tilde{\theta})\varphi_{12}$. This also saturates the zero modes χ_{12}, $\overline{\chi}_{12}$. The remaining zero modes χ_{21}, $\overline{\chi}_{21}$ can be soaked up by bringing down two insertions of $\varphi_{12}\chi_{21}\varphi_{12}\chi_{21}$ from $S_{\chi^2\phi^2}$ and two insertions of its complex conjugate operator. Bringing everything together, and integrating over the (saturated) fermionic zero modes, we get the following 2-instanton contribution:

$$\int d^4x_+ d^2\theta_+ [d\varphi]\, \exp\{-S_D - S_F\}\, |\varphi_{12}|^4 \tag{6.12}$$

where $x_+ = x_1 + x_2$, $\theta_+ = \theta_1 + \theta_2$ are the surviving zero modes of the instanton. Note that the φ integral converges since there are no flat directions in the $(\varphi_{12}, \varphi_{21})$ space, as is easily seen from the form of S_D and S_F. There are other similar contributions from other combinatorics of soaking up zero modes. The overall result is a non-zero contribution to the superpotential from the 2-instanton process.

The above mechanism is very similar to the lifting of accidental zero modes by world-volume interactions in other situations. For instance in the study of instanton effects on 4d $\mathcal{N} = 4$ supersymmetric theories, where a world-volume 4-fermion interaction lifts fermion zero modes in groups of four (and allows multi-instanton processes contribute to the same 4d effective action terms as single-instanton ones). The analogy could be made much more explicit by integrating over the bosonic modes above, generating world-volume 4-fermion interactions. This is, to our knowledge, the first explicit realization of a similar mechanism in the computation of nonperturbative D-brane instanton superpotentials in $\mathcal{N} = 1$ theories. Notice also the interesting fact that in such situations the usual recipe of adding the contributions from the individual instantons misses these new contributions.

The spacetime picture of the above mechanism is of the kind shown in Figure 6.2, with two fermion zero modes of each instanton saturated against each other, and two left-over fermion zero modes.

As a last comment, note that the above system fits nicely with the concept of quasi-instanton as described in [97]. Namely the bosonic modes φ can be described as quasi-zero modes, and they parametrize a quasi-moduli space

[2] In fact it is possible, and not much harder, to carry out the computation allowing for arbitrary $x_1 - x_2$. Namely one can perform the Gaussian integration over these bosonic zero modes, and conclude that the result is localized (with some exponentially vanishing tail) onto $x_1 = x_2$. We omit the detailed analysis since the conclusions are essentially unchanged, and the simplified discussion is enough to show that the 2-instanton process at hand provides a non-trivial contribution.

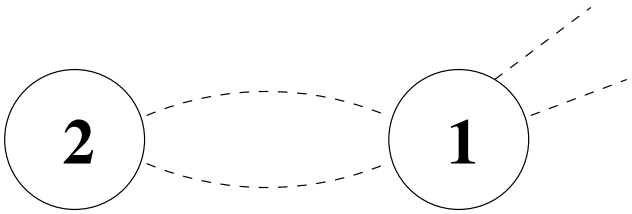

Figure 6.2: Schematic picture of a multi-instanton configuration contributing to the superpotential. A number of additional fermion zero modes are saturated against each other, due to interaction terms in the world-volume effective action of the 2-instanton system. The two left-over fermion zero modes are the Goldstinos of the overall BPS D-brane instanton system, and are saturated against the $d^2\theta$ integration in the induced 4d effective action superpotential term.

of quasi-instantons, in the sense that they correspond to a moduli space of instantons, which are lifted by a world-volume potential whose effects can be studied perturbatively in the value for the bosonic fields. Although strictly speaking such configurations do not correspond to BPS instantons, they can provide the dominant dynamical effect in the semiclassical approximation to certain quantities. Note that the additional Goldstinos (those associated to the supersymmetries preserved by BPS instantons) are not turned on in the first correction, and the effect of larger values for the bosonic fields is suppressed due to the exponential damping.

Nonperturbative lifting of zero modes of the $U(1)$ instanton

One can interpret the appearance of the non-trivial contribution to the superpotential as the instanton 2 generating an effective interaction term for the additional zero modes of the instanton 1. Indeed the piece

$$\Delta S_{\rm inst1} = \int d^2\theta_2\, d^4\chi\, d^4\varphi\, \exp[\,(\theta_1-\theta_2)\,\varphi\,\chi + \tilde{\theta}_1\,\overline{\varphi}\,\overline{\chi}+\chi^2\,\varphi^2 + V(\varphi)\,] \quad (6.13)$$

of the integral above can be regarded as computing the nonperturbative contribution of the instanton 2 to the effective action of the instanton 1. The result corresponds to an effective mass term (of nonperturbative strength e^{-S}) for the extra fermion zero modes of the instanton 1. Hence the amplitude of the instanton 1 is sketchily of the form

$$\begin{aligned} S_{4d} &\simeq \int d^4x\, d^2\theta\, d^2\tilde{\theta}\, \exp\,(\,-T_1\, -\, e^{-S}\,\tilde{\theta}\tilde{\theta}) \\ &= \int d^4x\, d^2\theta\, e^{-S} e^{-T_1} \,=\, \int d^4x\, d^2\theta e^{-T} \end{aligned} \quad (6.14)$$

namely the appropriate superpotential term.

In Section 6.3.2 we will provide yet another viewpoint regarding the nonperturbative lifting of fermion zero modes.

It is very interesting that $U(1)$ instantons can contribute to nonperturbative superpotentials via this mechanism of nonperturbative lifting of the extra zero modes. We also expect other instantons with additional universal fermion zero modes, like $Sp(2)$ instantons, to similarly contribute under special circumstances. It would be interesting to use this mechanism to revisit the role of interesting $U(1)$ and $Sp(2)$ instantons in model building applications, like the instanton scan in [98]. In fact, multi-instanton processes can already arise in simple toroidal orientifolds (see [99] for an explicit $\mathbb{T}^6/\mathbb{Z}_3$ example).

A comment on 4d charged matter insertions

The bottom line of the above sections is that nonperturbative superpotentials for non-gauge D-brane instantons are continuous across lines of marginal stability. The microscopic instanton physics mechanism relies on the fact that additional zero modes in multi-instanton processes can be saturated by interactions, leaving only a few zero modes to be saturated by external insertions in 4d correlators. The initial instanton amplitude is thus fully reconstructed by a multi-instanton amplitude.

Let us comment on the situation where the initial instanton intersects some of the 4d space filling D-branes in the system. There are fermion zero modes charged under the 4d gauge group at those intersections. In order to contribute to the superpotential, these additional fermion zero modes should be coupled to operators involving the 4d charged matter fields, so that upon integration over them (or pulling down these interactions) one generates insertions of the 4d charged matter fields in the 4d effective superpotential as discussed in [100, 101, 102, 103].

The appearance of the same insertions in the multi-instanton amplitude at the line of marginal stability is easy to show: notice that the homology charge of the contributing D-brane instanton system is preserved in the process of reaching the line of marginal stability. This ensures that the number of charged fermion zero modes is preserved in the process, and that the insertions of 4d fields are suitably generated. We refrain from delving into a more detailed discussion of concrete examples, and prefer to move on.

6.2.2 $O(1)$ splitting as $U(1)$ instanton

In this section we would like to consider another possible splitting of an $O(1)$ instanton across a line of marginal stability, in which it splits as a $U(1)$ instanton and its image. In fact this kind of process was already considered in [96], with the conclusion that such instantons cannot contribute to the superpotential due to the presence of additional zero modes. We will find

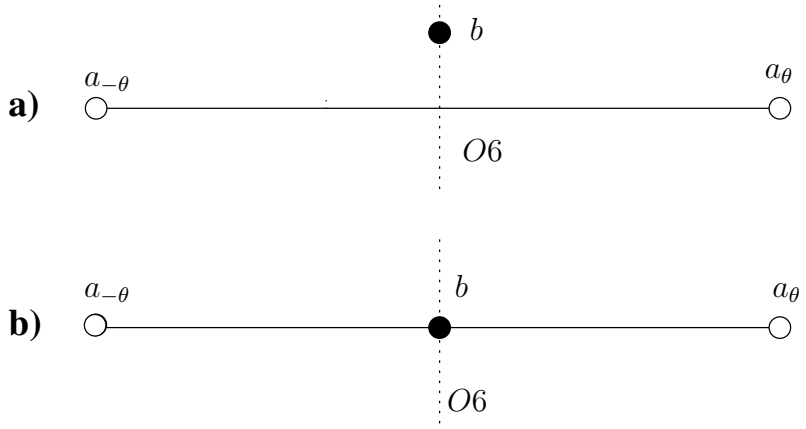

Figure 6.3: Configuration of an $O(1)$ instanton splitting as a $U(1)$ instanton (and its orientifold image). Interpreted as a HW setup, the dots b, $a_{\pm\theta}$, denote the locations in the 67 plane for an unrotated NS-brane, and NS5-branes rotated by angles $\pm\theta$ in the 4589 directions. Interpreted as D1-brane instantons in a threefold geometry, the dots $a_{\pm\theta}$, b denote a projection of the degenerations loci of a $\mathbb{C}^*$ fiber. D1-brane instantons wrap 2-cycles obtained by fibering the latter over segments defined by such degenerations, and are supersymmetric when the segments lie horizontally.

that our explicit example evades this no-go result, the reason being that there exists an F-term interaction in the world-volume of the instanton (not considered in [96]) which lifts the additional fermion zero modes.

The geometry in this configuration is similar, but slightly different from those introduced in Section 6.1. It is better to introduce the configuration in terms of a type IIA Hanany-Witten setup. Consider a NS-brane along 012345, and two NS-branes along 0123 and rotated by angles θ and $-\theta$ in the planes 45 and 89 (so we denote them NS_θ and $\mathrm{NS}_{-\theta}$). One can discuss the relevant part of the geometry by depicting the positions of the different branes in the $z = x^6 + ix^7$ plane, as shown in Figure 6.3. In our configuration, the NS-brane is located at $z = i\epsilon$, while the $\mathrm{NS}_{\pm\theta}$-branes are located at $z = \pm t$, with $t, \epsilon \in \mathbb{R}$. We consider instantons arising from euclidean D0-branes suspended between the different NS5-branes, thus corresponding to segments between the different NS5-brane locations in the z-plane. BPS instantons correspond to horizontal segments.

The above kind of configuration can be T-dualized using [104] into a type IIB geometry similar to those in Section 6.1 (and similar to those studied in [105, 106]). As a complex variety, the geometry can be described as an unfolding of an A_2 singularity

$$xy = u(u + \alpha v)(u - \alpha v) \tag{6.15}$$

with $\alpha = \tan\theta$. It can be regarded as a $\mathbb{C}^*$ fibration over the (u, v) space,

and degenerating at the loci $u = 0$, $u = \pm\alpha v$. The directions u, v are closely related to the directions 45 and 89 in the HW setup, and the degeneration loci correspond to the NS5-brane volumes in those directions. The geometry contains non-trivial 2-cycles, obtained by fibering the circle in the $\mathbb{C}^*$ over a segment joining two degeneration loci. There are D-brane instantons arising from D1-branes wrapping these 2-cycles. The description of the geometry as a complex manifold provided in (6.15) does not encode the parameters ϵ, t, which are Kahler parameters and control the lines of marginal stability of our instantons. We will rather use pictures like Figure 6.3, which can be regarded as a depiction of the blow-up structure of the above geometry, or the representation of the 67 plane in the HW configuration. Since the spectrum of instanton zero modes and their interactions can be obtained from the latter using standard rules, we stick to this language, although it is straightforward to translate into the geometric one.

Let us introduce an O6-plane along 0123789 in the HW setup, which thus corresponds to a fixed line along the vertical axis on the z-plane. The O6-plane intersects the NS-brane (in an intersection preserving 8 supercharges) mapping it to itself, while it exchanges the $\mathrm{NS}_{\pm\theta}$-branes. We choose the O6-plane charge such that it leads to $O(1)$ Chan-Paton symmetry on instantons along horizontal segments crossing the O6-plane.

Consider the configuration for non-zero ϵ, see Figure 6.3a. The only BPS instanton is given by a D0-brane stretched between the $\mathrm{NS}_{-\theta}$ and NS_{θ} branes. It has $O(1)$ Chan-Paton symmetry and has just 2 fermion zero modes (for non-zero θ), and thus leads to a nonperturbative superpotential contribution $W \simeq e^{-T}$, with T the chiral multiplet with real part t.

Consider the configuration for $\epsilon = 0$, where the previous instanton reaches a line of marginal stability and splits into a $U(1)$ instanton 1 (a D0-brane between the $\mathrm{NS}_{-\theta}$ and the NS branes) and its orientifold image $1'$ (between the NS and NS_{θ} branes). At the Gaussian level, the instanton has many additional zero modes beyond the required set of two fermion zero modes, hence naively it would not contribute to the superpotential. However, it is easy to go through the analysis of zero modes and their interactions, and realize that the additional fermion zero modes are lifted. The argument is very similar to that in the previous section, so our discussion is sketchy.

In the 11 sector of open strings with both endpoints on the instanton, there are four translational Goldstone bosonic zero modes x^μ, and four fermionic zero modes, two of them θ^α associated to Goldstinos of the 4d $\mathcal{N} = 1$, and two $\tilde{\theta}_{\dot{\alpha}}$ associated to the accidental enhancement to $\mathcal{N} = 2$. In the $11'$ sector of open strings between the instanton and its image, we have a hypermultiplet (given by the pair of chiral field Φ and Φ' in $\mathcal{N} = 1$ language) of zero modes φ, φ', χ_α, χ'_α with $U(1)$ charges ± 2 for unprimed/primed

fields. The couplings between the 11 and $11'$ fields are

$$S = \tilde{\theta}\,(\,\varphi\overline{\chi} - \overline{\chi}'\varphi'\,) \tag{6.16}$$

From the HW construction it is possible to derive that there are interactions among fields in the $11'$ sector. Given the amount of susy, it is possible to describe them by a superpotential $W \simeq (\Phi\Phi')^2$. Namely, there are scalar potential terms (involving also a D-term contribution)

$$\begin{aligned} V_D &\simeq (\,|\varphi|^2 - |\varphi'|^2\,)^2 \\ V_F &\simeq |\varphi\varphi'\varphi|^2 + |\varphi'\varphi\varphi'|^2 \end{aligned} \tag{6.17}$$

and most importantly couplings to the $11'$ fermions

$$S_{\varphi\chi} \simeq \chi\chi\varphi'\varphi' + 2\,\chi\varphi\chi'\varphi' + \varphi\varphi\chi'\chi' \tag{6.18}$$

As discussed in previous examples, all additional zero modes can be saturated by pulling down interaction terms from the instanton effective action. The only left-over fermion zero modes are the two Goldstinos θ^α, hence the $U(1)$ instanton contributes to the superpotential. Note that in contrast with the previous examples, the lifting of zero modes of the $U(1)$ instanton is purely perturbative (although is reminiscent of the nonperturbative lifting in previous section when regarded in the covering space).

Since the volume of the instanton and its image add up to the volume of the original $O(1)$ instanton, the complete superpotential is continuous.

6.2.3 A remark about the $O(1) \to O(1) \times O(1)$ (non)splitting

In the previous sections we have described examples where an $O(1)$ instanton decays into a set of two instantons of $U(1) \times O(1)$, or a $U(1)$ instanton and its orientifold image. Here we show that it is not possible to have one $O(1)$ instanton decay into two $O(1)$ instantons (or more generally, that an instanton mapped to itself under the orientifold action cannot decay into two instantons invariant under the orientifold action). The argument is general, and applies to any BPS instanton, contributing to the superpotential or to higher-fermion F-terms.

The general argument that forbids such instantons from crossing such marginal stability lines goes as follows. In order to contribute to F-terms, the instanton must be BPS, so the cycle it wraps must calibrated by $e^{i\varphi}\Omega$ with some constant phase φ:

$$\arg\Omega|_\Xi = \pi\varphi. \tag{6.19}$$

The phase φ of the calibration determines what is called in the Π-stability literature the *grading* of the brane, we will adopt this terminology here. This grading determines the supersymmetry conserved by the brane, and also the

mass of the lightest bosonic string mode between the decay products Ξ_1 and Ξ_2:

$$m^2 = \frac{1}{2}(\varphi_1 - \varphi_2). \tag{6.20}$$

When the gradings φ_1 and φ_2 of the decay products coincide Ξ_1 and Ξ_2 are mutually supersymmetric, the boson is massless, and we are on the marginal stability wall. Once we move slightly off the wall, the gradings will become different and bound state formation becomes possible. Whether we have a bound state or a stable superposition of two mutually non-supersymmetric branes depends on the sign of the boson mass: on one side of the wall it will become tachyonic, triggering bound state formation, while in the other side of the wall it will be massive, and the superposition of Ξ_1 and Ξ_2 is stable.

Here the main point of interest for our discussion is that the $\Omega \to \overline{\Omega}$ action of the orientifold acts on these gradings as $\varphi \to -\varphi$, so invariant instantons must have integer grading. This obstructs the decay of the $O(1)$ instanton into two $O(1)$ factors: there is no question of continuity of the nonperturbative superpotential since the gradings of the branes are frozen by the orientifold.

It is possible to argue the same thing in a slightly different way. Imagine D6 branes wrapping the same cycles in the internal space as the instantons. In this case the process of brane recombination is typically seen as a Higgsing, triggered by a Fayet-Iliopoulos term. The interpretation of the discussion above in terms of the gauge theory living on the brane is that due to the orientifold, the gauge group on the brane gets reduced from $U(1)$ to $O(1)$, and the Fayet-Iliopoulos is projected out. There is no continuous way of Higgsing $O(1) \times O(1)$ to $O(1)$.

We conclude by pointing out that our argument above does not exclude other more exotic possibilities to split an instanton invariant under the orientifold action into two instantons invariant under the orientifold action. In fact, there is a simple example of such transition, which is related to those in [75], as we now describe. Consider a geometry of the kind considered in Section 6.1, as shown in Figure 6.4. The configuration includes an orientifold plane associated to the action $\Omega R(-1)^{F_L}$, with R given by

$$z \to \overline{z} \quad ; \quad (x, y) \to (\overline{y}, \overline{x}) \quad ; \quad (x'y') \to (\overline{y}', \overline{x}') \tag{6.21}$$

or

$$z \to \overline{z} \quad ; \quad (x, y) \to (\overline{x}, \overline{y}) \quad ; \quad (x'y') \to (\overline{x}', \overline{y}') \tag{6.22}$$

The two choices lead to orientifold planes whose projection on the z-plane is the horizontal axis. They act differently on the $\mathbb{C}^*$ fibers, and lead to slightly different structures for the orientifold projection[3]. Namely the O6-

[3]The two choices correspond in the HW dual to introducing O4- or O8-planes, respectively.

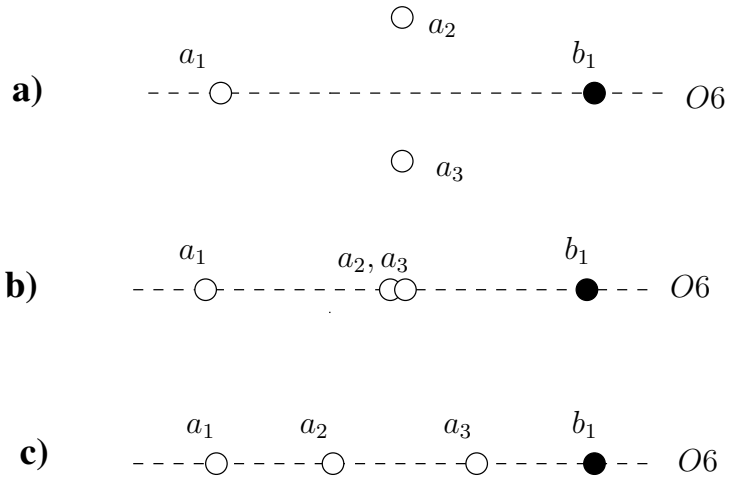

Figure 6.4: Splitting an instanton invariant under the orientifold action into two invariant instantons via a process involving a singular configuration.

plane defined by (6.21) is split when it encounters a $\mathbb{C}^*$ degeneration, and it changes from $\mathrm{O6}^+$ to $\mathrm{O6}^-$ (and vice versa). The O6-plane defined by (6.22) is not split and has a fixed RR charge. This distinction will not be relevant for us, and for concreteness we focus on an orientifold of the kind (6.22), and choose the orientifold to lead to $O(1)$ symmetries for D2-branes instantons.

Consider the transition shown in Figure 6.4. We consider the fate of the $O(1)$ instanton arising from a D2-brane on the 3-cycle $[a_1, b_1]$. As the two degenerations a_2, a_3 approach the orientifold plane (in a way consistent with the orientifold action), we reach a singular configuration, Figure 6.4b, where the $O(1)$ instanton is split into two $O(1)$ instantons. At this point a new branch emerges, where a_2, a_3 can separate along the horizontal axis, and the original instanton is split into three $O(1)$ instantons (for the orientifold action (6.21), the middle 3-cycle would lead to an USp instantons). It is thus possible to split $O(1)$ instantons by a physical process, but which is in fact unrelated to (and more exotic than) lines of marginal stability. Indeed, notice that the transition is not triggered by a Fayet-Iliopoulos parameter.

In fact, it is questionable that the transition has a simple description from the viewpoint of the instanton world-volume. Notice that the transition involves passing through a singular configuration, on which the 2-sphere of the 3-cycle $[a_2, a_3]$ shrinks to zero size. This is an orientifold quotient of the singular CFT point of the A_1 geometry, where the theory (at least before orientifolding) develops enhanced gauge symmetry, with additional massless gauge bosons arising from wrapped D2-branes. We thus expect that the nonperturbative superpotential can be discontinuous across this kind of transition. Indeed, in [75] similar transitions lead to discontinuous

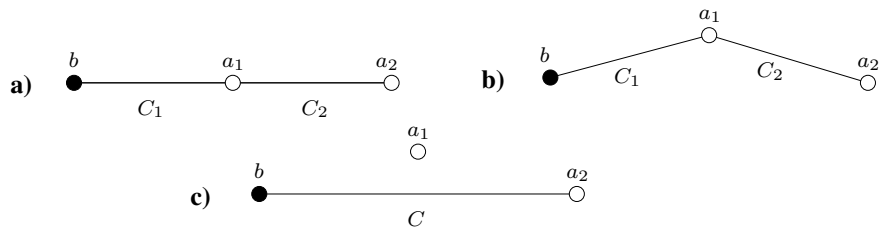

Figure 6.5: a) Marginally stable configuration. b) Moving a_1 away from the horizontal axis renders the configuration nonsupersymmetric, so it can c) decay to a supersymmetric configuration by brane recombination.

phenomena, like chirality changing phase transitions, not compatible with a local field theory description. It would be interesting to investigate these transitions in more detail, perhaps along the lines in [107].

6.3 Gauge D-brane instantons

Let us proceed to systems which are more familiar, namely configurations where the nonperturbative superpotential can be regarded as generated by gauge theory instantons. The idea is to consider a simple example of gauge sector with a nonperturbative superpotential, engineered via D-branes, and to consider its fate as one crosses a line of marginal stability. The general lesson of this example is the following. In this kind of setup, the crossing of lines of marginal stability in moduli space is basically described in terms of a Higgsing/unHiggsing in the field theory. Also, the dependence of the superpotential on the relevant moduli is encoded in the dynamical scales of the gauge factors associated to the 4d spacetime filling D-branes (since they control the gauge couplings). Thus the statement about the continuity of the superpotential across lines of marginal stability corresponds to the familiar matching of dynamical scales of a gauge theory in a Higgsing/unHiggsing process, at energies above and below the relevant vevs. Given this interpretation and the construction and discussion below, it is easy to find other examples of similar behaviour.

6.3.1 A $N_f < N_c$ SQCD example: spacetime view

Let us describe a system of D6-branes crossing a line a marginal stability in a geometry of the kind introduced in Section 6.1. Consider the geometry in Figure 6.5, having two a-type degenerations and one b-type degeneration, ordered as b, a_1, a_2 from left to right along the real axis. We consider a set of N D6-branes wrapped on the 3-cycle $C_1 = [b, a_1]$ and N D6-branes on $C_2 = [a_1, a_2]$. This configuration is supersymmetric as long as the degeneration

a_1 is aligned with the other two. Moving a_1 away from the horizontal axis forces the D6-branes on C_1 and C_2 to misalign, and their tension increases. The system of branes can relax by forming a bound states, described by N D6-branes on the 3-cycle $C = [b, a_2]$. Namely, the locus in moduli space where a_1 aligns with b, a_2 corresponds to a line of marginal stability for a D6-brane on C, which become unstable against decay into D6-branes on C_1, C_2.

The above phenomenon of brane dynamics has a counterpart in classical gauge field theory. The system of N D6-branes on C_1, C_2 leads to a $U(N)_1 \times U(N)_2$ $\mathcal{N} = 1$ supersymmetric gauge theory (see later for a discussion of the $U(1)$ factors), with chiral multiplets Q, $\tilde{Q}$ in the $(\Box_1, \overline{\Box}_2)$, $(\overline{\Box}_1, \Box_2)$, and Φ in the adjoint of $SU(N)_2$. There is a classical superpotential

$$W = \mathrm{Tr}\, Q\Phi\tilde{Q} \tag{6.23}$$

The parameters of the gauge theory are the gauge couplings g_i, and theta angles θ_i, which are classically related to C_i by

$$T_i = \frac{1}{g_i^2} + i\theta_i = \frac{1}{g_s}\int_{C_i} \Omega + i\int_{C_i} A_3 \tag{6.24}$$

where A_3 is the type IIA RR 3-form. In the quantum theory, these parameters are traded for dynamical scales

$$\Lambda_1 = \exp\left(-\frac{T_1}{2N}\right) \quad ; \quad \Lambda_2 = \exp\left(-\frac{T_2}{N}\right) \tag{6.25}$$

The change in the complex structure associated to moving a_1 off the horizontal axis corresponds to turning on a Fayet-Iliopoulos parameter ξ for the difference of the two $U(1)$'s. This triggers a vev for the bi-fundamental flavours Q or $\tilde{Q}$, depending on the sign of ξ, and breaking the gauge group to the diagonal $U(N)$. Assuming that Q acquires the vev, the fields Φ, $\tilde{Q}$ become massive by the superpotential and disappear. We are left with a $U(N)$ pure SYM gauge theory, with complex gauge coupling

$$T = T_1 + T_2 = \int_C \Omega + \int_C A_3 \tag{6.26}$$

This agrees with the picture of the D6-branes recombining into D6-branes wrapped on C.

It is worth noting that the $U(1)$ generators have BF Stuckelberg couplings with closed string moduli, which make the gauge bosons massive, so the $U(1)$ factors are really absent from the low energy effective theory. This modifies the above discussion very mildly. Namely, instead of turning on a FI parameter, the above transition can be regarded as moving along the baryonic branch of the $SU(N)_1 \times SU(N)_2$ theory, to yield a pure $SU(N)$ SYM theory.

We would now like to consider the nonperturbative superpotential in these two systems, showing that it is continuous across the line of marginal stability. Interestingly, the nonperturbative effects have a microscopic description in terms of D2-brane instantons on the relevant 3-cycles, along the lines described in Appendix D. In the discussion here we stick to the description in gauge theory language. Also for convenience we use the description where the $U(1)$'s are not included in the low-energy dynamics.

Consider first the system of N D6-branes on C. Since it corresponds to a pure SYM theory, it confines and develops a gaugino condensate. There is a nonperturbative superpotential

$$W \,=\, \Lambda^3 \,=\, (\, e^{-T/3N}\,)^3 \tag{6.27}$$

Consider now the situation when the instanton reaches the line of marginal stability. We consider the system of N D6-branes on C_1 and N D6-branes on C_2, so we essentially have to study the dynamics of the $SU(N)_1 \times SU(N)_2$ gauge theory. Let us focus in the regime where $\Lambda_1 \gg \Lambda_2$, so the dynamics of $SU(N)_1$ dominates.

In this case the $SU(N)_1$ group confines first. It has $N_f = N_c$, so the instanton on C_1 is a Beasley-Witten instanton, which induces a quantum deformation on the moduli space. Instead of using the intrinsic picture in moduli space and inducing an operator of the form (D.5), we prefer to work as usual in field theory analysis, by imposing the deformation by a quantum modified constraint. We describe the system is in terms of mesons M and baryons $B\tilde{B}$, with superpotential:

$$W = \mu\Phi M + \mu^{-2N+2}\, X\,(\det M - B\tilde{B} - \Lambda_1^{2N}) \tag{6.28}$$

where we have introduced the scale μ to keep the dimension of the operator in the superpotential invariant. This dynamical scale will be of the order of Λ_1, so we use it in what follows.

The F-term for Φ enforces $M = 0$, and vice versa. The fields Φ and M are massive, so we can integrate them out. We are left with a pure $SU(N)_2$ SYM theory, with dynamical scale Λ_f, to be determined later. In addition we have the singlets X, B, $\tilde{B}$, with superpotential

$$W \simeq X\,(\, B\tilde{B} + \Lambda_1^{2N}\,) \tag{6.29}$$

The theory has a one-complex dimensional baryonic moduli space, but these singlets do not modify the theory otherwise.

The dynamical scale Λ_f is determined by the matching, in analogy with the discussion in Appendix D.1, as

$$\Lambda_f^{3N} = \Lambda_2^N \Lambda_1^{2N} \tag{6.30}$$

and is in fact the same as the Λ introduced above.

In this left-over $SU(N)_2$ pure SYM theory, the effect of the (fractional) instanton on C_2 is simply to develop a gaugino condensate nonperturbative superpotential

$$W = \Lambda_f^3 = (e^{-T/3N})^3 \tag{6.31}$$

in agreement with (6.27).

This example provides a non-trivial and simple realization of the continuity of superpotentials across lines of marginal stability. The instanton wrapping C reaches the line of marginal stability, at which it splits into two BPS instantons, wrapping C_1 and C_2. The instanton on C_1 is of Beasley-Witten type and deforms the moduli space. The instanton on C_2, once the effect of the instanton on C_1 is taken into account, induces a nonperturbative superpotential. The total effect neatly adds up to the effect of the single instanton on C before crossing the line of marginal stability.

For completeness, let us mention that the discussion with $U(1)$'s in the effective action is similar. There are no baryonic operators, so there are no fields left out after integrating out M, Φ. The one-dimensional moduli space is realized in this view in the closed sector, as the FI term for the relative $U(1)$ corresponding to the position of a_1 off the horizontal axis.

6.3.2 Microscopic interpretation

In this section we discuss the microscopic interpretation of the continuity of the nonperturbative superpotential of the above configuration in terms of D-brane instanton physics.

The 2-instanton process

In analogy with the discussion for non-gauge instanton in Section 6.2.1, and from the above discussion, it is clear that the superpotential contribution at the line of marginal stability arises from a two-instanton process, involving the instantons C_1 and C_2. In fact, it is possible to compute the set of zero modes for the two-instanton system, and their interactions.

We skip the detailed discussion and just sketch the result. The contributions to the superpotential localize on configurations of instantons coincident in 4d. In addition the 3-cycle C_1 is non-rigid, and there is a bosonic zero mode ϕ parametrizing a branch where the instanton on C_1 slides away from the D6-branes on C_1. Along this branch the configuration has additional zero modes χ, $\overline{\chi}$ (the partners of ϕ), which are not saturated. Hence the contributions to the superpotential localize at $\phi = 0$. At this point one can easily check that all fermion zero modes except for the two overall Goldstinos $\theta_1 + \theta_2$ have non-trivial interactions, which can be pulled down to saturate the corresponding integrals.

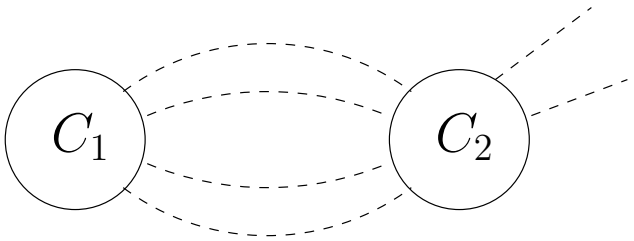

Figure 6.6: Schematic picture of the multi-instanton configuration discussed in the text.

The whole process can be described in spacetime in terms of the diagram shown in Figure 6.6. The instanton C_2 has six unsaturated fermion zero modes, since it is a Beasley-Witten instanton with $N_f = N_c$ (thus leading to two unsaturated fermion zero modes beyond the two $\mathcal{N} = 1$ Goldstinos) and two additional fermion zero modes χ, $\overline{\chi}$ from being on a non-rigid cycle. The instanton C_1 has four unsaturated fermion zero modes, since it is an $N_f = N_c$ Beasley-Witten instanton. In the two-instanton process, one can generate interactions between the zero modes of the two instantons via the bosonic zero modes charged under both, which allow to contract four fermion zero modes, leading to an overall process with only two fermion zero modes.

Nonperturbative lifting of zero modes

Along the lines of the discussion in Section 6.2.1, we would like to improve on the additional viewpoint of the process as a lifting of fermion zero modes of the instanton C_2 by a nonperturbative effect induced by the instanton C_1. In fact, for gauge instantons the mechanism can be posed in a much sharper setup. Consider a gauge instanton A, with field configuration $\mathcal{A}(x^\mu; \varphi, \psi)$, as a function of the sets of bosonic and fermionic zero modes, φ, ψ. Here $\mathcal{A}$ denotes the set of all 4d fields involved in the configuration. The classical effective action for the zero modes $S_{\text{inst.}}(\varphi, \psi)$ can be obtained by replacing the instanton field configuration on the 4d action $S_{4d}[\mathcal{A}] = \int d^4x\, \mathcal{L}[\mathcal{A}]$, namely

$$S_{\text{inst}}(\varphi, \psi) \;=\; \int d^4x\, \mathcal{L}[\mathcal{A}(x^\mu; \varphi, \psi)] \tag{6.32}$$

From this point of view, any additional term in the 4d effective action $\delta S_{4d}[\mathcal{A}]$ induces a corresponding term on the effective action $\delta S_{\text{inst}}(\varphi, \psi)$ for the instanton:

$$\delta S_{\text{inst}} \;=\; \int d^4x\, \delta\mathcal{L}[\mathcal{A}(x^\mu; \varphi, \psi)] \tag{6.33}$$

When the additional term in the 4d effective action δS_{4d} is induced by another instanton B, the term $\delta S_{\text{inst.}}(\varphi, \psi)$ can in a very precise sense be

regarded as a nonperturbative interaction term for the zero modes of A induced by the instanton B. In particular interaction terms of this kind involving the fermion zero modes ψ of A are nonperturbatively lifted by the instanton B. Notice that the g_s dependence arranges in such a way that the total 4d effect is suppressed by the exponential factors of both instantons A and B, as in equation (6.14).

On general grounds, we may expect that an instanton B with k fermion zero modes induces a 4d F-term leading to contributions to S_{4d} with k 4d fermion insertions. This will in general induce an interaction term $S_{\text{inst.}}(\varphi, \psi)$ on the instanton A lifting k fermion zero modes. The spacetime picture of the process is a two-instanton process where k fermion zero modes of the two instantons are contracted against each other. In particular, in our gauge theory example, the instanton C_2 induces a 4d effective operator corresponding to a 4-fermion F-term, which then induces a 4-fermion interaction term on the effective action for the zero modes of instanton C_1. Since the instanton C_1 has six fermion zero modes, the lifting of four leaves only the two Goldstinos, so that there is a non-trivial contribution to the superpotential.

To conclude, we would like to add yet another equivalent, but related, viewpoint on the nonperturbative lifting of zero modes. The idea is based on a generalization of the analysis in Section 4.3 of [108], which discussed the effects of a (perturbative) superpotential mass term on instantons with additional fermion zero modes. Consider an instanton A with $k = 2n$ fermion zero modes beyond the two Goldstinos, and leading to a 4d higher F-term similar to the one in equation (D.5)

$$\int d^4x\, d^2\theta\, \mathcal{O}_w \;=\; \int d^4x\, d^2\theta\; w_{\bar{i}_1\bar{j}_1\ldots\bar{i}_n\bar{j}_n}(\Phi)\, \mathcal{O}^{\bar{i}_1\bar{j}_1}\ldots\mathcal{O}^{\bar{i}_n\bar{j}_n} \tag{6.34}$$

with

$$\mathcal{O}_{\bar{i}\bar{j}} \;=\; \overline{D\Phi}^{\bar{i}}\,\overline{D\Phi}^{\bar{j}} \tag{6.35}$$

The operator $\mathcal{O}_w$ is chiral (despite its appearance). In the presence of an additional superpotential $W(\Phi)$, the supersymmetry algebra is modified (since the fermion variations change, $\delta\psi = F = -\overline{\partial W/\partial\Phi}$) and $\mathcal{O}_w$ is no longer chiral. Still, since the instanton A remains BPS, it should induce an F-term. Indeed, in [108] it was argued that (for superpotential mass terms), there is a suitable deformation $\tilde{\mathcal{O}}_w$ of $\mathcal{O}_w$ which is chiral in the presence of the superpotential. The instanton amplitude is now given by

$$\int d^4x\, d^2\theta\, \tilde{\mathcal{O}}_w \;=\; \int d^4x\, d^2\theta\; w_{\bar{i}_1\bar{j}_1\ldots\bar{i}_n\bar{j}_n}(\Phi)\, \tilde{\mathcal{O}}^{\bar{i}_1\bar{j}_1}\ldots\tilde{\mathcal{O}}^{\bar{i}_n\bar{j}_n} \tag{6.36}$$

where, generalizing the result in [108], $\tilde{\mathcal{O}}_{\bar{i}\bar{j}}$ has schematically the structure

$$\tilde{\mathcal{O}}^{\bar{i}\bar{j}} \;=\; \overline{D\Phi}^{\bar{i}}\,\overline{D\Phi}^{\bar{j}} \;+\; W^{\bar{i}\bar{j}} \tag{6.37}$$

Note that the total effect is that the instanton generate effective vertices not only with $2n$ fermionic external legs, but also with $2n-2p$ fermionic external legs (with p taking several possible values, depending on the detailed structure of W). The 4d interpretation is that $2p$ fermionic legs have been soaked up by p insertions of the superpotential interaction.

In fact, one is lead to suspect a further generalization of the above argument. Consider the instanton A in the presence, not of a 4d superpotential term, but of a higher F-term (which could be of perturbative or nonperturbative origin). Consider the latter to be of the form

$$\delta S_{4d} \,=\, \int d^4x\, d^2\theta\, W_{\bar{i}_1\bar{j}_1\ldots\bar{i}_m\bar{j}_m}(\Phi)\, \overline{D\Phi}^{\bar{i}_1}\, \overline{D\Phi}^{\bar{j}_1}\ldots \overline{D\Phi}^{\bar{i}_m}\, \overline{D\Phi}^{\bar{j}_m} \qquad (6.38)$$

Namely it leads to 4d interactions with $2m$ 4d fermions, and we assume $m < n$. Although we do not have a precise argument based on the supersymmetry algebra, we expect the amplitude of the instanton A to be modified in the presence of such term in the 4d action. Let us define $\tilde{n} = n \bmod m$ and $r = (n-\tilde{n})/m$, hence $n = rm + \tilde{n}$. The instanton amplitude is expected to take the schematic form

$$\int d^4x\, d^2\theta\, w_{\{\bar{i}_1\bar{j}_1\}\ldots\{\bar{i}_r\bar{j}_r\}\bar{p}_{\tilde{n}}} \mathcal{O}^{\{\bar{i}_1\bar{j}_1\}}\ldots\mathcal{O}^{\{\bar{i}_r\bar{j}_r\}}\, \overline{D\Phi}^{\bar{k}_1}\, \overline{D\Phi}^{\bar{p}_1}\ldots \overline{D\Phi}^{\bar{k}_{\tilde{n}}}\, \overline{D\Phi}^{\bar{p}\tilde{n}} \qquad (6.39)$$

where $\{i_q, j_q\}$ denotes an m-plet of indices $i_{q1}, j_{q1}\ldots i_{qm}j_{qm}$, and

$$\mathcal{O}^{\{\bar{i}\bar{j}\}} \,=\, \mathcal{O}^{\bar{i}_1\bar{j}_1\ldots\bar{i}_m\bar{j}_m} \,=\, \overline{D\Phi}^{\bar{i}_1}\, \overline{D\Phi}^{\bar{j}_1}\ldots \overline{D\Phi}^{\bar{i}_m}\, \overline{D\Phi}^{\bar{j}_m} \,+\, W^{\bar{i}_1\bar{j}_1\ldots\bar{i}_m\bar{j}_m} \qquad (6.40)$$

The interpretation is that in the presence of the 4d F-term (6.38), the instanton with $2n$ fermion zero modes can generate effective vertices with $2n-2m$ external fermionic legs, by having sets of $2m$ fermionic legs soaked up by the F-term (6.38).

The above discussion can be carried out to the situation where the modification to the 4d action is induced by a second instanton B with $2m$ fermion zero modes (which could be a gauge instanton or a non-gauge D-brane instanton). In the spacetime picture, we would have a multi-instanton process involving A and B, in which some of the fermionic external legs of the instanton A are soaked up by the 4d effective interaction induced by B. A simple example would be to consider the instanton B to have two fermion zero modes, so it generates a superpotential, thus fitting into the situation leading to (6.37). In fact, a particular case fitting within the analysis in [108] can be obtained by considering the instanton B to be a non-gauge D-brane instanton inducing a superpotential mass term in the 4d action. Explicit examples of this have been considered e.g. in [109, 55, 99]. Our example of gauge theory instantons above corresponds to a more general situation of the kind (6.40), with the instantons A, B given by the instantons C_1, C_2 (and $n=3$, $m=2$)

As a last remark, we expect processes with non-gauge instantons to admit a similar interpretation. Thus the contribution to the superpotential arising from the two-instanton process involving the $U(1)$ and the $O(1)$ instantons can be regarded as the 4d effective term induced by the $U(1)$ instanton in the presence of the additional 4d interaction induced by the $O(1)$ instanton.

6.3.3 Adding semi-infinite D-branes

It is interesting to consider some simple modifications of the above discussion in the presence of additional semi-infinite D6-branes sticking out of the $\mathbb{C}^*$ degenerations. From the field theory viewpoint they correspond to the addition of extra flavours for some of the gauge factors. From the viewpoint of the instantons, they lead to additional fermion zero modes. In this section we consider a few possibilities

In the above situation we have focused on a case where the nonperturbative dynamics reduces to that of pure SYM. However, it is straightforward to modify the setup to SQCD with N_f flavors. It suffices to introduce a stack of N_f D6-branes wrapping the non-compact 3-cycle obtained from a horizontal semi-infinite line starting from the degeneration a_2 (this can be regarded as a limit of infinite 3-cycle volume of a geometry with a second b-type degeneration, located on the far right of the figure). The above argument goes through, and implies the continuity of the nonperturbative superpotential across the line of marginal stability. Notice that in the particular case of $N_f = N-1$ the instantons under discussion are familiar gauge theory instantons.

Another straightforward addition of semi-infinite branes is to consider adding K D6-branes stretching from the a_1 degeneration horizontally to the left infinity. Note that for the configuration in Figure 6.5a, these D6-branes hit the b degeneration, so the configuration can be regarded as K D6-branes stretching along $(-\infty, b]$, $N+K$ on $[b, a_1]$ and N on $[a_1, a_2]$. For the configuration in Figure 6.5c, we have N D6-branes on $[b, a_2]$ and a disconnected set of K D6-branes from left infinity to a_1.

It is easy to carry out an analysis similar to the above to derive the continuity of the superpotential. In the initial configuration, the gauge factor $SU(N+K)$ has $N_f = N_c$ and thus a Beasley-Witten instanton deforming its moduli space and forcing the gauge factor onto the baryonic branch. The adjoint of the $SU(N)$ factor pairs up with some of the mesons and becomes massive, so the left over pure SYM theory develops a gaugino condensation superpotential. One recovers the same result from the instanton contribution in the final configuration Figure 6.5c (upon matching of scales along the lines in Appendix D).

6.3.4 Gauge theory instantons and Seiberg duality

In this section we elaborate on an interesting point. It is a familiar fact that the realization of Seiberg duality in terms of the D-brane construction of gauge theories corresponds to a motion in moduli space (in which D-branes typically break up and recombine) [64, 95, 110, 111, 112] (see also [113, 114, 115] for other related approaches). Therefore they provide a large class of examples of motion across lines of marginal stability in which the nonperturbative superpotential is continuous.

A comment is in order here. From field theory experience we know that Seiberg duality involves a non-trivial change of variables in the 4d chiral multiplets. We also know that tree level superpotentials are crucial in matching properties of two Seiberg-dual theories. Both properties are related to the following fact. Seiberg dualities in the D-brane realization of field theories can be described as a motion between two points P and Q in moduli space, at each of which we have D-branes wrapped on cycles, whose sizes control the gauge couplings and thus the strength of instanton effects. This motion typically involves a region in moduli space larger than the radius of convergence of the instanton expansion at either point. In other words, the operation can also be described as a continuation past infinite coupling, in the sense that they can be obtained by shrinking a cycle C on which 4d space filling branes wrap and growing a cycle C' which is in the opposite homology class $[C'] = -[C]$. The point O where the cycle shrinks is strongly coupled from the viewpoint of the original instanton at P, but a different weakly coupled description is available at Q (and vice versa). The change of description has several effects, which we be taken into account implicitly in our discussions below:

• It relates the strengths of the instantons as $e^{-T} = (e^{-T'})^{-1}$, where T, T' control the sizes of C, C'. This underlies the fact that matching of scales in the Seiberg duality encodes the continuity of the superpotential as a function of the closed string moduli.

• It implies a non-trivial change of variables in the 4d chiral multiplets, hence the comparison of the superpotentials at P and Q requires expressing the open string 4d multiplets in terms of gauge invariant operators.

• It can map tree-level and nonperturbative superpotentials to each other. Thus the continuity applies to the full superpotential.

The D-brane realization of Seiberg duality for large classes of field theories thus provides a large class of examples of continuity of the nonperturbative superpotential across lines of marginal stability (with the appropriate change of variables for the charged matter fields). We restrict to the description of this phenomenon with simple examples, which are illustrative for this whole class.

Notice that it is easy to provide a D-brane realization of the original Seiberg duality [116] using the above geometries following [95], as we review

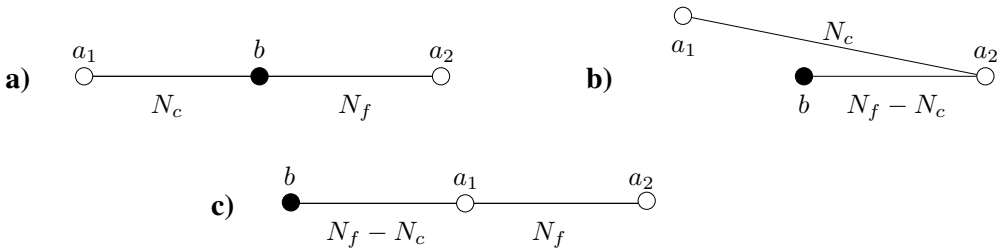

Figure 6.7: Realizing Seiberg duality in terms of D-branes: a) The electric configuration. b) We move a_1 up a bit. The original branes are now nonaligned, so they recombine to minimize their tension. c) Finally moving a_1 all the way to the middle position we get the magnetic dual theory.

now, see Figure 6.7.

Consider a geometry with three aligned degenerations ordered as a_1, b, a_2, and introduce N_c D6-branes on $[a_1, b]$ and N_f on $[b, a_2]$, with $N_f \geq N_c$, Figure 6.7a. This describes the electric theory of $SU(N_c)$ SQCD with N_f flavours, with a gauged flavour group. Now move up the degeneration a_1. The minimal energy configuration is obtained when N_c D6-branes recombine at b, so we have N_c D6-branes on the tilted[4] segment $[a_1, a_2]$ and $N_f - N_c$ on $[b, a_2]$, Figure 6.7b. Now move a_1 to the right and bring it down between b and a_2. The $N_c - N_f$ D6-branes on $[b, a_2]$ split, so we are left with $N_f - N_c$ D6-branes on $[b, a_1]$ and N_f on $[a_1, a_2]$. This describes the magnetic theory (again with gauged flavor group). Note that the gauging of the flavor group is just for the purposes of introducing configurations to be used later; a realization of the pure Seiberg duality can be obtained simply by sending the degeneration a_2 to right infinity.

Clearly the possibility of embedding Seiberg dualities in terms of D-branes provides a huge class of examples of brane systems crossing walls of marginal stability. The continuity of the nonperturbative superpotential in these processes is automatically guaranteed by the field theory argument for the matching of scales, as discussed above. We will not delve into a more detailed discussion, and simply discuss some particular examples related to systems in other sections.

Let us focus on some particularly simple examples where the basic splitting processes of the D6-branes are of the kind analyzed in the previous section. Consider the situation with N D6-branes on $[b, a_2]$ and no D6-branes on $[a_1, b]$. The a_1 degeneration has no D6-branes attached, so moving it

[4]The tilting breaks supersymmetry in the intermediate steps of the argument; there are however simple modifications of the setup which allow to preserve supersymmetry throughout the process [95]. We skip their discussion since they will not be needed in our examples below.

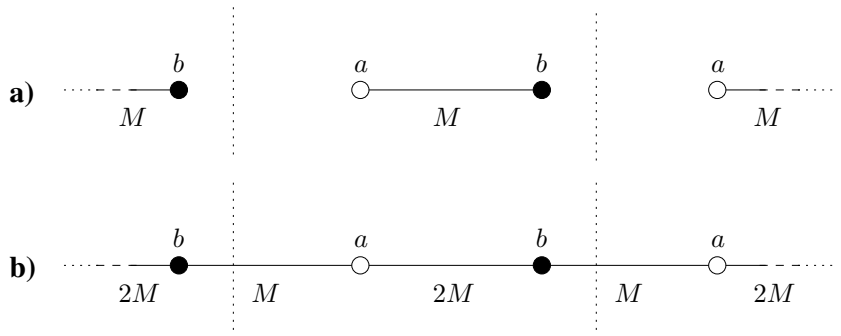

Figure 6.8: The periodic configuration dual to the conifold. The dotted vertical line denotes the period. a) Final step of the cascade. b) One step up in the cascade. We reach this point by moving all a degenerations one cell to the left.

between the degenerations b, a_2 is exactly the inverse process of the one in Figure 6.5, studied in Section 6.3.1.

For future convenience let us consider another example, now involving semi-infinite D6-branes. Consider the initial configuration with degenerations ordered as a_1, b, a_2 and introduce N D6-branes on $(-\infty, a_1)$, no D6-branes on $[a_1, b]$ and K D6-branes on $[b, a_2]$. As one moves the a_1 degeneration between b, a_2, it drags the K semi-infinite D6-branes, which end up split in the final configuration. In the latter we have K D6-branes on $(-\infty, b)$, $N + K$ D6-branes on (b, a_1), and N D6-branes on (a_1, a_2). The splitting process of the semi-infinite D6-branes is exactly as in the last system of Section 6.3.3, where we showed the continuity of the nonperturbative superpotential.

As a final example based on the configuration in the previous paragraph, let us consider a type IIA configuration mirror to D-branes at the conifold, and (one of the steps of) the celebrated Klebanov-Strassler duality cascade [89]. Following [104, 117], a system of D-branes at a conifold can be realized in terms of D4-branes suspended (along a circle direction) between two rotated NS-branes. Equivalently, one can use an infinite periodic array of rotated NS-branes with suspended D4-branes. This systems can be mapped to one of our familiar double $\mathbb{C}^*$-fibration geometries by simply introducing a periodic array of degenerations $\ldots, a, b, a, b, \ldots$, with D6-branes on the finite segments, as shown in Figure 6.8. This is equivalent to (but easier to visualize than) a double $\mathbb{C}^*$ fibration over a cylinder, with one degeneration of each type.

Consider the configuration on Figure 6.8a, with M D6-branes on the intervals of type $[a, b]$, and no D6-branes on those of type $[b, a]$. This describes the theory at the end of the duality cascade, and corresponds to $SU(M)$ SYM, with a nonperturbative superpotential induced by a $1/M$-

fractional instanton. Consider now the geometric operation that takes us one step up the cascade. This corresponds to moving the a-type degenerations once around the period, coming back to its original position in the periodically identified geometry but moving one period to the left in the covering space we are drawing. We do this in the same way as above: moving up the a singularity a bit, taking it one cell to the left, and finally returning it to its original vertical position. The resulting configuration is shown in Figure 6.8b and contains M D6-branes on the $[b, a]$ intervals and $2M$ D6-branes on the $[a, b]$ intervals. The geometric process, and in particular the splitting of branes, is exactly as that considered two paragraphs above, for $K = N \equiv M$. The continuity of the superpotential is easily derived, by showing (using the instanton interpretation of the field theory analysis in [118]) that the Beasley-Witten instanton of the $SU(2M)$ theory (which has $N_f = N_c$) deforms the moduli space of this theory and forces it into the baryonic branch, while the $1/M$-fractional instanton on the left over $SU(M)$ theory (with scale suitably computed by matching) generates the superpotential.

6.4 Exotic instantons becoming gauge instantons

In the previous sections we have argued continuity of the nonperturbative superpotential for gauge and non-gauge D-brane instantons, in several examples. In this section we would like to consider a slightly more general situation where the nature of the instanton changes in the process of crossing lines of marginal stability. Namely a non-gauge D-brane instanton ends up as a gauge D-brane instanton after some motion in moduli space.

A prototypical situation where this takes place is in duality cascades [89] (see also e.g. [119, 86, 90, 87]) of quiver gauge theories, in which one of the nodes of the quiver becomes eventually empty of 4d space filling branes. D-brane instantons which occupied this node change from gauge to non-gauge instantons in the motion in moduli space associated to the cascade. Since we are interested in studying contributions to the superpotential, one would need to consider cascades of orientifolded quiver gauge theories. In fact, this kind of analysis has been carried out in [120] in one particular example, focusing on the relevant part of the superpotential for the infrared theory. In Section 6.4.2 we revisit the system in our language, and recover that the full superpotential is well-behaved in the process. Our analysis reproduces some pieces dropped in [120], which are irrelevant in the infrared, but are still part of the full superpotential of the theory.

Before revisiting the example of the duality cascade, let us consider the simplest case where a non-gauge D-brane instanton becomes a gauge theory effect.

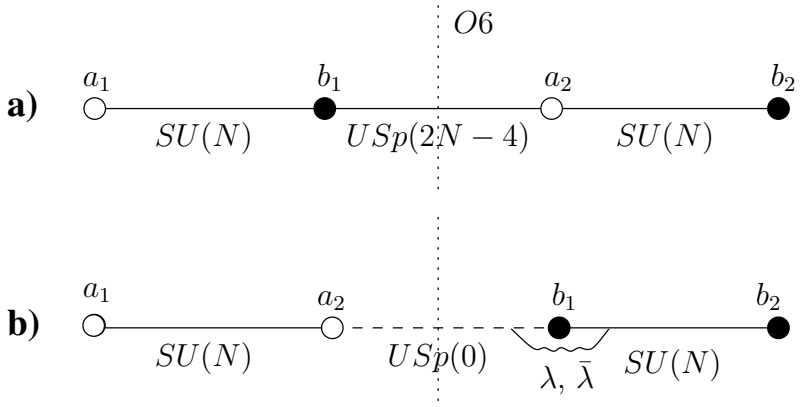

Figure 6.9: Prototypical example of a D-instanton effect being equivalent to a gauge theory effect via Seiberg duality. Figure a) shows the geometry leading to a $USp \times SU$ gauge theory upon wrapping D6-branes on the appropriate 3-cycles. The dotted line denotes the orientifold plane. Figure b) shows the configuration after the motion in moduli space corresponding to Seiberg duality. There are no D6-branes in the 3-cycle $[a_2, b_1]$, but an instanton (dashed line) wrapped on it can contribute to the superpotential. We have indicated the charged fermionic zero modes λ, $\bar{\lambda}$ between the D-brane instanton and the gauge D-brane.

6.4.1 Dualizing the $O(1)$ instanton

Let us consider a geometry of the kind in Section 6.1, with an O6-plane, see Figure 6.9. Let us wrap stack of D6-branes on the different 3-cycles corresponding to the configuration in Figure 6.9a. The low energy dynamics of this configuration is given a $SU(N) \times USp(2N-4)$ gauge theory, with quarks $q \in (\Box_{SU}, \Box_{USp})$, $\tilde{q} \in (\bar{\Box}_{SU}, \Box_{Usp})$ and superpotential

$$W = q\tilde{q}q\tilde{q} \tag{6.41}$$

Let us focus on the strong dynamics for the USp theory[5]. As argued in [121], when the USp node becomes strongly coupled the theory has an effective description (corresponding to its Seiberg dual) in which the USp group confines completely, and the fundamental degrees of freedom are the mesons:

$$M_{\begin{smallmatrix}\Box\\\Box\end{smallmatrix}} = q \cdot q \ ; \qquad M_{\begin{smallmatrix}\bar{\Box}\\\bar{\Box}\end{smallmatrix}} = \tilde{q} \cdot \tilde{q} \ ; \qquad M_{Adj} = q \cdot \tilde{q} \tag{6.42}$$

[5]There are additional nonperturbative effects from the $SU(N)$ factor, which can also be followed along the transition below, in analogy with our examples above (in fact, they map to 2-instanton effects after the transition). We skip their discussion in order to emphasize the main point.

where we have expressed the mesons in terms of the electric fields[6], and the dot denotes contraction in the USp indices, which antisymmetrizes the fields. The subindex denotes the representation of the $SU(N)$ group under which the meson transforms. There is also a superpotential implementing the classical constraint between the mesons, which can be written as

$$W_0 = \mathrm{Pf} \begin{pmatrix} M_{\square\,\square} & M_{Adj} \\ -M_{Adj} & M_{\overline{\square}\,\overline{\square}} \end{pmatrix} \tag{6.43}$$

Adding the original superpotential in terms of the mesons we obtain

$$W = W_0 + M_{\overline{\square}\,\overline{\square}} M_{\square\,\square} \tag{6.44}$$

We can solve the equations of motion for the massive mesons $M_{\overline{\square}\,\overline{\square}}$, $M_{\square\,\square}$ just by setting them to zero. The resulting superpotential is then given by:

$$W = \mathrm{Pf} \begin{pmatrix} 0 & M_{Adj} \\ -M_{Adj} & 0 \end{pmatrix} = \det M_{Adj}. \tag{6.45}$$

We can now perform a brane motion taking the configuration to that in Figure 6.9b, where there is no brane stretching on the 3-cycle $[a_2, b_1]$. This result takes into account the brane creation effects due to the presence of the orientifold planes, as discussed in [95]. Despite the non-trivial change in the brane configuration, the superpotential is continuous. Namely the above superpotential is still generated, but now via an exotic $O(1)$ instanton on $[a_2, b_1]$ which can contribute[7]. The calculation in this case is simple. In Figure 6.9b, the theory on the $SU(N)$ brane is locally $\mathcal{N} = 2$, in particular it has an adjoint, which we identify with the adjoint meson of the gauge analysis (in both cases it parametrizes sliding the D6-branes along the two b-type degenerations, and their images along the a-type ones). The zero modes λ, $\bar{\lambda}$ between the D2-brane instanton and the $SU(N)$ brane couple to this adjoint via a term

$$S = \ldots + \lambda M_{Adj} \bar{\lambda} \tag{6.46}$$

in the instanton action (this has the same origin as the usual coupling between the adjoint and the flavors in $\mathcal{N} = 2$ theories). Integrating over the fermionic zero modes gives us the determinant operator we found in

[6] We have omitted here the meson singlet under the $SU(N)$. In the stringy setup is will get a mass due to a coupling related by the $\mathcal{N} = 2$ susy to the one giving mass to the $U(1)$ gauge boson.

[7] Recall that the orientifold projection acts oppositely on 4d space filling D6-branes and D2-brane instantons, so an orientifold giving a USp gauge group will give a $O(1)$ D-instanton. This works in the same way as for the perhaps more familiar D5-D9 system.

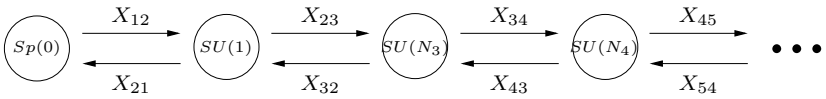

Figure 6.10: Relevant nodes of the quiver theory for the orbifolded conifold. We have indicated the ranks at the bottom of the cascade. There can be more $SU(N)$ nodes to the right, ending with another $USp(N)$ group. X_{ij} denotes the bifundamental from node i to node j.

equation (6.45). We thus recover the same kind of superpotential, with an exponential dependence on the closed string modulus associated to the 3-cycle defined by the degenerations b_1 and a_2. Thus the result is continuous across the motion in moduli space, in which gauge and non-gauge instantons turn into each other[8].

6.4.2 A duality cascade example

Let us proceed to the more complicated case of the duality cascade studied in [120], and show the continuity of the nonperturbative superpotential along a complicated chain of Seiberg dualities.

The theory under consideration is given by the quiver in Figure 6.10, with gauge group at the bottom of the cascade given by $USp(0) \times SU(1) \times SU(N_3) \times \ldots$ with $N_3, \ldots$ arbitrary. The superpotential is given by:

$$W = \sum_{i=1}^{N_{factors}} (-1)^i X_{i,i+1} X_{i+1,i+2} X_{i+2,i+1} X_{i+1,i}. \tag{6.47}$$

This theory can be easily realized in string theory by modding out an orbifold of the conifold [104] by a suitable orientifold action [122]. In terms of the geometries in Section 6.1, we can consider a periodic array of degenerations $a_1, b_1, a_2, b_2, a_3, b_3, a_4, b_4$ and introducing an orientifold quotient $\Omega R(-1)^{F_L}$, with R given by equation (6.4).

In terms of the geometrical setup, the cascade of Seiberg dualities simply amounts to a motion in moduli space, generalizing that discussed above. In this situation there are also some brane creation effects due to the presence of the orientifold planes, as discussed in [95]. The configuration one step up in the cascade is given by the same quiver but with different ranks:

$$USp(2N_2 - 4) \times SU(N_2) \times SU(N_4 - 1) \times SU(N_4) \times \ldots \tag{6.48}$$

[8] One may try to discuss a similar configuration without the external degenerations and with semi-infinite branes. In this case the computation for Figure 6.9a gives a non-zero superpotential, while in Figure 6.9b there are no dynamical mesons to help saturate the fermion zero modes of the instanton, hence there is no superpotential. The mismatch is related to the non-compact D-branes in the configuration (see comment at the beginning of Section 6.1). Upon "compactification" by adding the external degenerations at a finite distance, one recovers the above full agreement.

In particular all nodes are occupied so there are no non-gauge instantons at this level.

The detailed gauge theory analysis of [120] for the initial configuration shows that the nonperturbative superpotential of the initial gauge theory configuration can be described in terms of the fields at the end of the cascade as

$$W_{np}^{bottom} = X_{23}X_{32} + \det(X_{34}X_{43}) + X_{23}X_{34}X_{43}X_{32} + \dots \tag{6.49}$$

where we have omitted some quartic terms of the same form as those in (6.47), which are tree level from the point of view of g_s, and thus not particularly interesting here. We rather focus on the first two terms, which are nonperturbative. Our aim is to recover them by studying possible D-brane instantons in the final configuration. Note that the determinant term was dropped as irrelevant in [120], since they were just interested in the infrared behaviour of the theory. We are interested in the continuity of the full superpotential so we should keep it, since it carries an implicit dependence on the closed string modulus controlling the corresponding cycle. For completeness, let us reproduce here a sketch of the gauge theory analysis done in [120]:

The gauge theory analysis

We will assume for simplicity a hierarchy of scales given by

$$\Lambda_1 \gg \Lambda_3 \gg \dots \gg \Lambda_2 \gg \Lambda_4 \gg \dots \tag{6.50}$$

We will choose the ranks in such a way that the bottom of the cascade is described by the quiver in Figure 6.10. This can be achieved by choosing the following ranks:

$$N_1 = 2N_2 - 4 \quad ; \quad N_3 = N_4 - 1. \tag{6.51}$$

Due to the hierarchy of scales we have chosen, the first node to become strongly coupled is the USp one. This goes just as in Section 6.4.1, and we end up with a $USp(0)$ group, some mesons M_{Adj} charged in the adjoint of $SU(N_2)$, and a nonperturbative superpotential:

$$W_{np} = \det M_{Adj} \tag{6.52}$$

Now we have to dualize the $SU(N_3)$ node. We have $N_f = N_2 + N_4$, so the dual description is in terms of a $SU(N_f - N_c = N_2 + 1)$ gauge group, and the dual quarks and mesons. The mesons get a mass due to the quartic terms in the superpotential 6.47, and they can be integrated out. Also, there is a mass coupling coming from the superpotential between M_{Adj} and the

meson $M_2^{(3)}$ of $SU(N_3)$ charged under the adjoint of $SU(N_2)$. The relevant term in the superpotential looks like:

$$W = \ldots + \det M_{Adj} + M_{Adj} M_2^{(3)} + M_2^{(3)} q_{23} q_{32} \tag{6.53}$$

with q the dual quarks. Integrating the mesons out, we end up with a superpotential:

$$W = \ldots + \det q_{23} q_{32} + q_{23} q_{34} q_{43} q_{32} \tag{6.54}$$

where we have included a piece of the quartic superpotential that will play a role in a moment.

Going down in energy, eventually the $SU(N_2)$ node will become strongly coupled. It has $N_f = N_2 + 1$, coming just from the third node, so the gauge group confines completely (let us call the resulting node "$SU(1)$", as in the stringy picture of the duality there is a single brane remaining). The description is in terms of mesons $M_3^{(2)}$ in the adjoint of the third node and baryons B_3, $\tilde{B}_3$ in the fundamental and antifundamental. There is a superpotential given by:

$$W = \ldots + B_3 M_3^{(2)} \tilde{B}_3 - \det M_3^{(2)} \tag{6.55}$$

When the second node confines the q_{23}, q_{32} quarks get confined into baryons and mesons. In particular, the superpotential 6.54 can be expressed as:

$$W = \ldots + B_3 \tilde{B}_3 + M_3^{(2)} q_{34} q_{43} \tag{6.56}$$

The last step in the chain of dualities, as far as the first three nodes are concerned, comes from dualizing the fourth node. This is important for our discussion as it gives a mass to $M_3^{(2)}$ via the dual of the last coupling in equation (6.56). After dualizing node 4, we end up with a superpotential:

$$W = \ldots + B_3 M_3^{(2)} \tilde{B}_3 - \det M_3^{(2)} + B_3 \tilde{B}_3 + M_3^{(2)} M_3^{(4)} - M_3^{(4)} X_{34} X_{43} \tag{6.57}$$

where we have denoted as X_{34}, X_{43} the dual quarks of node 4 charged under node 3. We see that the mesons of node 3 get massive as expected. Integrating them out, one gets:

$$W = \ldots + B_3 X_{34} X_{43} \tilde{B}_3 - \det X_{34} X_{43} + B_3 \tilde{B}_3 \tag{6.58}$$

which is the same as the one in equation (6.49) up to a relabeling of the baryons as X_{23}, X_{32}.

D-instanton effects at the bottom of the cascade

Let us now consider the final configuration, where the 4d space filling D6-brane configuration gives rise to a structure $USp(0) \times SU(1) \times SU(N_3) \times \ldots$

with $N_3, \ldots$. There are two instantons which can contribute to the superpotential. There is a non-gauge D-brane instanton arising from the cycle corresponding to the node of the quiver with no 4d space filling branes. As argued in [120] and we now review, it leads to the first mass terms in (6.49). The instanton has $O(1)$ symmetry and has two neutral fermion zero modes. In addition it has two fermion zero modes α and β from the open strings going from the D-instanton to the $SU(1)$ brane. The instanton action contains a coupling of the form $\alpha X_{23} X_{32} \beta$, arising from the same disk instantons that produce the terms in (6.47). Integrating over these fermionic zero modes, we get a mass contribution to the superpotential:

$$\begin{aligned} W &= \ldots + \int d\alpha d\beta \ \alpha X_{23} X_{32} \beta \\ &= \ldots + X_{23} X_{32}. \end{aligned} \tag{6.59}$$

There is another D-brane instanton which contributes to the nonperturbative superpotential, and which involves a somewhat novel effect. It corresponds to a D-brane instanton on the node with 4d group "$SU(1)$". This instanton does not have a proper gauge theory interpretation, but still it shares some common features with gauge instantons. Namely, since it is a $U(1)$ instanton, not mapped to itself by the orientifold action, it has four fermion zero modes. The two Goldstinos of $\mathcal{N} = 1$ supersymmetry remain, while the two accidental $\mathcal{N} = 2$ Goldstinos have non-trivial couplings with the bosonic and fermionic zero modes in the sector of open strings between the instanton and the $SU(1)$-brane. For gauge D-brane instantons, integration over these zero modes imposes the fermionic ADHM constraints [123], and reproduces the correct measure on instanton (super)moduli space. In the present setup, we lack an appropriate gauge theory interpretation for the coupling, but its effect of leading to the saturation of the additional fermion zero modes remains. We are therefore left with the two Goldstinos θ^α needed for contributing to the superpotential. We still need to saturate the charged zero modes going from the D-instanton to the $SU(N_3)$ group, there are $2N_c$ of these, N_c of each chirality. Let us call them λ_{23} and λ_{32}. They can be saturated via the same kind of quartic coupling $\lambda_{23} Y_{34} Y_{43} \lambda_{32}$ as above. Expanding the instanton action we get a contribution to the superpotential:

$$\begin{aligned} W &= \ldots + \int [d\lambda_{23}][d\lambda_{32}] \ \exp\left(\lambda_{23} Y_{34} Y_{43} \lambda_{32}\right) \\ &\simeq \ldots + \epsilon^{i_1 \ldots i_{N_3}} \epsilon^{k_1 \ldots k_{N_3}} (Y_{34} Y_{43})_{i_1, k_1} \cdot \ldots \cdot (Y_{34} Y_{43})_{i_{N_3}, k_{N_3}} \\ &\simeq \ldots + \det(Y_{34} Y_{43}). \end{aligned} \tag{6.60}$$

which correctly reproduces the second term in the nonperturbative superpotential 6.49.

We see that there is a beautiful agreement between both computations. Clearly, there are plenty of other systems where the agreement between the

superpotential up in the cascade and at the lower steps can be checked. We leave this analysis for the interested reader.

6.5 Topology changing transitions in F-theory

In this section we comment on an intriguing implication of the continuity of the nonperturbative superpotential, when considering the F-theory viewpoint on nonperturbative effects on systems of D7-branes near lines of marginal stability. The process of D7-branes splitting/recombining corresponds to a topology changing transition in F/M-theory, along the lines of [124]. Our results therefore imply a non-trivial relation between the nonperturbative superpotentials on topologically different Calabi-Yau fourfolds.

We restrict to a simple local analysis of such D7-brane system, and of its F-theory lift. Consider the type IIB D7-brane realization of the D-brane configuration studied in Section 6.3.1. There are two stack of D7-branes wrapped on two holomorphic 4-cycles C_1 and C_2, intersecting over a complex curve Σ. It is possible to consider concrete examples of Calabi-Yau threefolds and 4-cycles with $h_{2,0}(C_1) = 1$, $h_{2,0}(C_2) = 0$, which would fit our example, but it is not necessary to illustrate the main point. In fact, the basic idea is already present in a local model in a neighborhood of a point P in Σ. Using local complex coordinates z, w, u we have D7-branes on C_1, described locally by $w = 0$ (and z, u arbitrary) and D7-branes on C_2, described locally by $z = 0$ (and w, u arbitrary). The curve Σ is locally parametrized by u. In this local analysis, the direction u is an spectator and we can ignore it in the following (although it can lead to global obstructions in the compact model). Thus we have a system of D7-branes wrapped on the locus $zw = 0$.

The F-theory lift of this configuration is described by an elliptic fibration over the threefold, with degenerate fibers (due to pinching of a 1-cycle) over the 4-cycle wrapped by the D7-branes. We can also work locally near the pinching of the elliptic fiber, and describe the geometry as a $\mathbb{C}^*$ fibration. For n, m D7-branes on the two different 4-cycles, the local description of the fourfold is thus given by the spectator direction u times the manifold

$$xy = z^n w^m \tag{6.61}$$

This kind of geometries were introduced in [104]. Let us focus on the simplest representative, $n = m = 1$, the conifold. In fact, the configuration corresponds to the resolved conifold, with the 2-cycle described as follows. The fiber on top of the intersection locus $z = w = 0$ on the base degenerates into two 2-spheres touching at two points. The class of the 2-cycle corresponds to one of these 2-spheres (while the sum is the class of the fiber). For intersecting D7-branes, the F/M-theory lift corresponds to the limit of vanishing 2-cycle (and no background 2-form potential can be turned on). We are thus at the singular conifold limit, in which there are massless states

[125] (arising from wrapped M2-branes in the M-theory picture). These are nothing but the open strings degrees of freedom between the two D7-brane stacks.

Consider now the D7-brane system away from the line of marginal stability. The D7-branes recombine into a single smooth one, wrapped on a 4-cycle which is a deformation of the above, namely $zw = \epsilon$. In the local model, ϵ corresponds to a modulus, a flat direction for the fields arising at the intersection of the D7-branes. In the global model the flat direction is obstructed by a D-term condition, and the value of ϵ is fixed by the closed string modulus moving us away from marginal stability. The F-theory lift of this configuration corresponds to the geometry

$$xy = zw - \epsilon \tag{6.62}$$

This describes the deformed conifold. This is expected, since the massless charged states have acquired a vev, thus triggering a topology changing transition [126]. The behaviour of the arbitrary $n = m$ case is similar, using the deformation $xy = (zw - \epsilon)^n$.

The local analysis shows that the crossing of a line of marginal stability corresponds to a topology change in the F/M-theory fourfold. The continuity of the nonperturbative superpotential in this case implies a non-trivial matching between topologically different spaces.

It would be interesting to have a more microscopic derivation of this result. We conclude by mentioning a few key points to this aim. The relevant instanton in the IIB picture is a D3-brane wrapped on the 4-cycle which splits at the line of marginal stability. As emphasized, the continuity of the process requires a non-trivial contribution from a 2-instanton process in the intersecting D7-brane configuration. In the F/M-theory lift, the effect arises from an M5-brane instanton wrapping a 6-cycle which splits, and there should exist a non-trivial contribution to the superpotential arising from a 2-instanton process involving the two M5-brane instantons wrapped on the two components of the split 6-cycle. Thus our analysis of superpotentials from multi-instantons should apply to M5-brane instantons on M-theory on CY fourfolds. Clearly this goes beyond the analysis in [127], since one would require a suitable generalization to M5-brane instantons on singular 6-cycles. In this respect, notice that one can rephrase the multi-instanton process as a nonperturbative lifting of zero modes of one M5-brane (A) by the effects of a second M5-brane (B). This is not inconsistent with the arguments in [127], which were based on counting fermion zero modes chiral with respect to the $U(1)$ symmetry acting on the normal directions transverse to the M5-brane A. Indeed the second M5-brane B can induce couplings which violate this $U(1)$ (which acts on directions along the volume of the M-brane B). Thus the nonperturbative lifting mechanism is powerful enough to allow the appearance of contributions from instantons which violate the celebrated

arithmetic genus condition in [127]. Concrete examples of this are provided by suitable F/M-theory versions of the type II models studied in this chapter.

Chapter 7

A gauge mediated model

In the previous chapters we have discussed different ways of embedding metastable supersymmetry breaking vacua in string theory. Of particular interest here will be the realization discussed in Chapter 4, where we described how DSB branes admit metastable vacua upon the addition of massive flavors.

In this chapter we will discuss how to apply this knowledge, together with the techniques of resolution and deformation of singularities studied in Chapter 5, in order to build a toy model of gauge mediated supersymmetry breaking. We will implement this scenario as a configuration of two stacks of branes in type IIB string theory located at the two daughter singularities of a slightly resolved or deformed singularity, so the main interaction between them is via open strings. One of the stacks models the observable sector (ideally the MSSM, but we will content ourselves with a simpler relative of it), while the other breaks supersymmetry, in our case by being trapped in a metastable non supersymmetric vacuum. This general framework was discussed in [46], which we follow here.

This chapter is organized as follows. We start in Section 7.1 by describing the main characteristics of the proposed framework for implementing GMSB in string theory. In Section 7.2 we discuss how is the sector of massive mediators determined in the construction, this section is essentially a review of the results of Section 5.1.3 in a slightly different language, we include it here for ease of reading. We proceed to discuss a simple toy model in Section 7.3. It is not intended to be an accurate description of reality, just some suggestive and simple example that highlights some points of this class of models. As a last point in Section 7.4 we discuss some possible interesting generalizations of the construction. As will hopefully become clear in this chapter, the procedure is quite flexible, we only illustrate some particularly representative directions in which it can be extended.

7.1 Overview of the construction

In this chapter we will try to construct models of gauge mediated supersymmetry breaking (GMSB) in string theory[1]. An important previous attempt to embed GMSB in string theory is [129], where the susy breaking in a sector of DSB branes is transmitted via gauge interactions (light open string modes) to a visible sector (a stack of branes a very short distance away in string units from the DSB branes). Here we will present a scenario with the same broad features to the one presented in [129], but with several advantages in the concrete implementation.

In particular, we will construct models in type IIB of branes at toric singularities. We will put branes on the singularity in such a way that when the singularity is partially smoothed (either via deformation or resolution) one stack of branes ends up in one of the daughter singularities, and another stack in the other daughter singularity (we can of course play the same game in the case where there are more than two daughter singularities). Thanks to the technology developed in Chapters 4 and 5 we will be able to realize two important features easily: the supersymmetry breaking sector can be realized as the metastable vacuum of a flavored DSB brane, and the mediator sector will come from the massless states in the mother singularity that become massive in the smoothing process, with masses given by the size of the blown-up cycle.

An important characteristic of the local setups we will be discussing is that they are manifestly insensitive to most UV details of the configuration, namely to the global structure of the internal space. Most physics can be understood from the local structure around the singularity, which allows us some freedom when we want to incorporate realistic gravity or closed string moduli stabilization into the models.

As a last remark, although we center our study in some simple examples, the construction is clearly very general. One can analyze a multitude of examples easily using the ideas described in this chapter.

7.2 Description of the mediator sector

Let us start by describing how to obtain in a simple way the sector of mediators. This can most easily be done in terms of dimer diagrams. In this language the resolution consists of splitting the original dimer diagram into two subdimers given by the removal of some edges in the original dimer diagram (equivalently, by the Higgsing of the corresponding gauge factors). We have described the rules for determining which edges get vevs in Chapter 5. We can also derive easily the spectrum of massive mediators, this was

[1]For an excellent review of GMSB the reader can consult [128].

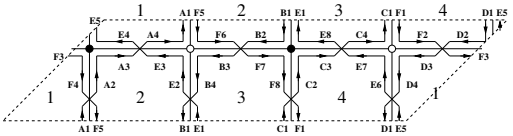

Figure 7.1: Zig-zag paths for the dimer diagram of the double conifold. The numbers label the different gauge factors.

done in Section 5.1.3, let us repeat the results of that section here for easier reading:

1. Each edge that disappears from a daughter dimer diagram gives rise to a massive vector multiplet in the adjoint of the resulting unified gauge factor. The vector multiplet comes from the non diagonal parts of the original factors, that get masses due to the Higgs mechanism.

2. Each face in the original dimer diagram gives rise to massive vector multiplets in bifundamentals of the corresponding gauge groups in the final dimer. If we denote the final gauge groups as N_1 and N_2 the resulting vector multiplet transforms in the $(N_1, \overline{N_2})$.

3. For each edge present in both daughter diagrams there is one chiral multiplet in the $(N_1, \overline{N_2})$ bifundamental representation, i.e., a bifundamental charged under the faces the edge separates (one factor being in the first dimer, and the other in the second). That the bifundamentals pair up consistently in order to form massive scalar multiplets is assured by the dimer diagram structure.

4. If the dimer diagram contains bi-valent nodes the corresponding edges each describe a massive scalar multiplet in the bi-fundamental of the two faces they separate.

5. For each D7-brane passing through an edge of type 1 there is a massive scalar multiplet in the fundamental representation of the $U(N_2)$ gauge factor corresponding to the resulting recombined face. Similarly for edges of type 2. When there are N_7 D7 branes across such an edge the massive multiplet transforms as $(N_{D3}, \overline{N_7})$.

All these rules are easy to understand just looking at open strings going from dimer to dimer. Let us illustrate the application of the rules in the case of the double conifold going to two conifolds. The dimers for this resolution have already been shown in Figures 5.4 and 5.7, we show them again in Figures 7.1 and 7.2, where we have also labeled the different gauge factors by integer numbers.

Applying the rules above one finds the following massive matter content after the resolution:

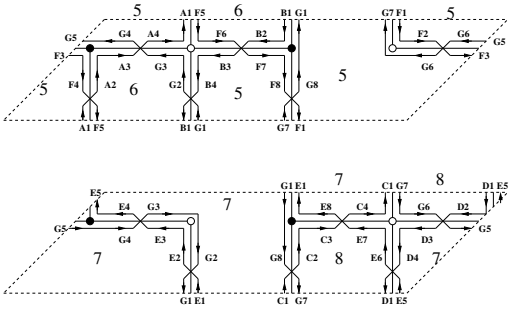

Figure 7.2: Zig-zag paths corresponding to the two daughter theories, in the splitting of the double conifold singularity to two conifold singularities, with the corresponding dimers shown as thick lines. The numbers label the different gauge groups.

- **Vector multiplets in the adjoint:** There are two edges of type 1, both giving rise to massive vector multiplets in the adjoint of the gauge factor 7. Similarly the two edges of type 2 give massive vector multiplets in the adjoint of 5.
- **Vectors in the bifundamental:** The massive vectors are found to be in the representation

$$(5, \overline{7}) + (6, \overline{7}) + (5, \overline{7}) + (5, \overline{8}) + \text{c.c.} \tag{7.1}$$

- **Scalar multiplets:** These are in the representation:

$$2(5, \overline{7}) + (6, \overline{7}) + (5, \overline{8}). \tag{7.2}$$

7.3 Our toy model

Let us proceed to the construction of our toy model. The strategy consists of putting branes in a "big" singularity in such a way that when doing the resolution of the singularity the two remaining singularities model a visible sector and a hidden supersymmetry breaking sector. The toric diagram for the "big" singularity is obtained by pasting the toric diagrams for the two small singularities along a common edge. In terms of web diagrams the same process is described as attaching two web diagrams through an external leg, making it internal. Our toy model consists of the pasting of dP_0 and dP_1, we show the pasting process that gives us the "big" singularity in Figure 7.3. The dimer diagram for this geometry has already been described in the literature [94], so we do not need to obtain it ourselves (although it is not difficult to do with the methods described in Section 5.1 starting from some orbifold of the conifold, for example). It is a member called $X^{3,1}$ of the infinite family $X^{p,q}$ [130]. We show its dimer diagram and the resolved geometry in Figures 7.4 and 7.5.

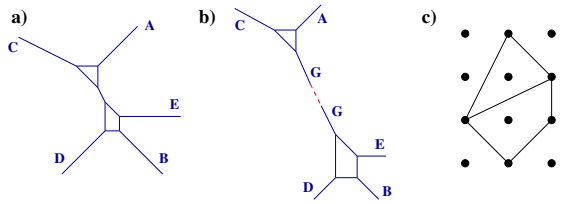

Figure 7.3: a) Web diagram for a local CY with dP_0 and dP_1 singularities, for generic sizes of all 2- and 4-cycles. b) The two singularities are obtained when the cycles corresponding to the two finite faces shrink to zero size, while the leg G remains finite and controls the distance between the singularities. c) Toric diagram for the geometry, with the partial resolution leading to the two separated singularities.

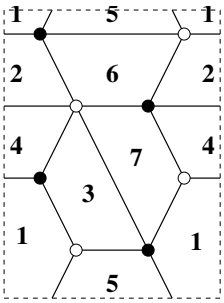

Figure 7.4: The dimer diagram for the $X^{3,1}$ theory.

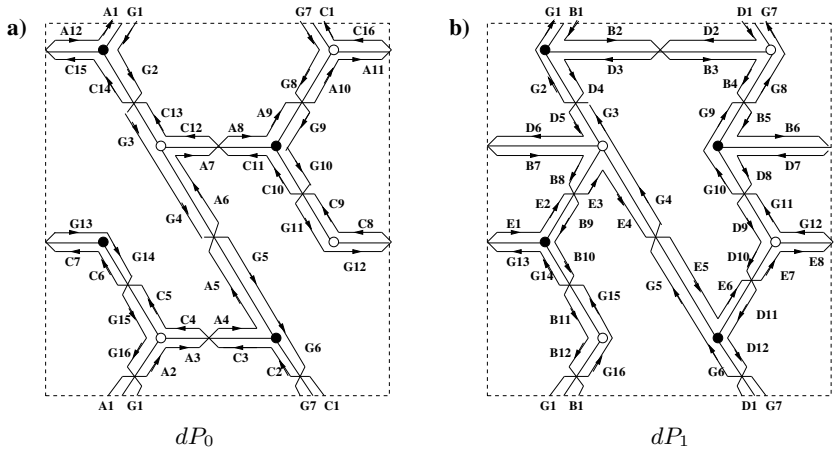

dP_0 dP_1

Figure 7.5: Daughter dimer diagrams obtained in the partial resolution of $X^{3,1}$ to a geometry with dP_0 and dP_1 singularities.

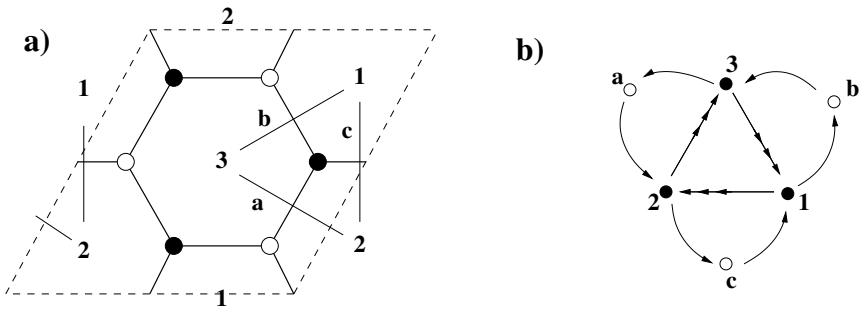

Figure 7.6: a) Extended dimer diagram of the dP_0 theory with D7-branes represented as segments across the edges. b) Quiver diagram including D7-branes (represented as white nodes). There are 33-37-73 couplings involving the 33 bifundamental across which the corresponding D7-brane stretches.

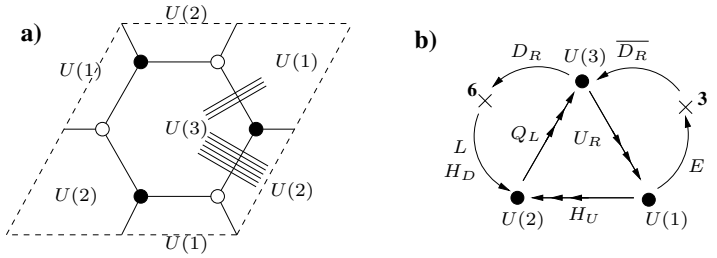

Figure 7.7: Dimer diagram (a) and quiver diagram (b) for a configuration of D3/D7 branes realizing a gauge theory close to the MSSM.

The visible sector

Our visible sector will be given by theory of (fractional) D3 branes at an orbifold of flat space, namely $\mathbb{C}^3/\mathbb{Z}_3$ or dP_0, as it is also known. We also introduce some flavor branes in order to have a matter content reasonably close to that of the MSSM. The relevant quiver and dimer diagrams are shown in Figure 7.6. In this theory there is just one massless $U(1)$, which is given by:

$$Q_Y = -\frac{1}{2}\left(\frac{1}{3}Q_3 + \frac{1}{2}Q_2 + Q_1\right), \tag{7.3}$$

where the Q_i charge refers to the charge under the $U(1)$ factor of $U(i)$ in the original theory. The rest of the $U(1)$s become massive and disappear from the low energy theory, so we are left with a $SU(3) \times SU(2) \times U(1)$ theory. Furthermore, the charge determined by equation (7.3) is such that it correctly reproduces the hypercharges of the MSSM fields. The resulting quiver gauge theory is shown in Figure 7.7, with labels indicating the analogous field in the MSSM. The matter content is that of the MSSM with the addition of some extra Higgs and vector matter, some further details of this model are studied in [131].

The hidden sector

For the sector breaking supersymmetry we can choose any of the metastable vacua described in Chapter 4. We will focus on the simplest one, the flavored DSB brane on the complex cone over dP_1, which we have already studied in detail in Section 4.2. As discussed there, the dP_1 theory when appropriately flavored has, in addition to the usual runaway vacuum due to the ADS superpotential, a metastable non supersymmetric local minimum. Let us quickly review here what we did in Section 4.2.

We will consider the DSB fractional brane in dP_1 described by the rank vector $(0, M, 2M, 3M)$. The $U(1)$ factors get massive due to the coupling to closed string modes, the resulting gauge group is then given by $SU(3M) \times SU(2M) \times SU(M)$. The superpotential for this theory is (this can be read from the dimer):

$$W = X_{23}X_{31}Y_{12} - X_{23}Y_{31}X_{12}, \tag{7.4}$$

where we have denoted the factors under which each bifundamental transforms. We also have a field Z_{12} which does not appear in the superpotential one reads from the dimer. When the $SU(3M)$ dynamics dominates the corresponding gauge factor confines and develops a (runaway) ADS superpotential, see [79, 132] for detailed discussions. Let us sketch the main point here. When the gauge factor confines a dual description in terms of mesons is more convenient, the appropriate mesons are given by $M_{21} = X_{23}X_{31}$ and $M'_{21} = X_{23}X_{31}$. Out of these we construct the mesonic matrix $\mathcal{M} = (M_{21}; M'_{21})$. The IR superpotential with the nonperturbative ADS term is then given by:

$$W = M_{21}Y_{12} - M'_{21}X_{12} + M\left(\frac{\Lambda_3^{7M}}{\det \mathcal{M}}\right)^{\frac{1}{M}}. \tag{7.5}$$

We easily see that the F-term equations push the vacuum towards infinity in field space. To see this, notice that the F-terms for X_{12} and Y_{12} impose $M_{21} = M'_{21} = 0$. Solving next the meson F-terms pushes the X_{12} and Y_{12} towards infinity (we assume canonical Kähler potential).

As discussed in Section 4.2, the introduction of massive (with masses well below the dynamical scale of the theory) flavors in this theory induces the existence of a local metastable vacuum. We show an example of a configuration giving local metastable non supersymmetric vacua in Figure 7.8.

Putting everything together

So far we have been slightly cavalier about the location of the D7 branes. If we are going to get the dP_0 and dP_1 geometries from a resolution of $X^{3,1}$ then the D7 branes in both sides need to obey certain consistency conditions, essentially being obtainable from a system of D7 branes in a $X^{3,1}$ singularity

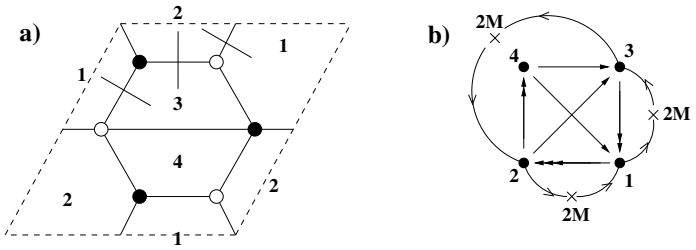

Figure 7.8: (a) Dimer diagram for a configuration of D3- and D7-branes in the dP_1 singularity leading to a gauge theory with meta-stable supersymmetry breaking vacua. (b) Extended quiver diagram for the theory.

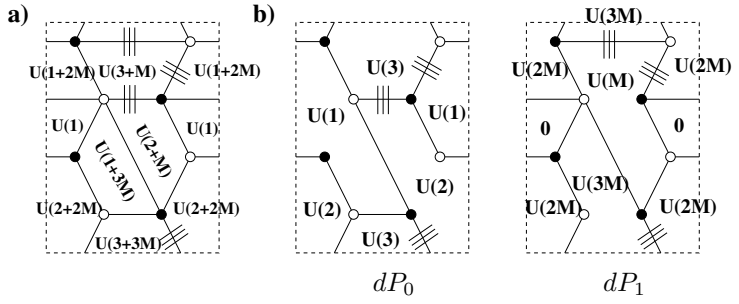

Figure 7.9: Gauge theories with D7-branes at (a) $X^{3,1}$, (b) dP_0 and dP_1 singularities obtained after partial resolution.

via a resolution. The effect of the resolution on the D7 branes has been described in Section 5.1.3. Another basic condition we have to fulfill is that the ISS analysis for the existence of a local long-lived metastable non supersymmetric vacuum is applicable. This restricts us to $M = 2$ in order to be in the free magnetic phase.

Luckily, both conditions can be satisfied at the same time, we show an example of an interesting configuration in Figure 7.9.

The mediator sector

As discussed in Section 7.2, the dimer diagram allows to easily read off the bi-fundamental vevs leading to this Higgsing, and to obtain the massive spectrum of mediators. We denote fundamental representations for the group $U(i)$ by i (for fields charged under the dP_0 sector) and fundamentals of $U(kM)$ by kM (for fields charged under the dP_1 sector), see Figure 7.9.

Vector multiplets in the adjoint: There are 7 massive vector multiplets in adjoint representations, coming from the 7 edges of type 2 (associated to the fields X_{56}, X_{24}, X_{43}, X_{71}) or type 1 (associated to X_{21}, X_{76} and X_{56}). They lead to massive vector multiplets in the representation

$$\mathrm{Ad}_2 \,+\, \mathrm{Ad}_3 \,+\, 2\,\mathrm{Ad}_1 \,+\, \mathrm{Ad}_M \,+\, \mathrm{Ad}_{2M} \,+\, \mathrm{Ad}_{3M} \tag{7.6}$$

Vectors in bi-fundamentals: There is one such massive vector multiplet for each face in the original gauge group. They transform in the representation

$$(2,\overline{2M}) + (1,\overline{2M}) + (1,\overline{3M}) + (3,\overline{3M}) + (3,\overline{M}) + (2,\overline{M}) \tag{7.7}$$

Note that face 4 of the $X^{3,1}$ dimer does not contribute, as the corresponding gauge factor in the dP_1 dimer has rank 0 with our choice of fractional branes.

Gauge scalar multiplets: One finds the following spectrum of scalar multiplets:

$$(1,\overline{2M}) + 2\,(2,\overline{3M}) + 2\,(3,\overline{2M}) + 2\,(1,\overline{M}) \tag{7.8}$$

Flavor scalar multiplets: From the strings between D7 branes localized at one daughter singularity, and the branes localized at the other daughter singularity, we get the following spectrum of scalar multiplets:

$$(\overline{F_1},3) + (\overline{F_0},M) \tag{7.9}$$

where F_i denotes the flavor group for the stack of D7 branes localizing at the dP_i daughter singularity, and disappearing from the other daughter singularity.

7.4 Generalizations

The class of models based on the previous ideas is quite wide, and it is relatively easy to build interesting generalizations. In this section we describe a few of them which are particularly interesting. We will only sketch the main ideas, as the detailed analysis, while possible in most cases using the tools we have described, is in practice quite involved and not particularly illuminating. We just want to illustrate the great flexibility of the setups we are considering.

Flavor universal models

One important constraint in supersymmetric model building is that of universality. A number of conflicts with observation goes away if we make the soft terms flavor independent.

The dP_0 singularity itself treats the three families equally, this is represented in terms of the web diagram as its invariance under the order 3 $SL(2,\mathbb{Z})$ rotation:

$$\begin{pmatrix} -1 & -1 \\ 1 & 0 \end{pmatrix}, \tag{7.10}$$

under which the diagram stays invariant (the individual legs get permuted). In this language it is easy to see how the problem of non universality arises,

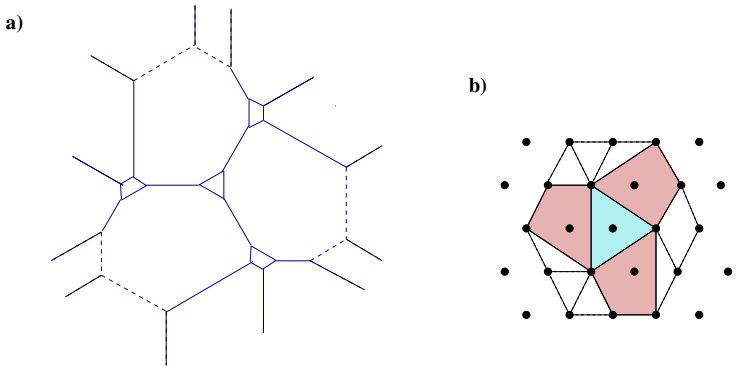

Figure 7.10: The web diagram (a) and toric diagram (b) for a singularity admitting a partial resolution with one dP_0 singularity (in blue) and three (symmetrically distributed) dP_1 singularities (in red).

it is a reflection of the fact that we have to choose a particular leg to attach to the dP_1 geometry in order to build the parent $X^{3,1}$ geometry. When we resolve the singularity the massless (flavor blind) sector is recovered, but the massive mediator sector, which induces the soft terms, is not invariant under the $\mathbb{Z}_3$ symmetry.

The good news is that this description of the problem also suggests a possible solution, namely one should attach three dP_1 geometries to the external legs in a symmetric way. The resulting toric variety is shown in Figure 7.10. It turns out that the convex hull of the minimal polygon one builds[2] is simply an orbifold of the complex cone over dP_3, a space we are already familiar with, so the detailed analysis should not be very difficult.

The Δ_{27} space

An interesting generalization is that to non toric Calabi-Yau spaces. Doing this in generality is beyond our tools, but some examples closely linked to toric varieties can be easily described. An interesting example that has been studied in the model building literature [131, 133, 134] is that of the simplest non A-D-E orbifold, named Δ_{27}. One simple way to describe it is as the quotient of $\mathbb{C}^3$ by the three actions:

$$\theta \;:\; (z_1, z_2, z_3) \to (\alpha z_1, \alpha^2 z_2, z_3) \tag{7.11}$$

$$\omega \;:\; (z_1, z_2, z_3) \to (z_1, \alpha z_2, \alpha^2 z_3) \tag{7.12}$$

$$\sigma \;:\; (z_1, z_2, z_3) \to (z_2, z_3, z_1), \tag{7.13}$$

where we have defined $\alpha = e^{2\pi i/3}$. We see that the first two actions define a $\mathbb{C}^3/(\mathbb{Z}_3 \times \mathbb{Z}_3)$ orbifold of flat space (which is describable as a toric variety),

[2] In other words, simply attaching three dP_1 geometries symmetrically does not give a convex polygon, so it does not define a toric variety. We have to add some extra triangles in order to achieve convexity, this gives the convex hull.

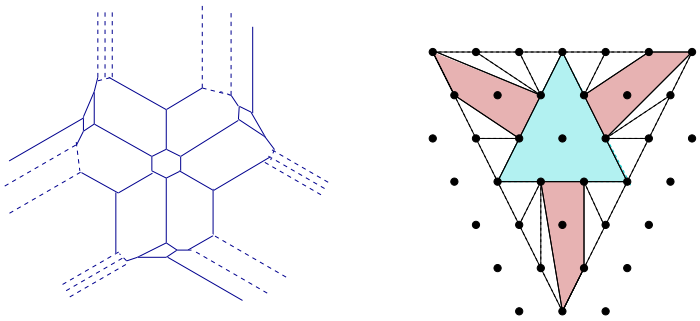

Figure 7.11: The parent toric geometry for the $\mathbb{C}^3/\Delta_{27}$ singularity with a supersymmetry breaking sector (given by dP_1) coupling in an universal way to the visible sector.

while the last one cyclically interchanges the coordinates. The trick will thus be considering the geometry described by $\mathbb{C}^3/(\mathbb{Z}_3 \times \mathbb{Z}_3)$ attached to three dP_1 geometries distributed in a way invariant under cyclic coordinate permutations, and then taking the quotient by σ. The parent geometry can be straightforwardly analyzed with the methods described, the toric diagram is shown in Figure 7.11. Once one has the theory describing the parent singularity the theory in the quotient can be easily found using standard techniques, see for example [104].

Complex deformations

Let us consider, as the last generalization of the ideas in this chapter, complex deformation instead of resolution as the process that gives us the two sectors. One advantage of this process compared to that of resolution consists of the automatic stabilization of the deformation modulus (it is a complex structure modulus describing the size of the $\mathbf{S}^3$ we grow). In the resolution case one needs additional input in order to stabilize the size of the $\mathbf{S}^2$, which is usually a source of UV sensitivity. I.e., the precise details of how the mass scale of the mediators arises depend usually on global details. This is not the case for complex deformations, where the complex deformation parameter can be described completely in terms of the gauge theory, as done in Section 5.2.2. The problem is one of studying (locally) fractional brane dynamics, where the only external input is the string coupling.

The fact that this process depends so much on strong coupling dynamics in gauge theory makes it harder than resolution in some respects, for example the study of massive mediators. In the case of resolution the mediator sector can be easily described as open strings going from one set of branes to the other, while in the deformation case they correspond (in the gauge theory language) to states that become massive due to strong coupling dynamics. In practice, at least with the current tools, this makes the problem intractable

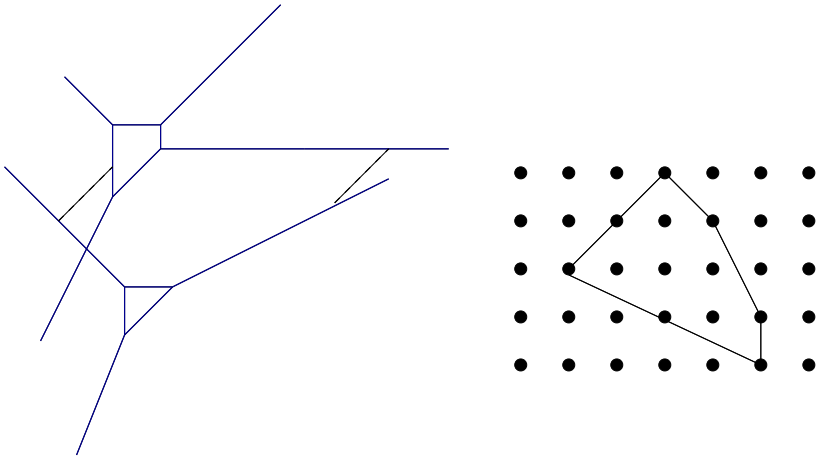

Figure 7.12: Web diagram and toric diagram of a singularity admitting a complex deformation to a geometry with a dP_0 and a dP_1 singularities. For clarity we have shown the web diagram explicitly split in two sub-webs, namely after the complex deformation. The finite size 3-cycle is shown as a dashed segment.

for the general case.

We will content ourselves with showing one geometry where complex deformation leads to the two sectors we have been studying, namely dP_0 and dP_1. The analysis of Section 5.2 provides us with the tools to study the process in gauge theory terms, and allows us to easily determine the fractional brane one should take in order to trigger the desired deformation (essentially draw in the Riemann surface a contour that divides the surface into the desired pieces, untwist the contour into the dimer, and then read the enclosed gauge groups). The relevant geometry is shown in Figure 7.12.

Chapter 8

Conclusions and future directions

In this work we have discussed a number of properties of D-branes at local Calabi-Yau geometries which are of interest for stringy model building. Let us shortly review them:

- In Chapter 3 we have discussed how to construct web of branes realizing the metastable ISS vacuum. The brane construction generalizes easily, and we discuss some of the generalizations that are expected to exhibit metastable vacua.
- In Chapter 4 we describe another system in string theory that is expected to have metastable vacua. This system is based on branes at toric singularities with obstructed complex deformations.
- In Chapter 5 we describe how the world volume theory in the branes feels the smoothing of the toric singularity. We find out that the end result is two or more sectors coupled only at the level of massive mediators.
- Chapter 6 contains a discussion of some interesting aspects of the continuity of the nonperturbative superpotential that might prove useful when building models involving D-instanton effects. These considerations are of interest not only for this class of examples, but are expected to also play a role in many other scenarios.
- In Chapter 7 we put together some of the pieces developed in the previous chapters, and show how brane configurations realizing a scenario of gauge mediated supersymmetry breaking can be easily constructed in local models. This is illustrated by some simple toy models.

The work described in this thesis can be extended in many directions. The most straightforward direction for extension corresponds to trying to

construct detailed realistic models using the ideas described here. In particular, in our discussion of the toy model of Chapter 7 any detailed analysis of the model presented beyond its very basic features is conspicuously absent. This was permissible in our situation as we were just illustrating how does the general mechanism work. In trying to construct any real phenomenological model one will face a number of generic interesting challenges that we ignored: moduli stabilization, including gravity, explaining the hierarchy, the μ problem, accommodating inflation, etc. Some of these could be solved by finding a consistent flux compactification where the singularity we focus on is at the bottom of some throat, perhaps something along the lines of [37, 135].

Another fruitful line of research concerns the direct embedding of the ISS vacua in string theory, as studied in Chapter 3. Using the brane web picture we were able to find some examples of theories where metastable vacua are expected to exist. One can use similar techniques to find plenty of other examples, see for example [136] and the references therein. It is also possible to find metastable vacua in other string systems, as mentioned in the introduction of Chapter 3. Some references for this are [54, 55, 56, 57, 58, 59, 60, 61, 62, 63].

One particularly interesting point of the brane configuration we study concerns its M-theory lift. As remarked in the introduction to Section 3.2, the M-theory lifts we describe in Chapter 3 for the metastable IIA configuration and the lift of the supersymmetric configuration have different asymptotic behavior, and thus are best thought of as states in different Hilbert spaces. In other words, in M-theory we do not have a metastable and a susy vacua for the same theory, as we have in gauge theory. It would be nice to find such a metastable susy breaking vacuum, staying as close to the ISS theory as possible.

This will probably be technically quite complicated, as the supergravity limit in which we have studied the M-theory curves is different from the gauge theory limit in which we obtain SQCD. There is no supersymmetry to protect the results as we change the relevant coupling constants, so anything can happen (and indeed, it seems like in the simplest case the metastable vacuum just disappears). A detailed discussion of these issues can be found in [53].

The discussion in Chapter 4 about finding metastable vacua in runaway quiver theories with flavors can also be extended in many ways. There are at least a couple of aspects of the construction which would be interesting to improve.

The first is the introduction of the small flavor masses. In our discussion the small masses for the flavors (required for the ISS analysis to be applicable) are tuned by hand. It would be much nicer to generate small masses in a more dynamical way, perhaps via D-instanton effects along the lines

sketched in Appendix D.

Another aspect of the construction which requires further study concerns the fate of the fields decoupled at tree level. As mentioned in the introduction to Chapter 4, and shown explicitly in some examples in that same chapter, in our constructions generically there are some fields not appearing in the tree level superpotential. Being decoupled from the superpotential at tree level, they are flat directions (assuming canonical Kähler potential) classically and at one-loop, but there is no reason to expect them to remain massless at higher orders, or nonperturbatively. Understanding whether these fields get positive or negative masses is essential for assessing the validity of the metastable solutions we found.

The discussion in Chapter 5 can also be improved in some ways. We could try to get a better qualitative understanding of the massive sector in the case of the deformation, and a better quantitative understanding of the resolution.

More generally, dimer models seem to be the proper language in which to discuss matters having to do with branes at toric singularities. Their utility is thus not limited for model building, they also seem to play an important but still relatively poorly understood role in crystal melting and black hole physics (see [137] and [138] for two recent papers exploring these topics).

As another two possible applications, they might also allow to study in a simpler way issues regarding the Π-stability [139] of D-branes in toric spaces, and they might be natural language in which to describe thermal Sasaki-Einstein backgrounds (for example in order to study thermal properties of dibaryons, which are generically abundant in AdS/CFT for Sasaki-Einstein spaces). It would be very interesting to develop these lines of research further.

Finally, the discussion in Chapter 6 can also be extended in a number of different directions.

An immediate application of the results presented here concerns a revision of previous scans for interesting D-instanton effects ([98] is one recent example). These scans dealt just with the one-instanton sector, so it would be interesting to see if interesting effects not present in the one-instanton sector appear in the multi-instanton sector.

Another aspect of the construction which could be explored further concerns contributions coming from BPS instantons which split into various instantons not mutually supersymmetric with respect to each other. If the continuity considerations still hold, and at this point we have no reason to expect them not to, this would be a nonsupersymmetric multi-instanton configuration contributing to the superpotential, which is somewhat amusing from the point of view of the usual localization theorems. It would be interesting to understand better how this works.

Yet another direction which could be considered further concerns the fate of nonperturbative higher F-terms across lines of marginal stability. The fact that under deformations of the supersymmetry algebra (by inserting mass terms, for example) higher F-terms may flow to superpotentials seems to be a strong hint for continuity, but it would be nice to check this in detail.

Capítulo 9

Conclusiones y direcciones futuras

(Spanish translation of Chapter 8)

En esta tesis hemos estudiado unas cuantas propiedades de D-branas en geometrías Calabi-Yau locales que pueden ser útiles para la fenomenología de cuerdas. Hagamos un pequeño resumen de éstas:

- En el Capítulo 3 discutimos cómo construir configuraciones de branas que reproduzcan el vacío meta-estable de ISS. Es sencillo generalizar la configuración de branas, mostramos algunas de las generalizaciones que se espera que den lugar a vacíos metas-estables.

- En el Capítulo 4 describimos otro sistema en teoría de cuerdas con vacíos meta-estables. Esta construcción está basada en branas en singularidades tóricas con deformaciones complejas obstruidas.

- En el Capítulo 5 estudiamos cómo ve la teoría en el volumen de la brana el suavizado de la singularidad tórica. Encontramos que el resultado final son dos o más sectores acoplados únicamente a través de mediadores masivos.

- El Capítulo 6 contiene una discusión de algunos aspectos interesantes de la continuidad de superpotencial no perturbativo que pueden resultar interesantes al construir modelos que involucren efectos de D-instantones. Esta discusión es interesante no sólo para esta clase de ejemplos, sino que también se espera que sean importantes en muchas otras situaciones.

- En el Capítulo 7 juntamos algunas de las piezas desarrolladas en los capítulos anteriores, y mostramos cómo de fácil se pueden construir en modelos locales configuraciones de branas que den GMSB. Ilustramos esto en algunos ejemplos de juguete.

El trabajo descrito en esta tesis se puede extender en muchas direcciones. La más evidente consiste en construir modelos detallados y realistas utilizando las ideas que hemos presentado. En particular, en nuestra discusión del modelo de juguete en el Capítulo 7, no hemos incluido ningún análisis detallado del modelo. Esto nos era permisible dado que sólo pretendíamos ilustrar cómo funciona el mecanismo en general. Cuando uno trate de construir un modelo detallado se deberá enfrentar genéricamente a un conjunto de dificultades que no hemos tenido en cuenta: estabilización de los moduli, incluir la gravedad, explicar la jerarquía, el problema μ, incluir inflación, etc. Algunos de estos problemas pueden ser resueltos al incluir nuestras configuraciones en compactificaciones con flujos en el fondo de gargantas, quizá de manera similar a [37, 135].

Otra línea de investigación fructífera trata sobre la inclusión directa de los vacíos ISS en teoría de cuerdas, como en el Capítulo 3. Utilizando la imagen de redes de branas hemos sido capaces de encontrar ejemplos de teorías en las que se espera que existan vacíos meta-estables. Uno puede utilizar técnicas similares para encontrar muchos otros ejemplos, véase por ejemplo [136], y los artículos que cita. También es posible encontrar vacíos meta-estables en otros sistemas de cuerdas, como hemos mencionado en la introducción del Capítulo 3. Algunas referencias sobre esto son [54, 55, 56, 57, 58, 59, 60, 61, 62, 63].

Un aspecto particularmente interesante de la configuración que estudiamos se refiere a su descripción en teoría M. Cómo hemos descrito en la introducción de la Sección 3.2, la realización en teoría M que damos en el Capítulo 3 para el vacío meta-estable en la teoría IIA y la realización de la configuración supersimétrica tienen distinto comportamiento asintótico, y por tanto es más preciso pensar en estas configuraciones como elementos de espacios de Hilbert distintos. En otras palabras, en teoría M no tenemos un vacío meta-estable y otro supersimétrico para la misma teoría, como tenemos en teoría gauge. Sería interesante encontrar un vacío meta-estable de este tipo, manteniéndonos tan cerca de la teoría ISS como nos sea posible.

Esto sea probablemente bastante complicado técnicamente, dado que el límite de supergravedad en el que hemos estudiado las curvas de teoría M es diferente al límite de teoría gauge en el que obtenemos SQCD. No hay ninguna supersimetría que proteja los resultados al variar las constantes de acoplo, de modo que cualquier cosa es posible (y de hecho, parece que en el caso más sencillo el vacío meta-estable simplemente desaparece). [53] hace un análisis detallado de estos asuntos.

La discusión del Capítulo 4 sobre cómo encontrar vacíos meta-estables en teorías quiver runaway con sabores también se puede extender en muchas direcciones distintas. Hay al menos un par de aspectos de la construcción que sería interesante mejorar.

El primero es cómo hemos introducido las masas pequeñas para los sabores. En nuestra discusión las masas pequeñas para los sabores (esto es necesario para que análisis de ISS funcione) son ajustadas a mano. Sería mucho más agradable si las masas pequeñas fueran generadas de un modo más dinámico, quizá a través de efectos de D-instantones de manera similar a lo discutido en el Apéndice D.

Otro aspecto de la conclusión que requiere un estudio más detallado concierne a los campos desacoplados a nivel clásico. Como hemos mencionado en la introducción al Capítulo 4, y hemos mostrado explícitamente en algunos ejemplos en el mismo capítulo, en nuestra construcción hay genéricamente algunos campos que no aparecen en el superpotencial clásico. Al no aparecer en el superpotencial son direcciones planas (si asumimos potenciales Kähler canónicos) clásicamente y a un loop, pero no hay ninguna razón para suponer que vayan a mantenerse sin masa a órdenes más altos, o no perturbativamente. Para asegurarse de que la construcción que hemos mostrado tiene sentido es necesario saber si estos campos toman masa positiva o negativa.

La discusión en el Capítulo 5 también puede ser mejorada. Podríamos intentar obtener una mejor comprensión cualitativa del sector masivo en el caso de la deformación, y una mejor comprensión cuantitativa de la resolución.

Más en general, los modelos de dímeros parecen ser el lenguaje adecuado en el que describir asuntos relacionados con branas en singularidades tóricas. Su utilidad, por tanto, no está limitada a cuestiones de fenomenología, también parecen jugar un papel importante (aunque todavía relativamente poco comprendido) en el derretido de cristales y física de agujeros negros (véanse [137] y [138] para dos artículos recientes explorando estos temas).

Dos posibles aplicaciones más son al estudio de cuestiones concernientes a la estabilidad Π [139] de branas en espacios tóricos, y a la comprensión de las geometrías Sasaki-Einstein térmicas (por ejemplo para estudiar propiedades térmicas de los dibariones, que son en general abundantes en AdS/CFT para espacios Sasaki-Einstein). Sería muy interesante desarrollar estas líneas de investigación.

Finalmente, la discusión en el Capítulo 6 también se puede extender en unas cuantas direcciones distintas.

Una aplicación inmediata de los resultados que presentamos es a la revisión de búsquedas anteriores de efectos de D-instantones interesantes ([98] es un ejemplo reciente). Estas búsquedas se limitaban al sector de un instantón, de modo que sería interesante ver si hay efectos interesantes en el sector de varios instantones que no estén presentes en el caso de un instantón.

Otro aspecto de la construcción que podría ser explorado más trata de las contribuciones que vienen de instantones BPS que se rompen en varios instantones mutuamente no supersimétricos. Si la discusión de continuidad

todavía es aplicable, y no tenemos ninguna razón para pensar que no lo va a ser, entonces esto sería un sistema de varios instantones no supersimétrico que contribuye al superpotencial, algo bastante curioso desde el punto de vista de los teoremas de localización habituales. Sería interesante ver cómo funciona esto en detalle.

Otra dirección más que podríamos considerar es intentar entender qué pasa con los términos F no perturbativos de orden más alto al cruzar líneas de estabilidad marginal. El hecho de que bajo deformaciones del álgebra de supersimetría (introduciendo términos de masa, por ejemplo) los términos F más altos puedan convertirse en superpotenciales apunta a que serán continuos, pero sería bueno entender esto en detalle.

Appendix A

The ISS model

A.1 Overview

In this appendix we shortly review some basic points of the analysis done in [41]. We will be focusing just on the issues closest to the analysis done in Chapters 3 and 4. The reader interested in a deeper treatment is advised to consult the insightful original paper [41] and the very pedagogical review [140].

The example analyzed in [41] is very simple, namely $\mathcal{N} = 1$ super Yang-Mills with massive flavors. The fact that there is a metastable vacuum in such a fundamental system suggests that the phenomenon will be very general.

In order to have good control over the theory, we work in the free magnetic range,

$$N_c + 1 \leq N_f < \frac{3}{2} N_c. \tag{A.1}$$

A very good thing about this interval is that we can study the magnetic dual quite easily[1]. This is because the Seiberg dual description is infrared free, and thus we can forget about the magnetic gauge dynamics in the deep infrared[2]. Also, since in doing the Seiberg duality we are correctly taking care of all massless degrees of freedom we know that the Kähler potential will be canonical in the infrared, with the only unknowns being the normalizations for the fields. This renders the system completely tractable.

The dual magnetic theory is $SU(N)$ SYM with $N = N_f - N_c$, and $SU(N_f) \times SU(N_f)$ flavor group. The matter content consists of the magnetic

[1] We will call the original theory "electric" and its Seiberg dual "magnetic", as is conventional in the literature.

[2] As long as the scale where the magnetic theory becomes strongly coupled is high enough compared to the scale of the supersymmetry breaking effects. This can be arranged by tuning the couplings.

quarks q and $\tilde{q}$ transforming respectively in the $(\square, \overline{\square}, 1)$ and $(\overline{\square}, 1, \square)$ of $SU(N) \times SU(N_f) \times SU(N_f)$, and the mesons Φ transforming in the $(1, \square, \overline{\square})$.

We will take a superpotential given by

$$W = h\mathrm{Tr}\,(q\Phi\tilde{q}) - h\mu^2\mathrm{Tr}\,\Phi, \tag{A.2}$$

which is the dual potential to massive flavored SQCD. The resulting model, ignoring gauge dynamics, breaks supersymmetry spontaneously at the classical level since not all F-term conditions can be satisfied at the same time. This is easy to see looking to the F-terms for Φ:

$$q\tilde{q} - \mu^2\mathbb{I}_{N_f} = 0 \tag{A.3}$$

Here $q\tilde{q}$ (there is a contraction in color indices here) has rank $N = N_f - N_c$, while the identity matrix $\mathbb{I}_{N_f}$ has rank N_f, so the system admits no solution. This mechanism for breaking supersymmetry is called the *rank condition*.

The classical moduli space of minima is parametrized by the following set of vevs:

$$\Phi = \begin{pmatrix} 0 & 0 \\ 0 & \Phi_0 \end{pmatrix}, \quad q = \begin{pmatrix} \varphi_0 \\ 0 \end{pmatrix}, \quad \tilde{q}^T = \begin{pmatrix} \tilde{\varphi}_0 \\ 0 \end{pmatrix}, \tag{A.4}$$

with Φ_0 an arbitrary $N_c \times N_c$ square matrix, and $\varphi_0, \tilde{\varphi}_0$ $N \times N$ square matrices. These last two matrices satisfy $\tilde{\varphi}_0\varphi_0 = \mu^2\mathbf{1}_N$, and are otherwise arbitrary.

A one loop computation (either calculating the Coleman-Weinberg potential as in Section A.2, or more directly calculating the one loop two point function of the pseudomoduli as in Chapter 4) shows that all the moduli that are not Goldstone bosons for broken symmetries get nonzero positive masses of order $m^2 \approx |h^4\mu^2|$, and that the one-loop minimum is located at $\Phi_0 = 0$, $\varphi_0 = \tilde{\varphi}_0 = \mu\mathbf{1}_N$.

Restoration of the supersymmetric minimum

In this theory there are $N_f - N = N_c$ minima. This is easiest to understand in the electric theory: since the quarks are massive we can integrate them out when studying the susy vacuum, and obtain pure $\mathcal{N} = 1$ SYM with N_c colors. This theory is well known to have N_c different supersymmetric vacua.

Although we will not be using this, it is nice to see how do the supersymmetric minima appear in the magnetic theory. In order to obtain them, we have to go to the region in field space where the gauge dynamics becomes important, namely the large field region $|\mu| \ll |\langle h\Phi\rangle|$. In this region the N_f flavors are very massive, and they can be integrated out without affecting

the IR dynamics, which becomes pure $SU(N)$ SYM, with a dynamical scale Λ' given by the matching at the mass scale of the magnetic quarks:

$$\Lambda'^{3N} = \frac{h^{N_f} \det \Phi}{\Lambda^{N_f - 3N}}, \tag{A.5}$$

with Λ the Landau pole of the original IR free theory. The resulting theory has a non perturbative contribution to the superpotential given by gaugino condensation, the end result for the IR superpotential is:

$$W = N(h^{N_f} \Lambda^{3N-N_f} \det \Phi)^{1/N} - h\mu^2 \mathrm{Tr}\, \Phi. \tag{A.6}$$

We can easily find the minima of this superpotential, they are given by the N_c roots of

$$\langle h\Phi \rangle = \mu \epsilon^{(3N-N_f)/N_c} \mathbf{1}_{N_f}, \tag{A.7}$$

with $\epsilon = \mu/\Lambda$. This parameter turns out to be very important in the complete analysis [41]. The condition $\epsilon \ll 1$ both justifies the above analysis in the low energy theory and assures us that the metastable minimum is long-lived.

A.2 One-loop masses for the pseudomoduli

Traditionally, the one-loop masses for the pseudomoduli are computed using the Coleman-Weinberg potential [141]. Let us include here for comparison how this method works.

Consider an $\mathcal{N} = 1$ theory with tree level bosonic mass matrix $\mathcal{M}_B$ and fermionic mass matrix $\mathcal{M}_F$. These mass matrices will be functions of the couplings of the theory and the tree level expectation values of the fields in the theory. For example, a (non-susy for simplicity) Lagrangian of the form:

$$\mathcal{L} = \phi\psi\psi + m\psi\psi \tag{A.8}$$

gives a tree level mass term for the fermion ψ equal to $m + \langle\phi\rangle$. We will restrict ourselves to spin less that one here since this is the case we will be considering in the main text, although the formula can be generalized for higher spins.

A simple one-loop calculation for the bubble diagram gives us the vacuum energy for the theory in terms of the mass matrices:

$$V^{(1)} = \frac{1}{64\pi^2} \mathrm{Tr} \left[\mathcal{M}_B^4 \log \frac{\mathcal{M}_B^2}{\Lambda} - \mathcal{M}_F^4 \log \frac{\mathcal{M}_F^2}{\Lambda} \right] \tag{A.9}$$

where Λ is the cutoff for our theory.

Once one calculates the one-loop potential in terms of the tree level couplings and vevs, extracting the one-loop mass matrix for the bosonic fields is simple:

$$\mathcal{M}_{ij}^{(1)} = \frac{\partial^2 V^{(1)}}{\partial\langle\phi_i\rangle \partial\langle\phi_j\rangle}. \tag{A.10}$$

Appendix B

Toric Geometry

In this appendix we will review some basic facts about toric varieties that will be useful in the following. The classical reference is the book by Fulton [142], although good introductory reviews for physicists exist, see for example [35, 143]. We will just give an short review of the main points we will be using.

For the reader encountering the ideas in this chapter for the first time the construction might seem formal and far from any interesting problem in physics. One of the main tasks of Appendix C consists of giving a nice physical link between the algebraic structure of the toric singularity described in this appendix and the physics of a D3 brane probing the singularity. We will find that many of the concepts in here admit simple and beautiful interpretations in the gauge theory describing the brane.

B.1 Toric varieties

The easiest way to picture a toric variety is as a fibration of a torus over some base, where the torus can degenerate over submanifolds of the base. As a trivial example, we can picture the two-sphere $\mathbb{P}^1$ as a fibration of the circle over a segment, where the fiber shrinks to zero size at the extrema of the segment. The next example is probably more interesting, let us try to picture the complex three-dimensional space $\mathbb{C}^3$ as a fibration of a three torus over some base. In order to do this, we can parametrize $\mathbb{C}^3$ by x, y and z. Now define the base as the modulus of these quantities, namely $|x|$, $|y|$ and $|z|$. The fiber will just be the corresponding phases, which form a three torus. It is also easy to identify which fibers degenerate: in this example the fiber associated with the phase of x should degenerate when $|x| = 0$, since changing the phase of 0 does not give different points in $\mathbb{C}^3$. The picture we get is thus the positive octant of $\mathbb{R}^3$, with a three torus fibered above it in the manner described.

It is possible to understand the kind of geometries above in another

way, as we will see in Section B.1.2. In essence, we generalize the idea of a projective space. The projective space $\mathbb{P}^n$ can be characterized by saying that it is $\mathbb{C}^{r+1} - \{0\}$, parametrized by $x_1, \ldots, x_{r+1}$, quotiented by the $\mathbb{C}^* = \mathbb{C} - \{0\}$ action:

$$x_i \to \lambda x_i,$$

where λ belongs to $\mathbb{C}^*$. A natural generalization of this is a weighted projective space, where now the $\mathbb{C}^*$ action acts on the coordinates as:

$$x_i \to \lambda^{w_i} x_i,$$

where w_i are positive integers. Toric spaces are the next simplest generalizations, where now we can quotient the original space by a number of different actions, not just one, and we allow the w_i to be negative or zero. Let us give a simple example, the conifold. In this case we quotient $\mathbb{C}^4 - \{0\}$ by the $\mathbb{C}^*$ action with charges $(1, 1, -1, -1)$. It is easy to see that it is a Calabi-Yau space, since the first Chern class is given by the addition of the charges, in the same way as in usual weighted projective spaces. This space will be an interesting example, and it presents already many of the main properties of general toric spaces, so let us study it in some detail before describing the main construction.

B.1.1 The conifold

Let us describe the conifold a bit more explicitly. Let us start with $\mathbb{C}^4 - \{0\}$, parametrized by $z_1, \ldots, z_4$. Now, let us quotient this space by the $\mathbb{C}^*$ action with the charges:

	z_1	z_2	z_3	z_4
$\mathbb{C}^*$	1	1	-1	-1

(B.1)

The resulting space can also be understood as a submanifold in $\mathbb{C}^4$. One way to see this is building all the independent $\mathbb{C}^*$ invariants and imposing any relations that follow from their expressions in terms of the z_i. It is a mathematical result that this characterizes completely the resulting space. The basic (in the ring sense) invariants are:

$$x = z_1 z_3 \tag{B.2}$$
$$y = z_2 z_4 \tag{B.3}$$
$$w = z_1 z_4 \tag{B.4}$$
$$z = z_2 z_3, \tag{B.5}$$

and the equation we have to impose is $xy = zw$. Changing variables linearly this can be written as:

$$x_1^2 + x_2^2 + x_3^2 + x_4^2 = 0, \tag{B.6}$$

which is one of the classical descriptions of the conifold. In particular, it clearly shows its cone structure. This follows from the fact that the defining equation (B.6) has a definite weight under real rescalings of the variables x_i.

It is easy to find the base of the cone, at least topologically. The easiest way to do this consists of going back to the formulation in terms of the z_i. Let us parametrize the $\mathbb{C}^*$ transformation by $se^{i\alpha}$, and first quotient by s, which belongs to $\mathbb{R}^*$. We can completely fix this rescaling freedom by imposing:

$$|z_1|^2 + |z_2|^2 = |z_3|^2 + |z_4|^2. \tag{B.7}$$

Choosing a section of the cone then amounts to imposing, for some constant $R \in \mathbb{R}^*$:

$$|z_1|^2 + |z_2|^2 = |z_3|^2 + |z_4|^2 = R^2. \tag{B.8}$$

We see that we have topologically a product of two three spheres. We still have to quotient by the action of the $U(1)$ part $e^{i\alpha}$. This has no fixed points (all fixed points under the $\mathbb{C}^*$ are removed in the toric construction) so we learn that topologically the conifold is a cone over $\mathbf{S}^3 \times \mathbf{S}^3/U(1) = \mathbf{S}^3 \times \mathbf{S}^2$.

More details about the conifold, and a beautiful application to AdS/CFT, can be found in [144].

B.1.2 GLSM

In this section we describe an interpretation of toric varieties as the moduli space of gauged linear sigma models (GLSM in what follows). This description will be very useful for our discussion on dimer models. The case of the conifold described in the previous section was a particular instance of this construction.

Let us consider a model of n chiral superfields ϕ_i with gauge group given by $U(1)^s$ and no superpotential. Then one gets a $n - s$ manifold of possible vacua, given by the gauge quotient of the solution of the D-term equations:

$$\sum_{i=0}^{n} q_i^a \, |\phi_i|^2 = r_a, \tag{B.9}$$

where q_i^a denotes the $U(1)$ charge of the i-th field under the a-th gauge group, and r_a is the Fayet-Iliopoulos term. It turns out that the resulting manifold is equivalent to the manifold given by the quotient of $\mathbb{C}^n$ by the complexification of $U(1)^s$, as in the example of the conifold in the previous section. In the literature the quotient by the complexified gauge group is called the *holomorphic quotient* construction for the manifold, while the GLSM one is called the *symplectic quotient*. Their equivalence can be understood from the fact that the D-term equation is essentially a gauge fixing for the $\mathbb{R}^*$ part of the $\mathbb{C}^*$ symmetry, as in equation (B.7). See [145] for the exact statement, and a more rigorous explanation of why this works.

In Appendix C we will see how to construct the GLSM describing the toric singularity from the dimer model describing the physics of a brane located at the singularity. These two objects are expected to be connected, since the dimer model encodes all information about the gauge theory, and the toric variety will be mesonic moduli space for a single D3-brane located at the singularity. The fact that they are very simply related through the concept of *perfect matchings* (to be explained in Appendix C) is nevertheless quite surprising.

B.2 Toric diagrams

For our study we will restrict to three dimensional toric varieties that are Calabi-Yau. In this case, we have a nice representation of the variety in terms of what are called toric diagrams. These are just convex polygons in a two dimensional integer lattice, and they encode most properties of the toric variety.

Let us first describe the algorithm that computes the toric diagram for a given GLSM. As usual, let us do it through one example, the conifold. The generalization to arbitrary toric varieties will be immediate.

Take the set of charges of the GLSM, as described in equation B.1, and which we reproduce here for convenience:

	z_1	z_2	z_3	z_4
$\mathbb{C}^*$	1	1	-1	-1

$(B.1)$

Now find a basis of independent linear relations between these charges. Let us choose for example:

$$q_1 + q_4 = 0 \tag{B.10}$$
$$q_1 + q_3 = 0 \tag{B.11}$$
$$q_1 + q_2 + q_3 + q_4 = 0 \tag{B.12}$$

Here q_i is simply the charge of z_i. We can represent this in matrix form as follows:

$$\begin{pmatrix} 1 & 0 & 0 & 1 \\ 1 & 0 & 1 & 0 \\ 1 & 1 & 1 & 1 \end{pmatrix} \tag{B.13}$$

Note that the last row amounts to the Calabi-Yau condition for the vanishing of the first Chern class. The resulting matrix defines some points in a two dimensional[1] lattice when read by columns, which in our case are four points

[1]The vectors live in a three dimensional lattice, but it is a general result that for a three dimensional Calabi-Yau the endpoints of the vectors actually live in a two dimensional hyperplane of the total lattice. In our example it is clear since the third coordinate is equal for all vectors.

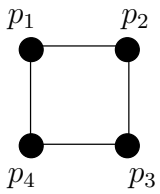

Figure B.1: Toric diagram for the conifold. We have labelled the positions of the vertices $p_1 \dots p_4$.

forming a square: $(1,1)$, $(0,0)$, $(0,1)$ and $(1,0)$. This is the toric diagram. We show it in Figure B.1. Notice that the construction is essentially unique except for the freedom in choosing which relations we choose as a basis, which gives us a $SL(2,\mathbb{Z})$ (recombination of the first two rows) plus displacement of the origin (adding the Calabi-Yau condition) freedom in choosing the diagram representing the geometry. The relation of this $SL(2,\mathbb{Z})$ to the modular group of some two torus will be explained in Appendix C.

This also shows how one can construct a GLSM from a given toric diagram: one has to invert the process above. The result is in general not unique. This non uniqueness is interesting, as its nontrivial part can be understood in the dimer model context as Seiberg duality, see for example [94]. Vertices are associated with the fields in the GLSM (with possibly more than one field per vertex), while the possible $SL(2,\mathbb{Z})$ invariant geometric relations between edges encode the GLSM charge vectors. That this is true is easy to see from the procedure above. For example, denoting the positions of the four vertices of the conifold $p_1 \dots p_4$, as done in Figure B.1, the possible $SL(2,\mathbb{Z})$ invariant geometric relations between the edges are generated by:

$$p_1 - p_2 + p_3 - p_4 = 0, \tag{B.14}$$

so we read the charges $(1,-1,1,-1)$ for the fields associated with the edges.

B.2.1 Web diagrams

It is possible to give a dual representation of the gauge theory that encodes more nicely its torus fibration structure, and turns out to have close links with the mirror of the toric variety, as we will explain in Appendix C. This representation is usually called web diagram. It is given by the planar dual of the toric diagram, let us see how can one construct it from the toric data in the case of the conifold.

The basic equation of the conifold $xy = zw$ can also be seen as a double $\mathbb{C}^*$ fibration over the complex plane given by:

$$xy = W \tag{B.15}$$

$$zw = W. \tag{B.16}$$

This fibration degenerates over $W = 0$. Each fiber has a $U(1)$ isometry given by:

$$U(1)_a \quad : \quad (x, y, z, w) \to (x, y, e^{i\theta_a} z, e^{-i\theta_a} w) \tag{B.17}$$

$$U(1)_b \quad : \quad (x, y, z, w) \to (e^{i\theta_b} x, e^{-i\theta_b} y, z, w). \tag{B.18}$$

We can rewrite these actions in terms of the original gauge dependent variables $z_1, \ldots, z_4$, they give the following action:

$$(z_1, z_2, z_3, z_4) \to (z_1 e^{-i(\theta_a - \theta_b)}, z_2, z_3 e^{i\theta_a}, z_4 e^{-i\theta_b}). \tag{B.19}$$

We know that the variety is actually a three dimensional toric Calabi-Yau, so it has a T^3 fibration structure. The $U(1)$ isometry that we have not included yet is that of changing the phase of W, which in terms of the GLSM fields can be written as:

$$U(1)_W : (z_1, z_2, z_3, z_4) \to e^{i\theta_W} (z_1, z_2, z_3, z_4). \tag{B.20}$$

So the third $\mathbf{S}^1$ is given by the phase of W. This $U(1)$ degenerates above $W = 0$.

It is possible to find out where the other two $U(1)$ isometries degenerate from the toric diagram itself. In fact, one of the usual definitions of toric varieties builds the toric diagram of a toric three dimensional Calabi-Yau as the projection on a hyperplane of something called a *fan*, which describes precisely the sets of limit points under the $(\mathbb{C}^*)^3$ action of the toric variety on itself, and gives rise to submanifolds invariant under the action of $U(1)$ fibers, or in other words submanifolds where the corresponding $U(1)$ action degenerates. Introductions for physicists to such an approach can be found in [35, 143].

The way this works in the conifold example (more complicated cases are similar, see the previous references for the general statements) starts with associating one field in the GLSM with each point in the toric diagram, as described before. Take for example the point in the toric diagram associated with z_1. Let us associate to it the divisor[2] $z_1 = 0$. In terms of the gauge invariant monomials this sets $x = w = 0$, and it is easy to realize that the $W + 2(b - a)$ subgroup of $U(1)_a \times U(1)_b \times U(1)_W$ leaves the points in the two dimensional manifold invariant (the notation for the subgroup represents the one dimensional abelian subgroup generated by $\theta \to (\theta_a, \theta_b, \theta_W) = (-2\theta, 2\theta, \theta)$).

It is possible to find all the other subspaces where the $U(1)$ actions degenerate, they come from edges and faces in the toric diagram. At this point, since higher dimensional curves in the toric diagram correspond to

[2]For our purposes, a divisor is the complex-codimension one submanifold of the variety one obtains when imposing $f(z) = 0$, with $f(z)$ some holomorphic and homogeneous function of the fields in the GLSM.

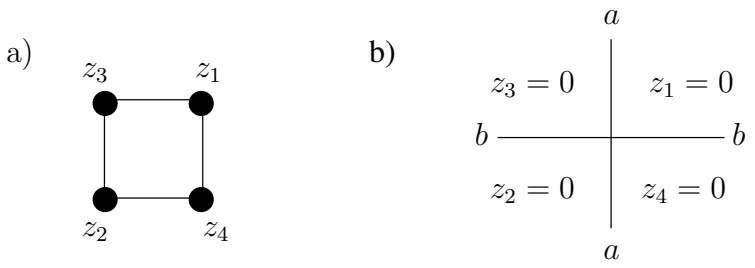

Figure B.2: Toric (a) and web (b) diagrams for the conifold. In the web diagram we have indicated which $U(1)$ symmetries degenerate over the edges.

lower dimensional curves in the variety (taking edges corresponds to imposing $x_i = x_j = 0$), it is convenient to switch to the planar dual of the toric diagram. This is the web diagram. It amounts to drawing (possibly semi infinite) lines perpendicular to the edges of the toric diagram. We illustrate the result for the conifold in Figure B.2.

It is easy to see that in the intersections of the divisors, given by the edges in the toric diagram (cones formed from the divisors in the complete fan) there is some combination of $U(1)_a$ and $U(1)_b$ that degenerates. Take for example $z_3 = z_2 = 0$. This set of points is described in a gauge invariant way by $x = y = z = 0$. In this description it is apparent that $U(1)_b$ degenerates. In terms of $(z_1, \ldots, z_4)$ we have the submanifold $(z_1, 0, 0, z_4)$, under which $U(1)_b$ acts as $(z_1 e^{i\theta_b}, 0, 0, z_4 e^{-i\theta_b})$, which is a complex line once one imposes the $U(1)$ GLSM symmetry. At the point where both edges meet in the web diagram we have both $U(1)_a$ and $U(1)_b$ degenerating. This point has also $W = 0$, so all fibers degenerate here. The conifold singularity is located in this point. The next section is devoted to understanding how to smooth out this singularity.

B.3 Acting on the variety

It is possible to take a singular manifold such as the conifold above and modify the singular point in such a way that the manifold is no longer singular. In particular, we have seen that the conifold is a cone with base $\mathbf{S}^2 \times \mathbf{S}^3$. It is thus possible to remove the singularity by "blowing up" a finite size two or three sphere at the origin. Blowing up means substituting the conifold by some smooth space that is isomorphic outside the singularity, but with a sphere where the singularity was. Let us see how to represent this in the toric and web diagrams. As usual, we center in the conifold.

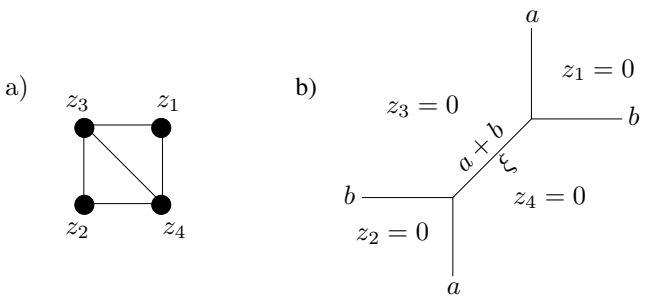

Figure B.3: Resolution of the conifold in terms of the toric diagram (a) and the web diagram (b).

B.3.1 Resolving the singularity

Blowing up the $\mathbf{S}^2$ is referred to as *resolving* the singularity. One simple way of describing this is in terms of the GLSM, in which we just switch on a nonzero Fayet-Iliopoulos term ξ in the D-term equations of the GLSM:

$$|z_1|^2 + |z_2|^2 - |z_3|^2 - |z_4|^2 = \xi. \tag{B.21}$$

We see that the condition for the existence of a singularity[3] no longer holds, so the manifold described by this equation is no longer singular. Let us try to understand better this operation in the toric variety. The most intuitive way to represent the resulting geometry is probably by means of the web diagram, so we will focus on this representation.

In the previous section we showed how the singularity can be associated with the point in the web diagram where all edges meet. It is a mathematical result that resolutions of toric Calabi-Yau varieties remain toric and Calabi-Yau[4], so we can draw a web diagram for the resolved geometry. It is easy to find the new points where the $U(1)$ actions degenerate. Take ξ positive, for example. Then $z_1 = 0$ and $z_2 = 0$ no longer intersect, as this would violate the D-term equations. $z_3 = z_4 = 0$ is still a possible locus where the fiber might degenerate, but note that in contrast to the singular case, only a specific combination of $U(1)_a$ and $U(1)_b$ degenerates, it is given by $a + b$. The action of the other $U(1)$ gives a non singular manifold. In fact the action of this $U(1)$ gives a $\mathbf{S}^1$ fibered over a segment and vanishing at the extrema of the segment. We saw in the introduction to this chapter that this is a way to represent $\mathbf{S}^2$ in toric geometry, so we find out that the web representation encodes in quite a visual way the growing of the resolution sphere. We show the resolved web diagram in Figure B.3b.

[3]For spaces defined by an equation $f = 0$ the condition for the existence of a singularity at a certain point is given by $df = f = 0$.

[4]Technically, this result requires that the singularities are what is called *canonical Gorenstein*, but this will always be the case in the setups we consider.

Looking to the resolved web diagram one might think that the locus $z_2 = z_3 = z_3 = 0$ where three lines of the diagram meet is singular, since at that point all three $U(1)$ actions degenerate (similarly for the locus $z_1 = z_3 = z_4 = 0$). Even if it is true that at that locus the T^3 degenerates, it does so in a smooth way. In fact the geometry near a point where just three legs intersect is locally $\mathbb{C}^3$. This is easy to see from the toric description of $\mathbb{C}^3$ we gave in the introduction: we have not provided the web diagram for $\mathbb{C}^3$, but it is easy to convince oneself that it is given by three legs that intersect at a point. Furthermore, all three leg web diagrams are related by $SL(2,\mathbb{Z})$ transformations, so they all represent flat space.

With the introduction of the sphere one has changed the Hodge numbers of the manifold[5], in particular we have increased in one unit $h^{1,1}$, adding a two-cycle. The (complexified with the B-field) Fayet-Iliopoulos ξ gives a measure of the (complexified) volume of the sphere. It is conventional to associate it with the length of the segment that we have grown.

It remains to describe the resolution in terms of the toric diagram. By dualizing the picture in Figure B.3b we obtain Figure B.3a, which represents the resolution in terms of toric diagrams. In fact, this fits nicely with the result, that we quote without proof, that a toric diagram describes a smooth surface if and only if it is triangulated into triangles of minimal area. Very sketchily, this result comes from the fact that a minimal area triangle describes a smooth $\mathbb{C}^3$ (this is just the graph dual of the statement for web diagrams, where three legs intersecting represent $\mathbb{C}^3$), and the common edges describe how to paste them into the final (smooth) space. Partial resolutions of a singularity are thus represented in this language by drawing internal lines in the toric diagram that divide it into pieces of smaller area. When all the pieces have area $\frac{1}{2}$ (one basic triangle) the space is smooth.

B.3.2 Deforming the singularity

The other possible way of obtaining a smooth space from the conifold corresponds to blowing up the $\mathbf{S}^3$. In terms of the defining equation for the conifold this can be written as follows:

$$xy - zw = a, \tag{B.22}$$

where $a \in \mathbb{C}^*$ is the complex deformation parameter. In Section 5.2 we will see how this process admits a nice interpretation as the quantum modification of the moduli space of a given confining gauge theory, but let us restrict ourselves to the purely geometrical description for the moment.

[5]With respect to the Hodge numbers of the complex deformed case to be studied later. This is what is called a drastic topology transition in [143]. There are also milder topological transitions that affect only the intersection forms, they are called *flops* and can be described essentially as a continuation of ξ to negative values.

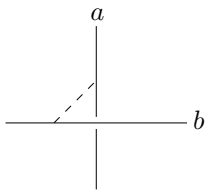

Figure B.4: Deformation of the conifold singularity. The dashed line indicates the $\mathbf{S}^3$ that deforms the singularity.

Let us describe how to see the three sphere in the geometry. Take $y = x^*$ and $w = -z^*$, rotating some phases to make a real and positive if necessary. The resulting equation describes a three sphere of radius $\sqrt{a}$:

$$|x|^2 + |z|^2 = a. \tag{B.23}$$

The description in terms of the toric diagram is slightly technical, and we will not be making much use of it. It can be found in [92, 93, 91]. We will focus instead in the description in terms of web diagrams [146, 147], which will prove to be more useful in Section 5.2 when we describe complex deformations in terms of dimer diagrams.

It turns out that complex deformed toric spaces are no longer toric, but can be described schematically as two toric spaces connected by a three sphere. Identifying the resulting web diagram in the case of the conifold is simple. Note that one still has $U(1)_a$ and $U(1)_b$ as isometries, but their degenerations no longer overlap. This is apparent from the fact that $U(1)_a$ degenerates over $z = w = 0$, while $U(1)_b$ degenerates over $x = y = 0$, and both equations cannot be true at the same time in the deformed conifold. Also note that $U(1)_W$ is no longer an isometry, this is a manifestation of the non-toric nature of the resulting manifold. We draw the resulting conventional web representation of the deformed space in Figure B.4.

In the general toric case the procedure is similar. It turns out that the effect of the deformation is dividing the original web into two subwebs in equilibrium, meaning that the take the original set of edges and divide it into two disjoint sets such that their slopes add up to zero. We have not discussed this last equilibrium condition in much detail, but it can be understood as a consequence of the fact that the toric diagram forms a closed polygon.

B.3.3 Taking orbifolds

As a last point we would like to describe a process that allows to take a singularity and obtain a worse one, that of orbifolding. We will focus on abelian orbifolds, given by the quotient of the original singularity by a $\mathbb{Z}_k$ action, where k is some positive integer. One of the simplest examples that yields a Calabi-Yau space is $\mathbb{C}^2/\mathbb{Z}_2 \times \mathbb{C}$, given by the identification of the

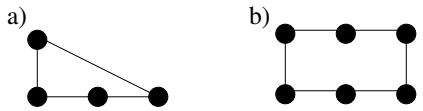

Figure B.5: (a) Toric diagram for the $\mathbb{C}/\mathbb{Z}_2 \times \mathbb{C}$ orbifold of flat space. The dots denote lattice points. (b) Toric diagram for the $\mathbb{Z}_2$ orbifold of the conifold.

points of flat space under the action:

$$\sigma : \quad (z_1, z_2, z_3) \to (-z_1, -z_2, z_3). \tag{B.24}$$

We can describe this in toric terms as follows. We introduce in the GLSM a new field w and a new gauge symmetry under which the fields have charges:

	z_1	z_2	z_3	w
$\mathbb{C}^*$	1	1	0	-2

(B.25)

In order to obtain the toric diagram one has to obtain the ring of invariants, it is given by:

$$\begin{aligned} x &= z_1^2 w \\ y &= z_2^2 w \\ w &= z_1 z_2 w \\ z &= z_3 \end{aligned} \tag{B.26}$$

with the constraint $f = xy - w^2 = 0$. We see already the singularity here, as $x = y = w = 0$ is a solution of $df = f = 0$. Let us draw the toric diagram. The matrix of vectors describing the ring of invariants is given by:

$$\begin{pmatrix} 2 & 0 & 0 & 1 \\ 0 & 2 & 0 & 1 \\ 1 & 1 & 0 & 1 \\ 0 & 0 & 1 & 0 \end{pmatrix} \tag{B.27}$$

If we read the columns we obtain the positions in the toric diagram. We have included a redundant relation to make the comparison with eq. (B.26) more straightforward. It is not hard to see that the four points are coplanar, and that they give rise to the drawing of Figure B.5a when projected into a plane. We see that the resulting toric diagram has area equal to two basic triangles, consistent with the fact that the space has a singularity.

The lesson is general. Taking an orbifold of a given toric variety is represented in terms of the toric diagram simply as refining the lattice in the directions associated to the orbifolded variables by an amount given by the rank of the orbifold group. An example describing the $\mathbb{Z}_2$ orbifold of the conifold is shown in Figure B.5b.

As a last comment, note that this process, in combination with resolution, allows us to construct a systematic algorithm for constructing any toric variety via orbifolding of the conifold (or flat space) and partial resolutions. Since both processes have simple descriptions in terms of the gauge theory describing D3 branes located at the singularity, this allows us to find in principle the gauge theory for arbitrary toric Calabi-Yau singularities.

Appendix C

Introduction to dimer models

In this appendix we will give a short review of the physics of dimer models, also called brane tilings, for branes at toric singularities. We will just discuss the points of more direct relevance for our work. The reader interested in a more general and thorough discussion of the subject is referred to the excellent review paper [148].

C.1 Branes at singularities

One simple way to build configurations in string theory such that their low energy dynamics reproduces complicated quantum field theories consists of placing D-branes at singularities. Let us give a short overview of some of the main points in this construction.

D-branes are objects in string theory defined by the property that open strings can end in them. Let us focus in type IIB D3 branes sitting at a point in flat $\mathbb{R}^6$ for the moment. The lighter vibrational modes of the strings ending the D3 brane can be described as quantum fields living in its world volume. The boundary condition describing the brane in the worldsheet theory breaks half of the supersymmetry of the background space, so we end up with 16 supersymmetries. Working out the interactions of the open string excitations, the theory in the brane can be seen to be $U(1)$ $\mathcal{N} = 4$ SYM. This theory, in $\mathcal{N} = 1$ language, has 3 vector multiplets in the adjoint. The vevs for the 6 real scalars in the vector multiplet parametrize the location of the brane in the internal $\mathbb{R}^6$.

Let us consider now the case of stacking multiple parallel D-branes together. Each brane has open strings starting and ending on it, so by the same reasons as before the gauge group of the field theory describing the low energy degrees of freedom contains $U(1)^N$, where N is the number of branes in the stack. From the open string scattering amplitudes one learns that oriented open strings stretching between different branes have charge $+1$ under the $U(1)$ factor corresponding to the brane where the string starts

and -1 under the $U(1)$ of the ending brane. The resulting multiplet is massive when the branes are not coincident, as the string has a nonzero length. When the D-branes coincide, the gauge symmetry is enhanced to a non-abelian one, as we have massless bosons charged under other gauge bosons. In fact, the algebra for the charges we just gave reproduces the $U(N)$ Lie algebra structure, so this is the gauge group when all branes coincide. When just a subset of the branes coincide only the corresponding k $U(1)$ factors get promoted to $U(k)$. We see that the positions of the branes in the internal $\mathbb{R}^6$ encode essentially the Coulomb branch moduli space, with points in the moduli space with enhanced gauge symmetry corresponding to points where branes coincide.

Our next step will be studying the theory in manifolds of more holonomy, in order to break some supersymmetry and get a more realistic theory in the world volume of the branes. In the next section we will study manifolds of $SU(3)$ holonomy, namely (local) Calabi-Yau spaces, so the resulting theory is $\mathcal{N} = 1$ SYM. We will find that the resulting gauge theory can be quite complicated, giving rise to involved gauge groups, matter content and superpotential terms.

C.2 Defining dimer models

In this section we will describe a nice way to characterize the gauge theory living in the world volume of D3 branes sitting at a Calabi-Yau toric singularity. This description is in terms of the so called *dimer models*[1], which are essentially tilings[2] of a two-torus such that each node can be colored black or white, and edges always connect white nodes with black nodes. One assigns a gauge theory to such a tiling in the following way:

- Each face corresponds to a $U(N)$ factor of the gauge group. We will take the rank of all gauge factors equal for the moment, and generalize to different ranks later on.

- Each edge corresponds to a bifundamental chiral field transforming in the fundamental of the face at one side and the antifundamental of the face at the other side. In order to distinguish sides, we draw for each edge an arrow perpendicular to it such that the field transforms in the antifundamental of the gauge group where the arrow comes from and in the fundamental of the group where it ends. Then we impose that the arrow flips direction as we traverse the edges in a face (it points

[1] In many places of this work, we will be slightly unconventional and refer to the dimer model simply as *dimer*. In the conventional nomenclature "dimer" refers to what we call here an edge. We will never refer to edges as dimers, so no confusion should arise.

[2] The terminology is that a tiling consists of faces, which are delimited by edges, and these edges end in nodes.

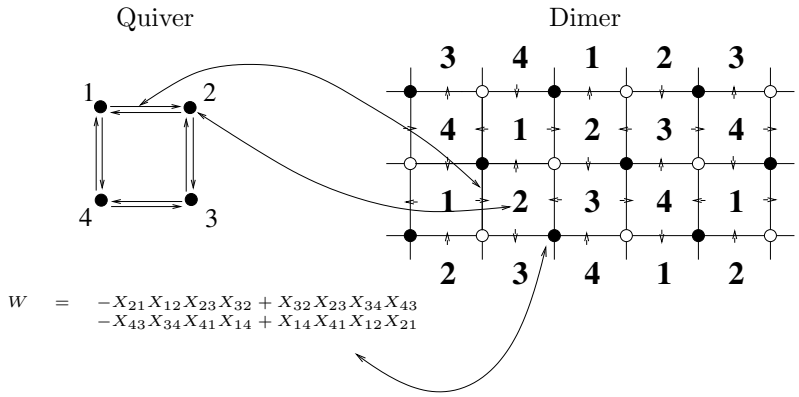

Figure C.1: Quiver and dimer for a $\mathbb{Z}_2$ orbifold of the conifold. Faces in the dimer correspond to gauge groups, edges correspond to bifundamentals and each vertex corresponds to a superpotential term. Edges have an orientation determined by the coloring of the adjacent nodes. There is an overall trace implicit in the superpotential.

inwards for the first edge, for example, then outwards from the face for the second, and so on). The net result is that the arrows circle black nodes clockwise and white nodes anticlockwise (or vice versa, depending on an overall sign convention).

- Finally, nodes are associated with superpotential terms. Each node contributes a term to the superpotential given by "following the arrows". Namely we follow the arrows as they go around the given node, and we write the ordered product of the fields we encounter. The sign is + for white nodes and − for black nodes, for example. Then we trace over the resulting monomial, making irrelevant which edge we decided to start from.

As an example of the application of these rules, let us consider the case of the dimer for a $\mathbb{Z}_2$ orbifold of the conifold, sometimes called the double conifold, which is defined as the surface $xy = z^2w^2$ in $\mathbb{C}^4$. It is shown in Figure C.1. In that figure the dimer representation of the theory is connected with the usual quiver representation, where gauge groups are points and bifundamentals are arrows between points (and the superpotential does not appear).

Another important concept present in dimer diagrams is that of zig-zag paths. They are paths on the dimer that run along edges and such that they turn maximally right at black nodes and maximally left at white nodes, where the color of the node is also conventional. The zig-zag paths for the case of the double conifold are shown in Figure C.2. The paths are A, B, C, D, E and F, and as it is customary we have divided each path in pieces highlighting the adjacency between paths, for example A4 and E3 are

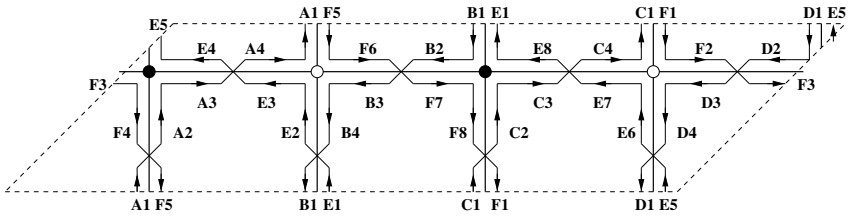

Figure C.2: Zig-zag paths for the dimer diagram of the double conifold.

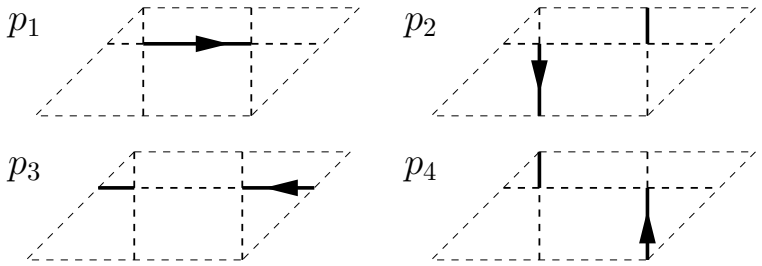

Figure C.3: Perfect matchings for the dimer graph of the conifold.

adjacent pieces.

As a first property of these zig-zag paths, note that they never intersect themselves. Another very useful property is that we can assign to each zig-zag path a (p, q) homology charge given by its winding numbers in the torus. It turns out that these charges, when represented in a plane, reproduce the web diagram of the toric variety describing the space of vacua of the gauge theory. From this information, it is extremely simple to find the geometry described by a given dimer. This surprising connection between zig-zag paths and the web diagram will be explained in Section C.3.

C.2.1 Perfect matchings

The last piece of information that will turn out to be important is the concept of *perfect matching*. We call a perfect matching a subset of edges in the dimer such that each node makes contact with one and only one edge in the perfect matching. The set of perfect matchings for the conifold is shown in Figure C.3.

It is possible to read the toric diagram also from the perfect matchings, and in some situations it might turn out to be more convenient to do things in this language. Note that each edge can be assigned a natural orientation, for example as going from white to black. We define subtraction of two perfect matchings $p_i - p_j$ as the oriented path that results in the dimer from concatenating p_i with the reversal of p_j. If the same edge appears in both perfect matchings, then it is removed in the end result. Let us denote as (p, q) the homotopy charge of the resulting cycle. The cycle need not

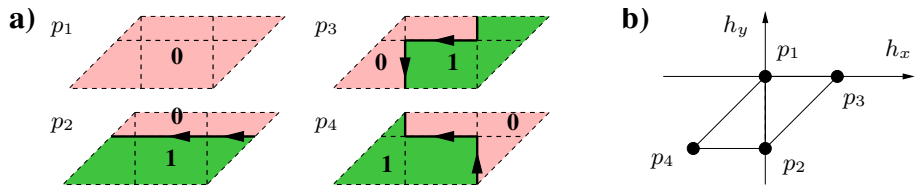

Figure C.4: Finding the toric diagram for the conifold from the perfect matchings of the corresponding dimer. In a) we show the paths in the dimer with the associated height functions, and in b) the resulting toric diagram.

be connected, in the case of multiple disconnected pieces we just add the homotopy charges of the different pieces.

In order to find the position in the toric diagram of a given perfect matching, one first takes any perfect matching as a reference (p_1, for simplicity), and situates it in the origin (again for simplicity) of the bi-dimensional integer lattice where we draw the toric diagram. The positions of the other perfect matchings in the toric diagram are then given by the (p, q) charges of the cycles $p_i - p_1$. The convex hull of the resulting set of points gives us the desired toric diagram. This is equivalent, but a bit simpler to picture, to the usual height function formalism [94]. There is an $SL(2, \mathbb{Z})$ transformation between the results of the two procedures (actually, simply a $\pi/2$ rotation). We choose to draw the resulting diagram as given in the height function formalism in order to make better contact with the existing literature. In Figure C.4 we illustrate the procedure for the case of the conifold. Note, as we pointed out in Section B.2, that this geometrizes the $SL(2, \mathbb{Z})$ arbitrariness of the toric diagram as the $SL(2, \mathbb{Z})$ freedom in electing the base cycles in the torus homology.

Perfect matchings and F-terms

Perfect matchings are the natural GLSM variables that trivialize the F-term conditions. This was conjectured in [94] and proved in [149]. It works as follows. In a toric field theory each field appears exactly twice in the superpotential, with opposite signs. In the dimer this is represented as the statement that each edge is bounded by two nodes, and that the graph is bipartite, with the color giving the sign of the corresponding superpotential term. Let us assign to each perfect matching a field p_i in a GLSM. Now construct composite fields X_a (one for each edge in the dimer) in terms of these basic perfect fields as:

$$X_a = \prod_i p_i^{\langle p_i, X_a \rangle}. \tag{C.1}$$

The product $\langle p_i, X_a \rangle$ is 1 if the edge corresponding to X_a is in the perfect matching corresponding to p_i, and 0 otherwise. The statement is that this

GLSM, with appropriately chosen $U(1)$ GLSM symmetries, has the same classical moduli space as the theory described by the dimer.

This statement divides into two parts. The first one amounts to describing precisely the $U(1)$ symmetries we will use in order to build the GLSM, and the charges of the p_i under these symmetries. We have already described how this can be done in the previous sections. Namely, one maps perfect matchings into positions in the toric diagram. The resulting positions in toric diagram fulfill linear relations of the type:

$$\sum_i n_i p_i = 0, \tag{C.2}$$

where $n_i \in \mathbb{Z}$, and $\sum n_i = 0$ (this last equality just encodes translational invariance of the relations). If we now interpret these relations as $U(1)$ symmetries and the coefficients n_i as the charges of the perfect fields under the $U(1)$ one has a well defined GLSM. The idea of associating $U(1)$ symmetries to these relations is just the restatement of the fact that the toric diagram is obtained as the cokernel of the charge matrix.

In the second part we should prove that the F-term equations hold (indeed they trivialize as we will see) when expressing the bifundamentals in terms of perfect fields. Remember that a basic fact about dimer models is that each bifundamental appears in the superpotential exactly twice, and with opposite signs. In terms of the dimer diagrams, this means that each edge E is bounded by a black and a white node. The F-term equation for E can be stated as the statement that the product of the fields at the white edge (excluding E) is equal to the product of the fields at the black node (again, excluding E). In terms of the perfect fields, this reads:

$$\prod_{\text{black } X_a} \prod_i p_i^{\langle p_i, X_a \rangle} = \prod_{\text{white } X_a} \prod_i p_i^{\langle p_i, X_a \rangle}, \tag{C.3}$$

with the understanding that the product excludes E. We can rewrite this in a bit more suggestive way:

$$\prod_i \left(\prod_{\text{black } X_a} p_i^{\langle p_i, X_a \rangle} \right) = \prod_i \left(\prod_{\text{white } X_a} p_i^{\langle p_i, X_a \rangle} \right). \tag{C.4}$$

Now we see the equation to be true, as every time a factor of p_i appears in the left side, meaning that the corresponding perfect matching touches the black node with an edge different from E, it also touches the white node with an edge different from E, so another factor of p_i appears in the right side.

C.3 String theory interpretation

It is possible to gain a better intuitive understanding of the relations we deduced above by studying the mirror configuration of branes. The contents

of this section were first discussed in [150], which we follow.

The manifold mirror to the toric variety is a non-compact Calabi-Yau that is most easily described as a double fibration over the complex plane, parametrized by $W \in \mathbb{C}$. One of the fibers is a (possibly singular at some points) $\mathbb{C}^*$ given by $uv = W$, with u and v both in $\mathbb{C}$, and the other is the non compact Riemann surface defined by $P(z, w) = W$, with z and w in $\mathbb{C}^*$. The total Calabi-Yau is thus the solution of the following set of equations:

$$\begin{aligned} W &= uv, \\ W &= P(z, w). \end{aligned} \tag{C.5}$$

We still need to describe what $P(z, w)$ is. It is given by what is called the *Newton polynomial* of the toric variety: associate one axis in the lattice where the toric diagram is defined with the variable z, and the other one with w. Each point in the toric diagram (possibly including interior points) has a position given by a pair of integers (p, q). To each such point we associate a term in the Newton polynomial given by:

$$P(z, w) = \ldots + c_{(p,q)} z^p w^q. \tag{C.6}$$

The coefficients $c_{(p,q)}$ are associated with complex deformations in the mirror, and thus to Kähler deformations in the original toric geometry. They will not play any important role in this section.

With such a definition, equation (C.5) defines a genus g punctured Riemann surface, where g is simply given by the number of interior points in the original toric diagram. The punctures will turn out to be important, they are associated with external legs in the web diagram. Each carries a natural (p, q) charge given by the (p, q) charge of the corresponding leg in the original web diagram. We will give a geometric interpretation of this charge in a moment.

Generically we call the Riemann surface Σ, but if we want to emphasize its dependence on the base point W we call it Σ_W instead. An essential fact about the Riemann surface is that it is given simply by a "thickening" of the web diagram for the toric geometry, meaning that we replace the one-dimensional lines in the web diagram by two dimensional cylinders, in the same way as we "thicken" the Feynman diagrams in string theory in order to obtain the worldsheet description of a given gauge theory process. This is illustrated for the double conifold in Figure C.5.

We still have to describe the 3-cycles wrapped by the D6 branes in this geometry. Studying the Newton polynomial it is found [150] that it degenerates in N points of the base, where N is twice the area of the corresponding toric diagram. Degeneration here means that there is a homotopically non-trivial[3] one cycle in the Riemann surface that contracts to a point. We

[3]The relevant homotopy here includes the punctures.

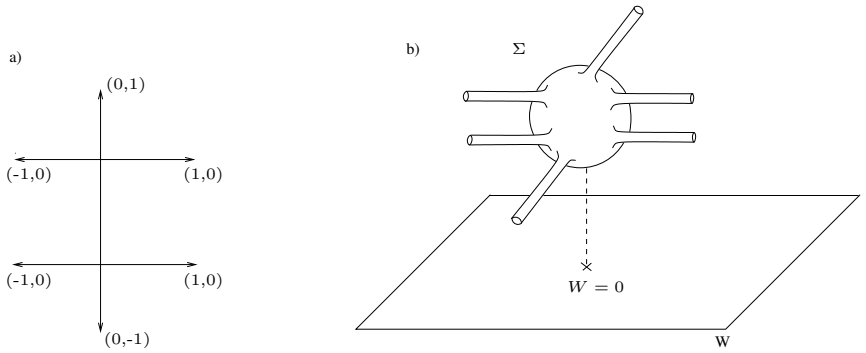

Figure C.5: The mirror for the double conifold. In a) we show the web diagram for the original geometry, and in b) the Riemann surface part of the fibration defining the mirror. The tubes going to infinity represent the punctures.

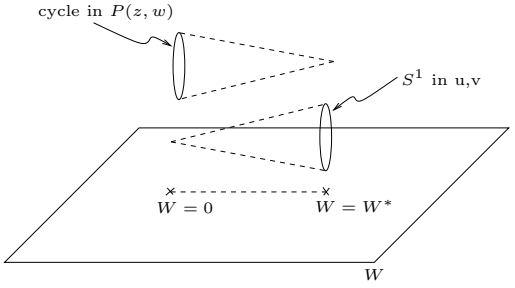

Figure C.6: The mirror geometry to the toric Calabi-Yau, where we have schematically shown the 3-cycle the D6 branes wrap. W^* denotes the critical points where the Riemann surface degenerates.

will associate one D6 brane with each such degeneration. Each of these D6 branes is mirror to one fractional brane of the IIB system.

On the other hand, note that the other fiber $W = uv$ is smooth and isomorphic to $\mathbb{C}^*$ except at $W = 0$, where the geometry becomes singular. The relevant 3-cycle wrapped by the D6 brane is then given by a 1-cycle around the origin in the $\mathbb{C}^*$ (which being volume minimizing contracts to the singular point at $W = 0$), the 1-cycle that degenerates at the critical points for the Riemann surface, and the line connecting the critical point and $W = 0$ in the base. The configuration is illustrated in Figure C.6.

The dimer in the mirror

It turns out that in a sense the dimer diagram is contained already in the mirror manifold. The different fractional branes intersect over $W = 0$, it is what happens at this point that determines the physics we are interested in. In particular, the D6 branes give the faces of the dimers, and their intersection corresponds to bifundamentals. Superpotential terms come from

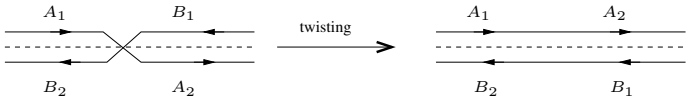

Figure C.7: Twisting the zig-zag paths A and B so they no longer cross over the edge in the dimer (depicted by the dashed line).

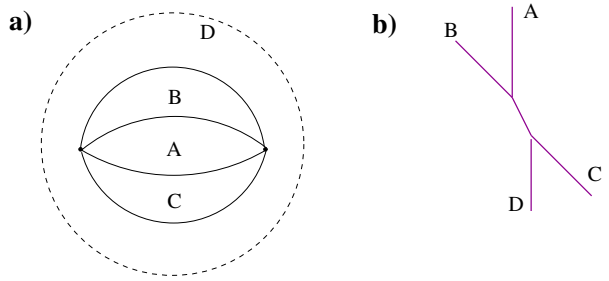

Figure C.8: a) Tiling of the Riemann surface (which is topologically a sphere, shown as the complex plane) for the case of D3-branes at a conifold singularity. b) The web diagram, providing a skeleton of the Riemann surface, with asymptotic legs corresponding to punctures (and hence to faces of the tiling of Σ, and zig-zag paths of the original dimer diagram).

to worldsheet disc instantons in the Riemann surface.

What we want to find is a map from Σ_0 to a T^2 representing the dimer. In order to see the map more clearly, recall that the mirror of a toric Calabi-Yau can be seen as a T^3 fibration over a base, where the three torus is the torus in which we perform three T-dualities [151]. It turns out that we can actually identify this T^2 inside the T^3 fiber, via what is called the *alga map* [150]. We will only describe a simplified version that is topologically equivalent and is easily implemented in terms of the dimer graphs. It is obtained via an operation called *twisting*, and maps the Riemann surface into a two torus isomorphic to the dimer model. The operation is defined in terms of zig-zag paths, and consists of undoing the natural crossing of the zig-zag paths over the edges, as shown in Figure C.7.

This operation maps a tiling of the two torus into a tiling of the Riemann surface in such a way that nodes go to nodes and edges go to edges. The fate of the faces of the dimer is a bit more subtle. What happens is that each zig-zag path surrounds in the Riemann surface a puncture. In this way we can assign to each puncture in Σ the (p, q) homotopy charge of the corresponding zig-zag path in the dimer. The faces then get mapped to paths in the Riemann surface such that the sum of the (p, q) charges of the punctures they enclose is zero (since the faces are contractible in the dimer). As an example, in Figure C.8 we show the tiling of the Riemann surface for the conifold.

C.4 Adding flavor

We have discussed in the previous sections how to describe the gauge theory on the D3 branes located at the toric singularity using dimer model techniques. Here we will describe a procedure for including flavors in such constructions. We use D7 branes for such purpose, as described in [152]. The discussion in the dimer model context has been done in [68], which we follow here.

Let us take as a working example the complex cone over dP_2. Its corresponding dimer model is shown in Figure C.9. As described in the previous section, D3–branes on a toric singularity are mirror to D6–branes on intersecting 3-cycles in a geometry given by a fibration of a Riemann surface Σ with punctures.

In [68], it was argued that D7–branes passing near the singular point can be described in the mirror Riemann surface Σ by non-compact 1-cycles which come from infinity at one puncture and go to infinity at another. One very heuristic way to motivate this is that in the web diagram for the toric singularity (of which Σ is just a thickening) 4-cycles are represented as the non compact regions of the plane bounded by the external legs. Since the mirror of a 4-cycle in a Calabi-Yau is always a 3-cycle (as the only non vanishing odd homology is the third one) we expect them to be represented, when restricted to Σ, by some one-cycle. From the web diagram description, it is reasonable to think that the corresponding one-cycle goes along the punctures, since they are the thickenings of the external legs, and these bound the holomorphic 4-cycle wrapped by the D7 in the original geometry. We can check that this curve gives us the correct matter spectrum and interactions in some simple cases.

Figure C.10 shows the 1-cycles corresponding to some D3- and D7-branes in the Riemann surface in the geometry mirror to the complex cone over dP_2. A D7-brane leads to flavors for the two D3-brane gauge factors whose 1-cycles are intersected by the D7-brane 1-cycle, and there is a cubic coupling among the three fields (related to the disk bounded by the three 1-cycles in the Riemann surface).

We will use this construction extensively in Chapter 4. There, given a gauge theory of D3-branes at a toric singularity, we will introduce massive flavors for some of the gauge factors in the following way. We pick a term in the superpotential, and we introduce flavors for all the involved gauge factors, and coupling to all the involved bifundamental multiplets. For example, the quiver with flavors for the dP_2 theory is shown in Figure C.11. We also introduce quadratic couplings between the D7 branes, giving mass to the flavors. Namely, we separate the D7 slightly from the singularity.

In the dimer model, this procedure amounts to picking a node and introducing D7-branes crossing all the edges ending on the node, see Figure C.10.

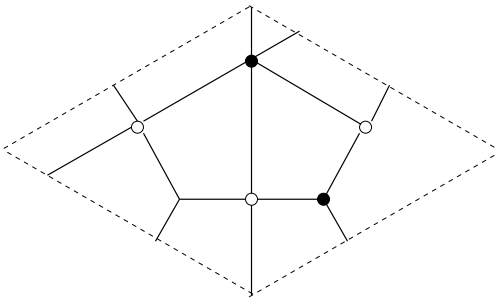

Figure C.9: Dimer diagram for D3–branes at a dP_2 singularity.

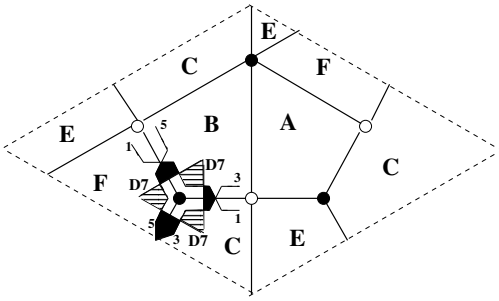

Figure C.10: Riemann surface in the geometry mirror to the complex cone over dP_2, shown as a tiling of a T^2 with punctures (denoted by capital letters). The figure shows the non-compact 1-cycles extending between punctures, corresponding to D7-branes, and a piece of the 1-cycles that correspond to the mirror of the D3-branes.

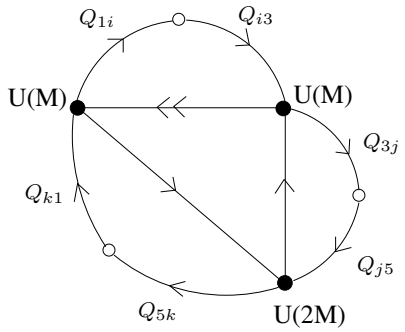

Figure C.11: Quiver for the dP_2 theory with M fractional branes and flavors.

In this example we obtain the superpotential terms

$$W_{flavor} = \lambda'(Q_{1i}\tilde{Q}_{i3}Y_{31} + Q_{3j}\tilde{Q}_{j5}X_{53} + Q_{5k}\tilde{Q}_{k1}X_{15}) \tag{C.7}$$

In addition we introduce mass terms

$$W_{mass} = m_1 Q_{1i}\tilde{Q}_{k1} + m_2 Q_{3j}\tilde{Q}_{i3} + m_5 Q_{5k}\tilde{Q}_{j5} \tag{C.8}$$

This procedure is completely general and applies to all gauge theories for branes at toric singularities we will be interested in. It does not apply if the superpotential (regarded as a loop in the quiver) passes twice through the node which is eventually dualized in the derivation of the metastable vacua. However we have found no example of this for any DSB fractional branes.

Appendix D

A short introduction to D-instantons

In dealing with euclidean brane instantons in string theory compactifications, it is convenient to make some general classifications and distinctions, which will be useful for the discussion in the main text. For concreteness we will focus on D-brane instantons, although the same effects can also arise from other types of instantons in dual pictures. A recent short review touching on many of the same topics that we discuss here can be found in [153].

D.1 Superpotentials from gauge D-brane instantons

A first class of D-brane instantons corresponds to those whose internal structure is exactly the same as some of the 4d space filling branes in the background. Namely, in geometric setups, Euclidean Dp-branes wrapping the same $(p+1)$-cycle (and carrying the same world-volume gauge bundle) as some D$(p+4)$-branes in the background configuration (in more abstract CFT terms, they should be described by the same boundary state of the internal CFT). Such D-brane instantons correspond to gauge instantons on the corresponding 4d gauge sector, and thus reproduce non-perturbative effects arising from strong gauge dynamics.

A prototypical case, which will appear in our examples, is the generation of the Affleck-Dine-Seiberg superpotential

$$W \,=\, (N_c - N_f) \left(\frac{\Lambda^{3N_c - N_f}}{\det M} \right)^{\frac{1}{N_c - N_f}} \tag{D.1}$$

on a set of 4d space filling branes whose low-energy dynamics corresponds to $SU(N_c)$ SQCD with N_f flavours (with dynamical scale Λ; here M denotes

the meson fields). For $N_f = N_c - 1$ this arises from classical 4d instanton field configurations, and has been recovered from D-brane instantons in several instances with different levels of detail [154, 155, 103, 156]. For other values of $N_f < N_c$, it does not arise from classical 4d field configurations, and is obtained indirectly. Alternatively, it can be obtained by considering the theory on $\mathbb{S}^1$, where there exist suitable 3d classical field configurations (sometimes denoted calorons) leading to a 3d superpotential, which can be argued to survive in the 4d decompactification limit (with a microscopic description in terms of putative objects denoted "fractional instantons" or "merons"). The latter description fits perfectly with the string theory realization. Indeed, the computation of e.g. the euclidean D3-brane instanton superpotential in type IIB configurations with gauge sectors on D7-branes on 4-cycles is usually described by invoking compactification on a circle in order to use an M-theory dual. Upon compactification, one may use T-duality, leading to a picture where instantons are D-branes stretched along the circle direction, and gauge D-branes are pointlike on it. In this picture the superpotential is generated by "fractional" D-branes, which are suspended between the gauge D-branes and thus stretch only a fraction of the period along the circle direction [157]. Equivalently, in the dual M-theory picture, the gauge D7-branes turn into degenerations of the elliptic fibration, such that the fiber over the 4-cycle on the base is a sausage of 2-spheres. The ADS superpotential is generated by M5-branes which wrap the 4-cycle times a 2-sphere (leading to "fractional" objects, in the sense that the standard 4d gauge instanton corresponds to an M5-brane wrapping the whole fiber) [155]. We will often abuse language and regard the 4d ADS superpotential as generated by (fractional) instantons, although strictly speaking only the 3d ADS superpotential has such a microscopic description.

It is interesting to point out that many of the manipulations in the analysis of $\mathcal{N} = 1$ supersymmetric field theories usually carried out in terms of the exact effective action, can be carried out microscopically in terms of the physics of the relevant (possibly fractional) instantons. For instance, an important point in working with gauge instantons in our examples is the derivation, from the instanton physics viewpoint, of the matching of scales in processes like integrating out massive 4d matter etc. Let us describe this in a simple example. Consider an $SU(N_c)$ theory with $N_f < N_c$ flavours with mass (matrix) m, with dynamical scale $\Lambda = (e^{-1/g^2})^{1/(3N_c - N_f)}$. Consider the situation where we neglect the effect of the mass term on the instanton physics. Then the instanton feels N_f massless flavors and the non-perturbative dynamics is described by the effect of a $\frac{1}{N_c - N_f}$-fractional instanton, leading to the total superpotential

$$W \,=\, (N_f - N_c) \left(\frac{\Lambda^{3N_c - N_f}}{\det Q\tilde{Q}} \right)^{\frac{1}{N_c - N_f}} \,+\, m\, Q\tilde{Q} \tag{D.2}$$

We may want to use an alternative description where we include the effect of the mass terms from the start. From the spacetime viewpoint, we integrate out the massive flavours. From the instanton perspective, the instanton feels that the $2N_f$ fermion zero modes α, β associated to the flavors (in the D-brane picture, open strings stretched between the instanton brane and the flavor branes) are actually massive[1]. Integrating out the term $S_{\rm inst} = m\alpha\beta$ in the instanton action leads to a prefactor of $\det m$ in the amplitude for the left-over $\frac{1}{N_c}$-fractional instanton. Therefore the superpotential is

$$W \,=\, N_c \left(\Lambda^{3N_c - N_f} \, \det m \right)^{\frac{1}{N_c}} \tag{D.3}$$

This is the standard $\frac{1}{N_c}$-fractional instanton amplitude for a SYM sector with effective scale Λ' defined by

$$\Lambda'^{3N_c} \,=\, \Lambda^{3N_c - N_f} \, \det m \tag{D.4}$$

Note that (D.3) in fact agrees with (D.2) upon integrating out the massive flavours in the latter. Also, the matching of scales is the familiar one in field theory.

For future reference, let us mention that D-brane instantons associated as above to 4d space filling D-branes, can lead to non-perturbative superpotentials despite the fact that there are 4 universal zero modes in the instanton-instanton open string sector. Indeed, two of these fermion zero modes have cubic couplings to the bosonic and fermionic zero modes in the mixed open string sector (strings stretched between the instanton and the gauge D-branes). Their role can be regarded as imposing the fermionic constraints to recover the ADHM instanton measure [123]. The two left-over fermion zero modes are Goldstinos of the $\mathcal{N} = 1$ supersymmetry, and are saturated by the $d^2\theta$ integration involved in the induced superpotential.

D.2 Non-gauge, "exotic" or "stringy" instantons

In general an euclidean D-brane instanton does not have the same internal structure as any gauge D-brane in the configuration. Such D-brane instantons do not have any known gauge field theory interpretation, and are thus sometimes dubbed "exotic" or "stringy" instantons. BPS instantons of this kind lead to superpotential terms only if they have two fermion zero modes, with additional fermion zero modes forcing multi-fermion insertions leading to higher F-terms as described below (additional fermions zero modes, with couplings to 4d chiral multiplets, are regarded here as non-zero modes, since

[1] This follows from the fact that the massive flavours are open strings from the color to the flavor branes, and that gauge brane instantons wrap exactly on top of the color branes.

they are lifted by background values of the latter; equivalently, integration over these zero modes leads to insertions of the 4d chiral multiplet in the induced superpotential). We are thus interested in stringy instantons with two fermion zero modes.

In the same way as for gauge instantons, there are 4 universal fermion zero modes in the instanton-instanton open string sector. However in this case, there are no bosonic zero modes which can lift the two non-goldstino modes. In the absence of other lifting mechanisms (like closed string flux backgrounds), the only mechanism which can eliminate these extra modes in type II perturbative models is an orientifold projection. Therefore, only instantons invariant under the orientifold action, and with a Chan-Paton action leading to an $O(1)$ symmetry, have two universal fermion zero modes, and have a chance of leading to a non-perturbative superpotential (of course if they do not have extra fermion zero modes in other sectors).

D.3 Higher F-terms from D-brane instantons

Besides D-brane instantons generating superpotentials, BPS D-brane instantons with additional fermion zero modes lead to higher F-terms in the effective action. These have been considered in [108, 158], and lead to operators with one insertion of $\overline{D\Phi}$ for each additional fermion zero mode. Roughly speaking they have the structure

$$\int d^4x\, d^2\theta\, w_{\bar{i}_1\bar{j}_1\ldots\bar{i}_n\bar{j}_n}(\Phi)\, \overline{D\Phi}^{\bar{i}_1}\, \overline{D\Phi}^{\bar{j}_1} \ldots \overline{D\Phi}^{\bar{i}_n}\, \overline{D\Phi}^{\bar{j}_n} \tag{D.5}$$

where the tensor $w(\Phi)$ depends holomorphically on the 4d chiral multiplets. The simplest situation is an instanton with two additional fermion zero modes, which is for instance realized for gauge instantons in $N_f = N_c$ SQCD. The corresponding operator has the above structure with $n = 1$ and implements the familiar complex deformation of the moduli space (in an intrinsic way, in the sense of the moduli space geometry).

The study of the interplay between non-perturbative higher F-terms and lines of marginal stability is beyond our scope here, although we expect that it admits a similar microscopic description in terms of multi-instanton contributions after instanton splitting. In any event, even for the analysis of superpotential terms, such instantons will play an interesting role in some of our examples. We refer to these instantons as Beasley-Witten instantons.

D.4 An example: dynamical mass terms

In this section we will discuss a simple example where instanton effects are important, and induce a mass term in the theory. The example is originally discussed in [55].

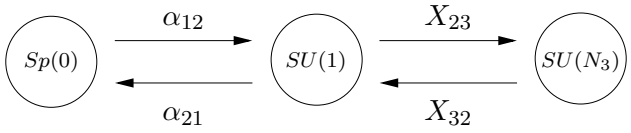

Figure D.1: Quiver for the fractional brane at the orientifolded orbifolded conifold we will study. The α are fermionic zero modes between the $SU(1)$ brane and the D-instanton.

We are going to consider the theory corresponding to a particularly simple set of fractional branes in the orientifolded orbifolded conifold, namely those that give the quiver in Figure D.1. This theory is much easier to analyze than the one studied in Section 6.4.2, and it already contains some interesting instanton effects.

There is no tree level superpotential for this theory, but there is a quartic coupling in the instanton action between the instanton zero modes and the X_{23}, X_{32} superfields:

$$S_{inst} \sim \frac{V}{g_s}\alpha_{12}X_{23}X_{32}\alpha_{21} \tag{D.6}$$

where g_s is the string coupling and V the volume of the cycle wrapped by the instanton. This coupling comes from a worldsheet disk instanton similar to the one that would have produced the usual quartic couplings in the conifold theories. In practice, the coupling in the instanton action is obtained simply by taking the known coupling in the conifold theory and substituting a couple of superfields by the corresponding fermionic zero modes.

In order to absorb the extra Goldstinos we have put an orientifold over node 1 (this is why in Figure D.1 we refer to this node as $USp(0)$). We now have just to integrate over the charged fermionic zero modes α. If we can saturate these α modes by insertions of the couplings in the instanton action we will have a contribution to the spacetime superpotential. This is indeed the case: bringing down one insertion of α one obtains the following contribution to the nonperturbative superpotential

$$W_{np} = \ldots + \int d\alpha_{12}d\alpha_{21}e^{S_{inst}} = \ldots + e^{-\frac{V}{g_s}}X_{23}X_{32} \tag{D.7}$$

We see that in this simple case instantons dynamically induce a mass term for some chiral fields in the theory. In particular, one could think of using configurations similar to the one studied here in order to give dynamically small masses to the flavors in the ISS-like constructions of Chapter 4. We could in this way remove the need for adding parametrically small masses by hand, at the expense of complicating the local geometry where we put our brane.

Bibliography

[1] Steven Weinberg. *The Quantum theory of fields. Vol. 1: Foundations.* Cambridge University Press (1995).

[2] Steven Weinberg. *The Quantum theory of fields. Vol. 2: Modern applications.* Cambridge University Press (1996).

[3] Michael E. Peskin and D. V. Shroeder. *An Introduction to quantum field theory.* Addison-Wesley (1995).

[4] R. D. Peccei. "Reflections on the strong CP problem" (1998). `hep-ph/9807514`.

[5] Michael B. Green, J. H. Schwarz and Edward Witten. *Superstring theory. Vol. 1: Introduction.* Cambridge University Press (1987).

[6] Michael B. Green, J. H. Schwarz and Edward Witten. *Superstring theory. Vol. 2: Loop Amplitudes, Anomalies and Phenomenology.* Cambridge University Press (1987).

[7] J. Polchinski. *String theory. Vol. 1: An introduction to the bosonic string.* Cambridge University Press (1998).

[8] J. Polchinski. *String theory. Vol. 2: Superstring theory and beyond.* Cambridge University Press (1998).

[9] K. Becker, M. Becker and J. H. Schwarz. "String theory and M-theory: A modern introduction". Cambridge, UK: Cambridge Univ. Pr. (2007) 739 p.

[10] M. Dine. "Supersymmetry and string theory: Beyond the standard model". Cambridge, UK: Cambridge Univ. Pr. (2007) 515 p.

[11] Clifford V. Johnson. "D-brane primer" (2000). `hep-th/0007170`.

[12] C. V. Johnson. "D-branes". Cambridge, USA: Univ. Pr. (2003) 548 p.

[13] Elias Kiritsis. "String theory in a nutshell". Princeton, USA: Univ. Pr. (2007) 588 p.

[14] B. Zwiebach. "A first course in string theory". Cambridge, UK: Univ. Pr. (2004) 558 p.

[15] Angel Uranga. "Graduate Course in String Theory". http://gesalerico.ft.uam.es/paginaspersonales/angeluranga/index.html.

[16] Dieter Lust. "String Landscape and the Standard Model of Particle Physics" (2007). arXiv:0707.2305 [hep-th].

[17] Joseph Polchinski. "Dirichlet-Branes and Ramond-Ramond Charges". *Phys. Rev. Lett.*, 75:4724–4727 (1995). hep-th/9510017.

[18] Edward Witten. "String theory dynamics in various dimensions". *Nucl. Phys.*, B443:85–126 (1995). hep-th/9503124.

[19] P. K. Townsend. "The eleven-dimensional supermembrane revisited". *Phys. Lett.*, B350:184–187 (1995). hep-th/9501068.

[20] Juan Martin Maldacena. "The large N limit of superconformal field theories and supergravity". *Adv. Theor. Math. Phys.*, 2:231–252 (1998). hep-th/9711200.

[21] Edward Witten. "Anti-de Sitter space and holography". *Adv. Theor. Math. Phys.*, 2:253–291 (1998). hep-th/9802150.

[22] S. S. Gubser, Igor R. Klebanov and Alexander M. Polyakov. "Gauge theory correlators from non-critical string theory". *Phys. Lett.*, B428:105–114 (1998). hep-th/9802109.

[23] Gerard 't Hooft. "Dimensional reduction in quantum gravity" (1993). gr-qc/9310026.

[24] Andrew Strominger and Cumrun Vafa. "Microscopic Origin of the Bekenstein-Hawking Entropy". *Phys. Lett.*, B379:99–104 (1996). hep-th/9601029.

[25] Thomas Mohaupt. "Supersymmetric black holes in string theory". *Fortsch. Phys.*, 55:519–544 (2007). hep-th/0703035.

[26] Kenneth A. Intriligator and N. Seiberg. "Lectures on supersymmetric gauge theories and electric- magnetic duality". *Nucl. Phys. Proc. Suppl.*, 45BC:1–28 (1996). hep-th/9509066.

[27] Amit Giveon and David Kutasov. "Brane dynamics and gauge theory". *Rev. Mod. Phys.*, 71:983–1084 (1999). hep-th/9802067.

[28] N. Seiberg and Edward Witten. "Electric - magnetic duality, monopole condensation, and confinement in N=2 supersymmetric Yang-Mills theory". *Nucl. Phys.*, B426:19–52 (1994). hep-th/9407087.

[29] Edward Witten. "Solutions of four-dimensional field theories via M-theory". *Nucl. Phys.*, B500:3–42 (1997). `hep-th/9703166`.

[30] Albrecht Klemm, Wolfgang Lerche, Peter Mayr, Cumrun Vafa and Nicholas P. Warner. "Self-Dual Strings and N=2 Supersymmetric Field Theory". *Nucl. Phys.*, B477:746–766 (1996). `hep-th/9604034`.

[31] Marcel Vonk. "A mini-course on topological strings" (2005). `hep-th/0504147`.

[32] Andrew Neitzke and Cumrun Vafa. "Topological strings and their physical applications" (2004). `hep-th/0410178`.

[33] Bertrand Eynard and Nicolas Orantin. "Invariants of algebraic curves and topological expansion" (2007). `math-ph/0702045`.

[34] M. Marino. "Chern-Simons theory, matrix models, and topological strings". Oxford, UK: Clarendon (2005) 197 p.

[35] K. Hori *et al. Mirror symmetry.* Providence, USA: AMS (2003).

[36] Michael R. Douglas and Gregory W. Moore. "D-branes, Quivers, and ALE Instantons" (1996). `hep-th/9603167`.

[37] J. F. G. Cascales, M. P. Garcia del Moral, F. Quevedo and A. M. Uranga. "Realistic D-brane models on warped throats: Fluxes, hierarchies and moduli stabilization". *JHEP*, 02:031 (2004). `hep-th/0312051`.

[38] M. Cvetic, H. Lu, Don N. Page and C. N. Pope. "New Einstein-Sasaki spaces in five and higher dimensions". *Phys. Rev. Lett.*, 95:071101 (2005). `hep-th/0504225`.

[39] Dario Martelli and James Sparks. "Toric Sasaki-Einstein metrics on S**2 x S**3". *Phys. Lett.*, B621:208–212 (2005). `hep-th/0505027`.

[40] Amihay Hanany and Edward Witten. "Type IIB superstrings, BPS monopoles, and three-dimensional gauge dynamics". *Nucl. Phys.*, B492:152–190 (1997). `hep-th/9611230`.

[41] Kenneth Intriligator, Nathan Seiberg and David Shih. "Dynamical SUSY breaking in meta-stable vacua". *JHEP*, 04:021 (2006). `hep-th/0602239`.

[42] Sebastian Franco, Inaki Garcia-Etxebarria and Angel M. Uranga. "Non-supersymmetric meta-stable vacua from brane configurations" (2006). `hep-th/0607218`.

[43] Inaki Garcia-Etxebarria, Fouad Saad and Angel M. Uranga. "Supersymmetry breaking metastable vacua in runaway quiver gauge theories". *JHEP*, 05:047 (2007). `arXiv:0704.0166 [hep-th]`.

[44] Inaki Garcia-Etxebarria, Fouad Saad and Angel M. Uranga. "Quiver gauge theories at resolved and deformed singularities using Dimers". *JHEP*, 06:055 (2006). `hep-th/0603108`.

[45] Inaki Garcia-Etxebarria and Angel M. Uranga. "Non-perturbative superpotentials across lines of marginal stability" (2007). `arXiv:0711.1430 [hep-th]`.

[46] Inaki Garcia-Etxebarria, Fouad Saad and Angel M. Uranga. "Local models of gauge mediated supersymmetry breaking in string theory". *JHEP*, 08:069 (2006). `hep-th/0605166`.

[47] Edward Witten. "Branes and the dynamics of QCD". *Nucl. Phys.*, B507:658–690 (1997). `hep-th/9706109`.

[48] Kentaro Hori, Hirosi Ooguri and Yaron Oz. "Strong coupling dynamics of four-dimensional N = 1 gauge theories from M theory fivebrane". *Adv. Theor. Math. Phys.*, 1:1–52 (1998). `hep-th/9706082`.

[49] N. Seiberg and Edward Witten. "Monopoles, duality and chiral symmetry breaking in N=2 supersymmetric QCD". *Nucl. Phys.*, B431:484–550 (1994). `hep-th/9408099`.

[50] S. Elitzur, A. Giveon, D. Kutasov, E. Rabinovici and A. Schwimmer. "Brane dynamics and N = 1 supersymmetric gauge theory". *Nucl. Phys.*, B505:202–250 (1997). `hep-th/9704104`.

[51] J. Park, R. Rabadan and A. M. Uranga. "Orientifolding the conifold". *Nucl. Phys.*, B570:38–80 (2000). `hep-th/9907086`.

[52] Hirosi Ooguri and Yutaka Ookouchi. "Meta-stable supersymmetry breaking vacua on intersecting branes" (2006). `hep-th/0607183`.

[53] I. Bena, E. Gorbatov, S. Hellerman, N. Seiberg and D. Shih. "A note on (meta)stable brane configurations in MQCD" (2006). `hep-th/0608157`.

[54] Riccardo Argurio, Matteo Bertolini, Sebastian Franco and Shamit Kachru. "Gauge/gravity duality and meta-stable dynamical supersymmetry breaking". *JHEP*, 01:083 (2007). `hep-th/0610212`.

[55] Riccardo Argurio, Matteo Bertolini, Sebastian Franco and Shamit Kachru. "Metastable vacua and D-branes at the conifold". *JHEP*, 06:017 (2007). `hep-th/0703236`.

[56] Mina Aganagic, Christopher Beem, Jihye Seo and Cumrun Vafa. "Geometrically induced metastability and holography". *Nucl. Phys.*, B789:382–412 (2008). `hep-th/0610249`.

[57] Changhyun Ahn. "Brane configurations for nonsupersymmetric metastable vacua in SQCD with adjoint matter". *Class. Quant. Grav.*, 24:1359–1370 (2007). `hep-th/0608160`.

[58] Amit Giveon and David Kutasov. "Gauge symmetry and supersymmetry breaking from intersecting branes". *Nucl. Phys.*, B778:129–158 (2007). `hep-th/0703135`.

[59] Herman Verlinde. "On metastable branes and a new type of magnetic monopole" (2006). `hep-th/0611069`.

[60] Hirosi Ooguri, Yutaka Ookouchi and Chang-Soon Park. "Metastable Vacua in Perturbed Seiberg-Witten Theories" (2007). `arXiv:0704.3613 [hep-th]`.

[61] Amit Giveon and David Kutasov. "Stable and Metastable Vacua in SQCD" (2007). `arXiv:0710.0894 [hep-th]`.

[62] Matthew Buican, Dmitry Malyshev and Herman Verlinde. "On the Geometry of Metastable Supersymmetry Breaking" (2007). `arXiv:0710.5519 [hep-th]`.

[63] P. G. Camara and Mariana Grana. "No-scale supersymmetry breaking vacua and soft terms with torsion" (2007). `arXiv:0710.4577 [hep-th]`.

[64] Shmuel Elitzur, Amit Giveon and David Kutasov. "Branes and N = 1 duality in string theory". *Phys. Lett.*, B400:269–274 (1997). `hep-th/9702014`.

[65] A. Brandhuber, N. Itzhaki, V. Kaplunovsky, J. Sonnenschein and S. Yankielowicz. "Comments on the M theory approach to N = 1 SQCD and brane dynamics". *Phys. Lett.*, B410:27–35 (1997). `hep-th/9706127`.

[66] J. L. F. Barbon. "Rotated branes and N = 1 duality". *Phys. Lett.*, B402:59–63 (1997). `hep-th/9703051`.

[67] E. Gava, K. S. Narain and M. H. Sarmadi. "On the bound states of p- and (p+2)-branes". *Nucl. Phys.*, B504:214–238 (1997). `hep-th/9704006`.

[68] Sebastian Franco and Angel M. Uranga. "Dynamical SUSY breaking at meta-stable minima from D-branes at obstructed geometries". *JHEP*, 06:031 (2006). `hep-th/0604136`.

[69] G. W. Gibbons and P. Rychenkova. "HyperKaehler quotient construction of BPS monopole moduli spaces". *Commun. Math. Phys.*, 186:585–599 (1997). `hep-th/9608085`.

[70] Jan de Boer, Kentaro Hori, Hirosi Ooguri and Yaron Oz. "Kaehler potential and higher derivative terms from M theory five-brane". *Nucl. Phys.*, B518:173–211 (1998). `hep-th/9711143`.

[71] Nick J. Evans, Clifford V. Johnson and Alfred D. Shapere. "Orientifolds, branes, and duality of 4D gauge theories". *Nucl. Phys.*, B505:251–271 (1997). `hep-th/9703210`.

[72] Shmuel Elitzur, Amit Giveon, David Kutasov, Eliezer Rabinovici and Gor Sarkissian. "D-branes in the background of NS fivebranes". *JHEP*, 08:046 (2000). `hep-th/0005052`.

[73] Karl Landsteiner, Esperanza Lopez and David A. Lowe. "Supersymmetric gauge theories from branes and orientifold six-planes". *JHEP*, 07:011 (1998). `hep-th/9805158`.

[74] Karl Landsteiner, Esperanza Lopez and David A. Lowe. "Duality of chiral N = 1 supersymmetric gauge theories via branes". *JHEP*, 02:007 (1998). `hep-th/9801002`.

[75] Ilka Brunner, Amihay Hanany, Andreas Karch and Dieter Lust. "Brane dynamics and chiral non-chiral transitions". *Nucl. Phys.*, B528:197–217 (1998). `hep-th/9801017`.

[76] Shmuel Elitzur, Amit Giveon, David Kutasov and David Tsabar. "Branes, orientifolds and chiral gauge theories". *Nucl. Phys.*, B524:251–268 (1998). `hep-th/9801020`.

[77] Amihay Hanany and Alberto Zaffaroni. "Chiral symmetry from type IIA branes". *Nucl. Phys.*, B509:145–168 (1998). `hep-th/9706047`.

[78] John H. Brodie and Amihay Hanany. "Type IIA superstrings, chiral symmetry, and N = 1 4D gauge theory dualities". *Nucl. Phys.*, B506:157–182 (1997). `hep-th/9704043`.

[79] Sebastian Franco, Amihay Hanany, Fouad Saad and Angel M. Uranga. "Fractional branes and dynamical supersymmetry breaking". *JHEP*, 01:011 (2006). `hep-th/0505040`.

[80] Ann E. Nelson and Nathan Seiberg. "R symmetry breaking versus supersymmetry breaking". *Nucl. Phys.*, B416:46–62 (1994). `hep-ph/9309299`.

[81] Jerome P. Gauntlett, Dario Martelli, James Sparks and Daniel Waldram. "Supersymmetric AdS(5) solutions of M-theory". *Class. Quant. Grav.*, 21:4335–4366 (2004). `hep-th/0402153`.

[82] Jerome P. Gauntlett, Dario Martelli, James Sparks and Daniel Waldram. "Sasaki-Einstein metrics on S(2) x S(3)". *Adv. Theor. Math. Phys.*, 8:711–734 (2004). `hep-th/0403002`.

[83] Jerome P. Gauntlett, Dario Martelli, James F. Sparks and Daniel Waldram. "A new infinite class of Sasaki-Einstein manifolds". *Adv. Theor. Math. Phys.*, 8:987–1000 (2006). `hep-th/0403038`.

[84] Dario Martelli and James Sparks. "Toric geometry, Sasaki-Einstein manifolds and a new infinite class of AdS/CFT duals". *Commun. Math. Phys.*, 262:51–89 (2006). `hep-th/0411238`.

[85] Sergio Benvenuti, Sebastian Franco, Amihay Hanany, Dario Martelli and James Sparks. "An infinite family of superconformal quiver gauge theories with Sasaki-Einstein duals". *JHEP*, 06:064 (2005). `hep-th/0411264`.

[86] C. P. Herzog, Q. J. Ejaz and I. R. Klebanov. "Cascading RG flows from new Sasaki-Einstein manifolds". *JHEP*, 02:009 (2005). `hep-th/0412193`.

[87] Andrea Brini and Davide Forcella. "Comments on the non-conformal gauge theories dual to Y(p,q) manifolds". *JHEP*, 06:050 (2006). `hep-th/0603245`.

[88] Luis E. Ibanez, R. Rabadan and A. M. Uranga. "Anomalous U(1)'s in type I and type IIB D = 4, N = 1 string vacua". *Nucl. Phys.*, B542:112–138 (1999). `hep-th/9808139`.

[89] Igor R. Klebanov and Matthew J. Strassler. "Supergravity and a confining gauge theory: Duality cascades and chiSB-resolution of naked singularities". *JHEP*, 08:052 (2000). `hep-th/0007191`.

[90] Sebastian Franco, Amihay Hanany and Angel M. Uranga. "Multi-flux warped throats and cascading gauge theories". *JHEP*, 09:028 (2005). `hep-th/0502113`.

[91] Samuel Pinansky. "Quantum deformations from toric geometry". *JHEP*, 03:055 (2006). `hep-th/0511027`.

[92] Klaus Altmann. "Infinitesimal Deformations and Obstructions for Toric Singularities" (1994). `alg-geom/9405008`.

[93] Klaus Altmann. "The versal Deformation of an isolated toric Gorenstein Singularity" (1994). `alg-geom/9403004`.

[94] Sebastian Franco, Amihay Hanany, Kristian D. Kennaway, David Vegh and Brian Wecht. "Brane dimers and quiver gauge theories". *JHEP*, 01:096 (2006). `hep-th/0504110`.

[95] Hirosi Ooguri and Cumrun Vafa. "Geometry of N = 1 dualities in four dimensions". *Nucl. Phys.*, B500:62–74 (1997). `hep-th/9702180`.

[96] Ralph Blumenhagen, Mirjam Cvetic, Robert Richter and Timo Weigand. "Lifting D-Instanton Zero Modes by Recombination and Background Fluxes". *JHEP*, 10:098 (2007). `arXiv:0708.0403 [hep-th]`.

[97] Nick Dorey, Timothy J. Hollowood, Valentin V. Khoze and Michael P. Mattis. "The calculus of many instantons". *Phys. Rept.*, 371:231–459 (2002). `hep-th/0206063`.

[98] L. E. Ibanez, A. N. Schellekens and A. M. Uranga. "Instanton Induced Neutrino Majorana Masses in CFT Orientifolds with MSSM-like spectra". *JHEP*, 06:011 (2007). `arXiv:0704.1079 [hep-th]`.

[99] L. E. Ibanez and A. M. Uranga. "Instanton Induced Open String Superpotentials and Branes at Singularities" (2007). `arXiv:0711.1316 [hep-th]`.

[100] Ori J. Ganor. "A note on zeroes of superpotentials in F-theory". *Nucl. Phys.*, B499:55–66 (1997). `hep-th/9612077`.

[101] Ralph Blumenhagen, Mirjam Cvetic and Timo Weigand. "Spacetime instanton corrections in 4D string vacua - the seesaw mechanism for D-brane models". *Nucl. Phys.*, B771:113–142 (2007). `hep-th/0609191`.

[102] L. E. Ibanez and A. M. Uranga. "Neutrino Majorana masses from string theory instanton effects". *JHEP*, 03:052 (2007). `hep-th/0609213`.

[103] Bogdan Florea, Shamit Kachru, John McGreevy and Natalia Saulina. "Stringy instantons and quiver gauge theories". *JHEP*, 05:024 (2007). `hep-th/0610003`.

[104] Angel M. Uranga. "Brane configurations for branes at conifolds". *JHEP*, 01:022 (1999). `hep-th/9811004`.

[105] Steven Gubser, Nikita Nekrasov and Samson Shatashvili. "Generalized conifolds and four dimensional N = 1 superconformal theories". *JHEP*, 05:003 (1999). `hep-th/9811230`.

[106] Esperanza Lopez. "A family of N = 1 SU(N)**k theories from branes at singularities". *JHEP*, 02:019 (1999). `hep-th/9812025`.

[107] Kentaro Hori, Kazuo Hosomichi, David C. Page, Raul Rabadan and Johannes Walcher. "Non-perturbative orientifold transitions at the conifold". *JHEP*, 10:026 (2005). `hep-th/0506234`.

[108] Chris Beasley and Edward Witten. "New instanton effects in supersymmetric QCD". *JHEP*, 01:056 (2005). `hep-th/0409149`.

[109] Massimo Bianchi and Elias Kiritsis. "Non-perturbative and Flux superpotentials for Type I strings on the Z_3 orbifold". *Nucl. Phys.*, B782:26–50 (2007). `hep-th/0702015`.

[110] Chris E. Beasley and M. Ronen Plesser. "Toric duality is Seiberg duality". *JHEP*, 12:001 (2001). `hep-th/0109053`.

[111] Bo Feng, Amihay Hanany, Yang-Hui He and Angel M. Uranga. "Toric duality as Seiberg duality and brane diamonds". *JHEP*, 12:035 (2001). `hep-th/0109063`.

[112] F. Cachazo, B. Fiol, K. A. Intriligator, S. Katz and C. Vafa. "A geometric unification of dualities". *Nucl. Phys.*, B628:3–78 (2002). `hep-th/0110028`.

[113] Kei Ito. "Seiberg's duality from monodromy of conifold singularity". *Phys. Lett.*, B457:285–290 (1999). `hep-th/9903061`.

[114] David Berenstein and Michael R. Douglas. "Seiberg duality for quiver gauge theories" (2002). `hep-th/0207027`.

[115] Christopher P. Herzog. "Seiberg duality is an exceptional mutation". *JHEP*, 08:064 (2004). `hep-th/0405118`.

[116] N. Seiberg. "Electric - magnetic duality in supersymmetric nonAbelian gauge theories". *Nucl. Phys.*, B435:129–146 (1995). `hep-th/9411149`.

[117] Keshav Dasgupta and Sunil Mukhi. "Brane constructions, conifolds and M-theory". *Nucl. Phys.*, B551:204–228 (1999). `hep-th/9811139`.

[118] Steven S. Gubser, Christopher P. Herzog and Igor R. Klebanov. "Symmetry breaking and axionic strings in the warped deformed conifold". *JHEP*, 09:036 (2004). `hep-th/0405282`.

[119] Sebastian Franco, Yang-Hui He, Christopher Herzog and Johannes Walcher. "Chaotic duality in string theory". *Phys. Rev.*, D70:046006 (2004). `hep-th/0402120`.

[120] Ofer Aharony and Shamit Kachru. "Stringy Instantons and Cascading Quivers". *JHEP*, 09:060 (2007). `arXiv:0707.3126 [hep-th]`.

[121] Kenneth A. Intriligator and P. Pouliot. "Exact superpotentials, quantum vacua and duality in supersymmetric SP(N(c)) gauge theories". *Phys. Lett.*, B353:471–476 (1995). `hep-th/9505006`.

[122] Sebastian Franco *et al.* "Dimers and Orientifolds". *JHEP*, 09:075 (2007). `arXiv:0707.0298 [hep-th]`.

[123] Marco Billo *et al.* "Classical gauge instantons from open strings". *JHEP*, 02:045 (2003). `hep-th/0211250`.

[124] Angel M. Uranga. "Localized instabilities at conifolds" (2002). `hep-th/0204079`.

[125] Andrew Strominger. "Massless black holes and conifolds in string theory". *Nucl. Phys.*, B451:96–108 (1995). `hep-th/9504090`.

[126] Brian R. Greene, David R. Morrison and Andrew Strominger. "Black hole condensation and the unification of string vacua". *Nucl. Phys.*, B451:109–120 (1995). `hep-th/9504145`.

[127] Edward Witten. "Non-Perturbative Superpotentials In String Theory". *Nucl. Phys.*, B474:343–360 (1996). `hep-th/9604030`.

[128] G. F. Giudice and R. Rattazzi. "Theories with gauge-mediated supersymmetry breaking". *Phys. Rept.*, 322:419–499 (1999). `hep-ph/9801271`.

[129] Duiliu-Emanuel Diaconescu, Bogdan Florea, Shamit Kachru and Peter Svrcek. "Gauge - mediated supersymmetry breaking in string compactifications". *JHEP*, 02:020 (2006). `hep-th/0512170`.

[130] Amihay Hanany, Pavlos Kazakopoulos and Brian Wecht. "A new infinite class of quiver gauge theories". *JHEP*, 08:054 (2005). `hep-th/0503177`.

[131] G. Aldazabal, Luis E. Ibanez, F. Quevedo and A. M. Uranga. "D-branes at singularities: A bottom-up approach to the string embedding of the standard model". *JHEP*, 08:002 (2000). `hep-th/0005067`.

[132] Kenneth Intriligator and Nathan Seiberg. "The runaway quiver". *JHEP*, 02:031 (2006). `hep-th/0512347`.

[133] David Berenstein, Vishnu Jejjala and Robert G. Leigh. "The standard model on a D-brane". *Phys. Rev. Lett.*, 88:071602 (2002). `hep-ph/0105042`.

[134] Herman Verlinde and Martijn Wijnholt. "Building the standard model on a D3-brane" (2005). `hep-th/0508089`.

[135] Juan F. G. Cascales, Fouad Saad and Angel M. Uranga. "Holographic dual of the standard model on the throat". *JHEP*, 11:047 (2005). `hep-th/0503079`.

[136] Changhyun Ahn. "Meta-Stable Brane Configurations by Quartic Superpotential for Bifundamentals" (2008). `arXiv:0801.0619 [hep-th]`.

[137] Vijay Balasubramanian, Bartlomiej Czech, Yang-Hui He, Klaus Larjo and Joan Simon. "Typicality, Black Hole Microstates and Superconformal Field Theories" (2007). `arXiv:0712.2434 [hep-th]`.

[138] R. Dijkgraaf, D. Orlando and S. Reffert. "Dimer models, free fermions and super quantum mechanics" (2007). `arXiv:0705.1645 [hep-th]`.

[139] Michael R. Douglas, Bartomeu Fiol and Christian Romelsberger. "Stability and BPS branes". *JHEP*, 09:006 (2005). `hep-th/0002037`.

[140] Kenneth Intriligator and Nathan Seiberg. "Lectures on Supersymmetry Breaking". *Class. Quant. Grav.*, 24:S741–S772 (2007). `hep-ph/0702069`.

[141] Sidney R. Coleman and E. Weinberg. "Radiative Corrections as the Origin of Spontaneous Symmetry Breaking". *Phys. Rev.*, D7:1888–1910 (1973).

[142] William Fulton. *Introduction to Toric Varieties*. Princeton University Press (1993).

[143] Brian R. Greene. "String theory on Calabi-Yau manifolds" (1996). `hep-th/9702155`.

[144] Igor R. Klebanov and Edward Witten. "Superconformal field theory on threebranes at a Calabi-Yau singularity". *Nucl. Phys.*, B536:199–218 (1998). `hep-th/9807080`.

[145] Edward Witten. "Phases of N = 2 theories in two dimensions". *Nucl. Phys.*, B403:159–222 (1993). `hep-th/9301042`.

[146] Naichung Conan Leung and Cumrun Vafa. "Branes and toric geometry". *Adv. Theor. Math. Phys.*, 2:91–118 (1998). `hep-th/9711013`.

[147] Mina Aganagic and Cumrun Vafa. "G(2) manifolds, mirror symmetry and geometric engineering" (2001). `hep-th/0110171`.

[148] Kristian D. Kennaway. "Brane Tilings". *Int. J. Mod. Phys.*, A22:2977–3038 (2007). `arXiv:0706.1660 [hep-th]`.

[149] Sebastian Franco and David Vegh. "Moduli spaces of gauge theories from dimer models: Proof of the correspondence" (2006). hep-th/0601063.

[150] Bo Feng, Yang-Hui He, Kristian D. Kennaway and Cumrun Vafa. "Dimer models from mirror symmetry and quivering amoebae" (2005). hep-th/0511287.

[151] Andrew Strominger, Shing-Tung Yau and Eric Zaslow. "Mirror symmetry is T-duality". *Nucl. Phys.*, B479:243–259 (1996). hep-th/9606040.

[152] Andreas Karch and Emanuel Katz. "Adding flavor to AdS/CFT". *JHEP*, 06:043 (2002). hep-th/0205236.

[153] Mirjam Cvetic, Robert Richter and Timo Weigand. "D-brane instanton effects in Type II orientifolds: local and global issues" (2007). arXiv:0712.2845 [hep-th].

[154] Bobby S. Acharya. "On realising N = 1 super Yang-Mills in M theory" (2000). hep-th/0011089.

[155] M. Bershadsky, A. Johansen, T. Pantev, V. Sadov and C. Vafa. "F-theory, geometric engineering and N = 1 dualities". *Nucl. Phys.*, B505:153–164 (1997). hep-th/9612052.

[156] Nikolas Akerblom, Ralph Blumenhagen, Dieter Lust, Erik Plauschinn and Maximilian Schmidt-Sommerfeld. "Non-perturbative SQCD Superpotentials from String Instantons". *JHEP*, 04:076 (2007). hep-th/0612132.

[157] John H. Brodie. "Fractional branes, confinement, and dynamically generated superpotentials". *Nucl. Phys.*, B532:137–152 (1998). hep-th/9803140.

[158] Chris Beasley and Edward Witten. "New instanton effects in string theory". *JHEP*, 02:060 (2006). hep-th/0512039.